ZooKeys 1012: 1–19 (2021)
doi: 10.3897/zookeys.1012.59854
https://zookeys.pensoft.net

RESEARCH ARTICLE

A peer-reviewed open-access journal
ZooKeys
Launched to accelerate biodiversity research

Five new *Sinopoda* species (Araneae, Sparassidae) from China and Thailand

Ziyi Wang[1], Wei Liang[1], Shuqiang Li[2]

1 *Ministry of Education Key Laboratory for Ecology of Tropical Islands, Hainan Normal University, 571158, Haikou, China* **2** *Institute of Zoology, Chinese Academy of Sciences, 100101, Beijing, China*

Corresponding author: Wei Liang (13976699091@139.com); Shuqiang Li (lisq@ioz.ac.cn)

Academic editor: I. Agnarsson | Received 20 October 2020 | Accepted 10 January 2021 | Published 26 January 2021

http://zoobank.org/1C55B70D-20B8-487D-92C2-40135CB85EA0

Citation: Wang Z, Liang W, Li S (2021) Five new *Sinopoda* species (Araneae, Sparassidae) from China and Thailand. ZooKeys 1012: 1–19. https://doi.org/10.3897/zookeys.1012.59854

Abstract

Five new species of the huntsman spider genus *Sinopoda* Jäger, 1999 are described: *S. hongruii* Wang & Li, **sp. nov.** (♂♀, forest in Anhui, China), *S. jiangzhou* Wang & Li, **sp. nov.** (♂♀, cave in Guangxi, China), *S. saiyok* Wang & Li, **sp. nov.** (♀, cave in Kanchanaburi, Thailand), *S. yanjin* Wang & Li, **sp. nov.** (♀, forest in Yunnan, China), and *S. yanzi* Wang & Li, **sp. nov.** (♂♀, cave in Hunan, China). A distribution map of the new species is provided.

Keywords

Biodiversity, distribution, huntsman spiders, taxonomy

Introduction

Sparassidae Bertkau, 1872 are small to large spiders with laterigrade legs. The genus *Sinopoda* was established by Jäger in 1999 and belongs to the subfamily Heteropodinae Thorell, 1873 (Jäger 1999). The genus can be distinguished from other huntsman spiders by the presence of an embolic apophysis and a membranous conductor in the male palp, and by the special internal ducts in female vulva (Jäger 1999; Liu et al.

2008; Zhang et al. 2015). *Sinopoda* is the fourth largest genus of Sparassidae, with 126 species from Asia reported: 65 from China, 16 from Laos, 12 from Malaysia, 11 from Japan and South Korea, nine from Thailand, five from Myanmar, four from Indonesia, three from Vietnam, and one from India (WSC 2020; Li 2020).

Sinopoda are non-web building spiders, living in leaf litter, rock crevices, caves, and on tree bark (Jäger 1999, 2012). *Sinopoda* spiders are difficult to collect in the field due to their cryptic life style and nocturnality; thus, about 40% of the species are known only from a single sex. In this paper, all five new *Sinopoda* species, including two known from females and three from both sexes, are found in typical habitat: three from caves and two from rock crevices in forests.

Methods

All the specimens were collected, preserved in 75% ethanol, and examined and measured with a Leica M205C stereomicroscope. After dissection of male palps and the epigynes, images were made with an Olympus C7070 wide zoom digital camera (7.1 megapixels) mounted on an Olympus BX51 compound light microscope. Images of the spiders' bodies were taken with an Olympus C7070 camera mounted on an Olympus SZX12 dissecting microscope. The epigynes were cleaned and treated in trypsin and, if necessary, in a boiling solution of potassium hydroxide (KOH) before being transferred to 75% ethanol for imaging. All images were assembled using Helicon Focus v. 6.7.1 software.

All measurements are in millimeters. Leg formula, spination, and measurements of palps and legs follow Jäger (2012). The point of origin of the embolus and conductor are given as "clock positions" on the left palps in ventral view.

Abbreviations used in the text:

ALE anterior lateral eyes;
AME anterior median eyes;
AW anterior width of prosoma;
CH clypeus height;
dRTA dorsal branch of RTA;
E embolus;
EA embolic apophysis;
EP epigynal pockets;
FB fusion bubble;
FD fertilization ducts;
LF lateral furrow;
LL lateral lobes;
LS lobal septum;
OL opisthosoma length;
OW opisthosoma width;
PL prosoma length;
PW prosoma width;
PLE posterior lateral eyes;
PME posterior median eyes;
PP posterior part of internal duct system;
SP spermophor;
RTA retrolateral tibial apophysis;
vRTA ventral branch RTA;
I, II, III, IV legs I to IV.

All material is deposited in the Institute of Zoology, Chinese Academy of Sciences (**IZCAS**) in Beijing, China.

Taxonomy

Family Sparassidae Bertkau, 1872
Subfamily Heteropodinae Thorell, 1873
Genus *Sinopoda* Jäger, 1999

***Sinopoda hongruii* Wang & Li, sp. nov.**
http://zoobank.org/A9AC1661-6533-4AE3-AFC4-D53660887306
Figs 1A–F, 2A, B, 9A, B, 10

Material examined. ***Holotype*** ♂ (IZCAS-Ar41604), China, Anhui Province, Lujiang County, Yefu Mountain National Forest Park; 31.5674°N, 117.5593°E; 170 m; 3 Jul. 2018; Hongrui Zhao leg. ***Paratypes*** 2 ♀ (IZCAS-Ar41605, IZCAS-Ar41606); China, Anhui Province, Lujiang County, Yefu Mountain National Forest Park; 31.2694°N, 117.2703°E; 50 m; 5 Sept. 2020; Ziyi Wang leg.

Diagnosis. The male of this new species resembles the male of *Sinopoda tengchongensis* Fu & Zhu, 2008 (Fu and Zhu 2008: 63, figs 1–5; Grall and Jäger 2020: 66, fig. 43a–c) in having the analogous conductor and embolus, but the new species can be recognized by the following: the distal part of vRTA is wider than the basal part in retrolateral view in this new species (Fig. 1A–D) but equal in width in *S. tengchongensis*; the tip of the embolus apophysis is flagelliform in the new species but flat in *S. tengchongensis*. The females of this new species are similar to *Sinopoda aequalis* Zhong, Jäger, Chen & Liu, 2019 (Zhong et al 2019: 8, figs 4D, E, 6A–D) in having the anterior part of the internal ducts similar and *S. tengchongensis* Fu & Zhu, 2008 (Fu and Zhu 2008: 63, figs 1–5; Grall and Jäger 2020: 66, fig. 43a–c) in having similar lateral lobes, but can be recognized by the following: the lobal septum is sharper than in *S. aequalis* and *S. tengchongensis*; the new species has blunt, swollen glandular appendages but in *S. aequalis* the glandular appendages are slender and longer; the posterior part of internal duct system as wide as the middle part of internal ducts (Fig. 2A, B) in the new species, while the posterior part of internal duct system swollen and much wider than the internal ducts in *S. aequalis*; the internal duct system is fused along whole median line in the new species but the anterior part is not fused in *S. tengchongensis*.

Description. Male (***holotype***, IZCAS-Ar41604) **Measurements:** PL 9.3, PW 8.8; AW 3.8; OL 9.9, OW 5.5. ***Eyes*:** AME 0.40, ALE 0.42, PME 0.39, PLE 0.59, AME-AME 0.37, AME-ALE 0.09, PME-PME 0.39, PME-PLE 0.29, AME-PME 0.47, ALE-PLE 0.26, CH AME 0.27, CH ALE 0.25. ***Palp*:** 12.34 (4.22, 2.04, 2.17, –, 3.91). ***Legs*:** I 34.06 (10.24, 3.55, 9.98, 6.84, 3.45); II 38.95 (10.81, 3.58, 10.62, 10.49, 3.45); III 28.77 (8.57, 3.45, 7.61, 6.65, 2.49); IV 26.99 (7.29, 2.68, 7.55, 6.59, 2.88). Leg formula: II-I-III-IV. **Spination: *Palp*:** 131 101 – 1100. ***Legs*:** Fe I–IV 232 Pa I–IV 101, Ti I–III 2326, IV 2337, Mt I–III 0004, IV 2025. ***Chelicerae*:** Furrow with four anterior teeth, four posterior teeth, and 27 denticles.

***Palp*:** as in diagnosis. The ratio of the length of the cymbium to the length of the tibia is approximately 2:1. The cymbium furrow is as long as 1/3 of the cymbium. The tip of the embolus apophysis is slightly pointy. Embolus S-shaped, arising from

Figure 1. *Sinopoda hongruii* sp. nov., holotype male from Yefu Mountain National Forest Park **A–C** left palp (**A** prolateral **B** ventral **C** retrolateral) **D** retrolateral view of RTA **E, F** habitus (**E** dorsal **F** ventral). Abbreviations: C conductor, dRTA dorsal branch of retrolateral tibial apophysis, E embolus, EA embolic apophysis, SP spermophor, ST subtegulum, T tegulum, vRTA ventral branch of retrolateral tibial apophysis. Scale bars: 0.5 mm (**A–D**); 2 mm (**E, F**).

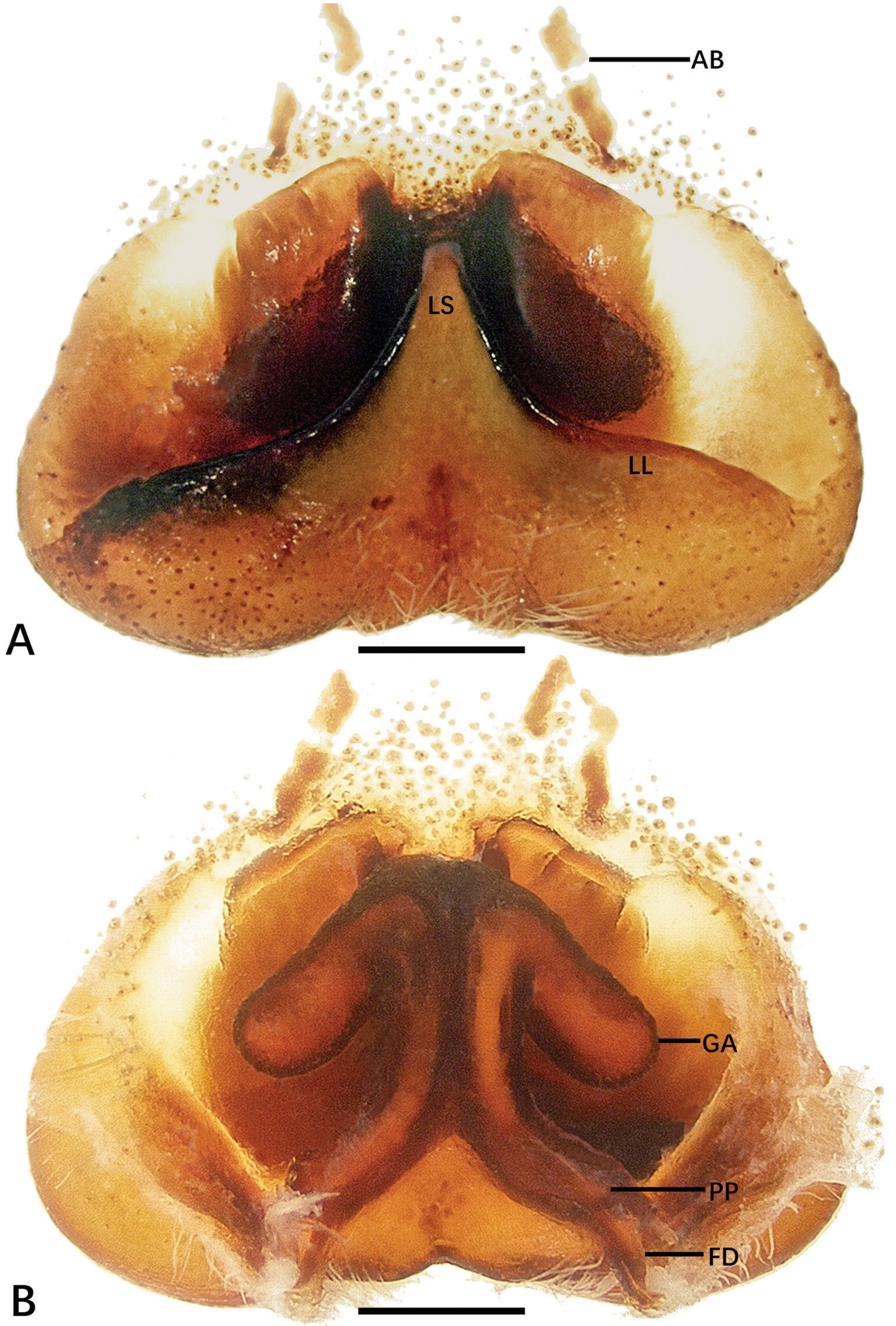

Figure 2. *Sinopoda hongruii* sp. nov., holotype female from Yefu Mountain National Forest Park **A** epigyne **B** vulval. Abbreviations: AB anterior bands, FD fertilization ducts, GA glandular appendages, LL lateral lobes, LS lobal septum, PP posterior part of internal duct system. Scale bars: 0.5 mm.

tegulum at nearly the 6-o'clock-position in ventral view. Conductor arising at 1-o'clock-position from tegulum, elongated, slightly bent. Spermophor slightly S-shaped. RTA arising basally from tibia; base of RTA with a brush of setae. vRTA smaller than dRTA, trapezoidal in retrolateral view. dRTA longer than tibia (Fig. 1A–D).

Coloration in ethanol: yellowish. ***Prosoma*:** dorsally yellowish, lateral margins dark with yellowish submarginal transverse interval. Labium and gnathocoxae light brownish. Fovea and radial furrow distinctly marked. Sternum yellowish, with margin yellowish brown. Chelicerae deep reddish brown. ***Legs*:** yellowish with dark spots. ***Opisthosoma*:** dorsally dark khaki covered with dark hairs; ventrally khaki with irregular pattern. Spinnerets yellowish brown (Fig. 1E, F).

Female (***paratype***, IZCAS-Ar41605) **Measurements:** PL 8.84, PW 8.39; AW 4.87; OL 9.42, OW 5.51. ***Eyes*:** AME 0.3, PME 0.4, ALE 0.55, PLE 0.5, AME-AME 0.37, AME-ALE 0.15, PME-PME 0.57, PME-PLE 0.67, AME-PME 0.52, ALE-PLE 0.6, CH AME 0.17, CH ALE 0.45. ***Palp*:** 8.5 (2.49, 0.64, 2.11, –, 3.26). ***Legs*:** I 27.66 (7.62, 2.62, 7.75, 7.11, 2.56); II 30.42 (8.58, 2.69, 8.9, 7.69, 2.56); III 25.35 (7.24, 2.43, 7.17, 6.02, 2.49); IV 27.86 (7.43, 2.56, 7.82, 7.3, 2.75). Leg formula: II-IV-I-III. **Spination:** ***Palp*:** 131 101 303 2222. ***Legs*:** Fe 323, IV 333, Pa 101, Ti I–III 1018, IV 2026, Mt I–III 0004, IV 2026. ***Chelicerae*:** Furrow with three anterior teeth, four posterior teeth, and 23 denticles.

***Copulatory organ*:** as in diagnosis. Epigynal field wider than long, with two short anterior bands close to the field. Lateral lobes fused. Lobal septum and lateral lobes almost triangular. Glandular appendages are slender and long, the posterior part of internal duct system swollen. Internal ducts half as wide as the epigynal field. Fertilization ducts arising posteriorly. Unexpanded membranous sac between fertilization ducts (Fig. 2A, B).

Coloration in ethanol: as in male (Fig. 9A, B).

Etymology. The specific name is dedicated to Mr Hongrui Zhao who collected this species; noun (name) in genitive case.

Distribution. Known only from the type locality (Fig. 10, China, Anhui).

Sinopoda jiangzhou Wang & Li, sp. nov.

http://zoobank.org/EAB771F1-EF19-49EC-ACF0-B2573B43D363
Figs 3A–F, 4A, B,9C, D, 10

Material examined. ***Holotype*** ♂ (IZCAS-Ar41607), China, Guangxi Zhuang Autonomous Region, Hechi City, Fengshan County, Jiangzhou Village, Underground Gallery; 24.3314°N, 106.9871°E; 449 m; 13 Sept. 2019; Ziyi Wang & Zhigang Chen leg. ***Paratype*** 1 ♂ (IZCAS-Ar41608), same data as holotype. 1 ♀ (IZCAS-Ar41609), same data as holotype, but 25 Mar. 2015; Yunchun Li & Zhigang Chen leg.

Diagnosis. This new species is similar to *Sinopoda tumefacta* Zhong, Jäger, Chen & Liu, 2019 (Zhong et al. 2019: 69, figs 53A–E, 54A–F, 55A–D) in the structure of the embolus and RTA but can be recognized by the following characters: in the male, the conductor is straight and fan-shaped, unlike in *S. tumefacta* (Zhong et al. 2019: fig. 53B) where the conductor is curved and covered by the embolus; the sub-tegulum

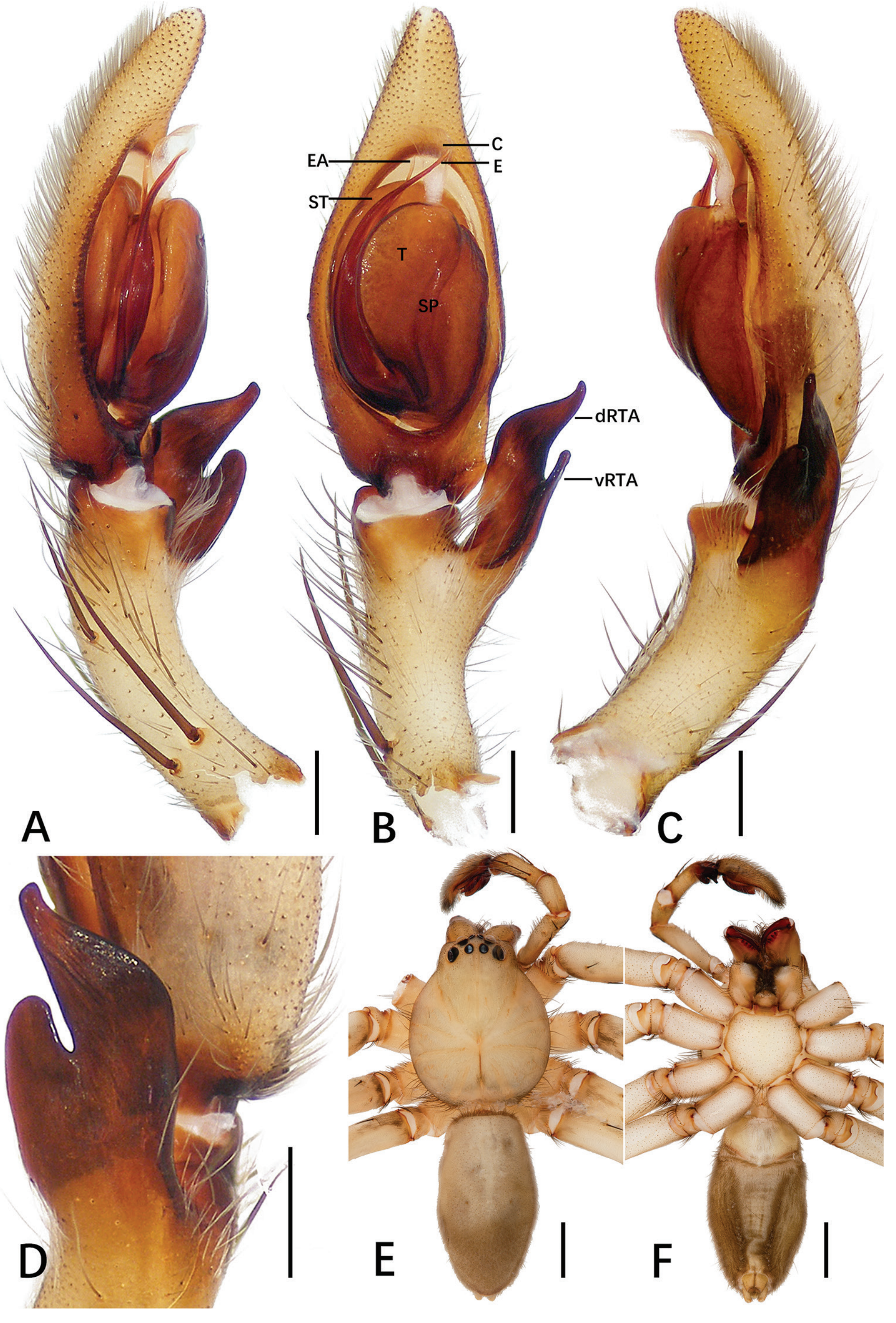

Figure 3. *Sinopoda jiangzhou* sp. nov., holotype male from Underground Gallery **A–C** left palp (**A** prolateral **B** ventral **C** retrolateral) **D** retrolateral view of RTA **E, F** habitus (**E** dorsal **F** ventral). Abbreviations: C conductor, dRTA dorsal branch of retrolateral tibial apophysis, E embolus, EA embolic apophysis, SP spermophor, ST subtegulum, T tegulum, vRTA ventral branch of retrolateral tibial apophysis. Scale bars: 0.5 mm (**A–D**); 2 mm (**E, F**).

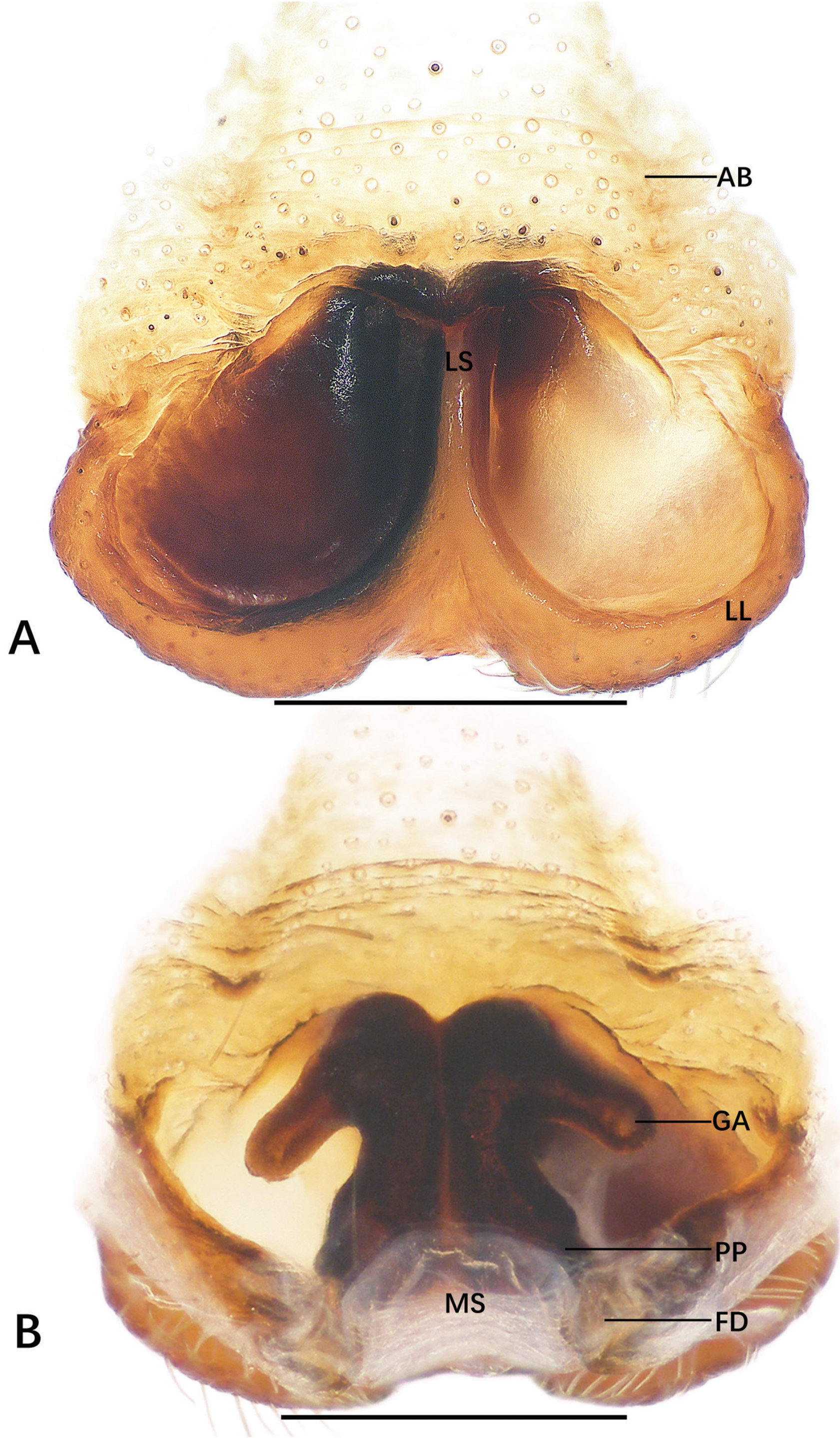

Figure 4. *Sinopoda jiangzhou* sp. nov., paratype female from Underground Gallery **A** epigyne **B** vulva. Abbreviations: AB anterior bands, FD fertilization ducts, GA glandular appendages, LL lateral lobes, LS lobal septum, MS membranous sac, PP posterior part of internal duct system. Scale bars: 0.5 mm.

is noticeably higher in the new species (Fig. 3A–D), but not in *S. tumefacta*; the embolus arises from the tegulum at the 6-o'clock position but at the 5-o'clock position in *S. tumefacta*. The female resembles *S. tumefacta* in the structure of the anterior part of internal ducts and the glandular appendages, which is longer than the posterior part of internal duct system but differs from *S. tumefacta* by: the lateral lobes of the new species (Fig. 4A, B) are narrow, but they are wider in *S. tumefacta* (Zhong et al. 2019: fig. 53D, E); the lobal septum is slender in the new species but broader in *S. tumefacta*.

Description. Male (***holotype***, IZCAS-Ar41607) **Measurements:** PL 5.7, PW 4.8; AW 2.43; OL 6.21, OW 3.52. ***Eyes*:** AME 0.17, PME 0.23, ALE 0.34, PLE 0.35, AME-AME 0.09, AME-ALE 0.03, PME-PME 0.18, PME-PLE 0.21, AME-PME 0.25, ALE-PLE 0.21, CH AME 0.23, CH ALE 0.2. ***Palp*:** 9.03 (3.26, 1.41, 1.6, –, 2.76). ***Legs*:** I 32.48 (8.78, 2.24, 9.74, 9.03, 2.69); II 35.62 (10.51, 2.05, 10.57, 9.74, 2.75); III 29.15 (8.14, 2.11, 8.33, 7.88, 2.69); IV 30.43 (8.01, 2.11, 8.84, 8.65, 2.82). Leg formula: II-I-IV-III. **Spination: *Palp*:** 131, 101, 2101. ***Legs*:** Fe 323, IV 123, Pa 101, Ti 2226, Mt I and II 1014, III and IV 2026. ***Chelicerae*:** furrow with three anterior teeth, four posterior teeth, and nine denticles.

***Palp*:** as in diagnosis. Cymbium longer than tibia. Embolus arising from tegulum at the 6-o'clock position, tip of embolus bent. Embolic apophysis bent at a right angle, slender. Tegulum covering middle of the embolus. Conductor arising from the tegulum at the 1-o'clock-position, elongated straight. Spermophor slightly bent. RTA arising from anterior part of tibia, vRTA smaller than dRTA (Fig. 3B).

Coloration in ethanol: yellowish brown. ***Prosoma*:** dorsally yellowish brown with fovea and cuticular with a radial pattern. Sternum and ventral coxae pale yellowish brown. Gnathocoxae reddish brown, labium yellowish brown. Chelicerae reddish brown. ***Legs*:** light yellowish brown. ***Opisthosoma*:** including spinnerets, khaki, sparsely covered with dark hairs (Fig. 3E, F); dorsally with some brown dots and ventrally with two long, distinct furrows posteriorly.

Female (***paratype***, IZCAS-Ar41609) **Measurements:** PL 4.23, PW 4.16; AW 2.49; OL 5.96, OW 3.26. ***Eyes*:** AME 0.14, PME 0.26, ALE 0.32, PLE 0.34, AME-AME 0.1, AME-ALE 0.06, PME-PME 0.22, PME-PLE 0.36, AME-PME 0.26, ALE-PLE 0.24, CH AME 0.14, CH ALE 0.18. ***Palp*:** 6.45 (1.66, 1.02, 1.21, –, 2.56). ***Legs*:** I 23.12 (6.41, 2.05, 6.47, 6.21, 1.98); II 24.07 (7.05, 2.17, 7.17, 5.44, 2.24); III 22.47 (6.53, 1.85, 6.02, 6.15, 1.92); IV 23.62 (6.66, 1.92, 6.79, 6.08, 2.17). Leg formula: II-I-IV-III. **Spination: *palp*:** 131 101 2130 4140. ***Legs*:** Fe 323, IV 123, Pa 101, Ti I and II 1018, III 2026, IV 2126, Mt I and II 1014, III and IV 2026. ***Chelicerae*:** furrow with three anterior teeth, four posterior teeth, and nine denticles.

***Copulatory organ*:** as in diagnosis. Epigynal field wider than long, with short anterior bands. Lateral lobes fused, with wide median incision and distinct, bilobed margin. Fertilization ducts arising posterolaterally. Unexpanded membranous sac between fertilization ducts (Fig. 4A, B).

Coloration in ethanol: as in male (Fig. 9C, D).

Etymology. The specific name refers to the type locality, Jiangzhou Village; noun in apposition.

Distribution. Known only from the type locality (Fig. 10, China, Guangxi).

***Sinopoda saiyok* Wang & Li, sp. nov.**
http://zoobank.org/329FFEC6-0A28-44AB-A33F-1383DD9D1CC1
Figures 5A, B, 9E, F, 10

Material examined. ***Holotype*** ♀ (IZCAS-Ar41647), Thailand, Kanchanaburi Province, Sai Yok District, Wang Krachae Subdistrict, unnamed cave; 14.2036°N, 99.0277°E; 82 m; 11 January 2014; Prasit Wongprom leg.

Diagnosis. This new species resembles *Sinopoda bifurca* Grall & Jäger, 2020 (Grall and Jäger 2020: 11, fig. 4d, e) in having similar lateral lobes, but it can be recognized by the uniquely rectangular lobal septum and the reduced posterior part of internal duct system (Fig. 5A, B), whereas the posterior part of internal duct system slightly swollen in *S. bifurca*.

Description. Female (***holotype***, IZCAS-Ar41647) **Measurements:** PL 3.28, PW 3.24; AW 1.88; OL 4.24, OW 2.64. ***Eyes*****:** AME 0.12, PME 0.08, ALE 0.14, PLE 0.16, AME-AME 0.10, AME-ALE 0.05, PME-PME 0.18, PME-PLE 0.22, AME-PME 0.13, ALE-PLE 0.15, CH AME 0.11, CH ALE 0.15. ***Palp*****:** 4.72 (1.53, 0.44, 1.34, –, 1.41). ***Legs*****:** I 15.04 (4.10, 1.66, 4.16, 3.84, 1.28); II 17.61 (5.06, 1.98, 4.93, 4.23, 1.41); III 15.18 (4.23, 1.73, 4.23, 3.65, 1.34); IV 15.43 (4.42, 1.41, 4.10, 3.97, 1.53). Leg formula: II-IV-III-I. **Spination:** ***palp*****:** 131 101 2130 3030. ***Legs*****:** Fe I–IV 323, Pa I–IV 111, Ti I–IV 2026, Mt I–IV 2026. ***Chelicerae*****:** furrow with three anterior teeth, four posterior teeth, and without denticles.

Copulatory organ**:** as in diagnosis. Epigynal field slightly wider than long, with two short anterior bands slightly fused with field, with one fusion bubble medially. The width of the lobal septum is equal to 1/3 the width of the epigynal field. The lobal septum is partly fused to the epigynal field. The anterior part of the internal ducts is discernibly swollen. The glandular appendages are blunt and bent at a right angle, extending laterally in posterior half of internal duct system. Internal duct system fused along whole median line. The posterior part of the internal duct system are miniaturized and narrower than anterior part of internal ducts and with the fertilization ducts arising posterolaterally. Unexpanded, membranous sac between fertilization ducts (Fig. 5A, B).

Coloration in ethanol: yellowish brown. ***Prosoma*****:** dorsally yellowish brown with fovea and cuticular with a radial, yellowish-brown pattern. Sternum and ventral coxae pale yellowish brown, gnathocoxae deep yellowish brown, labium reddish brown. Chelicerae deep reddish brown. ***Legs*****:** yellowish brown. ***Opisthosoma*****:** including spinnerets, greyish brown to yellowish brown, sparsely covered with brown hairs (Fig. 9E, F).

Male: unknown.

Etymology. The specific name refers to the type locality, Sai Yok District; noun in apposition.

Distribution. Known only from the type locality (Fig. 10, Thailand, Kanchanaburi).

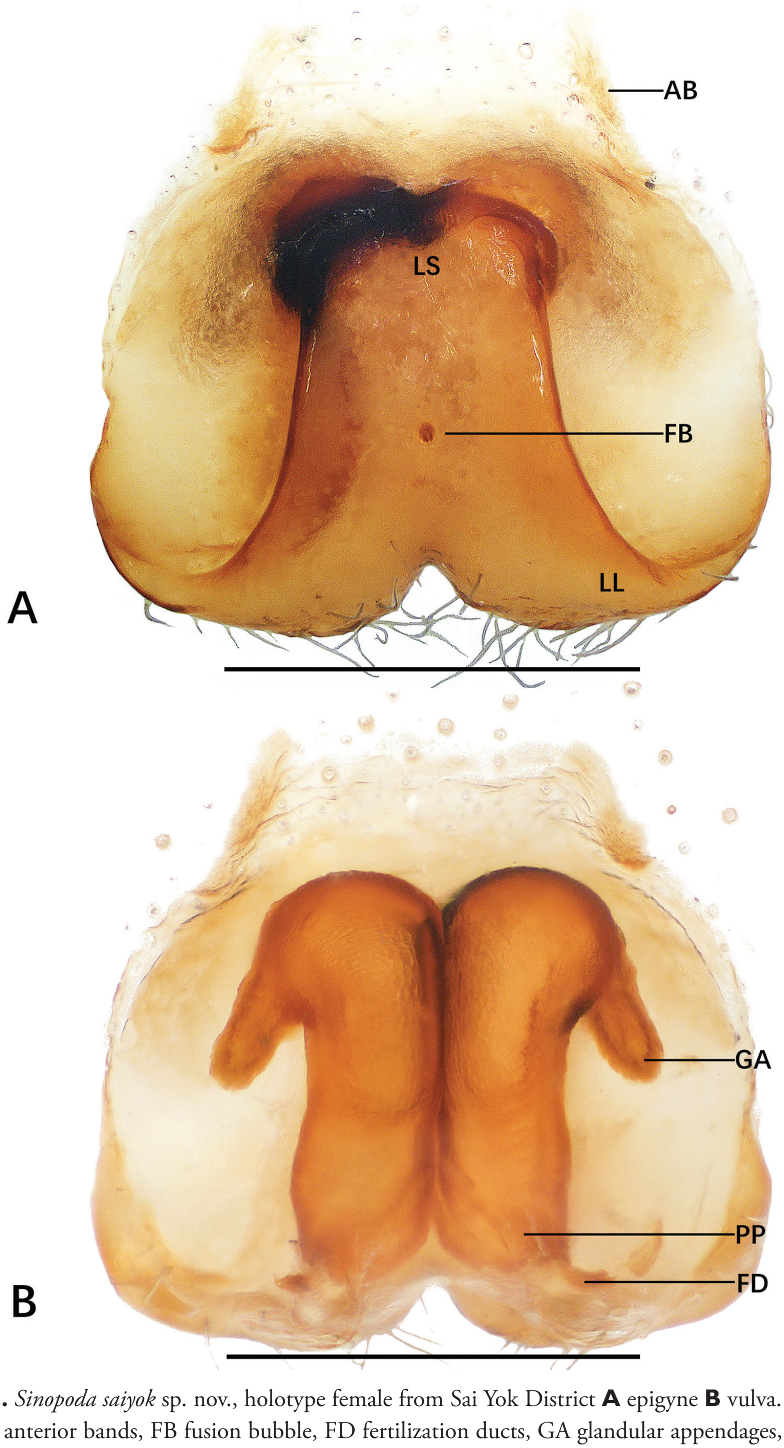

Figure 5. *Sinopoda saiyok* sp. nov., holotype female from Sai Yok District **A** epigyne **B** vulva. Abbreviations: AB anterior bands, FB fusion bubble, FD fertilization ducts, GA glandular appendages, LL lateral lobes, LS lobal septum, PP posterior part of internal duct system. Scale bars: 0.5 mm.

Sinopoda yanjin **Wang & Li, sp. nov.**
http://zoobank.org/85904853-5C78-4507-A8F7-566A075721C8
Figs 6A, B, 9G, H, 10

Material examined. ***Holotype*** ♀ (IZCAS-Ar41610), China, Yunnan Province, Zhaotong City, Yanjin County, Doushaguan Town, near Xiangshui Cave, unnamed cave; 28.0381°N, 104.07986°E; 774 m; 15 March 2015; Yunchun Li & Jinchen Liu leg. ***Paratypes*** 4 ♀ (IZCAS-Ar41611 to IZCAS-Ar41614); China, Yunnan Province, Zhaotong City, Yanjin County, Doushaguan Town, Wuchidao Scenic Area; 28.0398°N, 104.1150°E; 548 m; 19 Sept. 2020; Ziyi Wang leg.

Diagnosis. This new species can be separated from other *Sinopoda* species by the unique arrow-shaped lobal septum; the internal duct system is conspicuously swollen and broad; the width of the glandular appendages is equal to the width of medial part of the internal ducts (Fig. 6A, B).

Description. Female (***holotype***, IZCAS-Ar41610) **Measurements:** PL 8.71, PW 8.52; AW 4.87; OL 10.83, OW 7.24. ***Eyes*****:** AME 0.34, PME 0.4, ALE 0.5, PLE 0.48, AME-AME 0.3, AME-ALE 0.36, PME-PME 0.48, PME-PLE 0.72, AME-PME 0.58, ALE-PLE 0.64, CH AME 0.2, CH ALE 0.4. ***Palp*****:** 12.16 (3.46, 1.85, 2.62, –, 4.23). ***Legs*****:** I 34.72 (9.67, 3.97, 9.42, 8.46, 3.20); II 37.21 (11.08, 4.23, 10.06, 8.90, 2.94); III 31.59 (9.23, 3.78, 8.78, 6.98, 2.82); IV 34.84 (9.99, 3.71, 8.52, 9.16, 3.46). Leg formula: II-IV-I-III. **Spination:** ***palp*****:** 131 101 2120 2030. ***Legs*****:** Fe I–III 323, IV 333, Pa I–IV 101, Ti I–IV 2224, Mt I–III 2024, IV 3034. ***Chelicerae*****:** Furrow with three anterior teeth, four posterior teeth, and 16 denticles.

Copulatory organ**:** as in diagnosis. Epigynal field wider than long, with one long anterior band partly integrated into the field and one slit sensillum on each side, close to the field. The lobal septum is not fused with epigynal field and has a distinct indentation medially. Lateral lobes fused, with median indentation. The anterior part of the internal ducts is wider than the posterior part. The glandular appendages are blunt and wide, extending posteriorly to the posterior half of the internal duct system. The width of the glandular appendages is equal to the width of medial part of the internal ducts. Lateral furrow partly fused, inconspicuous. The posterior part of internal duct system bulging slightly laterally, fertilization ducts arising posteriorly from the posterior part of the internal duct system. Unexpanded membranous sac between fertilization ducts (Fig. 6A, B).

Coloration in ethanol: brown. ***Prosoma*****:** dorsally reddish brown with distinct radial furrow and fovea, sparsely covered with dark hairs. Labium and gnathocoxae deep reddish brown, with dark margin. Sternum bright yellowish brown, with reddish brown margin. ***Legs*****:** khaki, with distal parts darker, covered with dark hairs. Chelicerae dark reddish brown. ***Opisthosoma*****:** dorsally and ventrally reddish, slightly brownish, with an irregular pattern; ventrally with two longitudinal red lines between epigastric furrow and spinnerets. Spinnerets khaki (Fig. 9G, H).

Male: unknown.

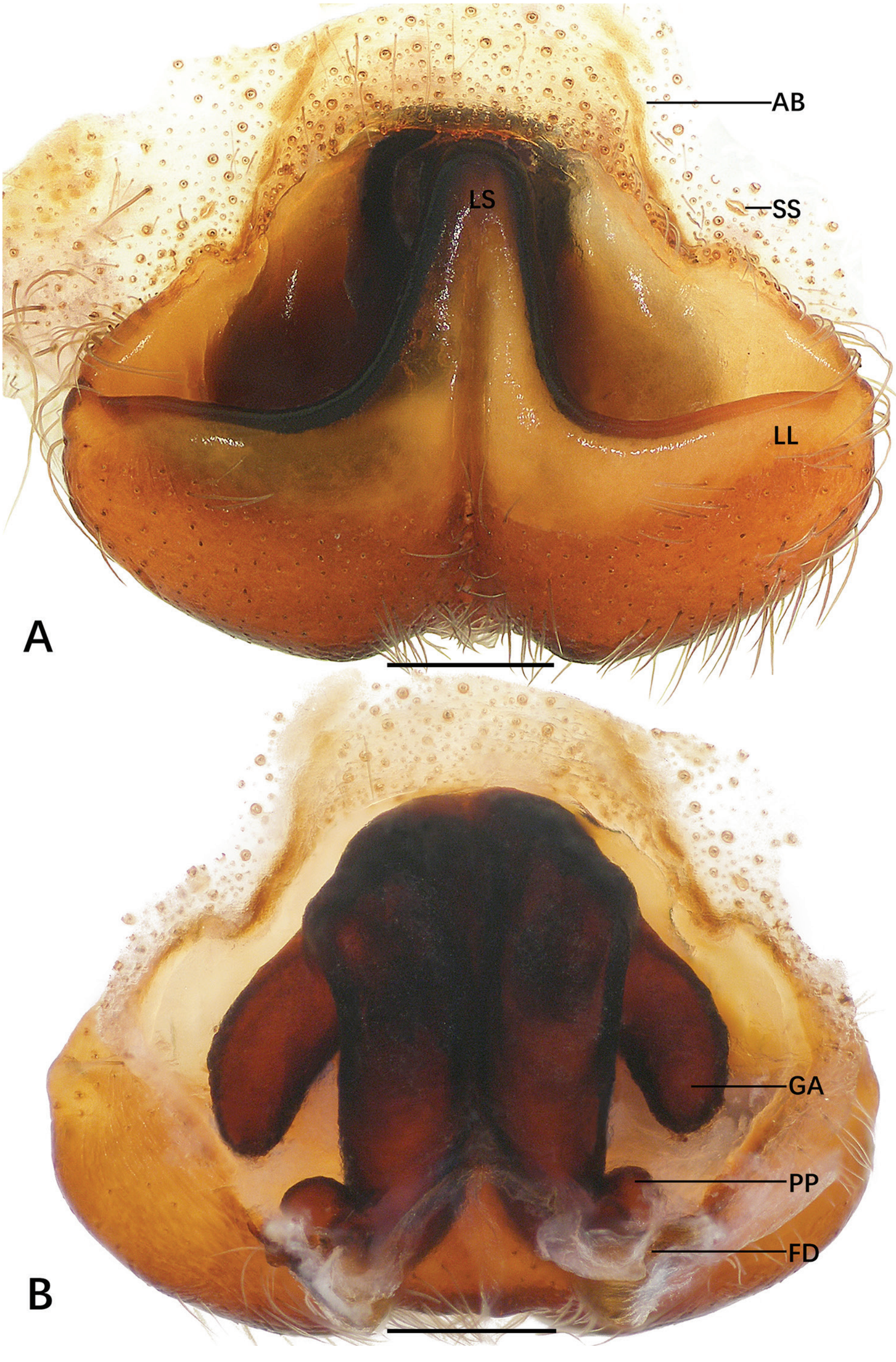

Figure 6. *Sinopoda yanjin* sp. nov., holotype female from Yanjin County **A** epigyne **B** vulva. Abbreviations: AB anterior bands, FD fertilization ducts, GA glandular appendages, LL lateral lobes, LS lobal septum, PP posterior part of internal duct system, SS slit sensillum. Scale bars: 0.5 mm.

Etymology. The specific name is taken from the type locality, Yanjin County; noun in apposition.

Distribution. Known only from the type locality (Fig. 10, China, Yunnan).

Sinopoda yanzi Wang & Li, sp. nov.

http://zoobank.org/4D942E8A-5EC2-4FE9-BB10-005EF4F8ADAB

Figures 7A–F, 8A, B, 9I, J, 10

Material examined. ***Holotype*** ♂ (IZCAS-Ar41615), China, Hunan Province, Huaihua City, Chenxi County, Huomachong Town, Yanzi Cave; 27.8545°N, 110.2605°E; 408 m; 6 Sept. 2019, Ziyi Wang & Zhigang Chen leg. ***Paratype*** 1 ♀ (IZCAS-Ar41627), same data as holotype, but 18 Mar. 2016; Yulong Li & Zhigang Chen leg. 1 ♀ (IZCAS-Ar41628), same data as holotype, 6 Sept. 2019; Ziyi Wang & Zhigang Chen leg.

Diagnosis. The male of this new species is similar to *Sinopoda tumefacta* Zhong, Jäger, Chen & Liu (Zhong et al. 2019: 69, figs 53A–E, 54A–F, 55A–D) in the shape of conductor, but it can be distinguished by the following: the dRTA is sharp, short, and triangular, while the dRTA is long and an irregular-quadrilateral in *S. tumefacta*; the vRTA is smooth in ventral view (Fig. 7A–D), while the vRTA is concave in ventral view in *S. tumefacta*. The female of this new species is similar to *S. dehiscens* Zhong, Jäger, Chen & Liu, 2019 (Zhong et al. 2019: 28, figs 20A, B, 21A–D) in having an analogous lobal septum and lateral lobes, but it can be separated by the following: the middle part of lateral lobes has a downward protrusion but there is no protrusion in *S. dehiscens*; the anterior part of the internal ducts is not fused with the median line, while in *S. dehiscens* the ducts are distinctly divided; the glandular appendages are wider than the posterior parts of the internal duct system in this new species, but the glandular appendages are as wide as the posterior parts of internal duct system in *S. dehiscens*; the posterior parts of internal duct system are swollen and slightly divided, while they are distinctly separated posterolaterally in *S. dehiscens*; this new species has fusion bubbles medially on the lobal septum, but *S. dehiscens* has no fusion bubble (Fig. 8A, B).

Description. Male (***holotype***, IZCAS-Ar41615) **Measurements:** PL 5.44, PW 4.87; AW 2.88; OL 6.08, OW 3.91. ***Eyes*:** AME 0.18, PME 0.26, ALE 0.3, PLE 0.32, AME-AME 0.24, AME-ALE 0.04, PME-PME 0.3, PME-PLE 0.34, AME-PME 0.4, ALE-PLE 0.28, CH AME 0.2, CH ALE 0.28. ***Palp*:** 8.12 (2.69, 1.02, 1.66, –, 2.75). ***Legs*:** I 25.11 (7.05, 1.92, 7.37, 6.66, 2.11); II 28.44 (8.14, 2.05, 8.07, 7.69, 2.49); III 22.42 (6.73, 1.98, 6.34, 5.32, 2.05); IV 24.01 (6.6, 1.79, 6.6, 6.85, 2.17). Leg formula: II-I-IV-III. **Spination:** ***palp*:** 131 101 – 3010. ***Legs*:** Fe 323, IV 123, Pa 101, Ti I and II 1318, III and IV 1216, Mt 1014, III 2024, IV 2026. ***Chelicerae*:** furrow with three anterior teeth, four posterior teeth, and six denticles.

***Palp*:** as in diagnosis. Cymbium almost twice as long as tibia. Embolus arising from tegulum in nearly the 5-o'clock-position. Embolic tip slightly longer than the embolic apophysis. Conductor arising from tegulum at the 1-o'clock-position, elongated flake with distal part flat. Tegulum covers medial part of embolus. Spermophor distinctly S-shaped. RTA arising from anterior part of tibia (Fig. 7B).

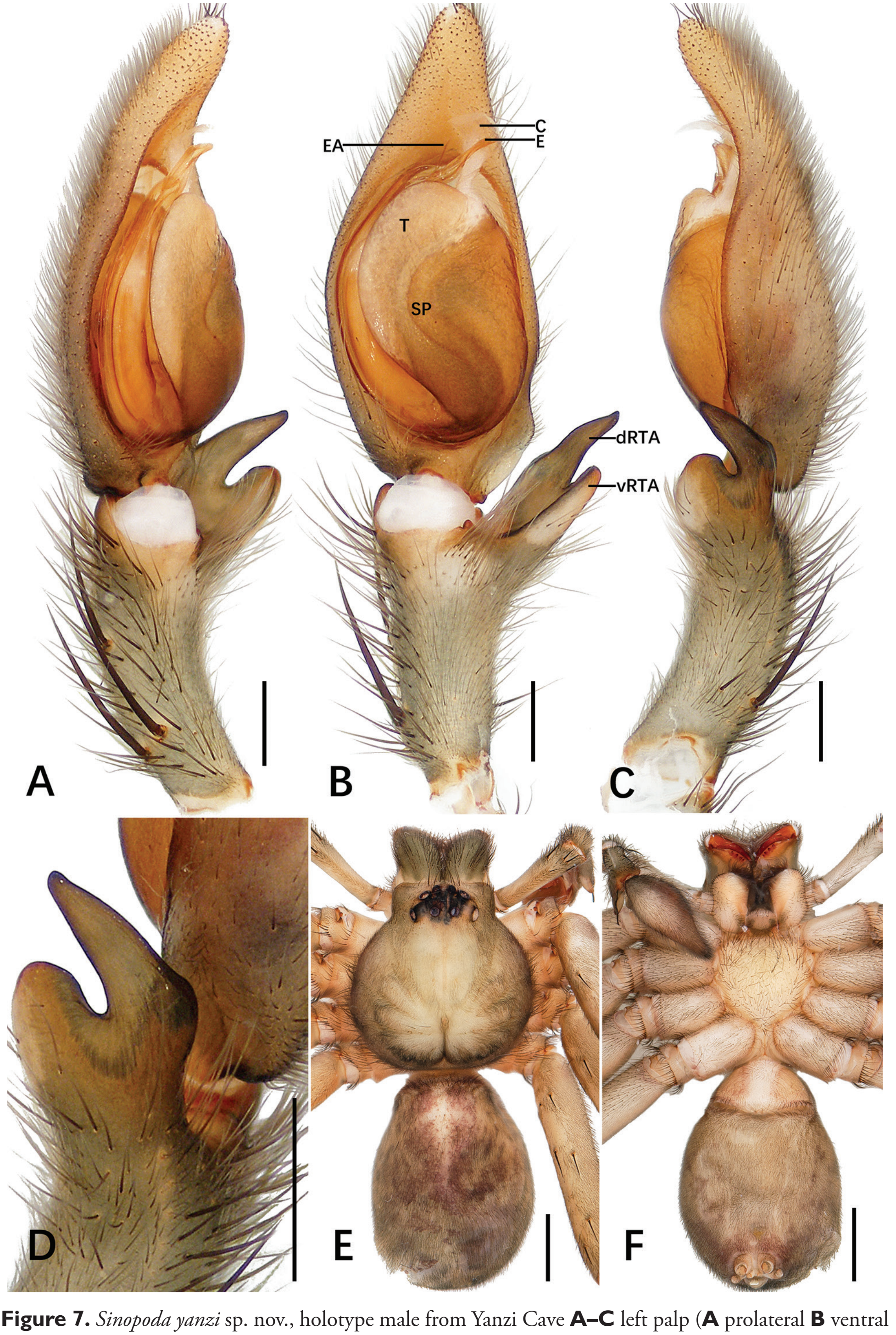

Figure 7. *Sinopoda yanzi* sp. nov., holotype male from Yanzi Cave **A–C** left palp (**A** prolateral **B** ventral **C** retrolateral) **D** retrolateral view of RTA **E, F** habitus (**E** dorsal **F** ventral). Abbreviations: C conductor, dRTA dorsal branch of retrolateral tibial apophysis, E embolus, EA embolic apophysis, SP spermophor, T tegulum, vRTA ventral branch of retrolateral tibial apophysis. Scale bars: 0.5 mm (**A–D**); 2 mm (**E, F**).

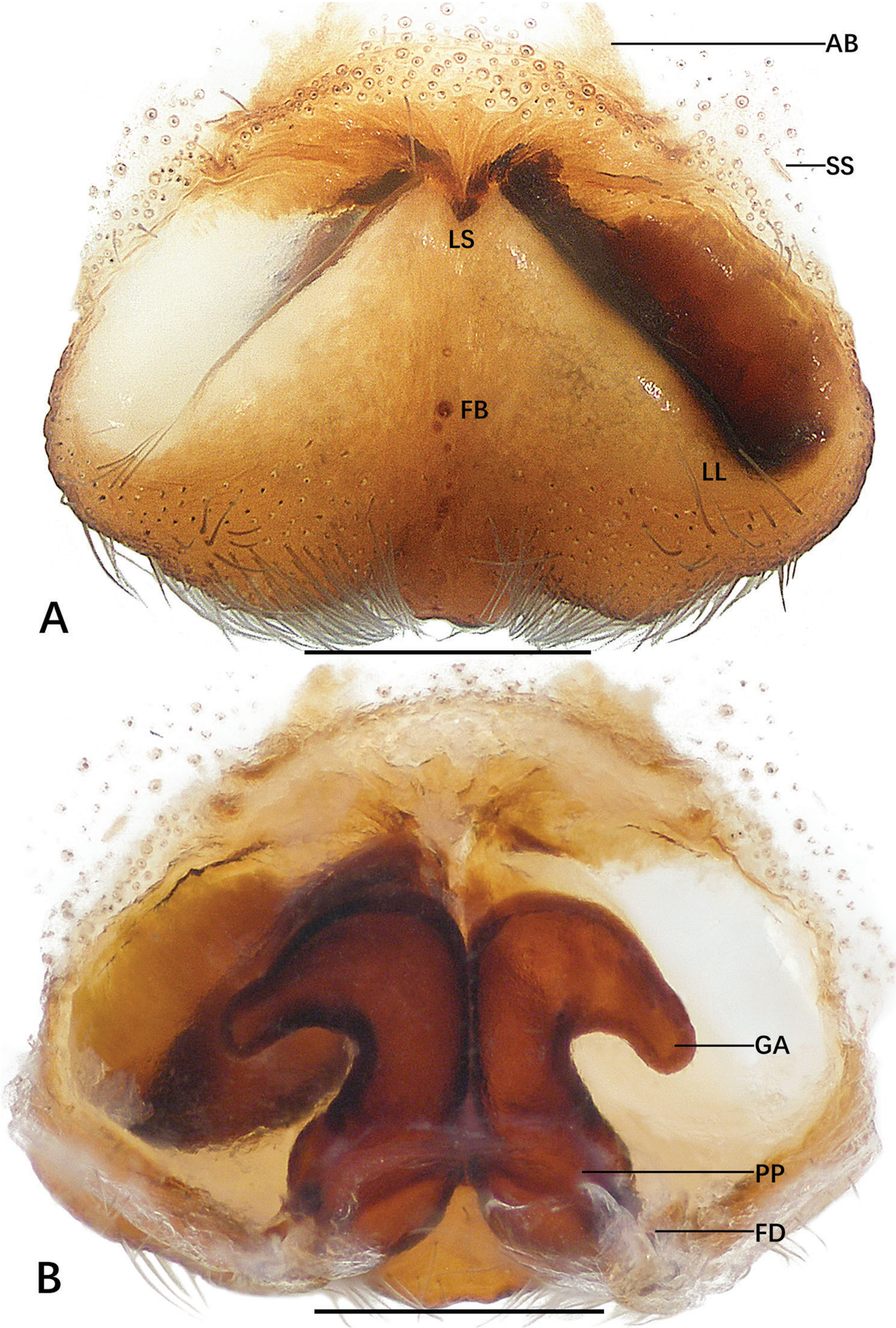

Figure 8. *Sinopoda yanzi* sp. nov., paratype female from Yanzi Cave **A** epigyne **B** vulva. Abbreviations: AB anterior bands, FB fusion bubble, FD fertilization duct, GA glandular appendages, LL lateral lobes, LS lobal septum, MS membranous sac, PP posterior part of internal duct system, SS slit sensillum. Scale bars: 0.5 mm.

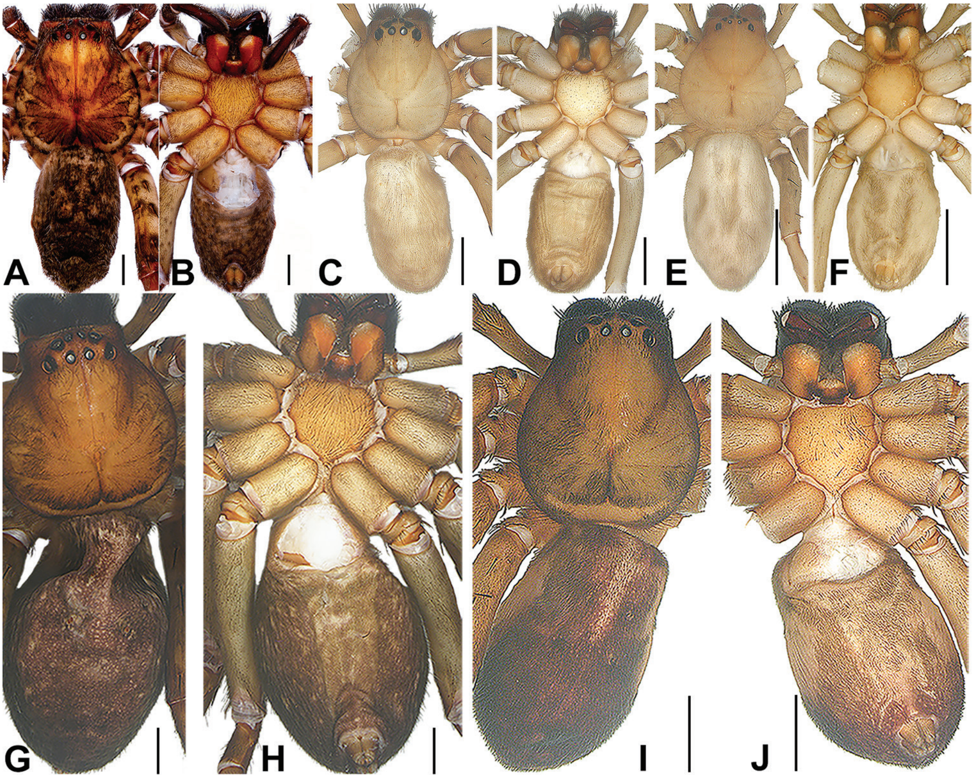

Figure 9. A, B *S. hongruii* sp. nov. female paratype **C, D** *S. jiangzhou* sp. nov. female paratype **E, F** *S. saiyok* sp. nov. female holotype **G, H** *S. yanjin* sp. nov. female holotype **I, J** *S. yanzi* sp. nov. female paratype. Scale bars: 2 mm.

Coloration in ethanol: yellowish brown. ***Prosoma*:** dorsally yellowish brown with distinct fovea and radial furrow, covered with dark hairs. Labium and sternum yellowish brown. Chelicerae deep reddish brown. ***Legs*:** yellowish brown. ***Opisthosoma*:** dorsally dark reddish brown, covered with dark hairs, with bright bands in anterior part; ventrally yellowish brown with bright band on both sides of central axis. Spinnerets yellowish brown (Fig. 7E, F).

Female (***paratype***, IZCAS-Ar41627) **Measurements:** PL 5.83, PW 5.32; AW 3.46; OL 7.05, OW 4.55. ***Eyes*:** AME 0.2, PME 0.22, ALE 0.3, PLE 0.32, AME-AME 0.22, AME-ALE 0.3, PME-PME 0.4, PME-PLE 0.48, AME-PME 0.32, ALE-PLE 0.1, CH AME 0.12, CH ALE 0.24. ***Palp*:** 8.62 (2.49, 1.02, 1.85, –, 3.26). ***Legs*:** I 21.25 (6.08, 2.56, 5.76, 4.93, 1.92); II 22.73 (6.73, 2.75, 6.21, 5.12, 1.92); III 20.16 (6.15, 2.43, 5.12, 4.8, 1.66); IV 21.65 (6.6, 2.24, 5.51, 5.25, 2.05). Leg formula: II-IV-I-III. **Spination: *palp*:** 131 101 213 3030. ***Legs*:** Fe I and II 323, III 333, IV 133, Pa 101, IV 000, Ti I and II 1018, III 2026, IV 2126, Mt 1014, IV 3034. ***Chelicerae*:** furrow with three anterior teeth, four posterior teeth, and 28 denticles.

***Copulatory organ*:** as in diagnosis. Epigynal field wider than long, with one short anterior band partly integrated with the field and one slit sensillum on each side close

Figure 10. Locality records for five new species of *Sinopoda*: **1** *S. hongruii* sp. nov. (Anhui, China) **2** *S. jiangzhou* sp. nov. (Guangxi, China) **3** *S. saiyok* sp. nov. (Kanchanaburi, Thailand) **4** *S. yanjin* sp. nov. (Yunnan, China) **5** *S. yanzi* sp. nov. (Hunan, China).

to the field. Lateral lobes fused, concave medially. Anterior and posterior part of internal ducts not fused along median line. Glandular appendages extending laterally in anterior half of internal duct system. Posterior part of internal duct system swollen, fertilization ducts arising posteriorly. Unexpanded membranous sac between fertilization ducts (Fig. 8A, B).

Coloration in ethanol: as in male, but dorsal prosoma yellowish brown, and posterior part with a bright band (Fig. 9I, J).

Etymology. The specific name refers to the type locality, Yanzi Cave; noun in apposition.

Distribution. Known only from the type locality (Fig. 10, China, Hunan).

Acknowledgements

The manuscript benefited greatly from comments by Ingi Agnarsson, Majid Moradmand, Yanfeng Tong, and Jie Liu. Sarah Crews checked the language. Zhigang Chen, Hongrui Zhao, Yunchun Li, Huifeng Zhao, Jincheng Liu, Yulong Li, Fengyuan Li, and Prasit Wongprom collected specimens. Theo Blick checked the etymology. This study was supported by the National Natural Science Foundation of China (NSFC-31530067).

References

Bertkau P (1872) Über die Respirationsorgane der Araneen. Archiv für Naturgeschichte 38: 208–233.

Folmer O, Black M, Hoeh W, Lutz R, Vrijenhoek R (1994) DNA primers for amplification of mitochondrial cytochrome oxidase subunit I from diverse metazoan invertebrates. Molecular Marine Biology and Biotechnology 3(5): 294–299.

Fu YN, Zhu MS (2008) A new species of the genus *Sinopoda* from China (Araneae, Sparassidae). Acta Arachnologica 57: 63–64. https://doi.org/10.2476/asjaa.57.63

Grall E, Jäger P (2020) Forty-seven new species of *Sinopoda* from Asia with a considerable extension of the distribution range to the south and description of a new species group (Sparassidae: Heteropodinae). Zootaxa 4797(1): 1–101. https://doi.org/10.11646/zootaxa.4797.1.1

Jäger P (1999) *Sinopoda*, a new genus of Heteropodinae (Araneae, Sparassidae) from Asia. Journal of Arachnology 27: 19–24.

Jäger P (2012) Revision of the genus *Sinopoda* Jäger, 1999 in Laos with discovery of the first eyeless huntsman spider species (Sparassidae: Heteropodinae). Zootaxa 3415: 37–57. https://doi.org/10.11646/zootaxa.3415.1.3

Li S (2020) Spider taxonomy for an advanced China. Zoological Systematics 45(2): 73–77. https://doi.org/10.11865/zs.202011

Liu J, Li S, Jäger P (2008) New cave-dwelling huntsman spider species of the genus *Sinopoda* (Araneae: Sparassidae) from southern China. Zootaxa 1857: 1–20. https://doi.org/10.11646/zootaxa.1857.1.1

WSC (2020) World Spider Catalog, version 21.5. Natural History Museum Bern. http://wsc.nmbe.ch [Accessed 29 March 2020]

Zhang BS, Zhang ZS, Zhang F (2015) Three new *Sinopoda* species (Araneae: Sparassidae) from southern China. Zootaxa 3974(1): 59–75. https://doi.org/10.11646/zootaxa.3974.1.4

Zhong Y, Cao XW, Liu J (2017) Six *Sinopoda* species (Araneae: Sparassidae) from Fujian and Yunnan Provinces in China. Zootaxa 4227(2): 151–172. https://doi.org/10.11646/zootaxa.4227.2.1

Zhong Y, Jäger P, Chen J, Liu J (2018) Taxonomic review of the *Sinopoda okinawana*-group (Araneae: Sparassidae) in China. Zootaxa 4388: 328–346. https://doi.org/10.11646/zootaxa.4388.3.2

Zhong Y, Jäger P, Chen J, Liu J (2019). Taxonomic study of *Sinopoda* spiders from China (Araneae: Sparassidae). Zootaxa 4607(1): 1–81. https://doi.org/10.11646/zootaxa.4607.1.1

ZooKeys 1012: 21–53 (2021)
doi: 10.3897/zookeys.1012.57047
https://zookeys.pensoft.net

RESEARCH ARTICLE

A peer-reviewed open-access journal
ZooKeys
Launched to accelerate biodiversity research

First records and three new species of the family Symphytognathidae (Arachnida, Araneae) from Thailand, and the circumscription of the genus *Crassignatha* Wunderlich, 1995

Francisco Andres Rivera-Quiroz[1,2], Booppa Petcharad[3], Jeremy A. Miller[1]

1 *Department of Terrestrial Zoology, Understanding Evolution group, Naturalis Biodiversity Center, Darwinweg 2, 2333CR Leiden, the Netherlands* **2** *Institute for Biology Leiden (IBL), Leiden University, Sylviusweg 72, 2333BE Leiden, the Netherlands* **3** *Faculty of Science and Technology, Thammasat University, Rangsit, Pathum Thani, 12121 Thailand*

Corresponding author: Francisco Andres Rivera-Quiroz (andres.riveraquiroz@naturalis.nl)

Academic editor: D. Dimitrov | Received 29 July 2020 | Accepted 30 September 2020 | Published 26 January 2021

http://zoobank.org/4B5ACAB0-5322-4893-BC53-B4A48F8DC20C

Citation: Rivera-Quiroz FA, Petcharad B, Miller JA (2021) First records and three new species of the family Symphytognathidae (Arachnida, Araneae) from Thailand, and the circumscription of the genus *Crassignatha* Wunderlich, 1995. ZooKeys 1012: 21–53. https://doi.org/10.3897/zookeys.1012.57047

Abstract

The family Symphytognathidae is reported from Thailand for the first time. Three new species: *Anapistula choojaiae* **sp. nov.**, *Crassignatha seeliam* **sp. nov.**, and *Crassignatha seedam* **sp. nov.** are described and illustrated. Distribution is expanded and additional morphological data are reported for *Patu shiluensis* Lin & Li, 2009. Specimens were collected in Thailand between July and August 2018. The newly described species were found in the north mountainous region of Chiang Mai, and *Patu shiluensis* was collected in the coastal region of Phuket. DNA sequences are provided for all the species here studied. The relations of these symphytognathid species were tested using previously published phylogenetic analyses on micro orb-weavers. Also, we used micro CT analysis to build 3D models of the male genitalia and somatic characters of two species of *Crassignatha* Wunderlich, 1995. The molecular phylogeny and 3D models were used to discuss the taxonomy and circumscription of the currently valid symphytognathid genera, with focus on *Crassignatha* and *Patu* Marples, 1951. Based on this, three new combinations are suggested: *Crassignatha bicorniventris* (Lin & Li, 2009), **comb. nov.**, *Crassignatha quadriventris* (Lin & Li, 2009), **comb. nov.**, and *Crassignatha spinathoraxi* (Lin & Li, 2009), **comb. nov.** A new record of *Crassignatha danaugirangensis* Miller et al. 2014 is reported from Brunei.

Keywords

3D reconstruction, *Anapistula*, Borneo, computed tomography, micro-CT, *Patu*, Sabah, Symphytognathoids

Introduction

The family Symphytognathidae includes some of the tiniest spiders known. According to a recent "Spider World Record" study (Mammola et al. 2017), this family holds the records for the smallest female, smallest male and smallest web. The Symphytognathidae has traditionally been put together with other small size araneoids (Anapidae, Mysmenidae, and Theridiosomatidae, sometimes with synaphrids and micropholcommatids) in a group informally called the symphytognathoids (Griswold et al. 1998; Hormiga and Griswold 2014). Although phylogenetic relationships among the Symphytognathidae have not been directly studied, some representatives have been used as part of other phylogenetic studies targeting the family Mysmenidae (Lopardo et al. 2011; Feng et al. 2019), as well as a broad scope analysis of the whole order Araneae (Wheeler et al. 2017; Kulkarni et al. 2020). Symphytognathids can be separated from other relatives by the following combination of characters: the loss of the posterior median eyes, reducing eye number to six (with the further loss of the anterior median eyes in the case of the four-eyed genus *Anapistula*), fusion of the chelicerae (but see below), extreme reduction or loss of female pedipalp, the labium being much wider than long, loss of the colulus, sternum broadly truncated posteriorly, the absence of book lungs, and the presence of one or two promarginal cheliceral teeth originating from a common base (Forster and Platnick 1977; Wunderlich 2004; Miller et al. 2009; Lopardo et al. 2011; Hormiga and Griswold 2014).

The family is widespread in the tropics and subtropical regions, with most species described from the southern hemisphere. At present 8 genera and 74 species are recorded worldwide. In Asia, six genera and 29 species have been recorded (WSC, 2020). From these, 19 species have been recorded from China (Tong and Li 2006; Lin and Li 2009; Miller et al. 2009; Lin et al. 2013; Lin 2019) and six from South East Asia (Indonesia, Malaysia and Vietnam) (Wunderlich 1995; Harvey 1998; Lin et al. 2009; Miller et al. 2014). Here, the family Symphytognathidae is formally reported from Thailand for the first time, although Lopardo et al. (2011) did include a Thai symphytognathid in their study, designated SYMP-004-THAI, which was later identified as *Crassignatha* (Lopardo, pers. comm.). We describe three new species of the genera *Anapistula* and *Crassignatha* and expand the known distribution of *Patu shiluensis.* We used a combination of newly generated sequences and sequences available in GenBank to build a molecular phylogeny of the Symphytognathidae, and related micro orb-weaver families, in order to test the familial placement of our new species. Additionally, we discuss the taxonomy of the Symphytognathidae with emphasis on the genera *Crassignatha* and *Patu*.

Materials and methods

Fieldwork

The symphytognathid specimens reported here were collected in Chiang Mai and Phuket, Thailand, between 16 July and 6 August 2018. All the specimens were captured using methods optimized for ground dwelling spiders: leaf litter sifting, Winkler extractors, pitfall traps and direct collecting on ground, and among sifted leaf litter.

Molecular data

To test the relationships and position of the novel species within the Symphytognathidae, we selected one specimen from each species we collected and used all four right legs to extracted genomic DNA and sequence six gene fragments: COI, H3, 12S, 16S, 18S, and 28S (primers in Suppl. material 1) following Miller et al. (2010) and Wheeler et al. (2017) protocols. Sequences were edited in Geneious Prime 2020.0.5 and deposited in GenBank; accession numbers are reported in Table 1. We used these sequences and a selection of taxa previously used to test the phylogeny of mysmenid spiders (Lopardo et al. 2011; Feng et al. 2019). In total, 47 species of "symphytognathoids" from the families Anapidae, Mysmenidae, Symphytognathidae and Theridiosomatidae were used. Two more species of Tetragnathidae were used as an outgroup to the symphytognathoids. We used MAFFT v.7.450 online (https://mafft.cbrc.jp/alignment/server/) with default parameters to align the sequences. Matrix was built using in Sequence Matrix v.1.8 (http://www.ggvaidya.com/taxondna/); matrix available in Suppl. material 1. Each locus was treated as a partition and examined with jModelTest2 (Darriba et al. 2012) in CIPRES (Miller et al. 2010) to get the best model fit for each; GTR+I+G was selected in all cases. Our datasets were analyzed using MEGA X (Kumar et al. 2018) for Maximum Parsimony (SPR, default values, bootstrap = 1000); RaXML (Stamatakis 2014) in CIPRES for Maximum Likelihood (GTR, bootstrap = 1000) and MrBayes v. 3.2.6 (Ronquist and Huelsenbeck 2003) in CIPRES for the Bayesian Inference (GTR+I+G, two independent runs with one cold and three heated chains, mcmc = 50,000,000 gen, samplefreq = 1000, burnin = 2500; partitions are indicated in the NEXUS file). The program Tracer v. 1.7.1 (Rambaut et al. 2018) was used to analyze the performance of our BI analyses.

Morphological data

Specimens were photographed with a Nikon DS-Ri2 camera attached to a Leica DM 2500 microscope. Specimens were observed in ethanol using semi-permanent

Table 1. GenBank accession numbers of DNA sequences generated for the present work.

Species	COI	H3	16s	12s	18s	28s
Anapistula choojaiae	MT712393	MT782018	–	MT711286	MT711238	MT711242
Crassignatha seedam	MT712396	MT782021	–	–	MT711241	–
Crassignatha seeliam	MT712394	MT782019	–	–	MT711239	–
Patu shiluensis	MT712395	MT782020	MT711285	–	MT711240	–

slide preparations (Coddington 1983). Female genitalia were dissected, digested using pancreatin solution (Alvarez-Padilla and Hormiga 2007), and cleared with methyl salicylate. For the 3D scans, whole male spiders were stained in 1% iodine in 70% et-OH for 24 hours. Specimens were fixed in a modified 10 ul pipette tip and scanned using a Zeiss X-radia 520 versa. 3D model and subsequent segmentation of the internal ducts of male pedipalps were done in Avizo 9.5.0. All the specimens have been deposited in the collection of the Naturalis Biodiversity Center, Leiden, the Netherlands. Additionally, two males of *Crassignatha danaugirangensis* Miller et al., 2014, recently collected in Brunei, were analyzed using micro-CT scanning. 3D reconstructions were used to clarify some anatomical details of this species and the genus *Crassignatha*, including the internal and external structure of the male pedipalp, cheliceral armature, and carapace texture.

Nomenclature of the genital structures was based on Harvey (1998) and Lin et al. (2013) for *Anapistula*, and Lin and Li (2009) and Miller et al. (2009) for *Crassignatha* and *Patu*. Abbreviations in text and figures: A – Epigynal atrium; AME – Anterior median eyes; BI – Bayesian Inference; C – Conductor; C1 – Conductor, anterior projection; C2 – conductor, posterior projection; Cd – Copulatory duct; Ch – Chelicera; ChT– cheliceral tooth; Co – Copulatory opening; Ct – cymbial tooth; Cy– Cymbium; E – Embolus; Em– Embolic membrane; EMD – Epigynal median duct; F – Femur; Fd – Fertilization duct; Lb – lateral branch of the EMD; LE – lateral eyes; Mcl – male leg II mating clasper; ML – Maximum Likelihood; MP – Maximum Parsimony; Pa – Patella; Pc – Paracymbium; PME – Posterior median eyes; S – Spermatheca; Sa – Secretory ampulla; Sc – Epigynal scape; Sd – Spermatic duct; T – Tibia.

Results

Phylogenetic analysis

Tree topologies inferred by the different phylogenetic analyses performed (Figs 1–3) show some consistencies in several groupings; however, low support values are common, especially in the MP and ML trees. There is an inconsistent and problematic placement of the Symphytognathidae in relation to the Anapidae. All tree analyses recovered Mysmenidae as monophyletic and a sister group of Anapidae + Symphytognathidae. Theridiosomatidae is recovered as monophyletic in the MP and ML analyses with medium to high support (Figs 1, 2); nevertheless, in the BI the position of this family is not resolved (Fig. 3). Similarly, the position of Micropholcommatinae, currently considered part of the Anapidae, is not clear, being found as paraphyletic in the MP, unresolved in the BI, and a poorly supported monophyletic clade in the ML analysis (Figs 1–3). The Anapidae is closely related to the Symphytognathidae in all our trees (with the notable exception of the two micropholcommatines in the ML and BI); however, it appears as a poorly supported monophyletic group in the ML

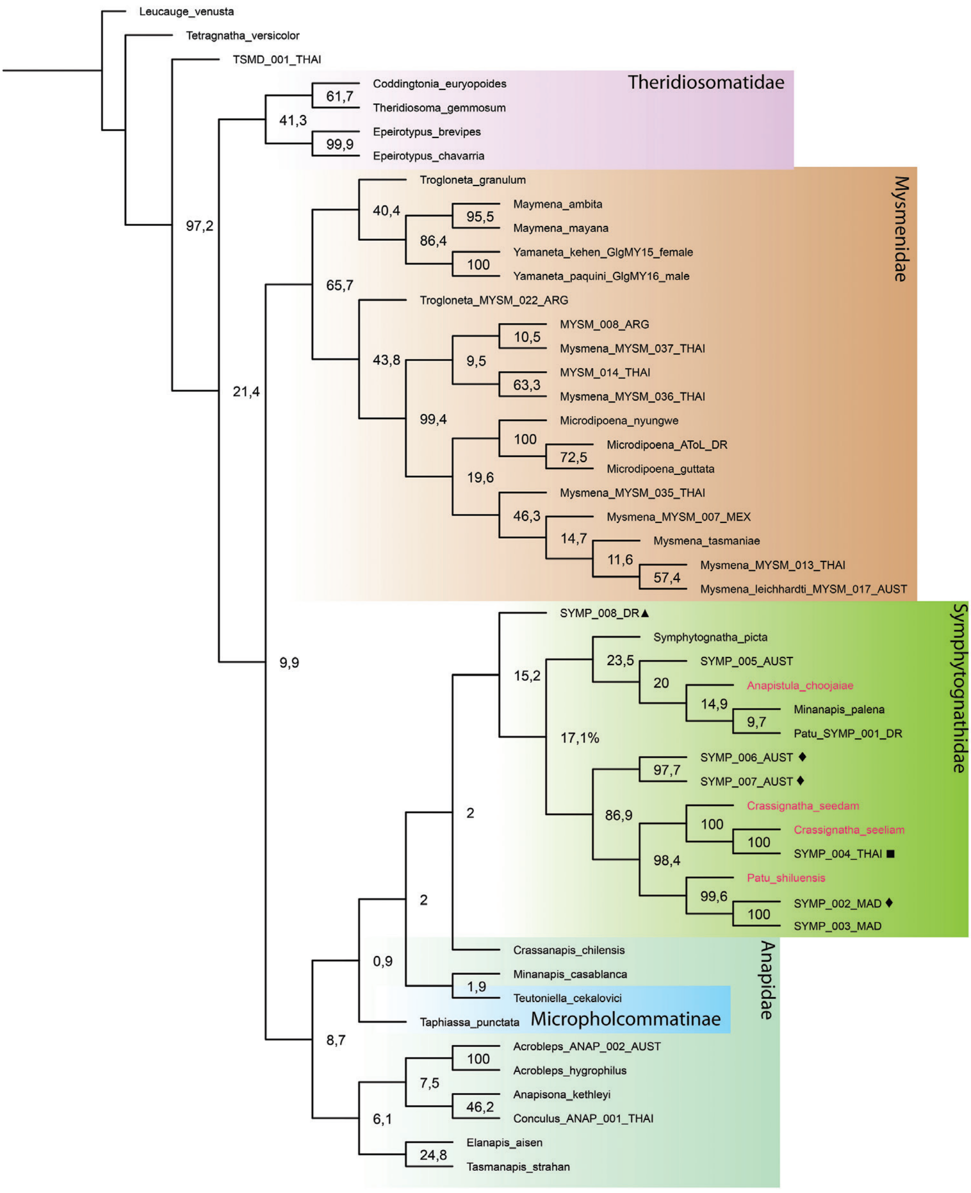

Figure 1. Tree topology obtained by Maximum Parsimony in MEGA-X using a modified version of Lopardo et al., (2011) and Feng et al., (2019) plus the four symphytognathid species from our study (in red). Numbers at nodes indicate bootstrap support. Note the paraphyly of Anapidae and the high support of *Crassignatha* and *Patu* in the Symphytognathidae. Molecular vouchers used for previous "symphytognathoid" studies (Lopardo et al. 2011; Lopardo and Hormiga 2015) identified to genus level by L. Lopardo (*pers. comm.*) as follows: ■ *Crassignatha* (apparently conspecific with *C. seeliam*); ◆ *Patu*; and ▲ *Symphytognatha*.

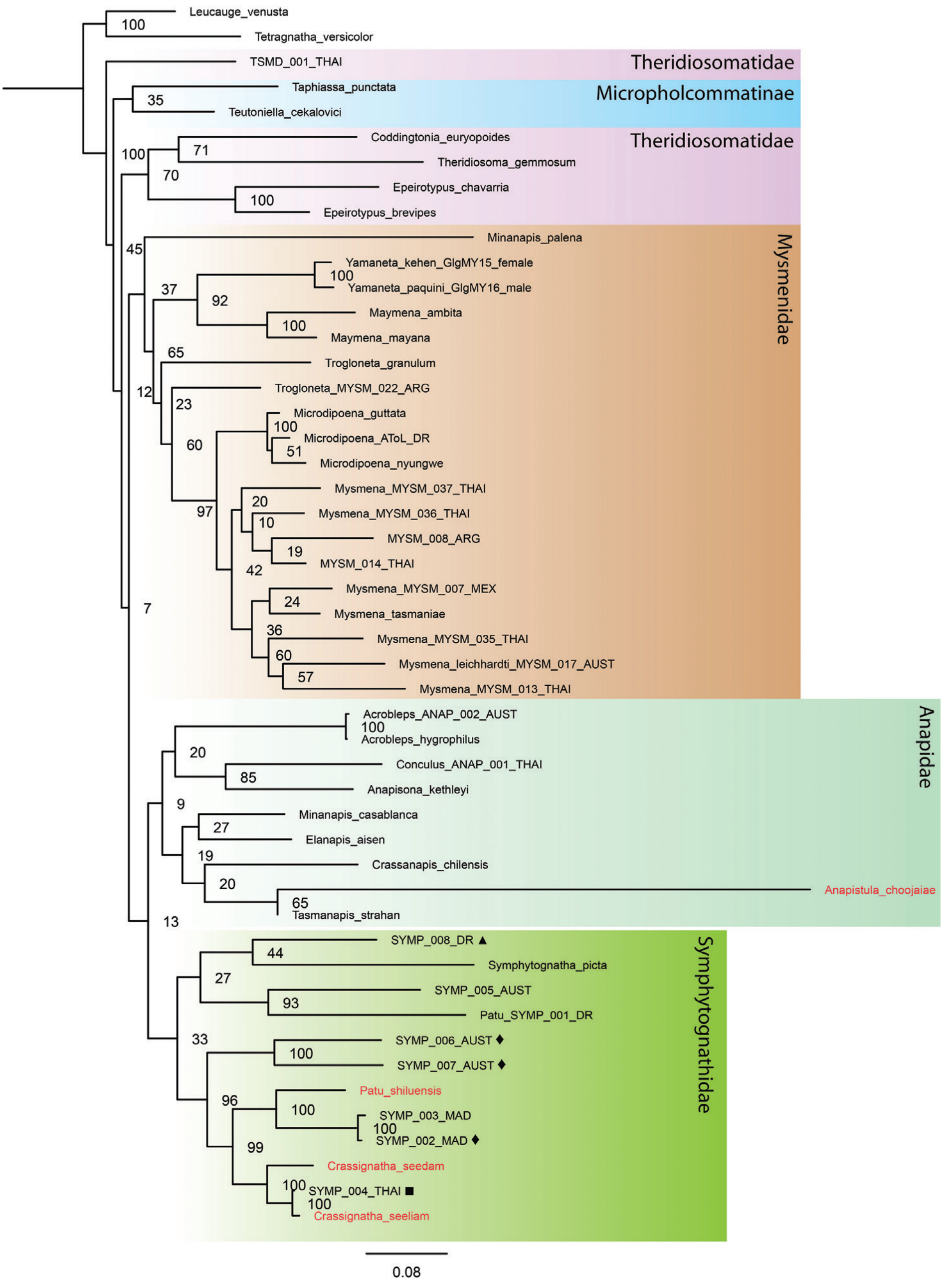

Figure 2. Tree topology obtained by Maximum Likelihood in RAxML using a modified version of Lopardo et al. (2011) and Feng et al. (2019) plus the four symphytognathid species from our study (in red). Numbers at nodes indicate bootstrap support. Note the long branch of *Anapistula* and its position within Anapidae; and the high support of *Crassignatha* and *Patu* in the Symphytognathidae. Molecular vouchers used for previous "symphytognathoid" studies (Lopardo et al. 2011; Lopardo and Hormiga 2015) identified to genus level by L. Lopardo (*pers. comm.*) as follows: ■ *Crassignatha* (apparently conspecific with *C. seeliam*); ◆ *Patu*; and ▲ *Symphytognatha*.

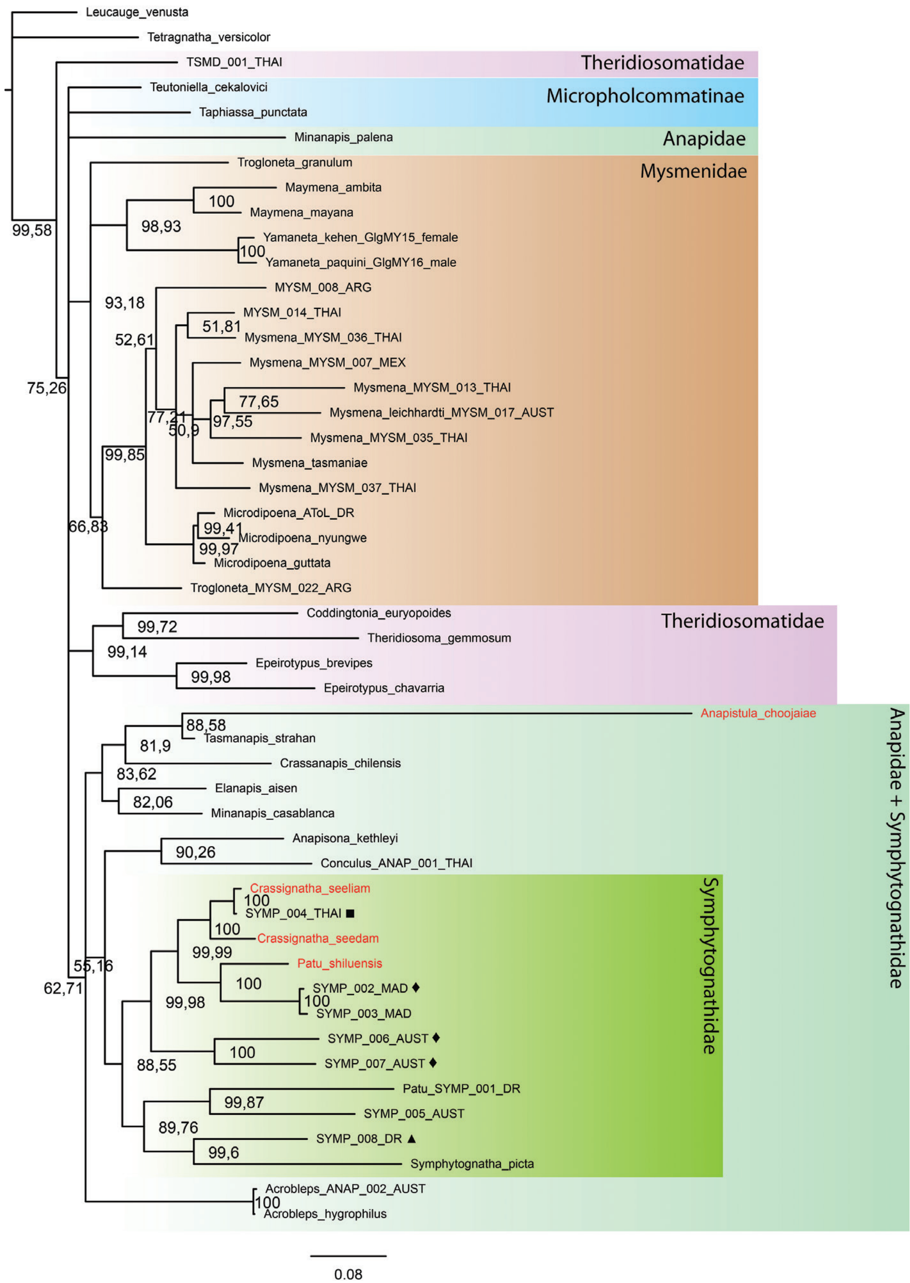

Figure 3. Tree topology obtained by Bayesian Inference in Mr. Bayes using a modified version of Lopardo et al. (2011) and Feng et al. (2019) plus the four symphytognathid species from our study (in red). Numbers at nodes indicate percent posterior probabilities. Note the unresolved relations of the Anapidae and the highly supported monophyly of Symphytognathidae. Molecular vouchers used for previous "symphytognathoid" studies (Lopardo et al. 2011; Lopardo and Hormiga 2015) identified to genus level by L. Lopardo (pers. comm.) as follows: ■ *Crassignatha* (apparently conspecific with *C. seeliam*); ◆ *Patu*; and ▲ *Symphytognatha*.

(Fig. 2), and paraphyletic in the MP and BI (Figs 1, 3). The Symphytognathidae appear monophyletic with moderate to high support in all the analyses (Figs 1, 2). In the BI analysis, this family is monophyletic and highly supported but found in an unresolved branch that includes the paraphyletic Anapidae (Fig. 3). The internal relations of the Symphytognathidae are similar in all our trees forming one clade that includes *Symphytognatha picta*, one species (SYMP_008_DR) identified as *Symphytognatha*, one as *Patu* (*Patu*_SYMP_001_DR), and one more (SYMP_005_AUST) that remained unidentified. The other clade recovers the rest of the *Patu* species + *Crassignatha*. Here, two terminals (SYMP_002_MAD and SYMP_003_MAD) are closer to *Patu shiluensis* and related to the three *Crassignatha* representatives; and two other (SYMP_006_AUS and SYMP_007_AUS) are consistently found outside of the *Crassignatha* + *Patu* clade. SYMP-004-THAI consistently clusters with *Crassignatha seeliam* sp. nov., and unpublished morphological observations (Lopardo, pers. comm.) are consistent with the possibility that these are conspecific.

Micro-CT and 3D modelling

The micro computed tomography scans allowed us to observe in detail small structures of the surface and internal ducts of the male genitalia (Fig. 4a–f). Structures like the cheliceral teeth (Fig. 5a), cephalothorax tubercles (Fig. 5b, c), and mating clasper on male tibia II (Fig. 5d, e) were also observed. We reconstructed 3D models of the whole body surface of *Crassignatha seeliam* (Fig. 6a, b) and *Crassignata danaugirangensis* (Fig. 6c, d). All of these images were important to examine, interpret and clarify the diagnostic characters of the genus *Crassignatha*. Additional views of the pedipalps, spermatic ducts and habitus can be found in the Suppl. material 2, 3)

Taxonomy

Family Symphytognathidae Hickman, 1931

Genus *Anapistula* Gertsch, 1941

Anapistula Gertsch, 1941: 2. Type species *Anapistula secreta* Gertsch, 1941.

Anapistula choojaiae **sp. nov.**
http://zoobank.org/916E1BC0-A72E-4B04-9C65-114FC0876E99
Figures 7–9

Material examined. ***Holotype*****:** Thailand • ♂; Chiang Mai, Pha Daeng National Park. Riparian tropical forest; 19°37.768'N, 98°57.257'E. 560 m; July 16–19, 2018; Booppa Petcharad, Jeremy Miller, F. Andres Rivera-Quiroz leg.; Winkler extractor; RMNH.ARA.18442. ***Paratypes*****:** Thailand • ♀ allotype; same data as holotype •

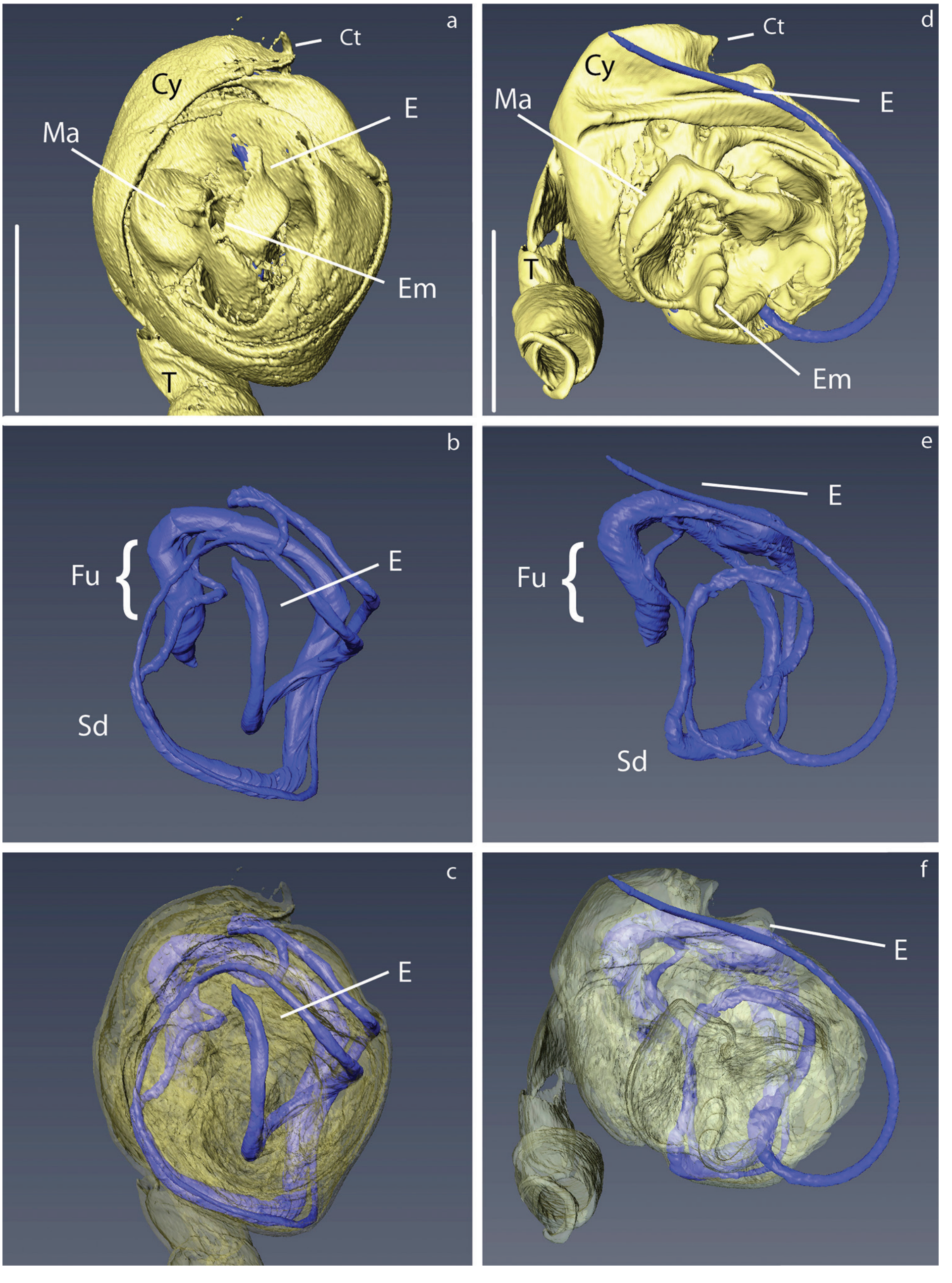

Figure 4. 3D reconstruction of the male palp of *Crassignatha* with detail in the spermatic ducts: **a–c** *C. seeliam* sp. nov. **d–f** *C. danaugirangensis*. Scale bars: 0.1 mm.

1♂ 1♀; same data as holotype; RMNH.5106639 • 2♀; Pha Daeng National Park. Bamboo forest; 19°37.668'N, 98°57.131'E. 573 m, same dates and collectors as holotype; RMNH.ARA.18443.

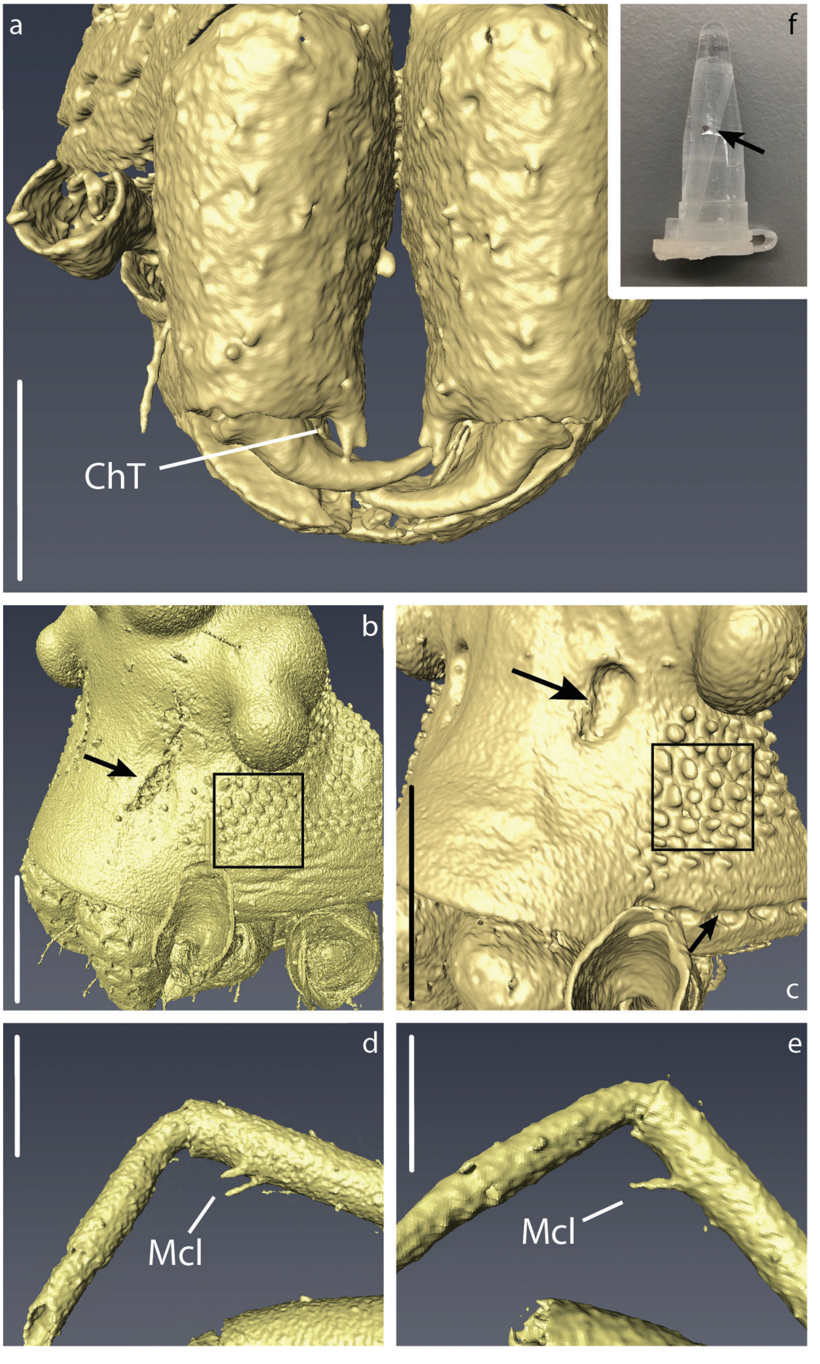

Figure 5. 3D reconstruction of some diagnostic characters of *Crassignatha* males: **a, c, e** *C. danaugirangensis* **b, d** *C. seeliam* sp. nov. **a** chelicerae, arrow pointing at the bifurcated tooth **b, c** detail of the carapace; cephalothorax tubercles (in the squares), and pore bearing sulcus (arrows) **d, e** male leg II clasper **f** whole male specimen of *C. danaugirangensis* prepared for micro-CT inside a modified 10 µl pipette tip and a 0.5 ml Eppendorf tube filled with 70% Et-OH. Scale bars: 0.06 mm (**a**); 0.1 mm (**b–e**).

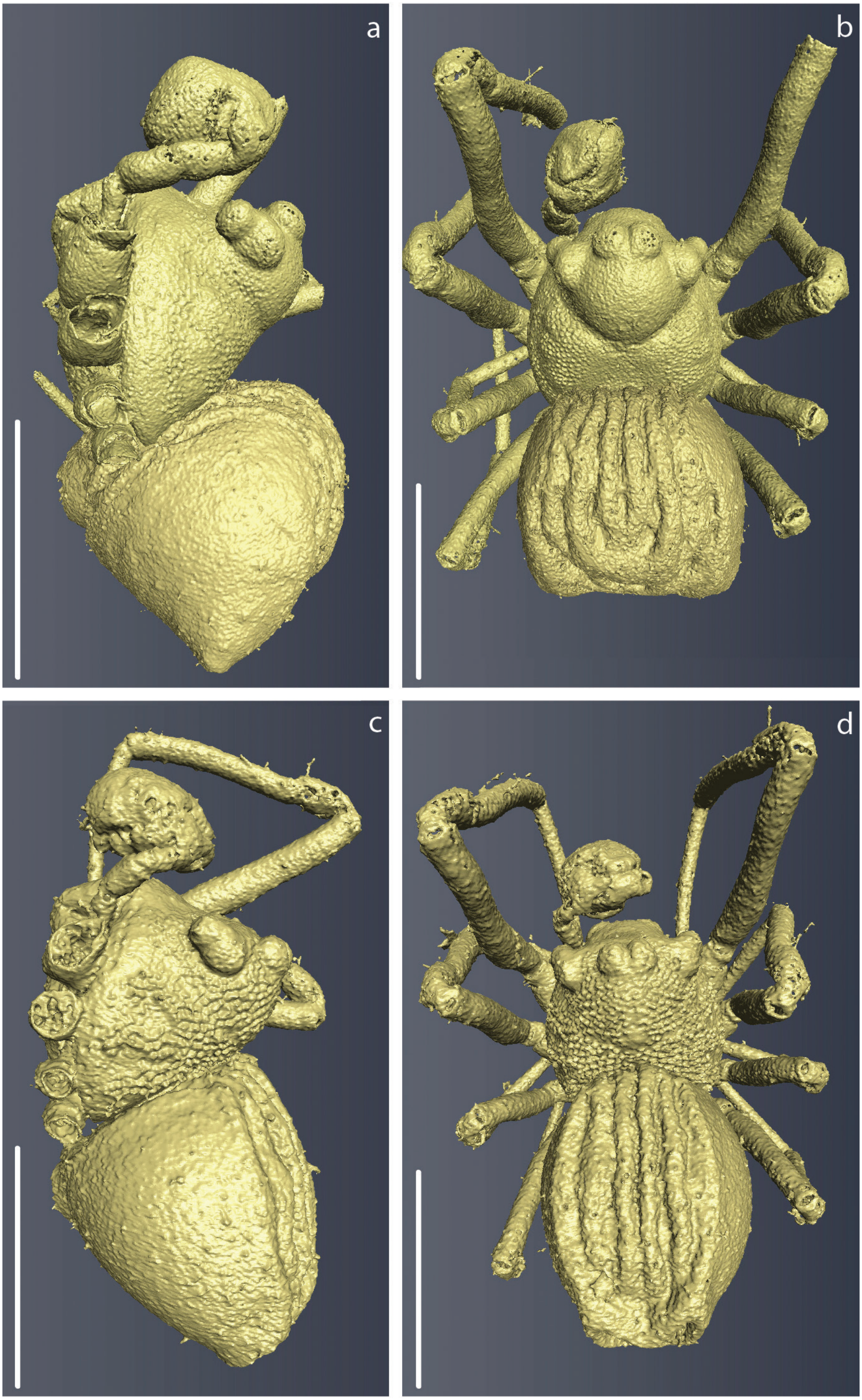

Figure 6. 3D reconstruction of the habitus of *Crassignatha* males: **a, b** *C. seeliam* sp. nov. **c, d** *C. danaugirangensis*. Right pedipalp was dissected previous to the scanning. Scale bars: 0.3 mm.

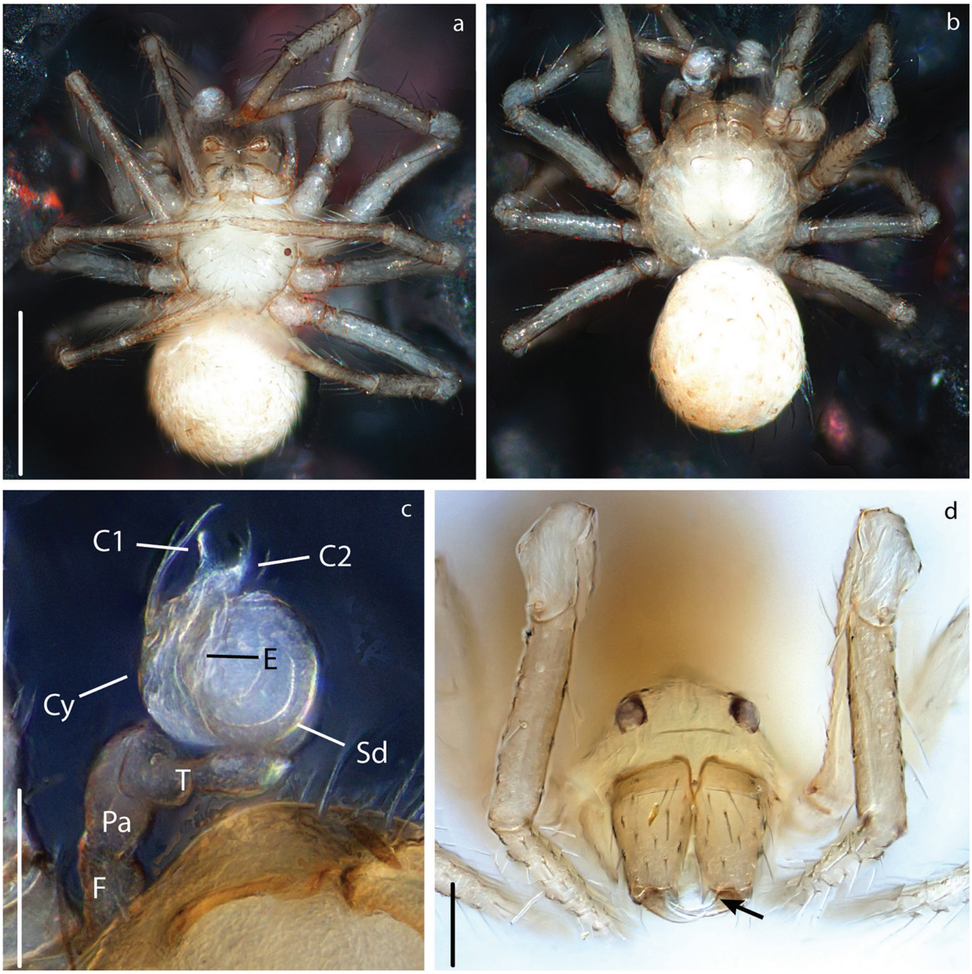

Figure 7. *Anapistula choojaiae* sp. nov. male: Habitus: **a** ventral view **b** dorsal view. Palp: **c** ventral view. Female: Prosoma: **d** anterior view. Scale bars: 0.2 mm (**a, b**); 0.07 mm (**c**); 0.06 mm (**d**). Arrow pointing to the cheliceral teeth.

Etymology. The species epithet is a Latinized matronym of the second authors' daughter.

Diagnosis. Female genitalia in *Anapistula* show little morphological variation between congeneric species making it generally difficult to tell species apart. However, *A. choojaiae* sp. nov. can be distinguished from most *Anapistula* species by the presence of an epigynal atrium; *A. aquytabuera* Rheims & Brescovit, 2003, *A. pocaruguara* and *A. ybyquyra* Rheims & Brescovit, 2003 from Brazil, *A. panensis* Lin, Tao, and Li 2013 and *A. zhengi* Lin, Tao, and Li 2013 from China, and *A. seychellensis* Saaristo, 1996 from the Seychelles also share this character. *A. choojaiae* differs from all of these by the relative size and shape of the atrium, the width of the EMD and the bifurcation of the Lb (compare Figs 8d and 9c to Rheims and Brescovit 2003: figs 16, 18, 21; Lin et al. 2013: figs 3, 4, 8, 9; and Saaristo 1996: fig. 3).

Figure 8. *Anapistula choojaiae* sp. nov. female: Habitus: **a** ventral view **b** dorsal view. Epigynum: **c** ventral view **d** dorsal view, cleared. Scale bars: 0.2 mm (**a, b**); 0.06 mm (**c**); 0.03 mm (**d**).

Male pedipalp of *A. choojaiae* similar to *A. panensis* in the overall shape of the palp and in having C1 and C2 roughly the same length, but differs on the width of C1 in respect to C2 and the length of the E in relation to C1 (compare Figs 7c, 9a to Lin et al. 2013: figs 1, 2).

Description. Carapace ovoid, yellowish-white with smooth texture (Figs 7a, b, 8a, b). AME absent (Fig. 7d). Male LE without pigmentation (Figs 7b, 8b). Chelicerae with two promarginal teeth (Fig. 7d). Legs same color as carapace with slightly darker color on distal segments. Abdomen sub-spherical with small sparse sclerotized patches, some bearing long setae (Figs 7b, 8b). Scuta absent in both sexes.

Male palp: Weakly sclerotized (Fig. 7c). Semicircular from ventral view (Figs 7c, 9a). With one wide sheet shaped conductor that presents two projections, here called C1 and C2 (Fig. 9a, b). Embolus short and transparent located posteriorly to C; very difficult to see (Figs 7c, 9a).

Vulva: Epigynal plate flat, without scape. Atrium semi-circular as wide as inner distance between S (Fig. 8c). Spermathecae spherical, heavily sclerotized in

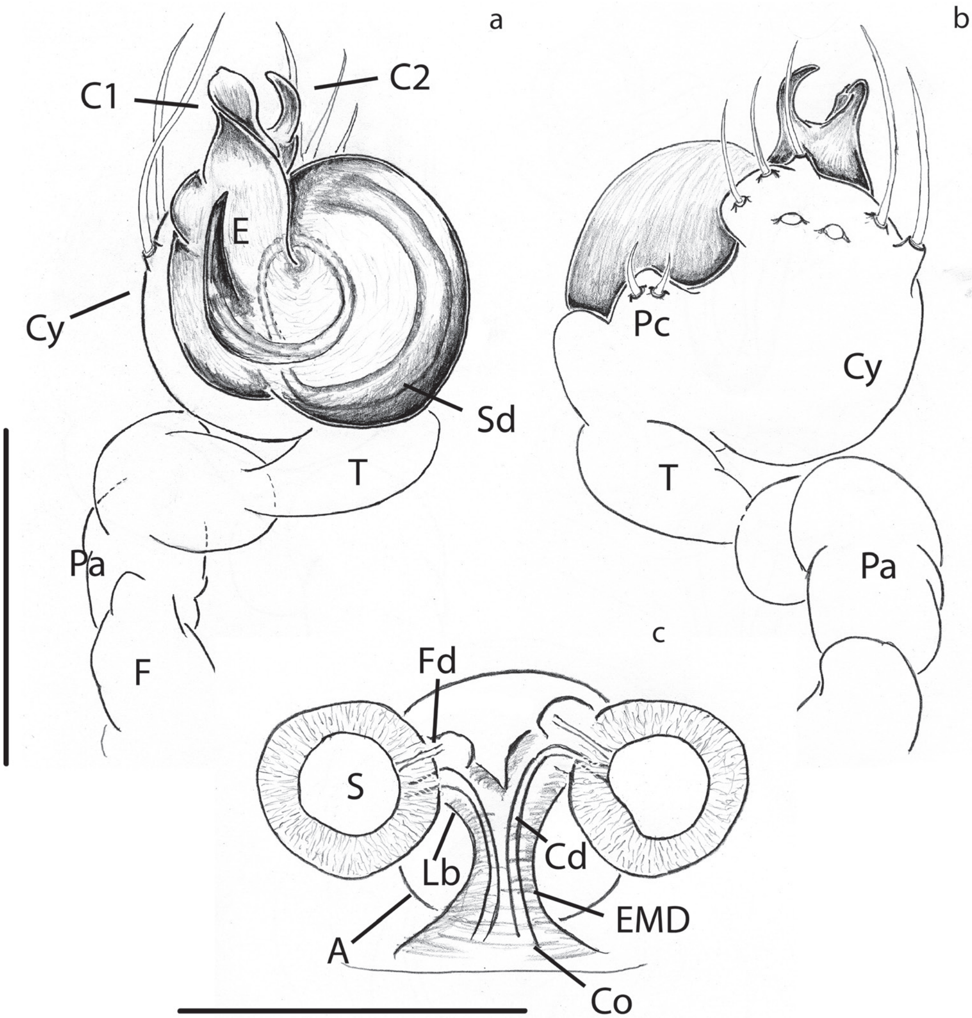

Figure 9. *Anapistula choojaiae* sp. nov., genitalia. Palp: **a** ventral view **b** dorsal view. Epigynum, cleared: **c** dorsal view. Scale bars: 0.07 mm (**a, b**); 0.06 mm (**c**).

relation to the rest of the body (Fig. 8d). Cd easy to distinguish inside the EMD. LB diverging from the EMD forming a "Y" (Figs 8d, 9c). Fertilization ducts very short and difficult to see, they appear as small bumps on the distal portion of Lb (Fig. 9c).

Male: Total length 0.4; carapace 0.2 long, 0.21 wide; clypeus 0.03; Chelicera 0.1 long, 0.06 wide; Leg I: femur 0.26, patella 0.1, tibia 0.17, metatarsus 0.09 tarsus 0.17; leg formula IV-I-II-III; abdomen 0.21 long, 0.21 wide.

Female: Total length 0.43, carapace 0.2 long, 0.21 wide; clypeus 0.3; Chelicera 0.1 long, 0.05 wide; Leg I: femur 0.20, patella 0.09, tibia 0.14, metatarsus 0.16, tarsus 0.1; leg formula IV-I-II-III; abdomen 0.24 long, 0.23 wide.

Genus *Crassignatha* Wunderlich, 1995

Crassignatha Wunderlich, 1995: 547. Type species *Crassignatha haeneli* Wunderlich, 1995.

Crassignatha seeliam sp. nov.

http://zoobank.org/DA61A955-A1D4-4B7D-A7A0-89AD024460A3
Figures 4a–c, 5b, d, 6a, b, 10–12

Material examined. ***Holotype*:** Thailand • ♂: Chiang Mai, Doi Inthanon National Park. Montane evergreen forest; 18°30.454'N, 98°30.584'E. 1605 m; July 21–24, 2018; Booppa Petcharad, Jeremy Miller, F. Andres Rivera-Quiroz leg.; direct hand coll.; RMNH.ARA.18444. ***Paratypes*:** Thailand • ♀ allotype; same data as holotype • 8 ♀; same data as holotype; RMNH.5106641• ♂ and ♀ Chiang Mai, Doi Suthep National Park. Montane evergreen forest with pine; 18°48.502'N, 98°53.528'E. 1409 m; July 24–28, 2018; same collectors as holotype; pitfall traps. RMNH.ARA.18445.

Etymology. The species epithet is a derivation of the Thai *seeliam* (square), in reference to the shape of the abdomen in dorsal view.

Diagnosis. Distinguished from other *Crassignatha* species except *Crassignatha quadriventris* (Lin & Li, 2009) by the semi-squared posterior of the abdomen in dorsal view (Figs 10b, 11b). Female can be separated from *C. quadriventris* by the coiling of the copulatory ducts in the epigynum (compare Figs 11d and 12c, d to Lin and Li 2009: fig. 10). Male differs on the size of tegular sclerites and the cymbial tooth being short and stout instead of hook-shaped (compare Figs 10c, d and 12a, b to Lin and Li 2009: fig. 8).

Description. Carapace coloration orange-brown covered by small tubercles (Figs 6a, b, 10a, b, 11a, b). Legs same color, slightly darker on distal portion its segments. Male Tibia II with two spines (mating claspers) (Fig. 5d). Abdomen black with light red patches; squared posteriorly, with sparse sclerotized patches, some bearing long setae (Figs 10b, 11b). Male with posterior scutum wrapping the abdomen. Male palp: slightly less sclerotized than carapace. Semicircular from ventral view (Figs 10c, 12a). Cymbium with distal tooth. Median apophysis as big as Ct (Fig. 12a). Embolus filiform, exposed when palp is expanded (Fig. 12c). Spermatic duct very long and coiling 2× inside the bulb (Fig. 4b, c).

Vulva: Epigynum with wide scape directed ventrally, heavily sclerotized at the tip (Fig. 11c). Copulatory opening at the tip of scape (Figs 11d, 12c, d). Spermathecae spherical, slightly more sclerotized than epigynum, separated by ca. 2× their diameter (Fig. 11d). Copulatory ducts very long, coiling over themselves before connecting to S. Fertilization ducts as long as S width, projecting dorsally (Figs 11d, 12c).

Male: Total length 0.68; carapace 0.36 long, 0.30 wide; clypeus 0.13; Chelicera 0.1 long, 0.07 wide; Leg I: femur 0.28, patella 0.12, tibia 0.37, metatarsus 0.17, tarsus 0.22; leg formula I-II-IV-III; abdomen 0.42 long, 0.38 wide.

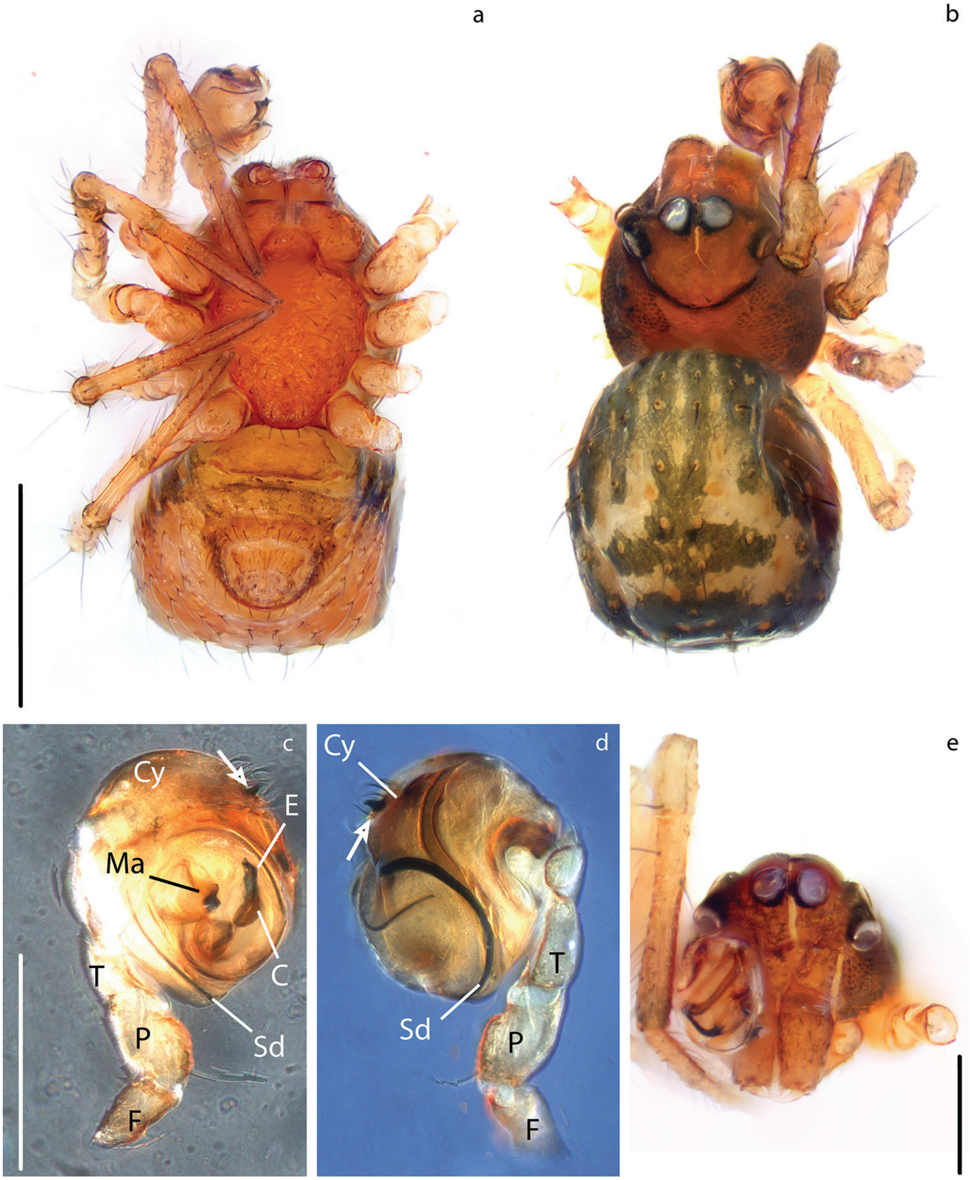

Figure 10. *Crassignatha seeliam* sp. nov., male: Habitus: **a** ventral view **b** dorsal view. Palp: **c** ventral view **d** retrolateral view. Prosoma: **e** anterior view. Scale bars: 0.3 mm (**a, b**); 0.15 mm (**c–e**). Arrow pointing at the cymbial tooth.

Female: Total length 0.69, carapace 0.44 long, 0.39 wide; clypeus 0.12; Chelicera 0.15 long, 0.1 wide; Leg I: femur 0.42, patella 0.15, tibia 0.53, metatarsus 0.22, tarsus 0.27; leg formula I-II-IV-III abdomen 0.44 long, 0.43 wide.

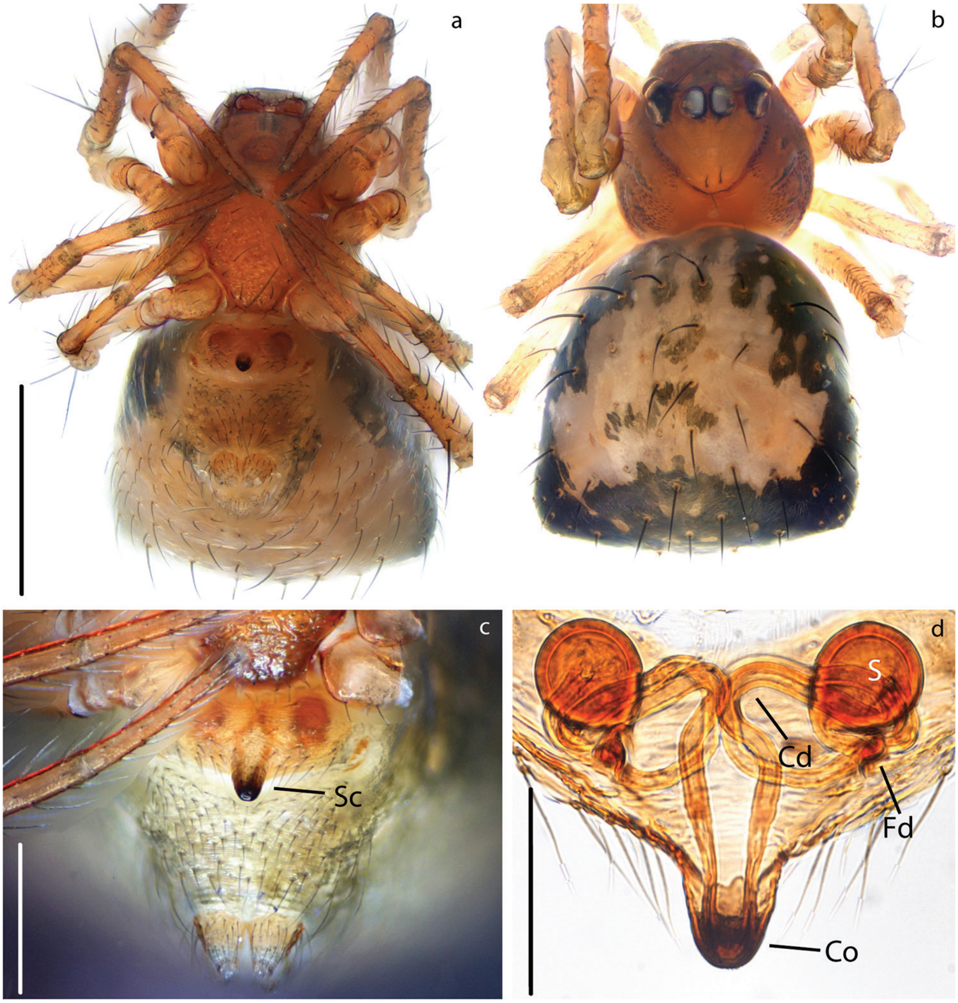

Figure 11. *Crassignatha seeliam* sp. nov. female: Habitus: **a** ventral view **b** dorsal view. Epigynum: **c** ventral view **d** dorsal view, cleared. Scale bars: 0.4 mm (**a, b**); 0.15 mm (**c**); 0.07 mm (**d**).

Crassignatha seedam sp. nov.

http://zoobank.org/0562D340-D322-49C4-A029-E95B47110BB5
Figures 13, 15b, d

Material examined. ***Holotype***: Thailand • ♀ Chiang Mai, Doi Suthep National Park. Montane evergreen forest with pine; 18°48.502'N, 98°53.528'E. 1409 m; July 24–28, 2018. Booppa Petcharad, Jeremy Miller, F. Andres Rivera-Quiroz leg.; direct hand coll.; RMNH.5106640. **Male** unknown.

Etymology. The species epithet is a derivation of the Thai *seedam* (black), in reference to the dark coloration of this species.

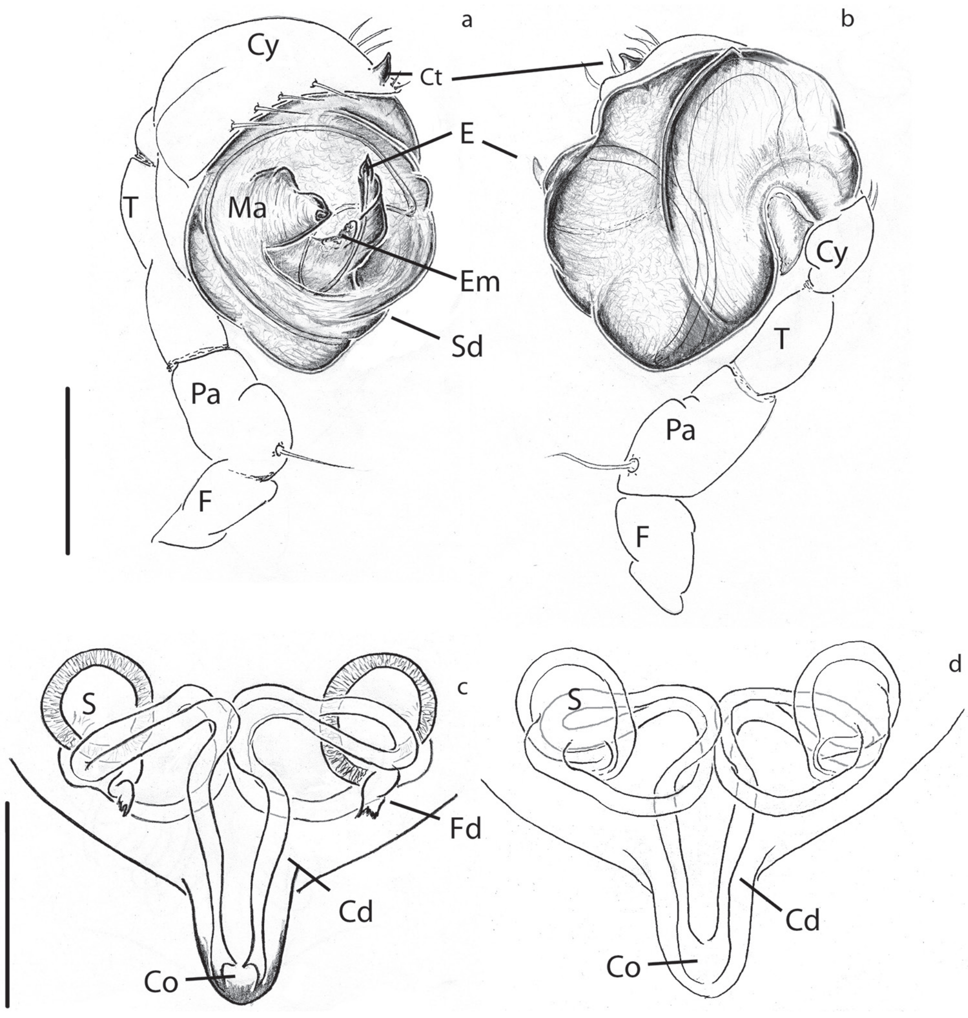

Figure 12. *Crassignatha seeliam* sp. nov., genitalia. Palp: **a** ventral view **b** dorsal view. Epigynum, cleared: **c** dorsal view **d** ventral view. Scale bars: 0.1 mm (**a, b**); 0.07 mm (**c, d**).

Diagnosis. *Crassignatha seedam* sp. nov. differs from other *Crassignatha* species by having a nearly round abdomen instead of triangular or squared, and having the epigynum bulging ventro-posteriorly but not forming an scape (compare Figs 13d and 15b, d to Fig. 12c; Lin and Li 2009: fig. 10; and Miller et al. 2009 fig. 76d, h).

Description. Carapace brown with smooth texture (Fig. 13b). Legs light brown, slightly darker on the distal portion its segments. Abdomen sub-spherical, darker than carapace with sparse light patches (Fig. 13a, b).

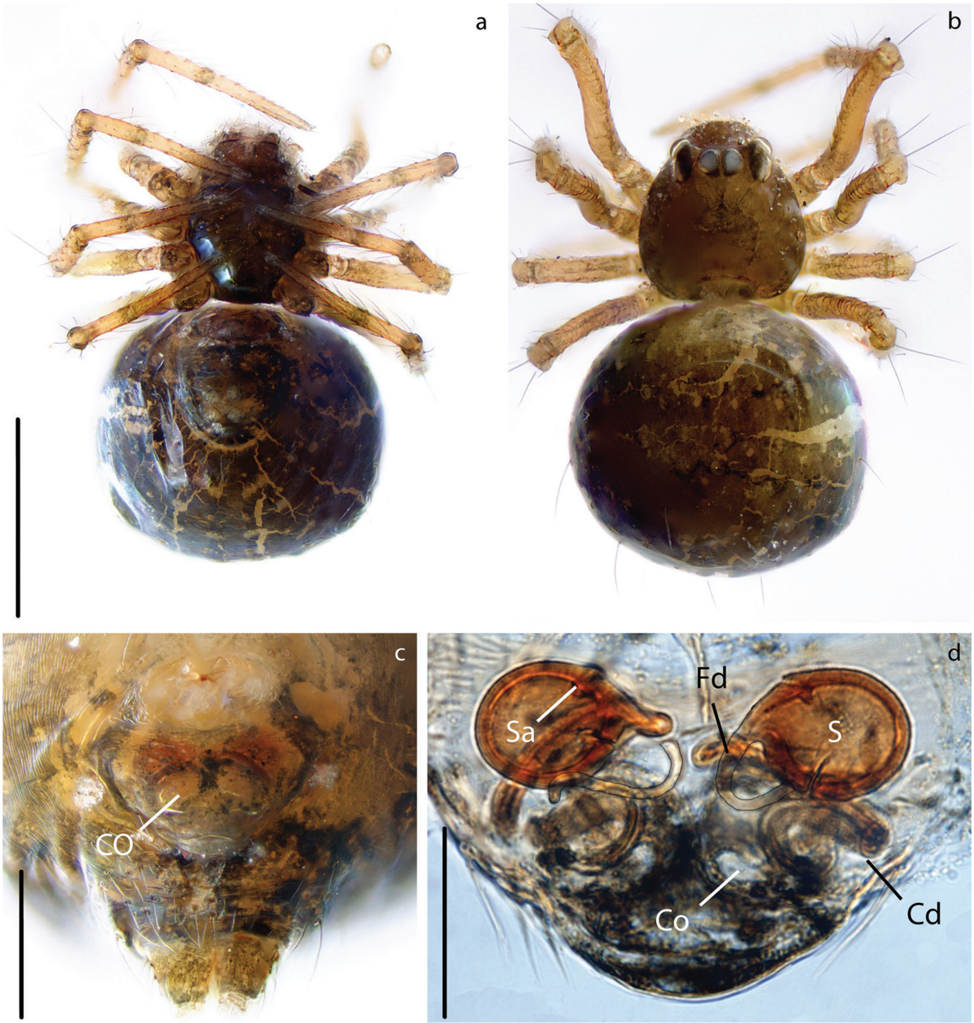

Figure 13. *Crassignatha seedam* sp. nov. female: Habitus: **a** ventral view **b** dorsal view. Epigynum: **c** ventral view **d** dorsal view, cleared. Scale bars: 0.3 mm (**a, b**); 0.1 mm (**c, d**); 0.05 mm (**d**).

Vulva: Epigynum weakly sclerotized but covered by small dark patches (Fig. 13d), bulging ventrally. Copulatory openings broad but not forming an atrium (Fig. 15b). Spermathecae spherical, much more sclerotized than epigynum, separated by 0.5× their diameter (Fig. 13d). Copulatory ducts long, coiling over themselves before connecting to S. Fertilization ducts as long as S width, connecting very close to Cd and projecting dorsally (Fig. 15b, d).

Female: Total length 0.56, carapace 0.28 long, 0.26 wide; clypeus 0.06; Chelicera 0.1 long, 0.07 wide; Leg I: femur 0.3, patella 0.1, tibia 0.22, metatarsus 0.13, tarsus 0.19; leg formula I-II-IV-III; abdomen 0.47 long, 0.41 wide.

***Crassignatha danaugirangensis* Miller et al., 2014**
Figures 4d–f, 5a, c, e, 6c, d

Crassignatha danaugirangensis Miller et al., 2014: 4, figs 1a–f, 3, 4.

New records. Brunei • 2♂; Temburong, Huala Belalong Field Studies Centre; 4.545°N, 115.157°E, 150 m; September 26 – October 6, 2018; Taxon Expeditions 2018 leg.; Winkler extractor; RMNH.5106643.

Genus *Patu* Marples, 1951

Patu Marples, 1951: 47. Type species *Patu vitiensis* Marples, 1951.

***Patu shiluensis* Lin & Li, 2009**
Figures 14, 15a, c

Patu shiluensis Lin & Li, 2009: 59, figs 11A, B, 12A, B, 13A–D.

Collected material. Thailand • 4♀; Phuket Province, Siray Island. Mixed tropical forest; 7°53.355'N, 98°26.083'E. 132 m; August 02–06, 2018; Booppa Petcharad, Jeremy Miller, F. Andres Rivera-Quiroz leg.; Winkler extractor; RMNH.5106642.

Distribution. Known only from its type locality, Shilu Town, Hainan Province, China and the specimens collected for the present work.

Morphological remarks. Carapace pale yellow with black margin, smooth texture (Fig. 14b). Legs black and semi-transparent. Abdomen oval, longer than wide (Fig. 14a, b). Ventrally same color as carapace, dorsally, darker with pale yellow patches.

Vulva: Epigynum weakly sclerotized, semi-transparent (Fig. 14c). Atrium semicircular slightly wider than inner distance between S (Figs 14c, 15c). Spermathecae spherical slightly more sclerotized than epigynum, separated by 0.5× their diameter (Fig. 14d). Copulatory ducts spring-like, spiraling 3× over themselves. Fertilization ducts as long as S width, projecting posteriorly (Figs 14d, 15a, c).

Female: Total length 0.52, carapace 0.21 long, 0.2 wide; clypeus 0.04; Chelicera 0.07 long, 0.05 wide; Leg I: femur 0.15, patella 0.07, tibia 0.1, metatarsus 0.07, tarsus 0.1; leg formula I-II-IV-III; abdomen 0.34 long, 0.28 wide.

Notes. Small somatic variations can be seen between the specimen we collected in Thailand and the ones previously described from China (compare Fig. 14b to Lin and Li 2009: fig. 11). However, we did not find any objective differences in the female genitalia.

Secretory ampullae (Figs 14d, 15a) were very evident in our specimens; these glandular structures might be homologous to the accessory glands in Lopardo and Hormiga (2015). These structures were found in one anapid (*Tasmanaspis*) and several mysmenids, but scored as absent or unknown for all the symphytognathids.

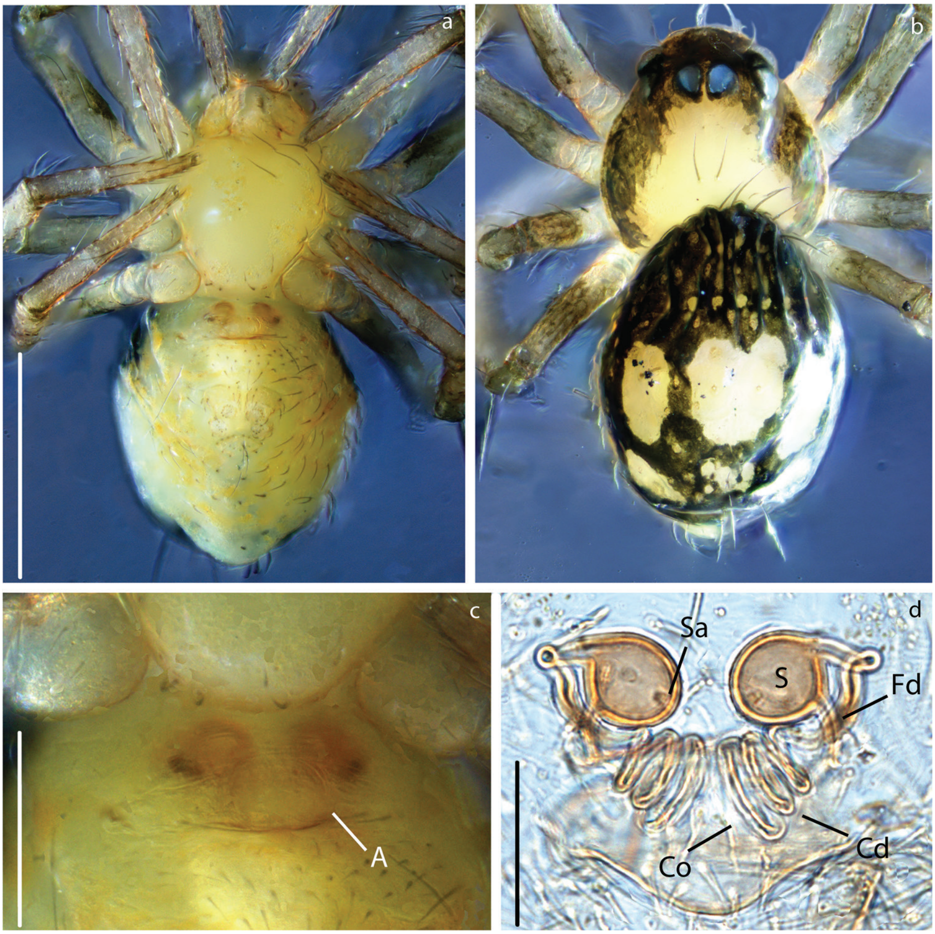

Figure 14. *Patu shiluensis* Lin & Li, 2009 female: Habitus: **a** ventral view **b** dorsal view. Epigynum: **c** ventral view **d** dorsal view, cleared. Scale bars: 0.2 mm (**a, b**); 0.06 mm (**c**); 0.03 mm (**d**).

The authors of this species mentioned it to be close to *Patu silho* Saaristo, 1996 from Seychelles. The possibility of *P. silho* not being a true *Patu* was discussed by its author (Saaristo 1996; 2010) mentioning evident differences on somatic and sexual characters between *P. silho* and other *Patu* species. Nevertheless, the author deemed appropriate to place it in this genus. We also consider this species might be misplaced in *Patu* but would need further and more detailed analysis out of the scope of this work to clarify it (see discussion on *Patu* relationships below).

Discussion

The monophyly of the Symphytognathidae and its relations to other symphytognathoid spiders have resulted in complications and inconsistencies across different

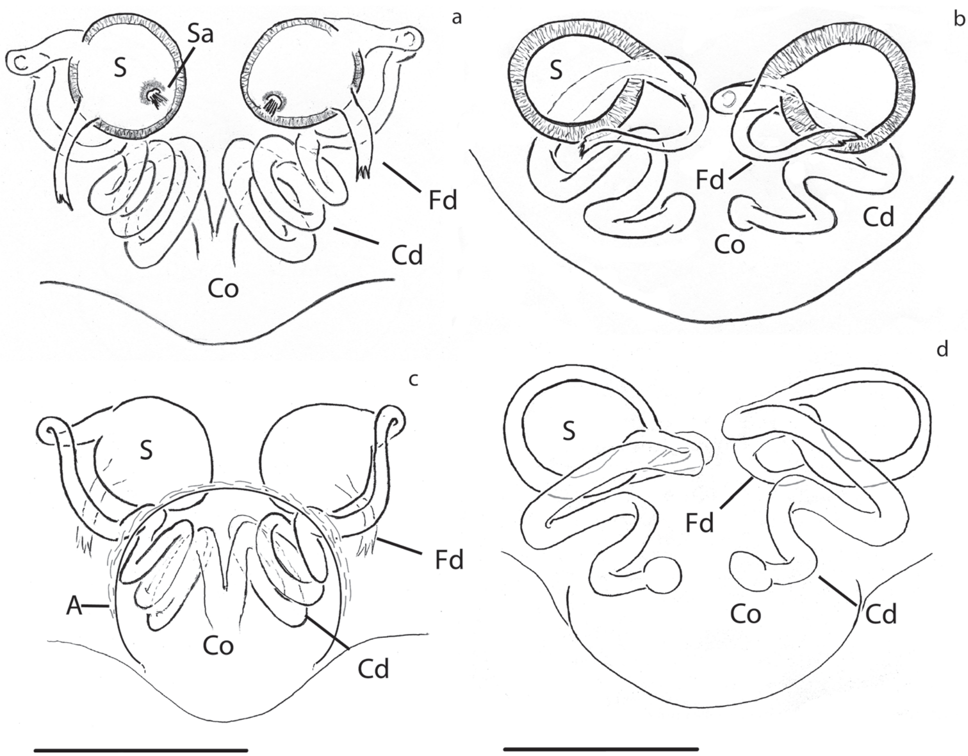

Figure 15. a, c *Patu shiluensis* Lin & Li, 2009 **b, d** *Crassignatha seedam* sp. nov. Epigynum, cleared: **a, b** dorsal view **c, d** ventral view. Scale bars: 0.03 mm (**a, c**); 0.05 mm (**b, d**).

studies. The symphytognathoids were first recognized in a morphological study being formed by four putatively monophyletic families Anapidae, Symphytognathidae, Mysmenidae and Theridiosomatidae (Griswold et al. 1998). The monophyly of this clade has been tested several times using different molecular approaches targeting specific families (Rix et al. 2008; Lopardo et al. 2011; Feng et al. 2019), the Orbiculariae (Fernández et al. 2014), and the whole order Araneae (Wheeler et al. 2017; Kulkarni et al. 2020). However, only a few representatives of the family Symphytognathidae have been used rendering their position and relations largely unexplored. Here, we built on two previous studies that used nine species of Symphytognathidae to test the relations of the Mysmenidae (Feng et al. 2019; Lopardo et al. 2011). Similarly to Feng et al. (2019) low node supports were common in our trees, especially for MP and ML; still, the topologies we observed when including our four species are consistent with the results from these studies. All of our analyses showed a close relationship between the Symphytognathidae and the Anapidae (Figs 1–3). This relationship has also been recovered in previous works (Griswold et al. 1998; Lopardo et al. 2011; Wheeler et al. 2017; Feng et al. 2019). Although tenuous due to the few terminals included, our study fails to recover the monophyly of the Anapidae and the position of micropholcommatids within this family. Our BI tree could not fully resolve the relations between the Anapidae and Symphytognathidae; similar issues have been observed before for the symphytognathoids (Rix et al. 2008; Lopardo et al. 2011; Dimitrov et al. 2012; Fernández et al. 2014; Feng et al. 2019). This has been explained by either the limited set of loci and the relatively low taxon sampling (Feng et al. 2019) or an indication of the polyphyly of the "symphytognathoids" as suggested by three broad scoped phylogenies (Dimitrov et al. 2012; Fernández et al. 2014; Wheeler et al. 2017). Nevertheless, Symphytognathoids were found to be a highly supported monophyletic group in a recent study that used ultraconserved elements (UCE) from 16 species across the four principal symphytognathoid families (Kulkarni et al. 2020)

The internal relations of the Symphytognathidae in our analyses are still unresolved. Most of Lopardo's identifications (pers. comm.) are found in the *Crassignatha* + *Patu* clade. From these, SYMP_004_THAI (identified to *Crassignatha*; presumably conspecific to *C. seeliam*), and SYMP_002_MAD and SYMP_003_MAD (*Patu*) group together with the other representatives of the genera they were identified to. But the placing of two more, SYMP_006_AUS and SYMP_007_AUS (*Patu*), is more ambiguous being found outside of the *Crassignatha* + *Patu* clade rendering *Patu* paraphyletic. This clade and its internal relations are highly supported in all our trees (Figs 1–3). Other two sequences, SYMP_008_DR (*Symphytognatha*) and Patu_SYMP_001_DR, are consistently grouped in another branch of the Symphytognathidae together with *Symphytognatha picta* and other unidentified symphytognathid (Figs 1–3) suggesting that Patu_SYMP_001_DR might be misidentified. The position of *Anapistula* within the Symphytognathidae is also problematic. *Anapistula choojaiae* has a very long branch that is recovered as a sister to *Tasmanapis strahan* Platnick & Forster, 1989 with moderate to high support in the ML and BI (Figs 2, 3). In these two analyses, this branch is related to other Anapidae having much higher support values in the BI than the ML (Figs 2, 3). Nevertheless, the recent UCE study by Kulkarni et al., (2020) places this genus next to *Patu* in a highly supported but taxonomically limited Symphytognathidae. Solving the internal relations of the families Anapidae and Symphytognathidae, and clarifying their delimitations would need a much more detailed examination with a broader taxonomic sample.

The minute size of the symphytognathid spiders complicates the observation of diagnostic traits. Examination and interpretation of many characters require higher magnifications than those a dissection microscope can give. Therefore, SEM images have been previously used in the taxonomy of this family (Forster and Platnick 1977; Rheims and Brescovit 2003; Miller et al. 2009, among others). Unfortunately, the process for getting SEM images is destructive; therefore, rare specimens or short series are not usually prepared in this way and some characters cannot be properly observed. Here we used micro-CT scanning to overcome this issue and get clear views of important characters without damaging the specimens. 3D reconstruction has been used before to elucidate surfaces and internal structures of spider genitalia (Lipke et al. 2015; Sentenská et al. 2017; Dederichs et al. 2019). Nevertheless, ours are, to the best of our knowledge, the smallest palps that have been processed using this method. This was challenging in itself since we wanted to preserve the samples without critical point drying, a method commonly used in micro-CT scanning (Sentenská et al. 2017; Keklikoglou et al. 2019; Steinhoff et al. 2017, 2020). The tiny size of the palps, less than 0.2 mm wide, did not allow to properly fix the dissected organ and keep it from moving during the scanning process. We attempted to fix the palp in agarose gel inside a 10 μl pipette tip, but the contrast of the resulting scans was too low to allow any observations. This problem was solved by scanning the entire spider (without dissecting the palp) in Et-OH 70% inside a modified 10 μL pipette tip that was in turn inside a 0.5 ml Eppendorf tube (Fig. 5f) in a similar fashion to Lipke et al. (2015), and Sombke et al. (2015). With this approach we were able to reconstruct the long and complicated internal ducts of the male genitalia (Fig. 4b, c, e, f), as well as the surface of the external somatic and genital morphology (Figs 4a, b, 5a–e, 6a–d; Suppl. material 2, 3). Other internal structures of the male palp, probably glands, could be observed but would require more detailed examination out of the scope of the present work to accurately determine their nature; therefore, they are not shown in our 3D models. Images obtained through 3D reconstruction were used to interpret and discuss the diagnostic characters of the genus *Crassignatha* and compare them to other Symphytognathid genera in Table 2.

Forster and Platnick (1977) reviewed the Symphytognathidae and its component genera. Five of the eight currently recognized symphytognathid genera were included: *Anapistula* Gertsch, 1941, *Curimagua* Forster & Platnick, 1977, *Globignatha* Balogh & Loksa, 1968, *Patu* Marples, 1951, and *Symphytognatha* Hickman, 1931. *Crassignatha* Wunderlich, 1995 was described based on a single male specimen from peninsular Malaysia. This genus has been associated with several families (Synaphridae, Anapidae, Mysmenidae, Symphytognathidae; Marusik and Lehtinen 2003; Wunderlich 2004; Miller et al. 2009; Lopardo and Hormiga 2015) and is currently considered a symphytognathid. Two other genera currently cataloged as Symphytognathidae, *Iardinis* Simon, 1899 *Anapogonia* Simon, 1905, are unrecognizable (Levi and Levi 1962; Forster and Platnick 1977; Platnick and Forster 1989; Lopardo and Hormiga 2015). Although spider taxonomy generally relies heavily on genitalia, little in the way of descriptive text or helpful depictions of genitalic characters was offered in Forster and Platnick's (1977) revision. Table 2 summarizes some important diagnostic characters of the currently accepted symphytognathid genera in an attempt to clarify the taxonomic inconsistencies in this family.

Other than their small size, the characteristic that is perhaps most strongly associated with the Symphytognathidae was the fusion of the chelicerae (Forster and Platnick 1977). But the degree of fusion is variable across the family and is particularly problematic in the genus *Patu*. The two species originally placed in *Patu* were reported as having the chelicerae fused for approximately half their length, but the degree of fusion was apparently less extensive in the genotype *Patu vitiensis* than in *Patu samoensis*, the other species described (Marples 1951). Subsequent authors have generally characterized *Patu* as having the chelicerae fused only at the base (Forster and Platnick 1977). Curiously, Forster (1959) made no mention of cheliceral fusion in *Patu*, but he did report basal fusion of the chelicerae in two genera (*Pseudanapis* and *Textricella*) that were subsequently transferred to Anapidae. So, assessing the presence or absence of basal cheliceral fusion is not always straight forward in practice. Some (but not all)

Table 2. Overview of diagnostic characters of the currently accepted genera of the Symphytognathidae.

	Anapistula Gertsch, 1941	*Anapogonia* Simon, 1905	*Crassignatha* Wunderlich, 1995	*Curimagua* Forster & Platnick, 1977	*Globignatha* Balogh & Loksa, 1968	*Iardinis* Simon, 1899	*Patu* Marples, 1951	*Symphytognatha* Hickman, 1931
Sexes known	♀♂	♀	♀♂	♀♂	♀	♂	♀♂	♀♂
Species number	25	1	9	2	2	(2)	18	15
Nomenclatural status	Valid	Valid	Valid	Valid	Valid	Nomen dubium*	Valid	Valid
Female genitalia, internal	Pair of round spermathecae connected by t-shaped duct	–	Large spermathecae, convoluted duct path (Fig. 12c, d)	Ducts follow nearly straight path posteriorly from round spermathecae	Spermathecae twisted anteriorly	N.A.	Spermathecae variable, sometimes elongate or reniform	Copulatory ducts loop around elongate spermathecae (Hickman 1931: figs 1–6, pl. 1, fig. 2)
Female genitalia, external	Transverse rounded lip overhanging furrow	–	Short robust scape (Fig. 11c, d)	Transverse rounded lip overhanging furrow	Transverse rounded lip overhanging furrow	N.A.	Transverse rounded lip overhanging furrow, or a flexible scape (Marples 1951: figs 1d, 2e)	Transverse rounded lip overhanging furrow
Tarsal claws	Homogeneous	–	Homogeneous	–	Homogeneous	–	Homogeneous	Multidentate only in anterior legs (Forster and Platnick 1977: figs 6, 7; Hickman 1931: fig. 2; Lin 2019: fig. 3)
Cheliceral fusion	Near the base	Absent	Near the base	Near the base	Almost entirely fused with no visible suture line (Forster and Platnick 1977: figs 41, 42)	–	Fused basally to ca. 1/2 their length	Fused for most of their length, with visible suture line
Cheliceral teeth	Two (Fig. 7d)	–	Single asymmetrically bifid tooth, or two teeth (Fig. 5a)	Absent	One large, two short (Forster and Platnick 1977: fig. 43)	One (Brignoli 1978: fig. 6)	Usually a single large tooth with 1–3 peaks	Two sinuous teeth (Forster and Platnick 1977: figs 3, 32, 36; Lin 2019: figs 2B, 2C; Lopardo and Hormiga 2015: fig. 122A)
Male tibia II clasper	Absent	N.A.	1–4 (Fig. 5d, e)	Absent	N.A.	–	Sometimes 1–2	Absent
Male abdominal scutum	Absent except in *A. boneti*	N.A.	Surrounding the posterior part of the abdomen. Usually present, except in *C. haeneli*	Absent	N.A.	–	Absent	Absent

	***Anapistula* Gertsch, 1941**	***Anapogonia* Simon, 1905**	***Crassignatha* Wunderlich, 1995**	***Curimagua* Forster & Platnick, 1977**	***Globignatha* Balogh & Loksa, 1968**	***Iardinis* Simon, 1899**	***Patu* Marples, 1951**	***Symphytognatha* Hickman, 1931**
Pars cephalica	usually only slightly raised, strongly raised in *A. boneti*	–	Strongly raised	Strongly raised	Strongly raised	Strongly raised	Strongly raised	Strongly raised
Eye arrangement	Usually four eyes (Fig. 8b), median eyes present in *A. boneti*	Six eyes in triads	Six eyes in diads (Figs 10b, e, 11b)	Six eyes in triads	Six eyes in diads	Six eyes in triads	Six eyes in diads (Fig. 14b)	Six eyes in diads
Female palp	Absent	–	Absent	Vestigial	Absent	N.A.	Absent	Absent
Carapace texture	Mostly smooth	–	Generally covered with tubercles (Fig. 5b, c)	Mostly smooth	Mostly smooth	–	Mostly smooth	Mostly smooth
Abdomen shape	Subspherical	–	Subspherical, sometimes with postero-lateral lobes (Fig. 6)	Subspherical	Subspherical	–	Subspherical, sometimes with lobes	Subspherical
Cymbium	With strong setae but without teeth or denticles	N.A.	With cymbial tooth (Fig. 4b, d)	With small bumps or denticles (Forster and Platnick 1977: fig. 66)	N.A.	–	–	–
Spermatic duct	Coiling 1.5× over itself (Fig. 9a)	N.A.	Long, coiling several times around itself (Fig. 4b, e)	–	N.A.	Coiling 1.5× over itself (Brignoli 1978: fig. 7; Lopardo and Hormiga 2015: fig 135a)	–	–
Embolus	Short less than 0.5× the diameter of the bulb (Figs 7c, 9a)	N.A.	Variable, short (Fig. 4c) or long, ca. the diameter of the palp (Fig. 4f)	Short, ca. 0.5× the diameter of the bulb (Forster and Platnick 1977: figs 67, 68)	N.A.	long, 0,5–1,5 the diameter of the bulb (Brignoli 1978: fig. 7; Brignoli 1980: figs 1, 2)	Long, ca. 1×the diameter of the bulb (Marples 1951: fig. 1e, f; Marples 1955: fig. 19)	Short, ca. 0.5× the diameter of the bulb (Forster and Platnick 1977: figs 8, 9)
Relevant literature	(Harvey 1998; Dupérré and Tapia 2017; Forster and Platnick 1977; Rheims and Brescovit 2003; Rubio and González 2010)	(Simon 1905; Platnick and Forster 1989)	(Wunderlich 2004; Miller et al. 2009; Lopardo and Hormiga 2015)	(Forster and Platnick 1977)	(Forster and Platnick 1977)	(Brignoli 1980; Forster and Platnick 1977; Gertsch 1960; Levi and Levi 1962; Lopardo and Hormiga 2015)	(Marples 1951, 1955; Forster 1959; Forster and Platnick 1977; Saaristo 1996)	(Hickman 1931; Forster and Platnick 1977; Lopardo and Hormiga 2015; Lin 2019)

Number of species is based on the WSC (2020). *Type species *Iardinis weyersi* Simon, 1899 is considered a *nomen dubium*; two species placed in this genus by Brignoli (1978, 1980) remain cataloged here (WSC 2020).

Patu species known from males have a number of ventral distal macrosetae on tibia II, a characteristic scored as present in Lopardo's *Patu* specimens SYMP_002_MAD and SYMP_006_AUS and absent in Patu_SYMP_001_DR and *Symphytognatha picta* (Lopardo and Hormiga 2015); this leg II clasper is otherwise found only in *Crassignatha*.

Genotype *Crassignatha haeneli* Wunderlich, 1995 features a textured carapace and a distinctive ventral spur on tibial II (Fig. 5d, e; Wunderlich 1995: figs 14, 15, 17). The chelicerae are not conspicuously fused and are armed with a single bifid tooth (Fig. 5a); a character also scored for three species (SYMP_002_MAD, SYMP_006_AUS and SYMP_007_AUS, later on identified as *Patu*) used in Lopardo and Hormiga (2015). Miller et al. (2009, 2014) placed several additional species in *Crassignatha*, including the first descriptions of females. In all of Miller's species where males are known, they possess a unique abdominal scutum surrounding the abdomen laterally and posteriorly. In most *Crassignatha* species, the female genitalia consists of a pair of robust round spermathecae separated by approximately their diameter, copulatory ducts that loop and switchback along their path, and a short, robust scape (Miller et al. 2009: figs 76, 79, 89A–D); only *C. longtou* and *C. seedam* sp. nov. have a transverse bulge and not a scape (Miller et al. 2009: figs 89E, F, 91F).

Wunderlich (1995) stated that *Crassignatha haeneli* lacked an abdominal scutum, and among the Symphytognathidae, only *Anapistula boneti* and Miller's *Crassignatha* species have a scutum (but see *Patu spinathoraxi*, below). A dissection of *Crassignatha* chelicerae indicated that they were indeed fused at the base (Miller et al. 2009: fig. 78A). It is however worth noting that the 3D scan of *Crassignatha* presented here do not appear to indicate cheliceral fusion (Fig. 5a). It was also determined that most of these *Crassignatha* species have an asymmetrical split in the cheliceral tooth with a small peak on the mesal side of the tooth; only *C. longtou* has two subequal teeth. *Crassignatha* species known from the male all have a group of 1–3 strong ventral setae on male tibia II (Miller et al. 2015: figs 74E, 77D, 80E, 83E; Miller et al. 2009: fig. 1F). One species had the abdomen modified with a pair of posteriolateral lobes (Miller et al. 2009: figs 86D–F), not as conspicuous in other species (Fig. 6b, d), or generally round or oblong.

Modern symphytognathid taxonomy in Asia

2009 was a big year for little spiders in Asia. Four papers described a total of 18 symphytognathid species from China, Japan, and Vietnam (Lin et al. 2009; Lin and Li 2009; Miller et al. 2009; Shinkai 2009). These were distributed across the genera *Anapistula*, *Crassignatha*, and *Patu*. Lin and Li (2009) described five new *Patu* species from China. Again, fusion of the chelicerae only near the base was declared as a characteristic of *Patu*. Chelicerae of all species were illustrated as fused, but no details were provided in the text. Of these five species, three show characters that match the diagnostic characters of *Crassignatha* instead of *Patu*:

Patu bicorniventris Lin & Li, 2009, known from the female only, has an asymmetrically bifid cheliceral tooth (Lin and Li 2009: figs 2C, 2D) resembling those typical of

Crassignatha (Miller et al. 2009: fig. 78A). It also has modifications to the abdomen consisting of two posteriolateral lobes and a straight posterior margin, resembling *Crassignatha ertou* (Miller et al., 2009 figs 86D-86F). The female genitalia of *Patu bicorniventris* resembles most *Crassignatha* females described in Miller et al. (2009), featuring conspicuous spermathecae with convoluted copulatory ducts leading to a knob-like median scape.

Patu quadriventris Lin & Li, 2009 shares with *P. bicorniventris* an abdomen that is truncated posteriorly, but lacks the posteriolateral lobes. The female genitalia is consistent with *Crassignatha*. The cymbium of the male pedipalp has a distal apophysis (CS in Lin and Li 2009: fig. 9C) that strongly resembles the Ct in *Crassignatha* (Figs 9a, 13a, d; Miller et al. 2009: figs 75, 77B, 81, 82B, 84, 87, 88).

Patu spinathoraxi Lin & Li, 2009 has distinctive spikey tubercles covering the carapace. It closely resembles (but is not conspecific with) *Crassignatha longtou* Miller, Griswold & Yin, 2009, which was described from the female only. The female genitalia of both species are similar, featuring round spermathecae with ducts that run ectally before turning back toward the middle and terminate in a pair of conspicuous posterior openings; they contrast with *Crassignatha* in that they lack a robust scape. The male has a medially split abdominal scutum, a single ventral macroseta on tibia II, and a distal apophysis of the cymbium similar to those found in *Crassignatha* (CS in Lin and Li 2009: fig. 16C). These two species are clearly congeneric; whether they are best placed together in *Crassignatha*, or in their own new genus, is debatable.

Current status and proposed changes

Of the eight valid symphytognathid genera, *Anapistula*, *Curimagua*, *Globignatha*, *Symphytognatha*, and *Crassignatha* seem morphologically coherent and recognizable; *Anapogonia* and *Iardinis* are currently unrecognizable; *Patu* remains problematic. However, some species currently placed in *Patu* show clear affinities with *Crassignatha*. We propose the following taxonomic changes: *Crassignatha bicorniventris* (Lin & Li, 2009) comb. nov., *Crassignatha quadriventris* (Lin & Li, 2009) comb. nov., and *Crassignatha spinathoraxi* (Lin & Li, 2009) comb. nov.

Acknowledgements

Thanks to Joe Dulyapat and Choojai Petcharad for their great assistance and participation during our fieldwork in Thailand. Thanks to Bertie van Heuven and Rob Langelaan for their help obtaining the 3D scans of the male genitalia, and Werner de Gier and Louk Seton for introducing us to the 3D software. Thanks to Menno Schilthuizen and the participants of the “Taxon expedition Brunei 2018” for lending us the specimens of *Crassignatha danaugirangensis.* Thanks to the subject editor Dimitar Dimitrov and the reviewers Lara Lopardo and Ivan Magalhaes for their valuable comments and suggestions.

Thanks to Lara Lopardo for the morphological identifications of the voucher specimens used in Lopardo et al. (2011). Funding for the first author was provided by CONACyT Becas al extranjero 294543/440613, Mexico. All specimens used in this study were collected under permit 5830802 emitted by the Department of National Parks, Wildlife and Plant Conservation, Thailand.

References

Alvarez-Padilla F, Hormiga G (2007) A protocol for digesting internal soft tissues and mounting spiders for scanning electron microscopy. Journal of Arachnology 35(3): 538–542. https://doi.org/10.1636/Sh06-55.1

Brignoli PM (1978) Spinnen aus Nepal, IV. Drei neue Symphytognathidae (Arachnida: Araneae). Senckenbergiana Biologica 59: 247–252.

Brignoli PM (1980) On few Mysmenidae from the Oriental and Australian regions (Araneae). Revue Suisse De Zoologie 87: 727–738. https://doi.org/10.5962/bhl.part.85542

Coddington JA (1983) A temporary slide-mount allowing precise manipulation of small structures. Verhandlungen des Naturwissenschaftlichen Vereins in Hamburg 26: 291–292.

Darriba D, Taboada GL, Doallo R, Posada D (2012) JModelTest 2: More models, new heuristics and parallel computing. Nature Methods 9: 772–772. https://doi.org/10.1038/nmeth.2109

Dederichs TM, Müller CHG, Sentenská L, Lipke E, Uhl G, Michalik P (2019) The innervation of the male copulatory organ of spiders (Araneae) – A comparative analysis. Frontiers in Zoology 16(39): 1–14. https://doi.org/10.1186/s12983-019-0337-6

Dimitrov D, Lopardo L, Giribet G, Arnedo MA, Álvarez-Padilla F, Hormiga G (2012) Tangled in a sparse spider web: Single origin of orb weavers and their spinning work unravelled by denser taxonomic sampling. Proceedings of the Royal Society B – Biological Sciences 279(1732): 1341–1350. https://doi.org/10.1098/rspb.2011.2011

Dupérré N, Tapia E (2017) On some minuscule spiders (Araneae: Theridiosomatidae, Symphytognathidae) from the Chocó region of Ecuador with the description of ten new species. Zootaxa 4341(3): 375–399. https://doi.org/10.11646/zootaxa.4341.3.3

Feng C, Miller JA, Lin Y, Shu Y (2019) Further study of two chinese cave spiders (Araneae, Mysmenidae), with description of a new genus. ZooKeys 870: 77–100. https://doi.org/10.3897/zookeys.870.35971

Fernández R, Hormiga G, Giribet G (2014) Phylogenomic analysis of spiders reveals nonmonophyly of orb weavers. Current Biology 24(15): 1772–1777. https://doi.org/10.1016/j.cub.2014.06.035

Forster RR (1959) The spiders of the family Symphytognathidae. Transactions and Proceedings of the Royal Society of New Zealand 86: 263–329.

Forster RR, Platnick NI (1977) A review of the spider family Symphytognathidae (Arachnida, Araneae). American museum novitates 2619: 1–29.

Gertsch WJ (1960) Descriptions of American spiders of the family Symphytognathidae. American Museum Novitates 1981: 1–40.

Griswold CE, Coddington JA, Hormiga G, Scharff N (1998) Phylogeny of the orb-web building spiders (Araneae, Orbiculariae: Deinopoidea, Araneoidea). Zoological Journal of the Linnean Society 123(1): 1–99. https://doi.org/10.1111/j.1096-3642.1998.tb01290.x

Harvey MS (1998) A review of the Australasian species of *Anapistula* Gertsch (Araneae: Symphytognathidae). Records of the Western Australian Museum 19: 111–120.

Hickman VV (1931) A new family of spiders. Proceedings of the Zoological Society of London 101(4): 1321–1328. https://doi.org/10.1111/j.1096-3642.1931.tb01063.x

Hormiga G, Griswold CE (2014) Systematics, Phylogeny, and Evolution of Orb-Weaving Spiders. Annual Review of Entomology 59: 487–512. https://doi.org/10.1146/annurev-ento-011613-162046

Keklikoglou K, Faulwetter S, Chatzinikolaou E, Wils P, Brecko J, Kvaček J, Metscher B, Arvanitidis C (2019) Micro-computed tomography for natural history specimens: a handbook of best practice protocols. European Journal of Taxonomy 522: 1–55. https://doi.org/10.5852/ejt.2019.522

Kulkarni S, Wood H, Lloyd M, Hormiga G (2020) Spider-specific probe set for ultraconserved elements offers new perspectives on the evolutionary history of spiders (Arachnida, Araneae). Molecular Ecology Resources 20: 185–203. https://doi.org/10.1111/1755-0998.13099

Kumar S, Stecher G, Li M, Knyaz C, Tamura K (2018) MEGA X: Molecular evolutionary genetics analysis across computing platforms. Molecular Biology and Evolution 35(6): 1547–1549. https://doi.org/10.1093/molbev/msy096

Levi HW, Levi LR (1962) The genera of the spider family Theridiidae. Bulletin of the Museum of Comparative Zoology 127: 1–71.

Lin Y (2019) First report of the spider genus *Symphytognatha* from Asia (Araneae, Symphytognathidae). Zootaxa 4638(2): 291–295. https://doi.org/10.11646/zootaxa.4638.2.8

Lin Y, Li S (2009) First described *Patu* spiders (Araneae, Symphytognathidae) from Asia. Zootaxa 2154: 47–68.

Lin Y, Pham DS, Li S (2009) Six new spiders from caves of Northern Vietnam (Araneae: Tetrablemmidae: Ochyroceratidae: Telemidae: Symphytognathidae). Raffles Bulletin of Zoology 57: 323–342. https://doi.org/10.11646/zootaxa.2154.1.3

Lin Y, Tao Y, Li S (2013) Two new species of the genus *Anapistula* (Araneae, Symphytognathidae) from Southern China. Acta Zootaxonomica Sinica 38(1): 53–58.

Lipke E, Hammel JU, Michalik P (2015) First evidence of neurons in the male copulatory organ of a spider (Arachnida, Araneae). Biology Letters 11(7): e20150465. https://doi.org/10.1098/rsbl.2015.0465

Lopardo L, Hormiga G (2015) Out of the twilight zone: Phylogeny and evolutionary morphology of the orb-weaving spider family Mysmenidae, with a focus on spinneret spigot morphology in symphytognathoids (Araneae, Araneoidea). Zoological Journal of the Linnean Society 173(3): 527–786. https://doi.org/10.1111/zoj.12199

Lopardo L, Giribet G, Hormiga G (2011) Morphology to the rescue: Molecular data and the signal of morphological characters in combined phylogenetic analyses-a case study from mysmenid spiders (Araneae, Mysmenidae), with comments on the evolution of web architecture. Cladistics 27(3): 278–330. https://doi.org/10.1111/j.1096-0031.2010.00332.x

Mammola S, Michalik P, Hebets EA, Isaia M (2017) Record breaking achievements by spiders and the scientists who study them. PeerJ 5: e3972. https://doi.org/10.7717/peerj.3972

Marples BJ (1951) Pacific Symphytognathid Spiders. Pacific Science 5: 47–51.

Marples BJ (1955) Spiders from Wesern Samoa. Journal of the Linnean Society of London, Zoology 42: 453–504. https://doi.org/10.1111/j.1096-3642.1955.tb02217.x

Marusik YM, Lehtinen PT (2003) Synaphridae Wunderlich, 1986 (Aranei: Araneoidea), a new family status, with a description of a new species from Turkmenistan. Arthropoda Selecta 11: 143–152.

Miller JA, Griswold CE, Yin C (2009) The symphytognathoid spiders of the Gaoligongshan, Yunnan, China (Araneae: Araneoidea): Systematics and diversity of micro-orbweavers. ZooKeys 11: 9–195. https://doi.org/10.3897/zookeys.11.160

Miller JA, Griswold CE, Haddad CR (2010a) Taxonomic revision of the spider family Penestomidae (Araneae, Entelegynae). Zootaxa (2534): 1–36. https://doi.org/10.11646/zootaxa.2534.1.1

Miller JA, Schilthuizen M, Burmester J, van der Graaf L, Merckx V, Jocqué M, Kessler P, Fayle T, Breeschoten T, Broeren R, Bouman R, Chua W-J, Feijen F, Fermont T, Groen K, Groen M, Kil N, de Laat H, Moerland M, Moncoquet C, Panjang E, Philip A, Roca-Eriksen R, Rooduijn B, van Santen M, Swakman V, Evans M, Evans L, Love K, Joscelyne S, Tober A, Wilson H, Ambu L, Goossens B (2014) Dispatch from the field: ecology of ground-web-building spiders with description of a new species (Araneae, Symphytognathidae). Biodiversity Data Journal 2: e1076. https://doi.org/10.3897/BDJ.2.e1076

Miller MA, Pfeiffer W, Schwartz T (2010b) Creating the CIPRES Science Gateway for inference of large phylogenetic trees. In: 2010 Gateway Computing Environments Workshop, GCE 2010, 1–8. https://doi.org/10.1109/GCE.2010.5676129

Platnick NI, Forster RR (1989) A revision of the temperate South American and Australasian spiders of the family *Anapidae* (Araneae, Araneoidea). Bulletin of the American Museum of Natural History 190:1–139.

Rambaut A, Drummond AJ, Xie D, Baele G, Suchard MA (2018) Posterior summarization in Bayesian phylogenetics using Tracer 1.7. Systematic Biology 67(5): 901–904. https://doi.org/10.1093/sysbio/syy032

Rheims C, Brescovit AD (2003) Description of six new species of *Anapistula* Gertsch (Araneae, Symphytognathidae) from Brazil. Bulletin of the British Arachnological Society 12(7): 324–330.

Rix MG, Harvey MS, Roberts JD (2008) Molecular phylogenetics of the spider family Micropholcommatidae (Arachnida: Araneae) using nuclear rRNA genes (18S and 28S). Molecular Phylogenetics and Evolution 46(3): 1031–1048. https://doi.org/10.1016/j.ympev.2007.11.001

Ronquist F, Huelsenbeck JP (2003) MrBayes 3: Bayesian phylogenetic inference under mixed models. Bioinformatics 19(12): 1572–1574. https://doi.org/10.1093/bioinformatics/btg180

Rubio GD, González A (2010) The first Symphytognathidae (Arachnida: Araneae) from Argentina, with the description of a new species of *Anapistula* from the Yungas Mountain rainforest. Revista Chilena de Historia Natural 83(2): 243–247. https://doi.org/10.4067/S0716-078X2010000200005

Saaristo MI (1996) Symphytognathidae (Arachnida, Araneae), a new spider family for the granitic islands of Seychelles. Phelsuma 4: 53–56.

Saaristo MI (2010) Araneae. In: Gerlach J, Marusik Y (Eds) Arachnida and Myriapoda of the Seychelles islands. Press Manchester, UK, 306 pp.

Sentenská L, Müller CHG, Pekár S, Uhl G (2017) Neurons and a sensory organ in the pedipalps of male spiders reveal that it is not a numb structure. Scientific Reports 7: e12209. https://doi.org/10.1038/s41598-017-12555-5

Simon E (1905) Arachnides de Java, recueillis par le Prof. K. Kraepelin en 1904. Mitteilungen aus dem Naturhistorischen Museum in Hamburg 22: 49–73.

Sombke A, Lipke E, Michalik P, Uhl G, Harzsch S (2015) Potential and limitations of X-Ray microcomputed tomography in arthropod neuroanatomy: A methodological and comparative survey. Journal of Comparative Neurology 523(8): 1281–1295. https://doi.org/10.1002/cne.23741

Stamatakis A (2014) RAxML version 8: A tool for phylogenetic analysis and post-analysis of large phylogenies. Bioinformatics 30(9): 1312–1313. https://doi.org/10.1093/bioinformatics/btu033

Steinhoff POM, Uhl G, Harzsch S, Sombke A (2020) Visual pathways in the brain of the jumping spider *Marpissa muscosa*. Journal of Comparative Neurology 528(11): 1883–1902. https://doi.org/10.1002/cne.24861

Steinhoff POM, Sombke A, Liedtke J, Schneider JM, Harzsch S, Uhl G (2017) The synganglion of the jumping spider *Marpissa muscosa* (Arachnida: Salticidae): Insights from histology, immunohistochemistry and microCT analysis. Arthropod Structure and Development 46(2): 156–170. https://doi.org/10.1016/j.asd.2016.11.003

Tong Y, Li S (2006) Symphytognathidae (Araneae), a spider family newly recorded from China. Zootaxa 1259: 33–38.

Wheeler WC, Coddington JA, Crowley LM, Dimitrov D, Goloboff PA, Griswold CE, Hormiga G, Prendini L, Ramírez MJ, Sierwald P, Almeida-Silva L, Alvarez-Padilla F, Arnedo MA, Benavides Silva LR, Benjamin SP, Bond JE, Grismado CJ, Hasan E, Hedin M, Izquierdo MA, Labarque FM, Ledford J, Lopardo L, Maddison WP, Miller JA, Piacentini LN, Platnick NI, Polotow D, Silva-Dávila D, Scharff N, Szüts T, Ubick D, Vink CJ, Wood HM, Zhang J (2017) The spider tree of life: phylogeny of Araneae based on target-gene analyses from an extensive taxon sampling. Cladistics 33: 574–616. https://doi.org/10.1111/cla.12182

WSC (2020) World Spider Catalog Version 21.0. Natural History Museum Bern. http://wsc.nmbe.ch

Wunderlich J (1995) Drei bisher unbekannte Arten und Gattungen der Familie Anapidae (s.l.) aus Süd-Afrika, Brasilien und Malaysia (Arachnida: Araneae). Beiträge zur Araneologie 3: 543–551.

Wunderlich J (2004) The fossil spiders of the family *Anapidae* s. l. (Aeaneae) [sic] in Baltic, Dominican and Mexican amber and their extant relatives, with the description of the new subfamily Comarominae. Beiträge zur Araneologie 3: 1020–1111.

Supplementary material 1

List of primers used in our study

Authors: F. Andres Rivera-Quiroz, Booppa Petcharad, Jeremy A. Miller

Data type: molecular data

Explanation note: List of primers used in our study, alignment of DNA sequence data used in phylogenetic analyses in nexus format, and Trace plot and histograms for both runs of the BI analysis observed in Tracer 1.7.1.

Link: https://doi.org/10.3897/zookeys.1012.57047.suppl1

Supplementary material 2

3D reconstructions *Crassignatha seeliam* sp. nov. male pedipalp and habitus

Authors: F. Andres Rivera-Quiroz, Booppa Petcharad, Jeremy A. Miller

Data type: multimedia

Link: https://doi.org/10.3897/zookeys.1012.57047.suppl2

Supplementary material 3

3D reconstructions *Crassignatha danaugirangensis* male pedipalp and habitus

Authors: F. Andres Rivera-Quiroz, Booppa Petcharad, Jeremy A. Miller

Data type: multimedia

Link: https://doi.org/10.3897/zookeys.1012.57047.suppl3

ZooKeys 1012: 55–69 (2021)
doi: 10.3897/zookeys.1012.55718
https://zookeys.pensoft.net

RESEARCH ARTICLE

A peer-reviewed open-access journal
ZooKeys
Launched to accelerate biodiversity research

The first record of *Tremoctopus violaceus sensu stricto* Delle Chiaje,1830 in southwestern Gulf of Mexico gives a hint of the taxonomic status of *Tremoctopus gracilis*

María de Lourdes Jiménez-Badillo[1], César Meiners-Mandujano[1], Gabriela Galindo-Cortes[1], Piedad S. Morillo-Velarde[1,2], Roberto González-Gómez[1,3], Irene de los Angeles Barriga-Sosa[4], Ricardo Pliego-Cárdenas[4,5]

1 *Laboratorio de Biología Pesquera y Acuicultura. Instituto de Ciencias Marinas y Pesquerías, Universidad Veracruzana. Hidalgo 617. Col. Río Jamapa. Boca del Río, Veracruz, México. C.P. 94290, Mexico* **2** *CONACYT-Instituto de Ciencias Marinas y Pesquerías, Universidad Veracruzana. Hidalgo 617. Col. Río Jamapa. Boca del Río, Veracruz, México. C.P. 94290, Mexico* **3** *Posgrado en Ecología y Pesquerías, Universidad Veracruzana. Mar Mediterráneo 314. Fracc. Costa Verde. Boca del Río, Veracruz, México. C.P. 94290, Mexico* **4** *Laboratorio de Genética y Biología Molecular, Planta Experimental de Producción Acuícola, Universidad Autónoma Metropolitana Unidad Iztapalapa. Av. San Rafael Atlixco 186. Col. Vicentina. Iztapalapa, Cd. de México. C.P. 09340, Mexico* **5** *Departamento de Biología Comparada, Facultad de Ciencias, Universidad Nacional Autónoma de México, Av. Universidad 3000, Ciudad Universitaria, Delegación Coyoacán, C. P. 04510, Mexico*

Corresponding author: María de Lourdes Jiménez-Badillo (ljimenez@uv.mx)

Academic editor: Jiri Frank | Received 23 June 2020 | Accepted 29 December 2020 | Published 26 January 2021

http://zoobank.org/602D0643-66AD-41EE-8C87-85896749DB69

Citation: Jiménez-Badillo ML, Meiners-Mandujano CS, Galindo-Cortes G, Morillo-Velarde P, González-Gómez R, Barriga-Sosa IA, Pliego-Cárdenas R (2021) The first record of *Tremoctopus violaceus sensu stricto* Delle Chiaje,1830 in southwestern Gulf of Mexico gives a hint of the taxonomic status of *Tremoctopus gracilis*. ZooKeys 1012: 55–69. https://doi.org/10.3897/zookeys.1012.55718

Abstract

Knowledge on species taxonomic identity is essential to understand biological and biogeographical processes and for studies on biodiversity. Species the genus *Tremoctopus* have been confused in the past and are inconsistently identified. To clarify of the taxonomic diagnosis *Tremoctopus violaceus* Delle Chiaje, 1830, an evaluation of morphological and meristic characters, as well as morphometric indices and genetic analyses, was undertaken. The analyzed octopod was an opportunistically collected mature female of 640 mm in total length, with a mantle length of 135 mm and a total weight of 1.02 kg. Evidence of autotomy as a defensive mechanism for protecting the egg mass is presented. The 16S haplotype sequenced from this specimen represents the first one publicly available for this species from the Gulf of Mexico. The genetic divergence between this haplotype and those reported from the Pacific Ocean is representative of interspecific variation in other taxa, which suggests that "*T. violaceus*" in the Pacific Ocean (KY649286, MN435565, and AJ252767) should be addressed as *T. gracilis* instead. Genetic evidence to separate *T. violaceus* and *T. gracilis* is presented. The studied specimen from the Gulf of Mexico represents the westernmost known occurrence of *T. violaceus* and the first record from the southwestern Gulf of Mexico.

Keywords

Blanket octopus, genetic divergence, geographic distribution, new record, range extension Mexico, Veracruz Reef System, 16S haplotype

Introduction

Tremoctopodidae is one of the four families within the superfamily Argonautoidea Cantraine, 1841 (Mollusca, Cephalopoda), all of which are characterized by marked sexual size dimorphism, with small or dwarf males and larger females, some of which reach 2 m long (Naef 1923; Norman 2000). Such extreme dimorphism is not seen in any other animal group (Norman et al. 2002). The Tremoctopodidae is represented by a single genus, *Tremoctopus* (blanket octopus), with four species currently recognized as valid: *Tremoctopus gelatus* Thomas, 1977 which is meso-bathypelagic, gelatinous, with circumtropical and temperate distribution; *Tremoctopus robsoni* Kirk, 1884 which was described from waters off New Zealand; *Tremoctopus gracilis* (Eydoux & Souleyet, 1852) which occurs in the Pacific and Indian oceans; and *Tremoctopus violaceus* Delle Chiaje, 1830 which is an epipelagic (1–250 m depth), muscular, heavily pigmented, and restricted from 40°N to 35°S in the Atlantic Ocean, including the Gulf of Mexico, Caribbean Sea, and Mediterranean Sea (Voss 1967; Thomas 1977; O'Shea 1999; Quetglas et al. 2013; Mangold et al. 2018).

The most comprehensive systematic review of Tremoctopidae was by Thomas (1977). Based on the morphological characteristics of the hectocotylus, he proposed two subspecies for *T. violaceus*: *T. v. violaceus* from the Atlantic and *T. v. gracilis* from the Indo-Pacific. More than two decades later they were reclassified as species using the same morphological considerations (Mangold et al. 2018). However, the difficulty in separating these taxa based solely on male morphology, as well as the absence of molecular phylogenetic analyses of the genus, has caused taxonomic confusion. This is evident in occurrence records of these two species that lie outside the geographical limits indicated by Thomas (1977) and Mangold et al. (2018). Examples of such cases are records published by Zeidler (1989), García-Domínguez and Castro-Aguirre (1991), Norman et al. (2002), Chesalin and Zuyev (2002), Nabhitabhata et al. (2009), Chiu et al. (2018), and many historical records in the Ocean Biogeographic Information System (OBIS 2020).

Specimens of *T. violaceus* and *T. gracilis* are relatively rare in catches and, therefore, remain poorly known, despite their sporadic appearance since 1914 (OBIS 2020). Information on *T. violaceus* has been obtained from three sources: 1) occasional encounters of living or dead individuals (Voss 1956; Thomas 1977; Lozano-Soldevilla 1991; Chesalin and Zuyev 2002; Díaz and Gracia 2004; Nabhitabhata et al. 2009; Almeida-Tubino et al. 2010; Quetglas et al. 2013), 2) collections or captures (Salisbury 1953; Thomas 1977; Arocha and Urosa 1983; Nesis 1987; Biagi and Bertozzi 1992; Judkins et al. 2017) and 3) as remains in stomach contents of large pelagic fishes (Bello 1993; Almeida-Tubino et al. 2010). Causes of the taxonomic uncertainty of these species are the intrinsic limitations in obtaining specimens, the difficulties in distinguishing morphologically similar species, and the limited number of genetic sequences currently available in GenBank for *T. violaceus*.

Therefore, the addition of sporadic findings of *Tremoctopus* species, like in the present study, is of utmost importance for the taxonomic clarification of the genus. Hence, this study reports the first record of *Tremoctopus violaceus sensu stricto* in the southwestern Gulf of Mexico, supported by an integrative taxonomic approach that includes both morphological and genetic analyses. This study also establishes the genetic baseline to resolve the phylogenetic relationships between *T. violaceus* and *T. gracilis*.

Methods

The studied specimen was found alive by fishermen in the Veracruz Reef System, at the fishing harbor of the town of Antón Lizardo (19°03'24"N, 95°59'17"W), Veracruz state, in the southwestern Gulf of Mexico (Fig. 1) on 20 July 2019 at approximately 13:00 hrs. The body condition, live coloration, and behavior were recorded *in situ*, then the specimen was preserved on ice and sent to the Laboratorio de Biología Pesquera y Acuicultura, Instituto de Ciencias Marinas y Pesquerías (Universidad Veracruzana) for study.

In the laboratory, a photographic record of the fresh octopod was obtained and the species was determined following Voss (1956), Thomas (1977), Roper and Voss (1983), and Mangold et al. (2018). The terminology and measurements used follows Thomas (1977) and Finn (2013). All measurements were made when the specimen was fresh and are given in millimeters; the total weight is in kilograms. The morphological indices are expressed as a percentage of the dorsal mantle length. The number of gill filaments and nuchal folds were also recorded.

Given the good condition of the specimen and to keep it intact, no internal organs were removed for analysis. Muscle tissue samples from the mantle and arm were taken for genetic analysis. Tissues were preserved in 95% ethanol and maintained at –4 °C for 72 h before processing for DNA extraction, following the procedure suggested by Wall et al. (2014). The specimen was fixed in 10% formalin, transferred to 75% ethyl alcohol, and deposited in the Colección Nacional de Moluscos, Universidad Nacional Autónoma de México (Mexico City) under the voucher number CNMO 8042.

The genetic analysis was conducted at the Laboratorio de Genética y Biología Molecular, Planta Experimental de Producción Acuícola, Universidad Autónoma Metropolitana Iztapalapa. Total DNA was extracted using the Wizard Genomic DNA Pu-

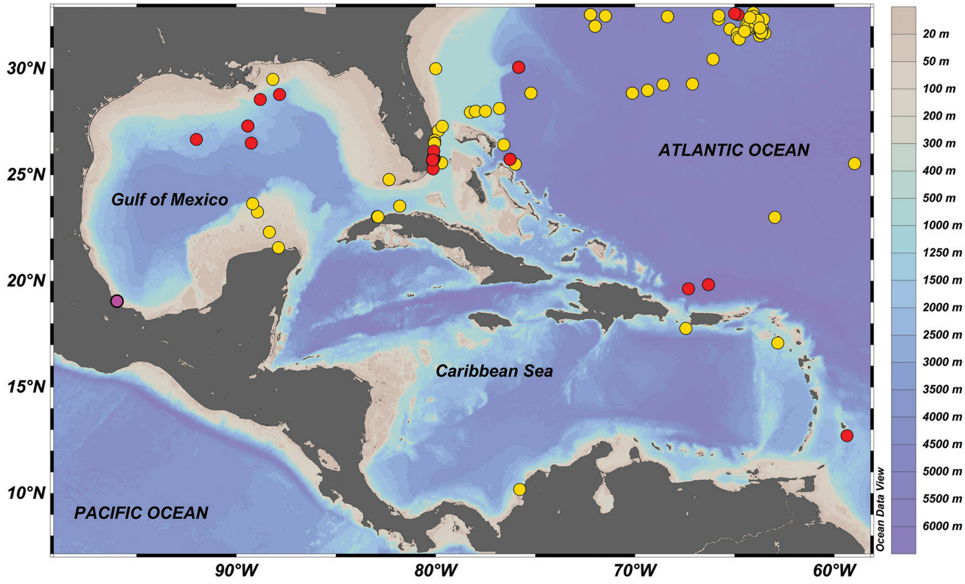

Figure 1. Observed distribution of *Tremoctopus violaceus* in Gulf of Mexico and adjacent areas based on Thomas (1977) (red dots), records contained in OBIS (2020) data base (yellow dots), and the new record from the southwestern Gulf of Mexico (present study; pink dot). Map prepared using Ocean Data View software (Schlitzer 2016).

rification Kit (Promega). DNA amplification was carried out through a polymerase chain reaction (PCR) using the ribosomal 16S primers from Simon et al. (1991). The mitochondrial fragment 16S is an effective DNA barcode marker for identifying cephalopod species (Dai et al. 2012; Pliego-Cárdenas et al. 2014, 2016; Flores-Valle et al. 2018). PCR conditions and sequencing are as in González-Gómez et al. (2018). The genetic analysis consisted of 1) identifying sequence homology in GenBank (NCBI) using the mega blast algorithm in Blast tool and 2) the phylogenetic inference analysis using the maximum likelihood (ML) method and the GTR+I+G model resolved by JModeltest (Darriba et al. 2012) in RaxMLGUI v. 1.5 (Silvestro and Michalak 2012). Branch support was assessed using 1000 bootstrap (bs) pseudo replicates under the rapid bootstrap algorithm.

Genetic divergences between the sequence obtained in this study and those that were the most similar according to Blast search from GenBank, were calculated in MEGA 7 (Kumar et al. 2016) using the Kimura two-parameter model (K2P). The following homologous sequences from genbank were used: *T. violaceus* (KY649286, MN435565, AJ252767), *Ocythoe tuberculata* Rafinesque, 1814 (GU288520), and *Haliphron atlanticus* Steenstrup, 1861 (AY616971). *Argonauta nodosus* Lightfoot, 1786 (AY545104), *A. hians* Lightfoot, 1786 (KY649285), and *A. argo* Linnaeus, 1758 (AB191108) were used as outgroups, based on the previous study of the phylogeny of Argonautoidea (Strugnell and Allcock 2010).

The results of the genetic analyses are discussed in context to the known distribution of Thomas's (1977) understanding of *T. violaceus* and *T. gracilis* as subspecies, and to the available records in OBIS (2020).

Results

Superfamily Argonautoidea
Family Tremoctopodidae
Genus *Tremoctopus*

***Tremoctopus violaceus* delle Chiaje, 1830**
Figures 2, 3

Material examined. Mexico • 1 female, 640 mm TL; 135 mm ML; southwestern Gulf of Mexico, Veracruz, Antón Lizardo; 19°03'24"N, 95°59'17"W; 20 July 2019; Jiménez-Badillo, L; recovered alive by fishermen; GenBank: MT271737; specimen code CNMO 8042.

The analyzed octopod was an adult female (TL of 640 mm, ML_d 135 mm, and TW 1.02 kg). It was found alive and was showing signs of disorientation and gross color pattern changes on the blanket from iridescent transparent to reddish-brown (Fig. 2A, D, F). The specimen had no apparent damage. Upon approach and handling by the fisherman, the octopus became threatened, extended her web, and jettisoned her eggs (Fig. 2B–D. A few meters away from the octopus, there appeared what was probably the eggs attached to a rod-like structure, but this could not be collected only recorded by video. This observation provides evidence of autotomy as a means of protection of the egg mass (Fig. 2G–I). The specimen is inferred to be sexually mature (Fig. 2E). Water pores, the coiled web on the ventral side of the animal, and some chromatophores on the web, which are characteristic of the species, were seen and recorded by video (Fig. 2A–D, G).

The fresh octopus had a brownish-purple color on the dorsal mantle and the head, while the ventral mantle was iridescent-silvery. The mantle was thick and muscular. The eyes were lateral. It had one pair of cephalic pores on the dorsal head between the eyes, and another, smaller pair on the ventral head adjacent to the funnel opening. The funnel extended beyond eye level and 14 gill filaments were counted. The arms were unequal in length and shape. The dorsal arms (arm pairs I and II) were much longer than the ventral arms (arm pairs III and IV); arms I and II were truncated. The suckers were biserial, decreasing in size towards the distal portion of each arm. One deep web was present between the four dorsal arms. The depth of the interdigital membrane was well developed and V-shaped. The nuchal folds numbered eight (Fig. 3A–E). The radula had seven teeth as well as two thin, rectangular marginal plates per transverse row. The rachidian teeth were tricuspid with an A2 seriation. The first lateral teeth were much smaller than the second lateral and rachidian teeth. The mar-

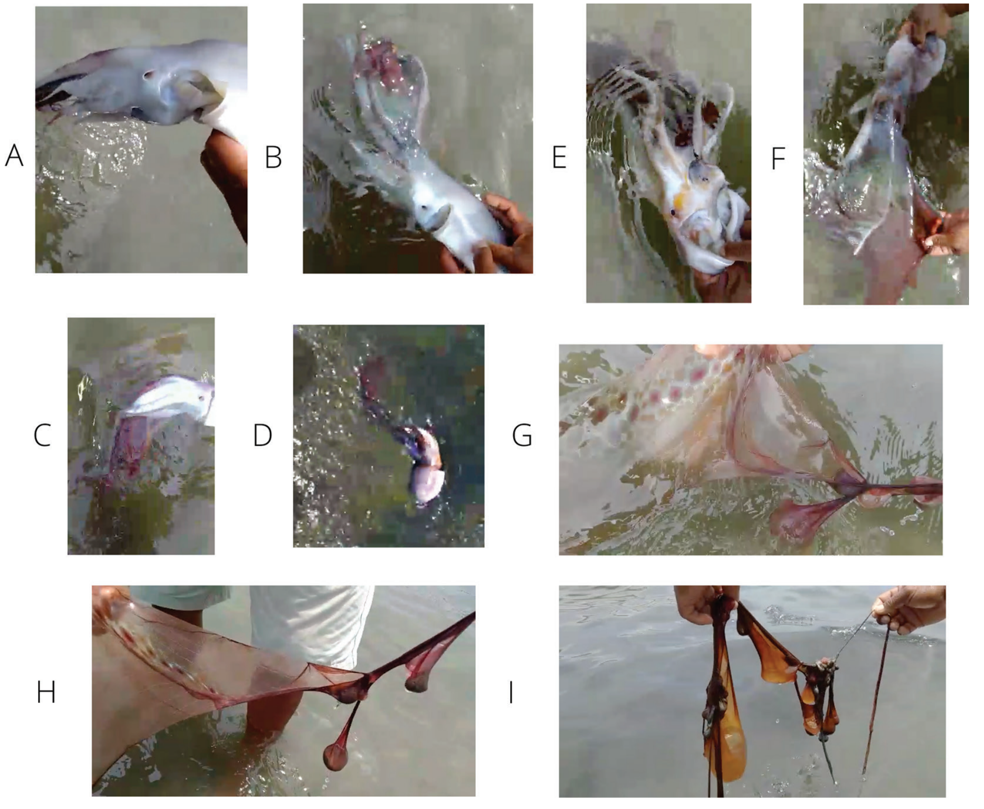

Figure 2. Photographic record of the *Tremoctopus violaceus* specimen (135 mm ML) in natural environment highlighting relevant characters for its taxonomic determination **A** ventral water pore **B–D** web of dorsal arms coiled on the ventral side and deployed when female was feeling threatened **E** egg mass **F** web displaying an iridescent greenish glow and a reddish brown color **G–I** evidence of autotomy: segments detached from interbrachial membrane showing slender arm, part of the connective tissue, circulatory system and chromatophores pattern characteristic of the species.

ginal teeth were long and slender and spine-shaped (Fig. 4). The color pattern and the morphological features described above as well as the body measurements and morphometric indices presented in Tables 1, 2 of the analyzed specimen fully correspond to *T. violaceus*, (Thomas 1977; Roper and Voss 1983; Orsi 2009; Mangold et al. 2018).

The compiled sequence of the mtDNA16S region (470 bp) obtained in this study (GenBank accession number MT271737) shows over 90% similarities to the *T. violaceus* homologue sequences from South Korea (MN435565), Taiwan (KY649286; Chiu et al. 2018), and Hawaii (AJ252767). This is the first mtDNA 16S haplotype publicly available in GenBank of *T. violaceus* from the Gulf of Mexico. Other public sequences for the species correspond to haplotypes of cytochrome c oxidase subunits I (COI) and III (COIII) genes (AF377978 and GU288522, respectively), and the voucher UMML:31.312. The genetic divergence among the Gulf of Mexico (Atlantic Ocean)

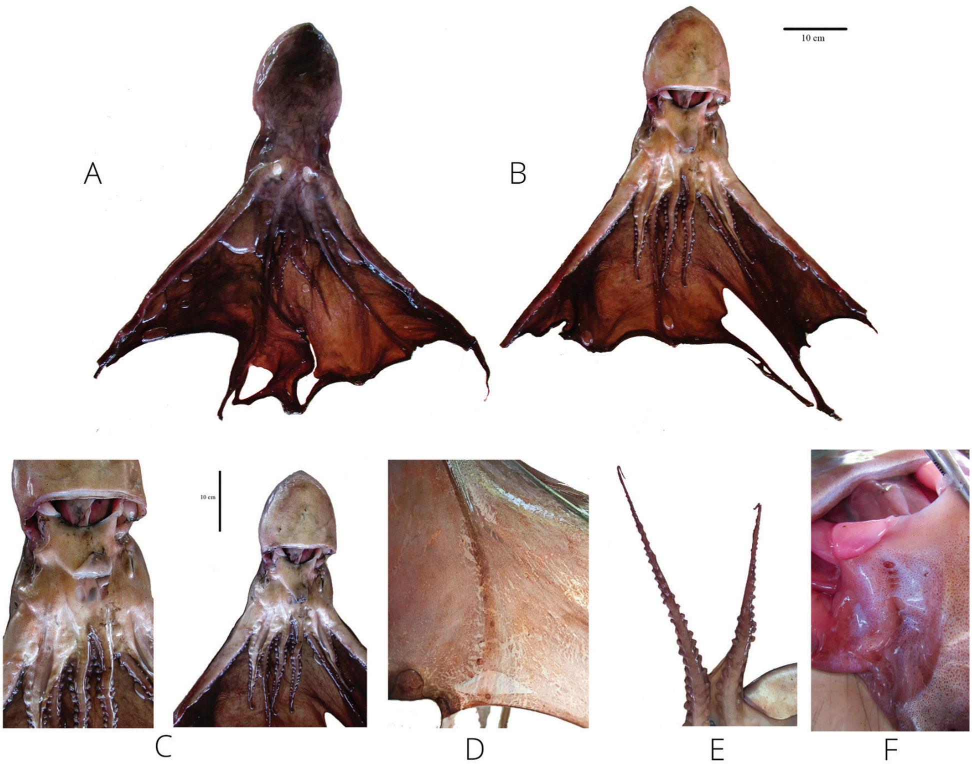

Figure 3. Photographic record of the *Tremoctopus violaceus* fresh specimen (135 mm ML) highlighting relevant characters for its taxonomic determination **A, B** dorsal and ventral view; arms unequal in length; one web between the four dorsal arms; two pairs of cephalic water pores, one pair located on dorsal surface of the head, slightly anterior to eyes at the base of first arms **C** second pair located ventrally, adjacent to funnel opening, at base of fourth arms; eyes large, laterally directed; funnel extends beyond eye level, distal one quarter free **D** bioluminescent tissue **E** biserial suckers on arms decreasing in size towards the distal portion **F** nuchal folds. To see the character dimensions, see Table 1. Scale bars: 10 cm (**A–C**).

specimen and the reference sequences from the Pacific Ocean is 6%, with 31 variable sites. All the *T. violaceus* 16S sequences are clustered in a well-supported monophyletic clade (bs = 100) (Fig. 5); however, the Atlantic Ocean specimen is in a separate clade from specimens from the Pacific Ocean.

Discussion

The octopus found in the southwestern Gulf of Mexico was a mature female belonging to the species *Tremoctopus violaceus* according to the morphometric, genetic, and biogeographic evidence, this identification is supported by the following features: color pattern, dorsal arms linked by a deep and broad web, arms proportions, sucker position, presence of conspicuous cephalic water pores, extended funnel, counts of gill

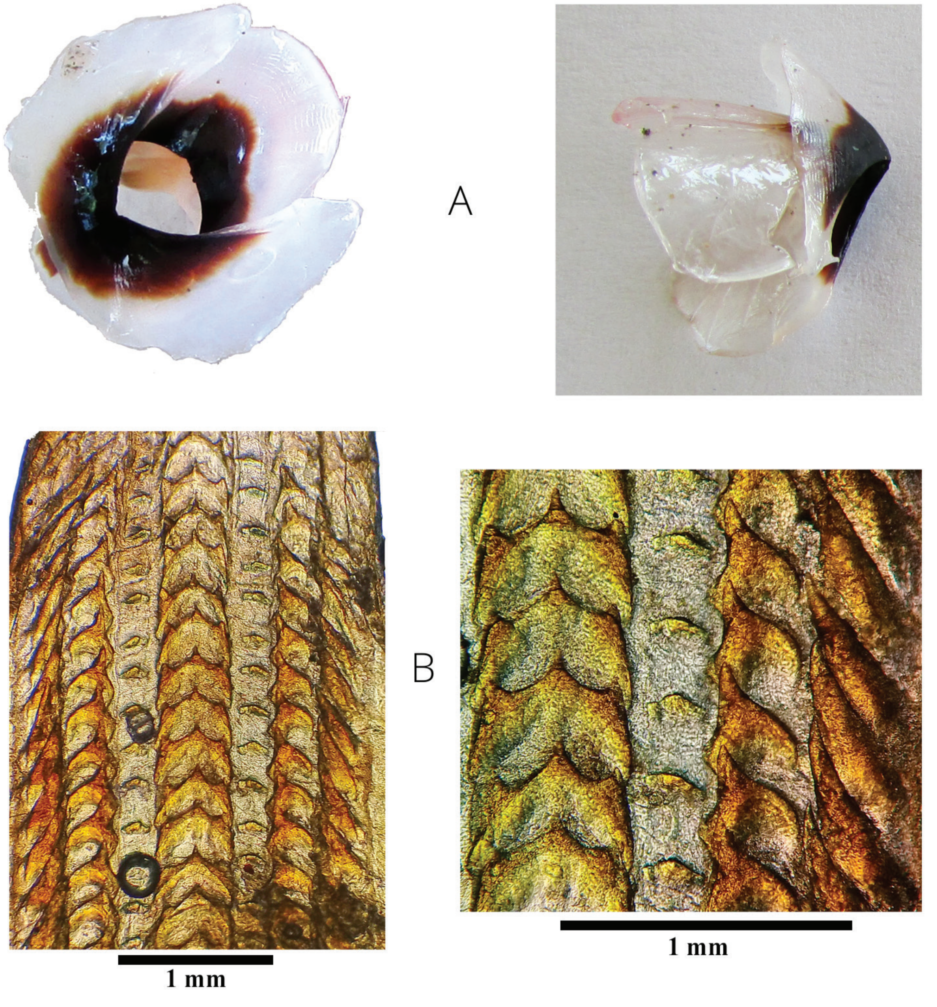

Figure 4. Photographic record of **A** upper and lower beak **B** radula, seven teeth and two marginal plates per transverse row are appreciated. On the approach (bottom right) rachidian teeth tricuspid with an A2 seriation is observed. For beak dimensions see Table 1. Scale bars:1 mm (**B**).

filaments, morphology of radular teeth, and eggs carried in arms (Voss 1956; Thomas 1977; Roper and Voss 1983; Orsi-Relini 2009; Mangold et al. 2018).

The studied specimen was found to be an adult female. Thomas (1977) indicated that the mantle shape depends on the size of the animals. Isometric growth of the mantle occurs in adults with a mantle length of 100–250 mm and not in juveniles. In this study, the mantle width index (MWI) was 53, which reflects a proportional growth between mantle width and mantle length. On the other hand, in adults, the mantle length continues to increase slightly faster than the head width, which is confirmed in the studied specimen by the head width index (HWI 70). In adult females, the funnel forms a broad transverse band with thin folds of glandular tissue. The funnel is mod-

Table 1. Body measurements (in mm) of the *Tremoctopus violaceus* specimen found in the southwestern Gulf of Mexico.

Character	CNMO 8042 specimen
Total length (TL)	640
Dorsal mantle length (ML_{d})	135
Ventral mantle length (ML_{v})	83
Mantle width (MW)	72
Head length (HL)	100
Head width (HW)	94
Arm length I (AL I) (left/rigth)	365*/330*
Arm length II (AL II) (left/rigth)	332*/473
Arm length III (AL III) (left/rigth)	161/162
Arm length IV (AL IV) (left/rigth)	152/179
Web depth interdigital A (WDI A)	Until tip of truncated arm
Web depth interdigital B (WDI B)	Until tip arm
Web depth interdigital C (WDI C)	78
Web depth interdigital D (WDI D)	65
Web depth interdigital E (WDI E)	54
Funnel length (FuL)	58
Free funnel length (FFL)	20
Funnel width (FW) at opening	25
Pallial aperture (PA)	89
Eye diameter (ED)	25
Pore size ventral (PS_{v}) (left/rigth)	16×11 / 16×13
Pore size dorsal (PS_{d}) (left/rigth)	27×18 / 27×17
Upper beak	
Hood length (HoL)	11.0
Beak height (BH)	17.8
Beak length (BL)	16.1
Beak width (BW)	16.5
Lower beak	
Rostral length (RL)	12.2
Wing length (WL)	18.0
Wing width (WW)	9.5
Beak height (BH)	5.7
Beak length (BL)	14.0
Beak width (BW)	19.1

* Truncated

erate in size, extending beyond the level of the eyes and is free for about a quarter of its length. In the studied specimen, the funnel length (FuL) was 58 mm and the free funnel length (FFL) was 20 mm, almost a quarter of the FuL.

In this species, the dorsal pores (PS_{d}) are usually larger than the ventral pores (PS_{v}), this was confirmed by 27×18 / 27×17 mm (left/right) vs 16×11 / 16×13 mm (left/right), respectively. The length of arms I and II is at least twice the mantle length, while the length of arms III and IV exceeds the mantle length by about 24 units. The arm formula (AF) 2, 1, 4, 3 agrees with that reported by Guerra (1992), Thomas (1977), and Finn (2014).

Autotomy was observed as a defense mechanism when the female felt threatened. Mangold et al. (2018) remarked that the web is only extended when the octopus is threatened. Nesis (1987) and Orsi-Relini (2009) also noted that both segments of the web and dorsal arms can be detached to protect the mass of embryos, which are

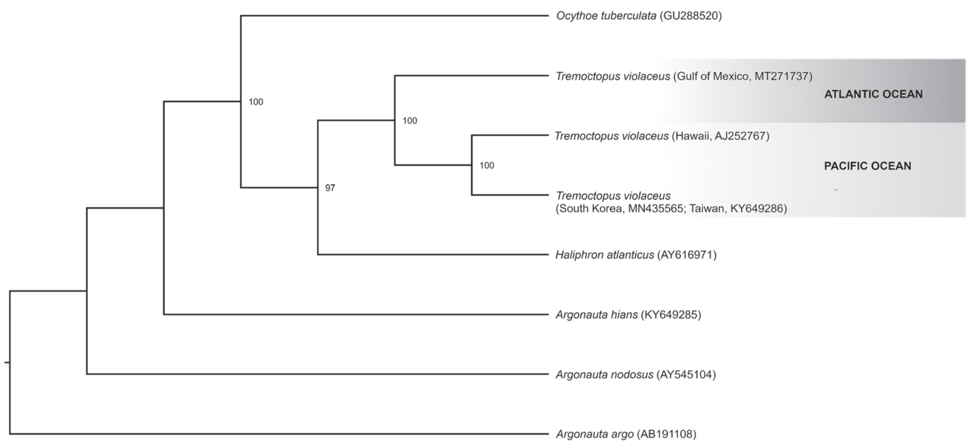

Figure 5. Maximum likelihood phylogenetic tree based on 16S sequences showing the relationships of *Tremoctopus violaceus*. Only bootstrap values above 90 are shown. Records from the Hawaiian Islands and South Korea–Japan were likely misidentified and correspond to *T. gracilis*.

Table 2. Morphometric indices of the *Tremoctopus violaceus* specimen found in the southwestern Gulf of Mexico.

Index	CNMO 8042 specimen
Pore length index dorsal (PLI_d)	20
Pore length index ventral (PLI_v)	12
Mantle width index (MWI)	53
Head width index (HWI)	70
Mantle arm index (MAI)	41
Arm length index I (ALI I) (left/rigth)	270 / 244
Arm length index II (ALI II) (left/rigth)	246 / 350
Arm length index III (ALI III) (left/rigth)	119 / 120
Arm length index IV (ALI IV) (left/rigth)	112 / 133
Arm formula (AF)	2,1, 4, 3
Arm width index (AWI)	19.26
Free funnel length index (FFuLI)	14.8
Funnel length index (FuLI)	42.9
Head length index (HLI)	74
Mantle width index (MWI)	53.3
Pallial aperture index (PAI)	65.9

brooded on the web until hatching (Portmann 1952). Figure 2G–I shows one segment of the web detached and with a chromatic pattern consisting of a large, round spot encircled by minor shapes, which is typical of *T. violaceus* (Orsi-Relini 2009).

The genetic analysis of the mtDNA 16S region revealed two important results. The phylogenetic inference confirms the identity of the Gulf of Mexico specimen as *T. violaceus*, i.e., within the same clade containing KY649286, MN435565, and AJ25276 (100 bootstrap support). The 6% genetic distance between analysed specimens suggests that the Gulf of Mexico and Pacific Ocean specimens belong to differ-

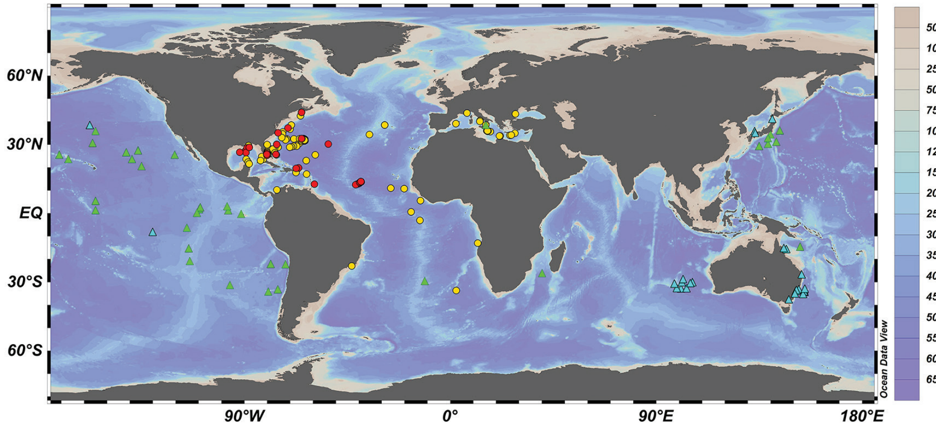

Figure 6. Observed distribution of coherent available records of *Tremoctopus violaceus* (dots) and *T. gracilis* (triangles) based on material examined by Thomas (1977) (red dots and green triangles), records contained in OBIS (2020) database and published records by Quetglas et al. (2013) and Almeida-Tubino et al. (2010) (yellow dots and blue triangles). Map prepared using Ocean Data View software (Schlitzer 2016).

ent species, with the Pacific Ocean species corresponding to *T. gracilis*. The average calculated interspecific genetic distance value for the mtDNA16S for cephalopods is 7.1% (range 1.3–12.7%) and for intraspecific genetic distances it is 0.5% (range 0.0–2.7%) (Dai et al. 2012). According to several authors (Thomas 1977; Almeida-Tubino et al. 2010; Quetglas et al. 2013; Finn 2014) and most of the records in OBIS (2020), *T. violaceus* occurs only in the Atlantic Ocean, whereas *T. gracilis* inhabits the Pacific and Indian oceans (Fig. 6). Therefore, it is likely that the octopods from the Pacific were misidentified and are in fact *T. gracilis*. The 16S marker is more variable than COI (Strugnell and Lindgren 2007) and is therefore a reliable marker for identifying species (Dai et al. 2012; Pliego-Cardenas et al. 2014, 2016; Flores-Valle et al. 2018). According to Chiu et al. (2018), *T. violaceus* is basal in the phylogenetic tree of Octopoda.

Data on the occurrence of *T. violaceus* are sporadic, with fewer than 350 records during the last hundred years, and many of these are from the Western Central Atlantic and the Mediterranean Sea (Fig. 6), which is consistent with the distribution of this taxon, as determined by Thomas (1977). From the Gulf of Mexico, available data are concentrated in the eastern portion of the Gulf (Fig. 1), near the influence of the Loop Current which exchanges water between the Caribbean Sea and the Eastern Seaboard. As far as we know, the specimen reported in this study is the first record of *T. violaceus sensu stricto* from the southwestern Gulf of Mexico.

Finally, the molecular evidence of the new 16S haplotype of *T. violaceus* undoubtedly separates it from the few available haplotypes of *Tremoctopus gracilis* of the Pacific. More studies, with consideration to inter- and intraspecific geographic dispersion, is required to fully solve the molecular phylogeny of the genus.

Acknowledgements

We thank the fishing cooperative Sociedad Cooperativa Arrecifes de Antón Lizardo, especially to Leodegario Castillo Marin for sharing the specimen studied. IDLABS thanks the Universidad Autónoma Metropolitana for grant no. 147.09.01. We are grateful to the reviewers and editor for providing helpful comments and contributions to the improvement of the manuscript.

References

Almeida-Tubino R, De Souza MLE, Rangel CA, Monteiro NC (2010) A new record for a *Tremoctopus violaceus* Chiaie, 1830 (Mollusca,Tremoctopodidae) from Rio de Janeiro coast, southeastern Brazil. Pan-American Journal of Aquatic Sciences 5(4): 572–576. https://panamjas.org/pdf_artigos/PANAMJAS_5(4)_572-576.pdf

Arocha F, Urosa LJ (1983) Notes on two Octopoda from Venezuelan waters. Bulletin of Marine Science 33(4): 941–942.

Bello G (1993) *Tremoctopus violaceus* (Cephalopoda: Tremoctopodidae) in the stomach content of a swordfish from the Adriatic Sea. Bolletino Malacologico 29(1–4): 45–48. https://www.biodiversitylibrary.org/page/49937296

Biagi V, Bertozzi A (1992) Presenza stagionale di *Tremoctopus violaceus* Delle Chiaie, 1830 (Cephalopoda: Octopoda) nel mare di Piombino (Li). Bolletino Malacologico 28(1–4): 47–54. https://www.societaitalianadimalacologia.it/Bollettino/Bollettino%201992/Boll.%20Mal.%201992%201-4.pdf

Chesalin MV, Zuyev GV (2002) Pelagic cephalopods of the Arabian Sea with an emphasis on *Sthenoteuthis oualaniensis*. Bulletin of Marine Science 71(1): 209–221. https://www.ingentaconnect.com/content/umrsmas/bullmar/2002/00000071/00000001/art00017

Chiu YW, Chang CW, Shen KN, Ju YM, Lin HD (2018) Complete mitochondrial genome and the phylogenetic position of the pelagic octopus *Tremoctopus violaceus* (Mollusca: Tremoctopodidae). Mitochondrial DNA Part B 3(2): 1248–1249. https://doi.org/10.1080/23802359.2018.1532347

Dai L, Zheng X, Lingfeng K, Li Q (2012) DNAbarcoding analysis of Coleoidea (Mollusca: Cephalopoda) from Chinese waters. Molecular Ecology Resources 12: 437–447. https://doi.org/10.1111/j.1755-0998.2012.03118.x

Darriba D, Taboada GL, Doallo R, Posada D (2012) jModelTest 2: more models, new heuristics and parallel computing. Nature Methods 9(8): e772. https://doi.org/10.1038/nmeth.2109

Díaz JM, Gracia CA (2004) Primer Registro de un pulpo de la familia Tremoctopodidae (Cephalopoda: Octopoda) para el caribe colombiano. Boletín de Investigaciones Marinas y Costeras 33(1): 285–288. http://ref.scielo.org/tw5sd3

Finn JK (2013) Taxonomy and biology of the argonauts (Cephalopoda: Argonautidae) with particular reference to Australian material. Molluscan Research 33(3): 143–222. https://doi.org/10.1080/13235818.2013.824854

Finn JK (2014) Family Tremoctopodidae. In: Jereb P, Roper CFE, Norman MD, Finn JK (Eds) Cephalopods of the World. An Annotated and Illustrated Catalogue of Cephalopod Species Known to Date (Vol. 3). Octopods and Vampire Squids. FAO Species Catalogue for Fishery Purposes, FAO, Rome, 240–243. http://www.fao.org/3/a-i3489e.pdf

Flores-Valle A, Pliego-Cárdenas R, Jiménez-Badillo L, Arredondo-Figueroa JL, Barriga-Sosa I (2018) First record of *Octopus insularis* (Leite and Haimovici, 2008) in the octopus fishery of a marine protected area in the Gulf of Mexico. Journal of Shellfish Research 37(1): 221–227. https://doi.org/10.2983/035.037.0120

García-Domínguez F, Castro-Aguirre JL (1991) Cuatro registros y algunas notas sobre la biología del pulpo pelágico Tremoctopus violaceus gracilis (Eydoux y Souleyet, 1852) (Octopoda: Tremoctopodidae) en México y en el Golfo de California. Investigaciones Marinas 6(1): 229–233. https://biblat.unam.mx/es/revista/investigaciones-marinas-cicimar/articulo/cuatro-registros-y-algunas-notas-sobre-la-biologia-del-pulpo-pelagico-violaceus-gracilis-eydoux-y-souleyet-1852-octopoda-tremoctopodidae-en-mexico-y-en-el-golfo-de-california

González-Gómez R, Barriga-Sosa I, Pliego-Cárdenas R, Jiménez-Badillo L, Markaida U, Meiners-Mandujano C, Morillo-Velarde P (2018) An integrative taxonomic approach revels *Octopus insularis* as the dominant species in the Veracruz Reef System (southwestern Gulf of Mexico). PeerJ 6: e6015. https://doi.org/10.7717/peerj.6015

Guerra A (1992) Mollusca, Cephalopoda. Fauna Ibérica (Vol. 1). Museo Nacional de Ciencias Naturales, CSIC, Madrid, 327 pp. http://www.fauna-iberica.mncn.csic.es/publicaciones/fi1.php

Judkins HL, Vecchione M, Cook A, Sutton T (2017) Diversity of midwater cephalopods in the northern Gulf of Mexico: comparison of two collecting methods. Marine Biodiversity 47: 647–657. https://doi.org/10.1007/s12526-016-0597-8

Kumar S, Stecher G, Tamura K (2016) MEGA7: Molecular Evolutionary Genetics Analysis version 7.0. for bigger data sets. Molecular Biology and Evolution 33(7): 1870–1874. https://doi.org/10.1093/molbev/msw054

Lozano-Soldevilla F (1991) Primera cita de *Tremoctopus violaceus violaceus* Delle Chiaje, 1830 (Octopoda: Tremoctopodidae) en aguas Canarias. Scientia Marina 55(3): 547–549. http://scimar.icm.csic.es/scimar/index.php/secId/10

Mangold KM, Vecchione M, Young RE (2018) Tremoctopodidae Tryon, 1879. *Tremoctopus* Chiaie, 1830. Blanket octopus. Version 29 March 2018. http://tolweb.org/Tremoctopus/20202/2018.03.29 in The Tree of Life Web Project. [Accessed 3.29.2020]

Nabhitabhata J, Sukhsangchan C, Wongkamhaeng K (2009) First record of two pelagic octopods, *Argonauta argo* and *Tremoctopus violaceus* cf. *gracilis* from the Andaman Sea, Thailand. Vie et Milieu Life & Environment 59(1): 39–45. https://wwwphp.obs-banyuls.fr/Viemilieu/index.php/volume-59-2009/59-issue-1/591-article-5.html

Naef A (1923) Cephalopoda. Fauna and Flora of the Bay of Naples. Monograph 35: 1–917. https://www.biodiversitylibrary.org/page/53459156

Nesis K (1987) Cephalopods of the world, Squids, Cuttlefishes, Octopuses and allies. TFH Publications, Neptune City, 351 pp.

Norman MD (2000) Chephalopods. A World Guide: Octopuses. Argonauts. Cuttlefish. Squid. Nautilus. Conchbooks, Harxheim, 320 pp.

Norman MD, Paul D, Finn J, Tregenza T (2002) First encounter with a live male blanket octopus: the world's most sexually size-dimorphic large animal. New Zealand Journal of Marine and Freshwater Research 36(4): 733–736. https://doi.org/10.1080/00288330.2002.9517126

OBIS (2020) Distribution records of *Tremoctopus violaceus* Delle Chiaje, 1830 and *Tremoctopus gracilis* (Souleyet, 1852). Dataset. Ocean Biogeographic Information System. Intergovernmental Oceanographic Commission of UNESCO. https://obis.org https://mapper.obis.org/?taxonid=141694,237820 [Accessed 5.7.2020]

Orsi-Relini L (2009) Notes about colour displays observed in female specimens of Tremoctopus (Cephalopoda: Octopoda) and their taxonomic value. Bolletino Malacologico 45: 13–16. https://www.societaitalianadimalacologia.it/Bollettino/Supplemento%208/05_Relini.pdf

O'Shea S (1999) The Marine Fauna of New Zealand: Octopoda (Mollusca: Cephalopoda). Biodiversity Memoir 112, National Institute of Water and Atmospheric Research, Wellington, 280 pp.

Pliego-Cárdenas R, Hochberg FG, García de León FJ, Barriga-Sosa IDLA (2014) Close genetic relationships between two American octopuses: *Octopus hubbsorum* Berry, 1953, and *Octopus mimus* Gould, 1852. Journal of Shellfish Research 33(1): 293–303. https://doi.org/10.2983/035.033.0128

Pliego-Cárdenas R, Flores L, Markaida U, Barriga-Sosa IDLA, Mora E, Arias E (2016) Genetic evidence of the presence of *Octopus mimus* in the artisanal fisheries of octopus in Santa Elena Peninsula, Ecuador. American Malacological Bulletin 34(1): 51–55. https://doi.org/10.4003/006.034.0102

Portmann A (1952) Les bras dorsaux de *Tremoctopus violaceus* Delle Chiaje. Revue Suisse de Zoologie 59: 288–293. https://doi.org/10.5962/bhl.part.75371

Quetglas A, Ordines F, González M, Zaragoza N, Mallol S, Valls M, De Mesa A (2013) Uncommon pelagic and deep-sea cephalopods in the Mediterranean: new data and literature review. Mediterranean Marine Science 14(1): 69–85. https://doi.org/10.12681/mms.320

Roper CFE, Voss GL (1983) Guidelines for taxonomic descriptions of cephalopod species. Memoirs of the National Museum of Victoria 44: 49–63. https://doi.org/10.24199/j.mmv.1983.44.03

Salisbury AE (1953) Mollusca of the University of Oxford Expedition to the Cayman Islands in 1938. Journal of Molluscan studies 30(1–2): 39–54. https://doi.org/10.1093/oxfordjournals.mollus.a064693

Schlitzer R (2016) Ocean Data View. http://odv.awi.de

Silvestro D, Michalak I (2012) RaxmlGUI: a graphical front-end for RAxML. Organisms Diversity & Evolution 12: 335–337. https://doi.org/10.1007/s13127-011-0056-0

Simon C, Franke A, Martin AP (1991) The polymerase chain reaction: DNA extraction and amplification. In: Hewitt GM, Johnston AWB, Young JPW (Eds) Molecular Techniques in Taxonomy. Springer, Berlin–Heidelberg, 329–355. https://doi.org/10.1007/978-3-642-83962-7_22

Strugnell JM, Lindgren AR (2007) A barcode of life database for the Cephalopoda? Considerations and concerns. Reviews in Fish Biology and Fisheries 17: 337–344. https://doi.org/10.1007/s11160-007-9043-0

Strugnell JM, Allcock AL (2010) Co-estimation of phylogeny and divergence times of Argonautoidea using relaxed phylogenetics. Molecular Phylogenetics and Evolution 54: 701–708. https://doi.org/10.1016/j.ympev.2009.11.017

Thomas RF (1977) Systematics, distribution, and biology of cephalopods of genus *Tremoctopus* (Octopoda: Tremoctopodidae). Bulletin of Marine Science 27(3): 353–392. https://www.ingentaconnect.com/contentone/umrsmas/bullmar/1977/00000027/00000003/art00001

Voss GL (1956) A review of the Cephalopods of the Gulf of Mexico. Bulletin of Marine Science of the Gulf and Caribbean 6(2): 85–178 https://www.ingentaconnect.com/content/umrsmas/bullmar/1956/00000006/00000002/art00001#

Voss GL (1967) The biology and bathymetric distribution of deep-sea cephalopods. Studies in Tropical Oceanography 5: 511–535. https://scholarlyrepository.miami.edu/trop_ocean/5

Wall AR, Campo D, Wetzer R (2014) Genetic utility of natural history museum specimens: endangered fairy shrimp (Branchiopoda, Anostraca). ZooKeys 457: 1–14. https://doi.org/10.3897/zookeys.457.6822

Zeidler W (1989) The pelagic octopus *Tremoctopus violaceus* Delle Chiaje, 1830, from Southern Australian Waters. Veliger 32(2): 166–170. https://www.biodiversitylibrary.org/page/43054034

Supplementary material 1

Data resources

Authors: María de Lourdes Jiménez-Badillo, César Meiners-Mandujano, Gabriela Galindo-Cortes, Piedad Morillo-Velarde, Roberto González-Gómez, Irene de los Angeles Barriga-Sosa, Ricardo Pliego-Cárdenas

Data type: occurences, genbank accession numbers, hyperlink of molecular sequences

Explanation note: We presented the biological material examined in this study. Also we presented a table with specimens name, catalog number, GenBank accession numbers and hyperlink of molecular sequences used in this study.

Link: https://doi.org/10.3897/zookeys.1012.55718.suppl1

ZooKeys 1012: 71–93 (2021)
doi: 10.3897/zookeys.1012.54779
https://zookeys.pensoft.net

RESEARCH ARTICLE

A peer-reviewed open-access journal
ZooKeys
Launched to accelerate biodiversity research

Rhodnius micki, a new species of Triatominae (Hemiptera, Reduviidae) from Bolivia

Yisheng Zhao[1], Cleber Galvão[2], Wanzhi Cai[1]

1 *Department of Entomology and MOA Key Lab of Pest Monitoring and Green Management, College of Plant Protection, China Agricultural University, Beijing 100193, China* **2** *Laboratório Nacional e Internacional de Referência em Taxonomia de Triatomíneos, Instituto Oswaldo Cruz, LNIRTT/IOC/FIOCRUZ, Pavilhão Rocha Lima, 5° andar, Avenida Brasil, 4365, Manguinhos, RJ, Brazil*

Corresponding author: Wanzhi Cai (caiwz@cau.edu.cn)

Academic editor: L. Livermore | Received 27 May 2020 | Accepted 2 December 2020 | Published 26 January 2021

http://zoobank.org/8CE02949-01D3-4409-8BEB-CCB9EACDC068

Citation: Zhao Y, Galvão C, Cai W (2021) *Rhodnius micki*, a new species of Triatominae (Hemiptera, Reduviidae) from Bolivia. ZooKeys 1012: 71–93. https://doi.org/10.3897/zookeys.1012.54779

Abstract

Rhodnius Stål, 1859 is the second largest genus of Triatominae after *Triatoma* Laporte, 1832, and includes several important Chagas vectors. Genitalia in Reduviidae are frequently used for species identification, but the current use of terminology for it is inconsistent in Triatominae. Here, *Rhodnius micki* **sp. nov.**, is described from Bolivia and considered as belonging to the *pictipes* group based on its morphological characters and distribution. Detailed documentation of the genitalia of *Rhodnius micki* **sp. nov.** is provided with emphasis on its everted phallus, especially the endosomal sclerites, which are potentially useful as species-level diagnostic features in *Rhodnius*. To further verify the validity of this species, the head shapes and wing venation patterns of five species in *Rhodnius* are compared with morphometric analysis. After reviewing taxonomic and comparative morphology papers of assassin bugs, a vocabulary with a terminology of morphological characters, especially of external male genitalic characters, is assembled with the preferred terms and the synonyms listed. Establishing a consistent terminological framework will greatly facilitate future research on the homology of these structures across Triatominae and will ultimately contribute to our understanding of the evolution of these groups.

Keywords

Comparative terminology, genitalia, geometric morphology, kissing bug, taxonomy

Introduction

Triatominae are a subfamily within Reduviidae that is known for its hematophagous feeding habit (Jansen and Roque 2010). Currently, there are 151 extant and three known fossil species assigned to 18 genera and five tribes in Triatominae (Lent and Wygodzinsky 1979; Justi and Galvão et al. 2017; Rosa et al. 2017a; Oliveira et al. 2018; Lima-Cordón et al. 2019; Nascimento et al. 2019; Poinar Jr 2019). All Triatominae possess a nearly straight labium with a flexible membranous connection between the second and third visible segments that allows upward pointing when feeding (Lent and Wygodzinsky 1979). Many species are competent vectors of Chagas disease transmitting *Trypanosoma cruzi* (Chagas, 1909) in their feces (Lent and Wygodzinsky 1979; Bern et al. 2011). Chagas disease is one of the ten most seriously neglected tropical diseases, which are currently estimated to affect nine million people, with more than 70 million people living under a serious risk of infection (Justi and Galvão 2017; WHO 2019).

The tribe Rhodniini currently contains two genera, *Rhodnius* Stål, 1859 (with 20 species) and *Psammolestes* Bergroth, 1911 (with three species) (Justi and Galvão et al. 2017; Rosa et al. 2017a; Nascimento et al. 2019). The main characters which distinguish *Rhodnius* and *Psammolestes* from the other genera of Triatominae are that their antenniferous tubercles do not close to eyes and the presence of callosities behind their eyes (Lent and Wygodzinsky 1979). *Rhodnius* is widely distributed in the Neotropical Region, and some species are the key vectors of Chagas disease in their respective ranges. *Rhodnius ecuadoriensis* Lent & León, 1958, for example, is one of the most important vector species of Chagas disease in Ecuador (Grijalva et al. 2015); *R. robustus* Larrousse, 1927 and *R. pictipes* Stål, 1872 are the vectors that cause public health problem in French Guiana (Barnabé et al. 2018). Most species of *Rhodnius* are arboreal, and their microhabitat preference patterns range from species that appear to inhabit a single species of palms (e.g., *R. brethesi* Matta, 1919 in *Leopoldinia piassaba*) to species that are found across several genera of palms (e.g., *R. pictipes* in *Attalea butyracea* and *Oenocarpus bataua*) (Lent and Wygodzinsky 1979; Barrett 1991; Carcavallo et al. 1998; Abad-Franch et al. 2005). *Rhodnius* is usually divided into three species groups, namely the *pictipes*, *prolixus*, and *pallescens* groups. *Pictipes* group includes six species, i.e., *R. amazonicus* Almeida, Santos & Sposina, 1973, *R. brethesi*, *R. paraensis* Sherlock, Guitton & Miles, 1977, *R. pictipes* Stål, 1872, *R. stali* Lent, Jurberg & Galvão,1993 and *R. zeledoni* Jurberg, Rocha & Galvão, 2009. *Prolixus* group includes eleven species, i.e., *R. barretti* Abad-Franch, Palomeque & Monteiro, 2013, *R. dalessandroi* Carcavallo & Barreto, 1976, *R. domesticus* Neiva & Pinto, 1923, *R. milesi* Carcavallo, Rocha, Galvão & Jurberg, 2001, *R. marabaensis* Souza et al., 2016, *R. montenegrensis* Rosa et al., 2012, *R. nasutus* Stål, 1859, *R. neglectus* Lent, 1954, *R. neivai* Lent, 1953, *R. prolixus* Stål, 1859, and *R. robustus*. *Pallescens* group includes three species, i.e., *R. colombiensis* Moreno Mejía, Galvão & Jurberg, 1999, *R. ecuadoriensis*, *R. pallescens* (Justi and Galvão 2017). These three species groups are currently recognized based on molecular data, distribution patterns, and morphometric analysis, and but not on qualitative morphological characters in the published literature (Dujardin et al. 1999; Lyman et al. 1999; Schofield and Dujardin 1999; Justi and Galvão 2017). The *pallescens* group is distributed to west of the Andes, whereas the *pictipes* and *prolixus* groups are mainly recorded to the east of the Andes (Abad-Franch and Monteiro 2007; Abad-Franch et al. 2009; Hernández et al. 2020).

The latest taxonomic revision of the entire genus was published approximately 40 years ago in the monograph on Triatominae by Lent and Wygodzinsky (1979) and contained descriptions of 11 of the 13 known species at that time. They regarded *R. amazonicus* as a synonym of *R. pictipes*, omitting *R. dalessandroi* because they were unable to examine specimens of this species. Bérenger and Pluot-Sigwalt (2002) and Rosa et al. (2017) made comparative studies between *R. pictipes* and *R. amazonicus* to prove the validity of *R. amazonicus.* The remaining seven species now included in *Rhodnius* were described after Lent and Wygodzinsky's (1979) monograph (Lent et al. 1993a; Mejia et al. 1999; Valente et al. 2001; Jurberg et al. 2009; Rosa et al. 2012; Abad-Franch et al. 2013; Souza et al. 2016). *Rhodnius taquarussuensis* Rosa et al., 2017a was described as a new species but is now considered a phenotypic form of *R. neglectus* instead of a distinct species (Nascimento et al. 2019). Bérenger and Pluot-Sigwalt (2002) published a key for the *pictipes* group and Galvão (2014) released a key in Portuguese which included 12 *Rhodnius* species.

Rhodnius is relatively easy to distinguish from other Triatominae genera because of its long head and coloration pattern but shows low non-genitalic morphological variability between species in the genus, which may account for the difficulties in species identification. The female external genitalia was described for most species of the subfamily (Lent 1948; Abalos and Wygodzinsky 1951; Sherlock and Serafim 1967), but their diagnostic importance was dismissed in papers published by Lent and Jurberg (1968, 1969, 1975) which considered them uniform and, not useful for specific identification. The resurrection of female genitalia, as an important taxonomic tool, was attributed to Rosa et al. (2010) through a detailed study by scanning electron microscopy. Subsequently, several studies corroborate the diagnostic value of female genitalia (Rosa et al. 2012, 2014, 2017b; Rodrigues et al. 2018). The male external genitalia are usually used for generic and specific differentiation in assassin bugs. All published species except *R. barretti* had been documented with the external male genitalia. However, most of these descriptions were restricted to describing or comparing the shapes of the median process of pygophore (Lent and Wygodzinsky 1979; Harry 1993; Lent et al. 1993a; Mejia et al. 1999; Valente et al. 2001; Rosa et al. 2012, 2017a, b; Souza et al. 2016). Six species (*R. zeledoni*, *R. marabaensis*, *R. milesi*, *R. montenegrensis*, *R. stali*, and *R. colombiensis*) had only detailed illustrations of non-everted phalli, thus restricting the possibility of comparison various structures on the phallosoma and endosoma, which may be helpful in species-level identifications (Lent et al. 1993a; Mejia et al. 1999; Valente et al. 2001; Rosa et al. 2012, 2017b; Zhao et at. 2015; Souza et al. 2016). Drawings of endosomal structures that show the individual sclerites rather than the complete everted endosoma were published for only three species, *R. stali*, *R. pictipes*, and *R. milesi* (Lent et al. 1993a; Valente et al. 2001).

When examining the specimens of *Rhodnius*, two specimens from Bolivia were distinctly different from any other species found. In this study, they are named *Rhodnius micki* sp. nov. and described. Male genitalia are important in identifying assassin bugs, especially for *Rhodnius* which has low non-genitalic morphological variability between species. Therefore, special emphasis is put on their everted phallus, allowing for detailed photographic documentation of the phallus, particularly the sclerites of the endosoma. The diagnosis of the new species takes advantage of qualitative morphological features including genitalic features, and of geometric morphometric approaches to better characterize head and forewing shapes. Combining morphometric characters with distribution, we propose that this new species should be classified in the *pictipes* group. We also provide a synopsis of genitalic terminology applied to Triatominae and offer preferred terms to facilitate future investigations into the homology of these structures across Triatominae and even Heteroptera.

Materials and methods

Specimens

Type specimens and an additional male specimen of *R. robustus* Larrousse, 1927 are deposited in The Natural History Museum (**NHMUK**), London, United Kingdom.

Specimens of *R. stali*, *R. pictipes*, *R. pallescens*, and *R. ecuadoriensis* which were used for the geometric analysis came from colonies reared at Fundação Oswaldo Cruz (FIOCRUZ) in Brazil and were deposited at Fundação Oswaldo Cruz (**FIOCRUZ**).

Dissections and measurements

After softening the abdomens of dried specimens with wet tissue, the pygophores were removed and soaked in 100% lactic acid overnight (Fig. 1). They were then boiled in 20% lactic acid solution for ~ 30 minutes to remove muscles (Fig. 2). Dissections were carried out in the lactic acid under a Motic binocular dissection microscope. At this point, the endosoma was gently stretched with a pair of forceps (Ideal-Tek SS.SA) and insect pins (0#). The tip of the pins should be blunt (Fig. 3). At first, we inserted the insect pin along the membrane of the endosoma from the opening where the endosoma is everting out, and then gently agitated the pin along the membrane from one side to the other to make the phallosoma loose and make the endosoma move towards the tip of phallosoma, so that the opening is big enough and the forceps would enable to touch the sclerites of endosoma without breaking the membrane (Figs 4, 5). Forceps were used to grasp the sclerite and to stretch the endosoma (Fig. 6). After taking the photographs and other procedures, the dissected genitalia were preserved in glycerol in plastic tubes which were pinned under the corresponding specimens. Measurements were made using a calibrated micrometer and given in millimeters.

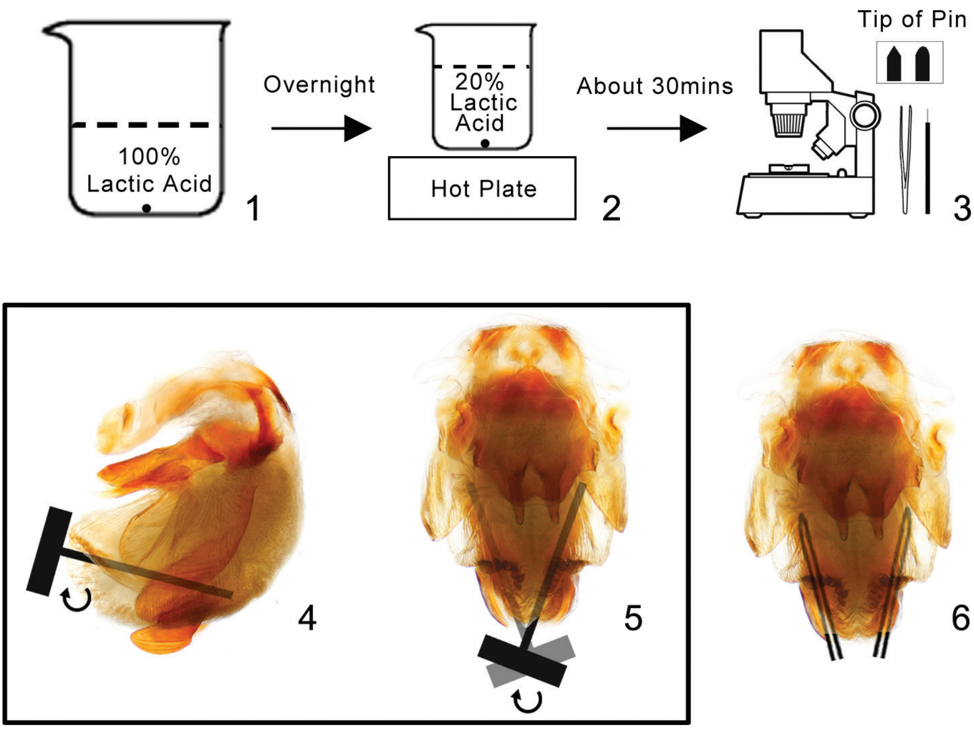

Figures 1–6. Process of dissection **1** soaking genitalia in 100% lactic acid overnight **2** boiling genitalia in 20% lactic acid solution for ~ 30 minutes **3–6** dissecting genitalia under microscope with forceps and blunted insect pin **4, 5** inserting the insect pin along the membrane of the endosoma and agitate the pin **6** using forceps to stretch the endosoma**.**

Terminology

Because of the inconsistent use of terminology in Triatominae, after reviewing many taxonomic and comparative morphology papers of assassin bugs, the terminology adopted in this paper are listed in Table 1. It includes the preferred terms, definition of terms, previously used terms, and references.

Images and image processing

Habitus images were obtained using a Canon EOS 7D and 60mm macro lens. Detail images of heads, pronota, and wings were obtained using a Microscope (Nikon SMZ18) with a Canon EOS 600D. Genital images were taken using an Olympus BX51 with a Canon EOS 450D. Images were stacked using the EOS Utility 2, and Helicon focus 5.3. Photographs were edited with Adobe Photoshop CS4, including adjustment of background color and cropping without modifying any characters. All the images were taken in the laboratory by the authors. The plate of male genitalia is that of the paratype.

Table 1. Terminology used in this study with synonyms from the literature.

Preferred term (abbreviation)	Definition	Previously used terms	References
Articulatory apparatus (AA)	System of plates and apodemes for suspension of phallus and attachment of its motor muscles	Articulatory apparatus (Apb) (apt)	Lent and Wygodzinsky 1979; Lent and Jurberg 1984; Lent and Jurberg 1987; Lent et al. 1993b; Mejia et al. 1999; Carcavallo et al. 2001; Valente et al. 2001; Sandoval et al. 2007; Jurberg et al. 2009; Forero et al. 2010; Berniker et al. 2011; Forero and Weirauch 2012; Gil-Santana and Galvão 2013; Jurberg et al. 2013; Castro-Huertas and Forero 2014; Gil-Santana 2017; Chłond et al. 2018
		Phallobase	Zhao et al. 2015
Basal plate (BP)	Paired major plates of articulatory apparatus	Basal plate (Plb)	Lent and Wygodzinsky 1979; Lent and Jurberg 1984; Lent and Jurberg 1987; Lent et al. 1993a; Mejia et al. 1999; Carcavallo et al. 2001; Valente et al. 2001; Cai and Tomokuni 2003; Weirauch 2008; Sandoval et al. 2007; Jurberg et al. 2009; Frías-Lasserre 2010; Forero et al. 2010; Berniker et al. 2011; Forero and Weirauch 2012; Rosa et al. 2012; Gonçalves et al. 2013; Jurberg et al. 2013; Zhao et al. 2015; Ishikawa and Naka 2016; Souza et al. 2016; Rosa et al. 2017a; Chłond et al. 2018; Oliveira et al. 2018
		Basal plate arm (bpa)	Gil-Santana 2017
		Basal arm	Gil-Santana and Galvão 2013
Basal plate extension (BPE)	Ventral sclerite arising from the basal plate	Basal plate extension (bpe)	Weirauch 2008; Berniker et al. 2011; Forero and Weirauch 2012; Oliveira et al. 2018
		Pedicel (ped) (pd)	Cai and Tomokuni 2003; Gil-Santana and Galvão 2013; Castro-Huertas and Forero 2014; Zhao et al. 2015; Gil-Santana 2017
		Median (Medium) extension of the basal plate (EPlb) (MeBp)	Lent and Jurberg 1984; Lent and Jurberg 1987; Lent et al. 1993a, b; Mejia et al. 1999; Carcavallo et al. 2001; Valente et al. 2001; Sandoval et al. 2007; Jurberg et al. 2009; Frías-Lasserre 2010; Rosa et al. 2012; Souza et al. 2016; Rosa et al. 2017a
		Median basal plate	Gonçalves et al. 2013
		Plate extension (pext)	Forero et al. 2010
Distal dorsal sclerite of endosoma (DDSEn)	Paired or single sclerite on the tip of endosoma which is on the dorsal side of the distal ventral sclerite	Process of endosoma	Jurberg et al. 2009
		Processes of endosoma 1 (PrEn 1)	Valente et al. 2001
		Processes of endosoma 2 (PrEn 2)	Lent et al. 1993a; Mejia et al. 1999
Distal ventral sclerite of endosoma (DVSEn)	A single sclerite on the tip of endosoma which is on the ventral side of the distal ventral sclerite	Processes of endosoma	Jurberg et al. 2009
		Processes of endosoma 1 (PrEn 1)	Lent et al. 1993a; Mejia et al. 1999
		Processes of endosoma 2 (PrEn 2)	Valente et al. 2001
Dorsal phallothecal sclerite (DPS)	Sclerotized proximal part of phallosoma	Dorsal phallothecal sclerite (dps)	Cai and Tomokuni 2003; Weirauch 2008; Forero et al. 2010; Berniker et al. 2011; Forero and Weirauch 2012; Castro-Huertas and Forero 2014; Zhao et al. 2015; Ishikawa and Naka 2016; Gil-Santana 2017; Chłond et al. 2018; Lapischies et al. 2019
		Phallosoma (Ph)	Lent and Jurberg 1984; Lent and Jurberg 1987; Lent et al. 1993a, b; Mejia et al. 1999; Carcavallo et al. 2001; Valente et al. 2001; Sandoval et al. 2007; Jurberg et al. 2009; Rosa et al. 2012; Gonçalves et al. 2013; Jurberg et al. 2013; Souza et al. 2016; Rosa et al. 2017a, b; Oliveira et al. 2018
		Dorsal phallotheca plate	Lent and Wygodzinsky 1979; Gil-Santana and Galvão 2013
		Phallotheca plate	Frías-Lasserre 2010

Preferred term (abbreviation)	Definition	Previously used terms	References
Dorsal sclerites of pygophore (DSPr)	Posterior dorsal sclerotization of pygophore	Dorsal sclerotization of genital opening, tergite 9 (t9)	Forero and Weirauch 2012
Endosoma (En)	Distal portion of phallus which can be reverted	Endosoma	Lent and Wygodzinsky 1979; Lent and Jurberg 1984; Lent and Jurberg 1987; Lent et al. 1993a, b; Mejia et al. 1999; Carcavallo et al. 2001; Valente et al. 2001; Cai and Tomokuni 2003; Jurberg et al. 2009; Frías-Lasserre 2010; Forero and Weirauch 2012; Jurberg et al. 2013; Castro-Huertas and Forero 2014; Zhao et al. 2015; Ishikawa and Naka 2016; Souza et al. 2016; Rosa et al. 2017a; Oliveira et al. 2018; Lapischies et al. 2019
Lateral flap-like prolongation of phallosoma (LFPPh)	Paired of sclerite on the lateral side of phallosoma	Lateral flat-like prolongation of the phallosoma	Forero and Weirauch 2012
		Processes of the conjunctiva 1 (PrCj 1)	Lent et al. 1993a; Mejia et al. 1999; Valente et al. 2001
		Processes of the conjunctiva	Jurberg et al. 2009
Mandibular plate	Laterad of clypeus and dorsad of maxillary plate	Mandibular plate	Weirauch 2008; Berniker et al. 2011; Ishikawa and Naka 2016
		Jugum	Lent and Wygodzinsky 1979; Lent et al. 1993a; Carcavallo et al. 2001; Gonçalves et al. 2013; Souza et al. 2016
Maxillary pate	Ventral to mandibular plate	Maxillary plate	Weirauch 2008; Berniker et al. 2011; Castro-Huertas and Forero 2014; Ishikawa and Naka 2016
		Gena (ge)	Lent and Wygodzinsky 1979; Lent et al. 1993a; Carcavallo et al. 2001; Sandoval et al. 2007; Jurberg et al. 2009; Gonçalves et al. 2013; Souza et al. 2016; Rosa et al. 2017a; Chłond et al. 2018; Oliveira et al. 2018
Medial basal sclerite of phallosoma (MBSPh)	Basal part of a phallosoma, often sclerotized	Vesica (V)	Lent and Wygodzinsky 1979; Lent and Jurberg 1987; Carcavallo et al. 2001; Cai and Tomokuni 2003; Sandoval et al. 2007; Gonçalves et al. 2013; Jurberg et al. 2013
		Median distal process	Gil-Santana and Galvão 2013
		Median process of endosoma	Gil-santana 2014
		Central sclerite of endosoma (cs)	Lapischies et al. 2019
		Median basal sclerotization (mbs)	Forero et al. 2010; Berniker et al. 2011
		Processes of conjunctiva 2	Lent et al. 1993a; Mejia et al. 1999
		Dorsobasal large sclerite	Ishikawa et al. 2007
Median process of pygophore (MPPy)		Median process of (the) pygophore (PrP)	Lent and Wygodzinsky 1979; Lent and Jurberg 1984; Lent et al. 1993a, b; Mejia et al. 1999; Carcavallo et al. 2001; Valente et al. 2001; Sandoval et al. 2007; Jurberg et al. 2009; Forero et al. 2010; Rosa et al. 2012; Gil-Santana and Galvão 2013; Castro-Huertas and Forero 2014; Souza et al. 2016; Rosa et al. 2017a; Oliveira et al. 2018
		Median pygophore process	Cai and Tomokuni 2003; Zhao et al. 2015
Phallosoma (Ph)	Proximal portion of phallus, between basal plate and endosoma.	Phallosoma	Lent and Wygodzinsky 1979; Forero and Weirauch 2012; Castro-Huertas and Forero 2014; Zhao et al. 2015
		Conjunctive	Lent and Jurberg 1984; Lent and Jurberg 1987; Lent et al. 1993a, b; Mejia et al. 1999; Carcavallo et al. 2001; Valente et al. 2001; Sandoval et al. 2007; Jurberg et al. 2009; Rosa et al. 2012; Gonçalves et al. 2013; Souza et al. 2016; Rosa et al. 2017a

Preferred term (abbreviation)	Definition	Previously used terms	References
Phallus (P)	Intromittent organ inside the pygophore	Phallus (Ph) (P)	Lent and Jurberg 1984; Lent and Jurberg 1987; Lent et al. 1993a, b; Mejia et al. 1999; Carcavallo et al. 2001; Valente et al. 2001; Cai and Tomokuni 2003; Ishikawa et al. 2007; Sandoval et al. 2007; Weirauch 2008; Jurberg et al. 2009; Frías-Lasserre 2010; Forero et al. 2010; Forero and Weirauch 2012; Rosa et al. 2012; Gonçalves et al. 2013; Gil-Santana and Galvão 2013; Jurberg et al. 2013; Castro-Huertas and Forero 2014; Zhao et al. 2015; Ishikawa and Naka 2016; Souza et al. 2016; Rosa et al. 2017a; Gil-Santana 2017; Oliveira et al. 2018; Lapischies et al. 2019
		Aedeagus	Lent and Wygodzinsky 1979
Struts	Paired sclerites on the ventral side of dorsal phallothecal sclerite	Struts (str)	Lent and Wygodzinsky 1979; Cai and Tomokuni 2003; Forero et al. 2010; Gonçalves et al. 2013; Gil-Santana and Galvão 2013; Zhao et al. 2015
		Phallosoma support (Sph)	Lent and Jurberg 1984; Lent and Jurberg 1987; Lent et al. 1993b; Carcavallo et al. 2001; Sandoval et al. 2007; Jurberg et al. 2013; Oliveira et al. 2018
		Struts of phallus	Ishikawa and Naka 2016
Synthlipsis	Minimum interocular distance	Synthlipsis	Lent and Wygodzinsky 1979; Valente et al. 2001; Sandoval et al. 2007; Jurberg et al. 2013; Zhao et al. 2015
		Interocular space	Ishikawa and Naka 2016; Gil-Santana 2017
		Interocular region	Valente et al. 2001; Jurberg et al. 2013
Transverse bridge of basal plate (TBBP)	Connection between two basal plate	Basal plate; Bridge (bpb)	Lent and Wygodzinsky 1979; Cai and Tomokuni 2003; Berniker et al. 2011; Castro-Huertas and Forero 2014; Ishikawa and Naka 2016; Gil-Santana 2017
		Basal bridge (PB)	Lent and Jurberg 1984; Lent and Jurberg 1987; Lent et al. 1993; Mejia et al. 1999; Carcavallo et al. 2001; Valente et al. 2001; Sandoval et al. 2007; Gonçalves et al. 2013; Gil-Santana and Galvão 2013; Jurberg et al. 2013
Transverse bridge of pygophore (TBPy)	Anterior dorsal sclerotization of pygophore	Transverse bridge of the pygophore (br)	Forero and Weirauch 2012; Castro-Huertas and Forero 2014
Ventral sclerite of phallosoma (VSPh)	Paired of sclerites on the ventral side of phallosoma	Processes of the conjunctiva 2 (PrCj 2)	Valente et al. 2001
		Processes of the conjunctiva (PrCj)	Lent et al. 1993b
		Processes of the conjunctiva 3 (PrCj 3)	Mejia et al. 1999

Morphometrics

In total, 42 specimens of five species, *R. ecuadoriensis* (ten specimens), *R. pallescens* (ten specimens), *R. pictipes* (ten specimens), *R. stali* (ten specimens), and *R. micki* sp. nov. (two specimens), were used in the analysis. and nine anatomical landmarks were extracted respectively on the heads and forewings. Thirteen landmarks of head (type II points, which combine geometric and biological or histological descriptions) (Gurgel-Gonçalves et al. 2008; Oliveira et al. 2017), and nine landmarks of wings (type I points, which homology comes from unique patterns in biological form) (Gurgel-Gonçalves et al. 2008; Feliciangeli et al. 2007; Costa et al. 2009; Oliveira et al. 2017) were extracted based on the landmarks used in previous works. These landmarks were digitized with tpsUtil 1.46 (Rohlf 2010) and tpsdig2 v.2.16 (Rohlf 2008). To quantify the shape variation related with the shape dimensions, the digitized data were analyzed using morphoJ 1.06d (Klingenberg 2011). Variability in the shape space was assessed using a Principal Component Analysis (PCA). To better visualize the shape variation, thin plate spline visualization was used to get the average shapes of these characters.

Taxonomy

Reduviidae Latreille, 1807
Triatominae Jeannel, 1919

***Rhodnius* Stål, 1859**

Type of genus. *Rhodnius prolixus* Stål, 1859.

***Rhodnius micki* sp. nov.**
http://zoobank.org/226A56E5-FDF8-4850-9426-80B3C4D79FC5

Type materials. Bolivia: Santa Cruz, Saavedra, C.J. Pruett [leg.], 1 male holotype, 10.v.1989, 1 male paratype, 1.iii.1989 (NMHUK).

Diagnosis. General coloration dark brown. Head relatively short, only slightly longer than the pronotum. Eyes small, width of the eye shorter than the synthlipsis. Central area of the anterior lobe of the pronotum conspicuously dark and its humeral angle of the posterior lobe relatively sharply curved. Legs brown. The median process of the pygophore long and bifid on the tip. The medial basal sclerite of the phallosoma with two straight and flat projections. One distal dorsal sclerite of the endosoma bifurcated, and its tip rounded and curved slightly inward.

Description. ***Coloration.*** Body generally dark brown. Head with light median longitudinal stripe extending from the apex of clypeus to the posterior portion of ocelli; eyes blackish; middle of third segment and posterior half of forth segment yellow; a pair of black stripes on the dorsal surface of neck, half of lateral side and ventral side dark. Pronotum with a pair of submedian carinae and lateral margin yellow; concave areas on anterior lobe, especially the central area darkened; posterior lobe dark with scattered irregular small yellow spots. Scutellum dark with a yellow "Y"-shaped ridge; the tip of scutellar process white. Hemelytra generally brown and mottled; corium with small lightly colored spots; membrane with narrowly rimmed pale-yellow veins, area between veins with scattered light color spots. Legs mottled with yellow spots; tarsi yellowish (Fig. 7). Connexivum dark and mottled with yellow spots, posterior one fourth of every segment almost yellow; ventral surface of the abdomen yellowish with scattered irregular dark brown spot; sternites light brown to black, with irregular dark brown spots, center of sternite II and a pair of sublateral elliptical spots of each segment dark (Fig. 9); spiracles with a brown narrowly margin (Fig. 8).

Structure. ***Head.*** Elongated and granulose, almost 2.5 × as long as width across eyes (1:2.6–2.59), slightly longer than length of pronotum (1:1.17–1.21); apex of

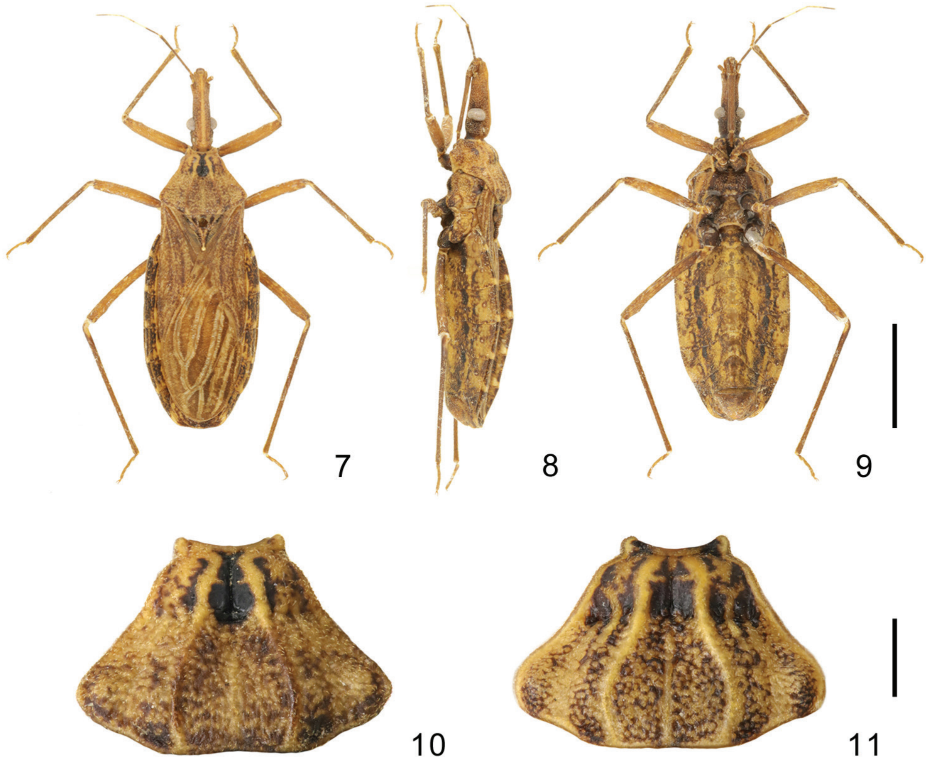

Figures 7–11. 7–9 holotype of *Rhodnius micki* sp. nov. **11** *Rhodnius stali* Lent, Jurberg & Galvão, 1993 **7** dorsal side **8** lateral side **9** ventral side **10, 11** pronotum. Scale bars: 5.00 mm (**7–9**); 1.00 mm (**10, 11**)

maxillary plate surpassing clypeus; anteocular region ~ 3 × as long as postocular region in length (1: 2.84–3.15); eyes small, width of eye in dorsal view shorter than synthlipsis (1:0.60); in lateral view, eyes far away from upper surface of head and approaching to lower surface; ratio of antennal segments 1:5.11–6.29:4.66–5.14:3.55–4.43; first labial segment proceeding toward antenniferous tubercle and second labial segment approaching to posterior margin of head. Ratio of labial segments 1:2.78–3.13:0.61–0.83. ***Thorax.*** Anterolateral angles triangle-like. Surface of pronotum granulose, length of posterior pronotal lobe ~ 2 × as that of anterior lobe (1:1.89–1.93); posterior pronotal lobe ~ 1.5 ×as wide as anterior lobe (1:1.52–1.74); median longitudinal furrow of anterior lobe deep on the median transverse furrow; humeral angles sharply curved relatively to other species of ***Rhodnius*** (Fig. 10). Scutellum triangular with a yellow Y-shaped ridge; subapical portion with a cone-shaped process. Pleura of meso- and metathoraxes winkled. Legs long and slender. Hemelytra approaching tip of abdomen. ***Male genitalia*** (Figs 12–26). Pygophore (Figs 12–14) globular with a tubercle on the bottom of the ventral surface (Fig. 13); transverse bridge of pygophore (TBPy) strongly sclerotized and narrow; a pair of dorsal sclerites of genital opening (DSPr) large; median process of pygophore (MPPy) long, bifid at apical portion and tilting 45 degrees to the dorsal side in lateral view. Parameres (Figs 15, 16) strongly curved

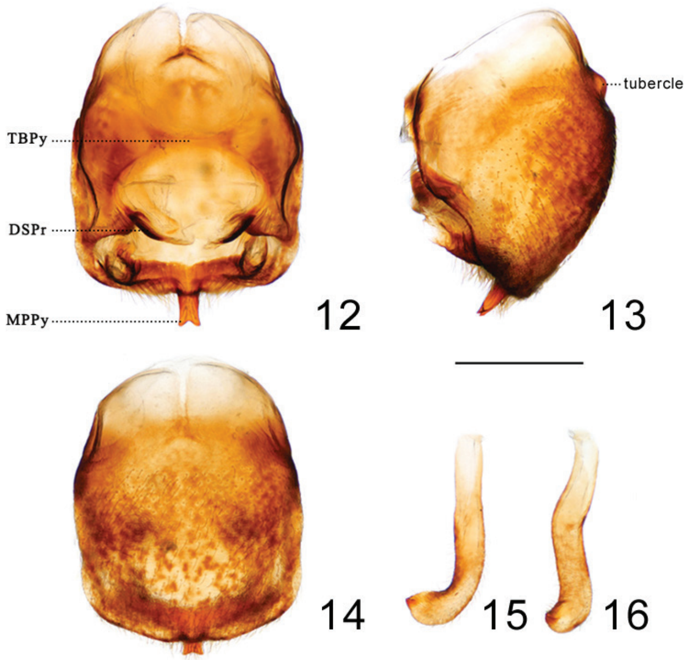

Figures 12–16. Pygophore and paramere of paratype of *Rhodnius micki* sp. nov. **12–14** pygophore **12** dorsal view **13** lateral view **14** ventral view **15, 16** paramere: **15** dorsal view **16** lateral view. Scale bars: 1.00 mm. Abbreviations: **DSPr** dorsal sclerites of pygophore **MPPy** Median process of pygophore **TBPy** Transverse bridge of pygophore.

at apex and with a denticle. Basal plate (BP) hexagonal in dorsal view, diameter of the arms similar to that of the transverse bridge of basal plate (TBBP) (Fig. 17); basal plate extension (BPE) short and approximately half shorter to arms of basal plate in length (Figs 18, 21); dorsal phallothecal sclerite (DPS) flat, as a subrectangular with round angles; medial basal sclerite of phallosoma (MBSPh) bifid with two straight and flat projections (Figs 17, 18, 20, 21), and both of them slightly swelled at base; lateral flap-like prolongation of phallosoma (LFPPh) large (Figs 17–22); two ventral sclerites of phallosoma (VSPh) elongated ovoid (Figs 17–22); the tip of non-everted phallus slightly sclerotized on the dorsal and lateral surface, and the surface of the phallosoma with indistinct stripes (Figs 17, 18); distal dorsal sclerite of endosoma (DDSEn) bifurcated, tips rounded, and curved inward lightly (Figs 20, 21, 24); distal ventral sclerite of the endosoma (DVSEn) smaller than the dorsal sclerite and bifurcated with two projections set far apart (Figs 21–23). The membrane of endosoma on the dorsal surface wrinkled and a bit thicker than other part of membrane.

Etymology. The species epithet is named in honor of Mr. Mick Webb (NHMUK), who had helped us in many ways in the study of Hemiptera.

Measurements. [in mm, ♂ (n = 2)] Total length to tip of abdomen 17.20–17.33. Length of head (exclude neck) 3.21–3.55; width of head 1.40–1.43; length of anteocular 2.27–2.30; length of postocular 0.73–0.80; width of eye 0.40–

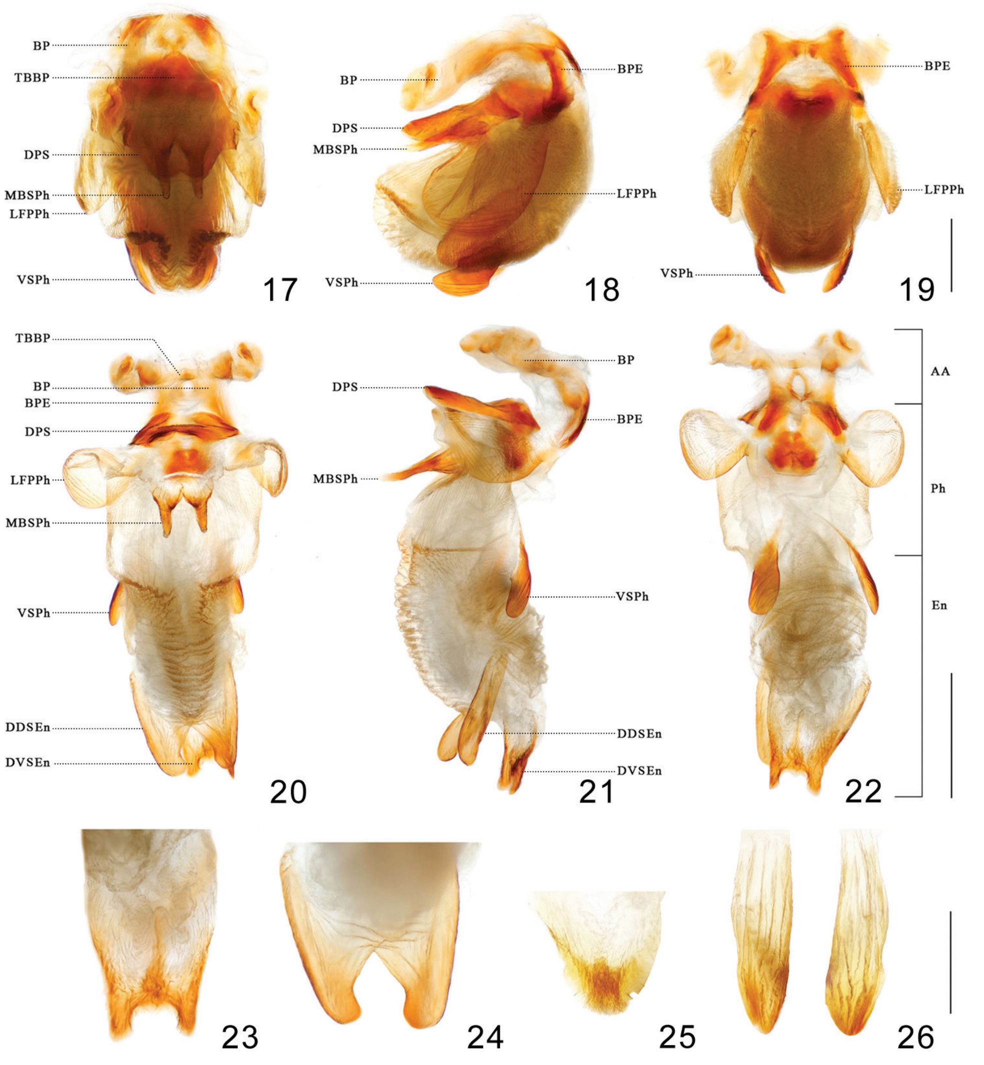

Figures 17–26. Pallus **17–24** *Rhodnius micki* sp. nov. **25, 26** *Rhodnius robustus* **17–19** non-everted phallus **20–26** everted phallus **17, 20** dorsal side **18, 21** lateral side **19, 22** ventral side **23, 25** distal ventral sclerite of endosoma **24, 26** distal dorsal sclerite of endosoma. Scale bars: 1.00 mm (**11–16**); 0.50 mm (**17–20**). Abbreviations: **BP** basal plate **TBBP** transverse bridge of basal plate **DPS** dorsal phallothecal sclerite **MBSPh** medial basal sclerite of phallosoma **LFPPh** lateral flat-like prolongation of phallosoma **VSPh** ventral sclerite of phallosoma **BPE** basal plate extension **DDSEn** distal dorsal sclerite of endosoma **DVSEn** distal ventral sclerite of the endosoma **AA** articulatory apparatus **Ph** phallosoma **En** endosoma.

0.44; length of synthlipsis 0.67–0.73. Length of antennal segments I–IV=0.35–0.45/2.20–2.30/1.80–2.10/1.55–1.60; length of visible labial segments I–III=0.80–0.90/2.50/0.60. Length of anterior lobe of pronotum 0.90–0.93; length of posterior pronotal lobe 1.70–1.93; width of anterior pronotal lobe 2.30–2.33; width of posterior pronotal lobe 4.00–4.15. Length of scutellum 1.70–1.75; width of scutellum 1.80–1.90; length of hemelytron 10.40–10.50. Width of abdomen 5.35–5.40. (all

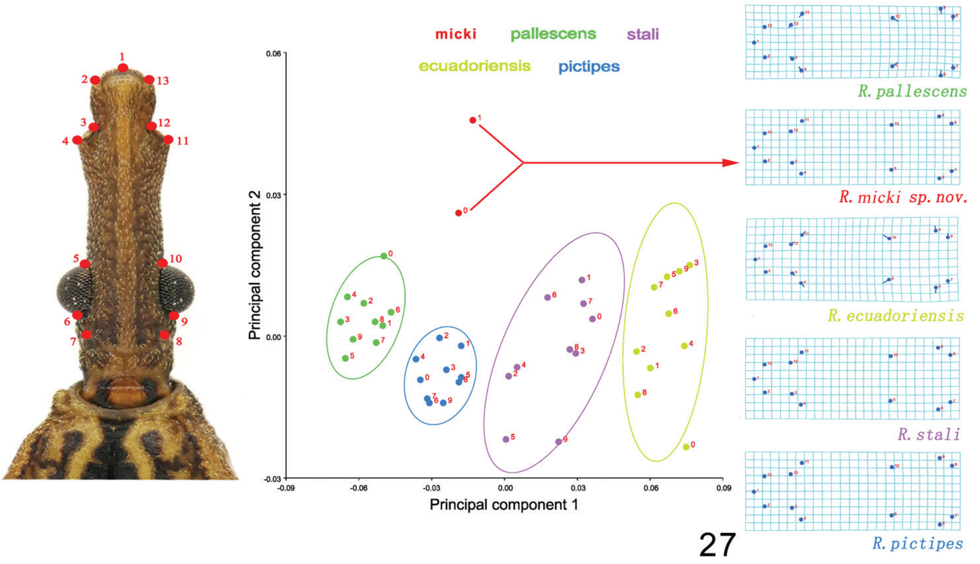

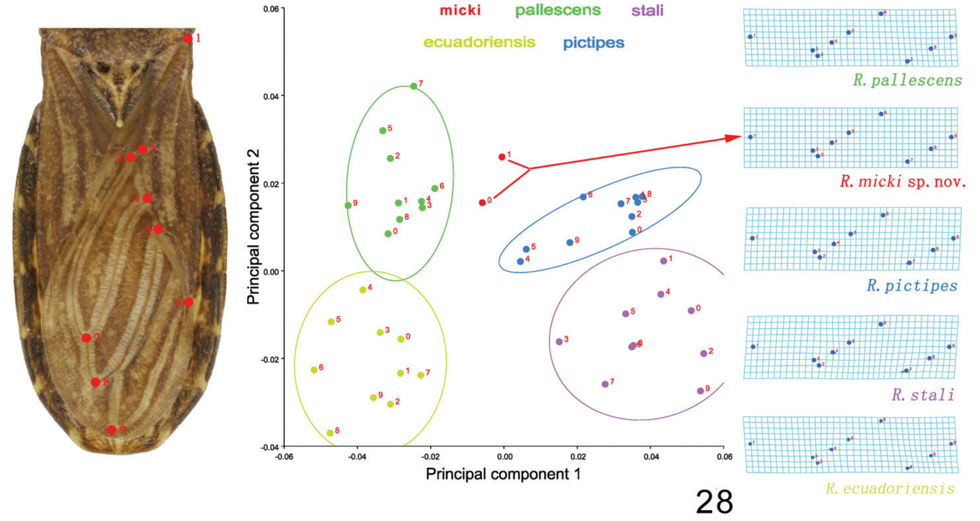

Figures 27, 28. Morphological variations of five *Rhodnius* species based on Principal Component Analysis. The 90% equal frequency ellipses containing approximately 90% of the data points are shown. The thin-plate splines show the average shape for each species, corresponding to the deformation of the landmarks compared with the origin (the average shape of all species) **27** head **28** fore wing.

the former numbers are for holotype, except length of total, anteocular, second and fourth segment, and width of abdomen).

Additional material. *Rhodnius robustus* Larrousse, 1927 (1♂, Brazil: Belém, Instituto Evandro Chagas, reared in lab, 20.II.1992) (NHMUK).

Geometric morphometrics (Figs 27, 28) On the one hand, *R. pictipes* and *R. stali* appear to be the most morphologically similar species to *R. micki* sp. nov. having relatively short head, only slightly longer than the pronotum, and a defined transverse sulcus on their pronotum. On the other hand, *Rhodnius ecuadoriensis*, *R. pallescens*, *and R. micki* sp. nov. do not have dark rings on the tibiae which is a significant diagnostic character of *Rhodnius*. Based on the morphometrics of the head and the particular coloration of the legs, we compared before mentioned four species to *R. micki* sp. nov. For head shape analysis (Fig. 27), the contribution of the first principal (PC1) component accounted for 81.79% of the total variation, whereas the second principal component (PC2) accounted for 6.26%. In the factorial map, five species were separated. The type specimens of *R. micki* sp. nov. were far away from the others. The thin plate spline visualization showed that the fifth and tenth landmarks located on the anterior margin of eye contributed most to the shape difference among these species. The size of the eye and the length of the anteocular and postocular regions might be the most significant differences among them. For wing vein analysis (Fig. 28), the contribution of the first principal (PC1) component accounted for 58.46% of the total variation and the second principal component (PC2) accounted for 22.21%. The points of *R. micki* sp. nov. were also distinct from those of the other four species, and these four species were separated from each other too. The thin plate spline visualization showed that the seventh landmark contributed most to the shape difference among these species. It implied that the position of the intersection of the Cu and An1 veins may be the most variable among them.

Discussion

Comparison with other species

It is relatively easy to distinguish this species from other *Rhodnius* species because of its relatively sharply curved humeral angles and unique color pattern. *Rhodnius stali* and *R. pictipes* are similar to *R. micki* sp. nov. because their heads are all relatively short, only slightly longer than their pronota, and their pronota have a defined transverse sulcus. However, the tibiae of *R. micki* sp. nov. are uniformly dark brown, the humeral angle is sharply curved (Fig. 10), and the third antennal segment is black, whereas the other two both have a distinct dark ring on each tibia, only the anterior half of the third antennal segment is black, and the humeral angle is broadly rounded (Fig. 11). *Rhodnius ecuadoriensis* and *R. pallescens* do not have any tibial rings. *Rhodnius ecuadoriensis* is smaller than *R. micki* sp. nov., and the head of *R. pallescens* is obviously longer than the pronotum. *Rhodnius micki* sp. nov. is darker and its submedian carinae on the posterior lobe are not obvious; the posterior quarter of every connexival segment on the dorsal side is yellow. Differences between *R. micki* sp. nov. and the other species in the male genitalia are significant. The median processes of the pygophore of *R. micki* sp. nov., *R. stali*, and *R. pictipes* are bifid, but the former one is bifid at its tip, with small projections, whereas the median processes of the pygophores of *R. stali* and *R. pictipes* are bifid (Lent et al. 1993a) at the base with long projections, and those of *R. ecuadoriensis* and *R. pallescens* are not bifid (Lent and Wygodzinsky 1979; Mejia et al. 1999). The parameres of *R. micki* sp. nov. are narrower than those of *R. stali* and *R. pictipes* (Lent et al. 1993). The medial basal sclerite of its phallosoma (MBSPh) is bifid with two flat and straight arms; other *Rhodnius* species do not have a medial basal sclerite or it is not bifid (Y. Zhao unpublished data). The distal ventral sclerite of the endosoma (DVSEn) of *R. micki* sp. nov. is smaller and less sclerotized than those in *R. stali* and *R. pictipes* (Lent et al. 1993a), and the distal dorsal sclerite (DDSEn) is bifurcated deeply, curved inward, and more heavily sclerotized than *R. ecuadoriensis* and *R. pallescens* (our unpublished data). Therefore, Genitalic structures, especially distal ventral sclerite of the endosoma (DVSEn) and distal dorsal sclerite of the endosoma (DDSEn), can provide more information to fully compare the species of *Rhodnius*. According to geometric morphological analysis, *R. micki* sp. nov. is relatively isolated on the factorial map, which suggests that the *R. micki* sp. nov. is also distinguished from those species relatively easily based on the shapes of the head and wing.

Species group assignment

Rhodnius micki sp nov. is known from Santa Cruz, Bolivia, where some species of *pictipes* group and *prolixus* group, i.e., *R. stali*, *R. pictipes*, and *R. robustus* are distributed (Chávez 2006; Schofield and Galvão 2009; Justi et al. 2010; Soto-Vivas et al. 2018). *Rhodnius stali* and *R. pictipes*, which are the most similar species to *R. micki* sp. nov. based on the non-genitalic characters mentioned above, both belong to the *pictipes* group. With respect to genitalic characters, they are also similar because they all have a single distal dorsal sclerite on the endosoma (Lent et al. 1993a). Based on our observations (unpublished), species in the *prolixus* group, such as *R. robustus*, have two symmetrical sclerites located in the same position, and the shape of the ventral sclerite of endosoma is triangle (Figs 25, 26). Therefore, we infer that *R. micki* sp. nov. should be included in the *pictipes* group based on distribution and genitalic characters.

Terminology of morphological characters

Historically, the terminology of Triatominae, especially male genitalic terms, has developed at least partially in isolation from that of Reduviidae. A plethora of terms have been used for homologous genitalic structures, and in some cases different structures have used the same name. This inconsistency results in incompatible and sometimes misleading terminology for taxonomic descriptions and diagnoses. For example, some researchers have variously used the terms aedeagus, phallus, phallosoma, conjunctiva and phallothecal plate when describing the apical apart of the intromittent organ, and the sclerotized plate beneath the basal plate (Lent and Wygodzinsky 1979; Mejia et al. 1999; Valente et al. 2001; Jurberg et al. 2009; Rosa et al. 2012; Gil-Santana and Galvão 2013; Souza et al. 2016; Oliveira et al. 2018). To avoid ambiguity and achieve consistency with the description of other assassin bugs, we adopt the following terms in this study. Male genitalia consist of pygophore, parameres, and phallus. The articulatory apparatus is composed of basal plate, basal plate bridge, and basal plate extension. The dorsal phallothecal sclerite (DPS) is regarded as the dorsal part of phallosoma. To clarify each sclerite's position, we rename these sclerites with adjectives describing their position, while being as consistent as possible with previous terms. We adopt medial basal sclerite of phallosoma to denote the sclerite on the dorsal side of phallosoma. Two pairs of sclerites on the lateral and ventral sides of phallosoma are called lateral flat-like prolongation of phallosoma (LFPPh) and ventral sclerite of phallosoma (VSPh) respectively. Sclerites at the tip of the endosoma are renamed distal dorsal sclerite of endosoma (DDSEn) and distal ventral sclerite of endosoma (DVSEn). All the preferred terms and synonyms are shown in Table 1.

Acknowledgements

We are grateful to Christiane Weirauch, her lab members, and Dimitri Forero for kindly reviewing the manuscript and greatly improving the final version. Special thanks to Carolina Dale for offering photos and kindly reviewing the manuscript. This research is financially supported by the National Natural Science Foundation of China (Nos. 31730086, 31772498).

References

Abad-Franch F, Monteiro FA (2007) Biogeography and evolution of Amazonian triatomines (Heteroptera: Reduviidae): implications for Chagas disease surveillance in humid forest ecoregions. Memórias do Instituto Oswaldo Cruz 102(1): 57–70. https://doi.org/10.1590/S0074-02762007005000108

Abad-Franch F, Palomeque FS, Aguilar VHM, Miles MA (2005) Field ecology of sylvatic *Rhodnius* populations (Heteroptera, Triatominae): risk factors for palm tree infestation in western Ecuador. Tropical Medicine and International Health 10(12): 1258–1266. https://doi.org/10.1111/j.1365-3156.2005.01511.x

Abad-Franch F, Monteiro FA, Jaramillo O, Gurgel-Gonçalves R, Dias FBS, Diotaiuti L (2009) Ecology, evolution, and the long-term surveillance of vector-borne Chagas disease: A multi-scale appraisal of the tribe Rhodniini (Triatominae). Acta Tropica 110(2–3): 159–77. https://doi.org/10.1016/j.actatropica.2008.06.005

Abad-Franch F, Pavan MG, Jaramillo O, Palomeque FS, Dale C, Chaverra D, Monteiro FA (2013) *Rhodnius barretti*, a new species of Triatominae (Hemiptera: Reduviidae) from western Amazonia. Memórias do Instituto Oswaldo Cruz 108(1): 92–99. https://doi.org/10.1590/0074-0276130434

Abalos JW, Wygodzinsky P (1951) Las Triatominae Argentinas (Reduviidae, Hemiptera). Instituto Médico Regional de Tucumán. Publicacíon 601, Monografia 2: 1–179.

Barrett TV (1991) Advances in triatomine bug ecology in relation to Chagas disease. In: Harris KF (Ed) Advances in Disease Vector Research. Springer, New York, 8: 143–176. https://doi.org/10.1007/978-1-4612-3110-3_6

Barnabé C, Brenière SF, Guégan JF, Blanchet D, Aznar C (2018) Molecular characterization of Rhodnius robustus specimens, potential vectors for Chagas disease in French Guiana, South America. Infection, Genetics and Evolution 59: 28–31. https://doi.org/10.1016/j.meegid.2018.01.019

Bern C, Kjos S, Yabsley MJ, Montgomery SP (2011) *Trypanosoma cruzi* and Chagas' Disease in the United States. Clinical Microbiology Reviews 24: 655–681. https://doi.org/10.1128/CMR.00005-11

Bérenger JM, Pluot-Sigwalt D (2002) *Rhodnius amazonicus* Almeida, Santos & Sposina, 1973, bona species, close to *R. pictipes* Stål, 1872 (Heteroptera, Reduviidae, Triatominae). Memórias do Instituto Oswaldo Cruz 97: 73–77. https://doi.org/10.1590/S0074-02762002000100011

Berniker L, Szerlip S, Forero D, Weirauch C (2011) Revision of the *crassipes* and *pictipes* groups of *Apiomerus* Hahn (Hemiptera: Reduviidae: Harpactorinae). Zootaxa 2949: 1–113. https://doi.org/10.11646/zootaxa.2949.1.1

Cai W, Tomokuni M (2003) *Camptibia obscura*, gen. and sp. nov. (Heteroptera: Reduviidae: Harpactorinae) from China. European Journal of Entomology 100(1): 181–185. https://doi.org/10.14411/eje.2003.028

Carcavallo RU, Jurberg J, Lent H, Galvão C, Steindel M, Pinto CJC (2001) Nova espécie do complexo *oliveirai* (nova denominação para o complexo *matogrossensis*) Hemiptera, Reduviidae, Triatominae) do estado do Rio Grande do Sul, Brasil. Memórias do Instituto Oswaldo Cruz 96: 71–79. https://doi.org/10.1590/S0074-02762001000100008

Carcavallo RU, Rodríguez MEF, Salvatella R, Curto de Casas SI, Sherlock IA, Galvão C, Rocha DS, GalíndezGirón I, Arocha MAO, Martinez A, Rosa JA, Canale DM, Farr TH, Barata JMS (1998) Habitats and related fauna. In: Carcavallo RU, Girón IG, Jurberg J, Lent H (Eds) Atlas of Chagas' Disease Vectors in the Americas (Vol. 2). Fiocruz, Rio de Janeiro, 561–600.

Castro-Huertas V, Forero D (2014) First record of the genus *Tagalis* Stål, 1860 (Hemiptera: Reduviidae: Saicinae) from Colombia with the description of two new species. Zootaxa 3838(4): 475–485. https://doi.org/10.11646/zootaxa.3838.4.6

Chagas C (1909) Nova tripanozomiaze humana: estudos sobre a morfolojia e o cicloevolutivo do *Schizotrypanum cruzi* n. gen, n. sp., ajente etiolojico de nova entidade morbida do homem. Memórias do Instituto Oswaldo Cruz 1: 159–218. https://doi.org/10.1590/S0074-02761909000200008

Chávez J (2006) Contribución al estudio de los triatominos del Perú: Distribución geográfica, nomenclatura y notas taxonómicas. Anales de la Facultad de Medicina 67(1): 65–76. https://doi.org/10.15381/anales.v67i1.1296

Chłond D, Guilbert E, Faille A, Baňař P, Davranoglou L-R (2018) A remarkable new species of cavernicolous Collartidini from Madagascar (Hemiptera: Heteroptera: Reduviidae). Zootaxa 4425(2): 372–384. https://doi.org/10.11646/zootaxa.4425.2.11

Costa J, Peterson AT, Dujardin JP (2009) Morphological evidence suggests homoploid hybridization as a possible mode of speciation in the Triatominae (Hemiptera, Heteroptera, Reduviidae). Infection, Genetics and Evolution 9: 263–270. https://doi.org/10.1016/j.meegid.2008.12.005

Dujardin JP, Chavez T, Moreno JM, Machane M, Noireau F, Schofield CJ (1999) Comparison of Isoenzyme Electrophoresis and Morphometric Analysis for Phylogenetic Reconstruction of the Rhodniini (Hemiptera: Reduviidae: Triatominae). Journal of Medical Entomology 36: 653–659. https://doi.org/10.1093/jmedent/36.6.653

Feliciangeli MD, Sanchez-Martin M, Marrero R, Davies C, Dujardin JP (2007) Morphometric evidence for a possible role of *Rhodnius prolixus* from palm trees in house re-infestation in the State of Barinas (Venezuela). Acta Tropica 101: 169–177. https://doi.org/10.1016/j.actatropica.2006.12.010

Forero D, Weirauch C (2012) Comparative genitalic morphology in the New World resin bugs Apiomerini (Hemiptera, Heteroptera, Reduviidae, Harpactorinae). Deutsche Entomologische Zeitschrift 59: 5–41.

Forero D, Berniker L, Szerlip S (2010) A polychromatic new species of *Apiomerus* (Hemiptera: Reduviidae: Harpactorinae) from Central America. Zootaxa 2522: 44–60. https://doi.org/10.11646/zootaxa.2522.1.2

Frías-Lasserre D (2010) A new species and karyotype variation in the bordering distribution of *Mepraia spinolai* (Porter) and *Mepraia gajardoi* Frías et al (Hemiptera: Reduviidae: Triatominae) in Chile and its parapatric model of speciation. Neotropical Entomology 39(4): 572–583. https://doi.org/10.1590/S1519-566X2010000400017

Galvão C (2014) Vetores da Doença de Chagas no Brasil. Sociedade Brasileira de Zoologia, Curitiba, 289 pp. https://doi.org/10.7476/9788598203096

Gil-Santana HR (2014) *Pothea berengeri* sp. nov. from Brazil, with taxonomic notes on *Pothea furtadoi* Gil-Santana & Costa and *Pothea jaguaris* (Carpintero) and reinstatement of *Parapothea* Carpintero as junior synonym of *Pothea* Amyot & Serville (Hemiptera: Heteroptera: Reduviidae: Ectrichodiinae). Zootaxa 3826(3): 497–516. https://doi.org/10.11646/zootaxa.3826.3.4

Gil-Santana HR (2017) A new species of *Zeraikia* Gil-Santana Costa with taxonomic notes on *Zeraikia novafriburguensis* Gil-Santana & Costa (Hemiptera, Reduviidae, Peiratinae). ZooKeys 716: 105–126. https://doi.org/10.3897/zookeys.716.20843

Gil-Santana HR, Galvão C (2013) Description of the male genitalia of *Belminus rugulosus* Stål and *Belminus corredori* Galvão & Angulo, and comments on the holotype of *Parabelminus yurupucu* Lent & Wygodzinsky (Hemiptera: Heteroptera: Reduviidae: Triatominae: Bolboderini). Zootaxa 3746(4): 587–596. https://doi.org/10.11646/zootaxa.3746.4.6

Gonçalves TCM, Teves-Neves SC, Santos-Mallet JR, Carbajal-de-la-Fuente AL, Lopes CM (2013) *Triatoma jatai* sp. nov. in the state of Tocantins, Brazil (Hemiptera: Reduviidae: Triatominae). Memórias do Instituto Oswaldo Cruz 108: 429–437. https://doi.org/10.1590/S0074-0276108042013006

Gurgel-Gonçalves R, Abad-Franch F, Ferreira JBC, Santana DB, Cuba CAC (2008) Is *Rhodnius prolixus* (Triatominae) invading houses in central Brazil? Acta Tropica 107: 90–98. https://doi.org/10.1016/j.actatropica.2008.04.020

Grijalva MJ, Villacis AG, Ocana-Mayorga S, Yumiseva CA, Moncayo AL, Baus EG (2015) Comprehensive survey of domiciliary triatomine species capable of transmitting chagas disease in Southern Ecuador. PLoS Neglected Tropical Diseases 9(10): e0004142. https://doi.org/10.1371/journal.pntd.0004142

Harry M (1993) Use of the median process of the pygophore in the identification of *Rhodnius nasutus*, *R. neglectus*, *R. prolixus* and *R. robustus* (Hemiptera: Reduviidae). Annals Tropical Medicine and Parasitology 87: 277–282. https://doi.org/10.1080/00034983.1993.11812767

Hernández C, Aristeu da Rosa J, Vallejo GA, Guhl F, Ramírez JD (2020) Taxonomy, Evolution, and Biogeography of the Rhodniini Tribe (Hemiptera: Reduviidae). Diversity 12(3): e97. https://doi.org/10.3390/d12030097

Ishikawa T, Naka T (2016) First record of the thread-legged assassin bug genus *Proguithera* from Japan, with description of a new species (Hemiptera: Heteroptera: Reduviidae). Zootaxa 4184(1): 184–196. https://doi.org/10.11646/zootaxa.4184.1.12

Ishikawa T, Toriumi W, Susila W, Okajima S (2007) *Sycanus aurantiacus* (Hemiptera: Heteroptera: Reduviidae), a new harpactorine species from Bali, Indonesia, with brief notes on its biology. Zootaxa 1615: 21–27. https://doi.org/10.11646/zootaxa.1615.1.2

Jansen AM, Roque ALR (2010) Domestic and wild mammalian reservoirs. In: Telleria J, Tibyarenc M (Eds) American Trypanosomiasis. Elsevier, London, 249–276. https://doi.org/10.1016/B978-0-12-384876-5.00011-3

Jurberg J, Rocha DS, Galvão C (2009) *Rhodnius zeledoni* sp. nov. afim de *Rhodnius paraensis* Sherlock, Guitton& Miles, 1977 (Hemiptera, Reduviidae, Triatominae). Biota Neotropica 9: 123–128. https://doi.org/10.1590/S1676-06032009000100014

Jurberg J, Cunha V, Cailleaux S, Raigorodschi R, Lima MS, Rocha DS, Moreira FFF (2013) *Triatoma pintodiasi* sp. nov. do subcomplexo *T. rubrovaria* (Hemiptera, Reduviidae, Triatominae). Revista Pan-Amazônica de Saúde 4: 43–56. https://doi.org/10.5123/S2176-62232013000100006

Justi SA, Galvão C (2017) The evolutionary origin of diversity in Chagas disease vectors. Trends in Parasitology 33(1): 42–52. https://doi.org/10.1016/j.pt.2016.11.002

Justi SA, Noireau F, Cortez MR, Monteiro FA (2010) Infestation of peridomestic *Attalea phalerata* palms by *Rhodnius stali*, a vector of *Trypanosoma cruzi* in the Alto Beni, Bolivia. Tropical Medicine and International Health 15: 727–732. https://doi.org/10.1111/j.1365-3156.2010.02527.x

Klingenberg CP (2011) MorphoJ: an integrated software package for geometric morphometrics. Molecular Ecology Resources 11: 353–357. https://doi.org/10.1111/j.1755-0998.2010.02924.x

Lapischies R, Forero D, Barcellos A, Salomão RP (2019) A new species of *Pyrrhosphodrus* (Hemiptera: Heteroptera: Reduviidae) from the Caatinga ecosystem in Brazil, with notes on the genus. Zootaxa 4543(3): 388–420. https://doi.org/10.11646/zootaxa.4543.3.4

Lent H (1948) O gênero *Rhodnius* Stål, 1859 (Hemiptera: Reduviidae). Revista Brasileira de Biologia 8: 297–339.

Lent H, Wygodzinsky P (1979) Revision of the Triatominae (Hemiptera, Reduvidae) and their significance as vectors of Chagas' disease. Bulletin of the American Museum of Natural History 163(3): 127–520. http://digitallibrary.amnh.org/handle/2246/1282

Lent H, Jurberg J (1968) Estudo morfológico comparativo de *Panstrongylus geniculatus* (Latreille, 1811) e *Panstrongylus megistus* (Burmeister, 1835) e suas genitálias externas (Hemiptera, Reduviidae, Triatominae). Revista Brasileira de Biologia 28: 499–520.

Lent H, Jurberg J (1969) O gênero *Rhodnius* Stål, 1859, com um estudo sôbre a genitália das espécies (Hemiptera, Reduviidae, Triatominae). Revista Brasileira de Biologia 29: 487–560.

Lent H, Jurberg J (1975) O gênero *Panstrongylus* Berg, 1879, comum estudo sobre a genitália externa das espécies (Hemiptera, Reduviidae, Triatominae). Revista Brasileira de Biologia 35: 379–438.

Lent H, Jurberg J (1984) A genitália externa na tribo Bolboderini (Hemiptera, Reduviidae, Triatominae). Memórias do Instituto Oswaldo Cruz 79: 1–27. https://doi.org/10.1590/S0074-02761984000100001

Lent H, Jurberg J (1987) A genitália externa dos machos de sete espécies de *Triatoma* Laporte, 1832 da regiãoNeártica (Hemiptera, Reduviidae). Memórias do Instituto Oswaldo Cruz 82: 227–246. https://doi.org/10.1590/S0074-02761987000200011

Lent H, Jurberg J, Galvão C (1993a) *Rhodnius stali* n. sp., afim de *Rhodnius pictipes* Stal, 1872 (Hemiptera, Reduviidae, Triatominae). Memórias do Instituto Oswaldo Cruz 88: 605–614. https://doi.org/10.1590/S0074-02761993000400019

Lent H, Jurberg J, Galvão C (1993b) Triatoma matsunoi Fernandez-Loayza, 1989 com um estudo sobre a genitália externa masculina (Hemiptera, Reduviidae, Triatominae). Memórias do Instituto Oswaldo Cruz 88: 615–619. https://doi.org/10.1590/S0074-02761993000400020

Lima-Cordon LA, Monroy CM, Stevens L, Rodas A, Rosas GA, Dorn PL, Justi SA (2019) Description of *Triatoma huehuetenanguensis* sp. n., a potential Chagas disease vector (Hemiptera, Reduviidae, Triatominae). ZooKeys 820: 51–70. https://doi.org/10.3897/zookeys.820.27258

Lyman DF, Monteiro FA, Escalante AA, Cordon-Rosales C, Wesson DM, Dujardin JP, Beard CB (1999) Mitochondrial DNA sequence variation among triatomine vectors of Chagas' disease. The American Journal of Tropical Medicine and Hygiene 60(3): 377–386. https://doi.org/10.4269/ajtmh.1999.60.377

Mejia JM, Galvão C, Jurberg J (1999) *Rhodnius colombiensis* sp. n. da Colômbia, com quadros comparativos entre estruturas fálicas do gênero *Rhodnius* Stal, 1859 (Hemiptera, Reduviidae, Triatominae). Entomología y Vectores 6: 601–617.

Nascimento JD, da Rosa JA, Salgado-Roa FC, Hernández C, Pardo-Diaz C, Alevi KCC, Ravazi A, de Oliveira J, de Azeredo Oliveira MTV, Salazar C, Ramírez JD (2019) Taxonomical over splitting in the *Rhodnius prolixus* (Insecta: Hemiptera: Reduviidae) clade: Are *R. taquarussuensis* (da Rosa et al. 2017) and *R. neglectus* (Lent, 1954) the same species? PLoS ONE 14(2): e0211285. https://doi.org/10.1371/journal.pone.0211285

Oliveira J, Marcet PL, Takiya DM, Mendonça VJ, Belintani T, Bargues MD, Mateo L, Chagas V, Folly-Ramos E, Cordeiro-Estrela P, Gurgel-Gonçalves R, Costa J, da Rosa JA, Almeida CE (2017) Combined phylogenetic and morphometric information to delimit and unify the *Triatoma brasiliensis* species complex and the *Brasiliensis* subcomplex. Acta Tropica 170: 140–148. https://doi.org/10.1016/j.actatropica.2017.02.020

Oliveira J, Ayala JM, Justi SA, Rosa JA, Galvão C (2018) Description of a new species of *Nesotriatoma* Usinger, 1944 from Cuba and revalidation of synonymy between *Nesotriatoma bruneri* (Usinger, 1944) and *N. flavida* (Neiva, 1911) (Hemiptera, Reduviidae, Triatominae). Journal of Vector Ecology 43: 148–157. https://doi.org/10.1111/jvec.12294

Poinar Jr G (2019) A primitive triatomine bug, *Paleotriatoma metaxytaxa* gen. et sp. nov. (Hemiptera: Reduviidae: Triatominae), in mid-Cretaceous amber from northern Myanmar. Cretaceous Research 93: 90–97. https://doi.org/10.1016/j.cretres.2018.09.004

Rodrigues JMS, Rosa JA, Moreira FFF, Galvão C (2018) Morphology of the terminal abdominal segments in females of Triatominae (Insecta: Hemiptera: Reduviidae). Acta Tropica 185: 86–97. https://doi.org/10.1016/j.actatropica.2018.04.021

Rohlf FJ (2008) tpsDig2, v2.16. Morphpometrics at suny stony Brook. https://life.bio.sunysb.edu/morph/

Rohlf FJ (2010) tpsUtil, Version 1.46. Morphpometrics at suny stony Brook. https://life.bio.sunysb.edu/morph/

Rosa JA, Mendonça VJ, Gardim S, Carvalho DB, de Oliveira J, Nascimento JD, Pinotti H, Pinto MC, Cilense M, Galvão C, Barata JM (2014) Study of the external female genitalia of 14 *Rhodnius* species (Hemiptera, Reduviidae,Triatominae) using scanning electron microscopy. Parasites & Vectors 7: 1–7. https://doi.org/10.1186/1756-3305-7-17

Rosa JA, Mendonça VJ, Rocha CS, Gardim S, Cilense M (2010) Characterization of the external female genitalia of six species of Triatominae (Hemiptera: Reduviidade) by scanning electron microscopy. Memórias do Instituto Oswaldo Cruz 105: 286–292. https://doi.org/10.1590/S0074-02762010000300007

Rosa JA, Justino HHG, Nascimento JD, Mendonça VJ, Rocha CS, Carvalho DB, Falcone R, Azeredo-Oliveira MTV, Alevi KCC, Oliveira J (2017a) A new species of *Rhodnius* from Brazil (Hemiptera, Reduviidae, Triatominae). ZooKeys 675: 1–25. https://doi.org/10.3897/zookeys.675.12024

Rosa JA, Souza ES, da Costa Teixeira A, Barbosa RR, Souza AJ, Belintani T, Nascimento JD, Gil-Santana HR, Oliveira J (2017b) Third record of *Rhodnius amazonicus* and comparative study with *R. pictipes* (Hemiptera, Reduviidae, Triatominae). Acta Tropica 176: 364–372. https://doi.org/10.1016/j.actatropica.2017.09.003

Rosa JA, Rocha CS, Gardim S, Pinto MC, Mendonça VJ, Filho JCRF, Carvalho EOC, Camargo LMA, Oliveira J, Nascimento JD, Cilense M, Almeida CE (2012) Description of *Rhodnius montenegrensis* sp. nov. (Hemiptera: Reduviidae: Triatominae) from the state of Rondônia, Brazil. Zootaxa 3478: 62–76. https://doi.org/10.11646/zootaxa.3478.1.8

Sandoval CM, Pabón E, Jurberg J, Galvão C (2007) *Belminus ferroae* n.sp. from the Colombian north-east, with a key to the species of the genus (Hemiptera: Reduviidae: Triatominae). Zootaxa 1443: 55–64. https://doi.org/10.11646/zootaxa.1443.1.5

Schofield CJ, Dujardin JP (1999) Theories on the evolution of *Rhodnius*. Actualidades Biológicas 70: 183–197.

Schofield CJ, Galvão C (2009) Classification, evolution, and species groups within the Triatominae. Acta Tropica 110: 88–100. https://doi.org/10.1016/j.actatropica.2009.01.010

Sherlock IA, Serafim EM (1967) *Triatoma lenti* sp.n., *Triatoma pessoai* sp.n. e *Triatoma bahiensis* sp.n. do estado da Bahia, Brasil (Hemiptera: Reduviidae). Gazeta Medica. Bahia: 67: 75–92.

Soto-Vivas A, Enríquez S, Villacrés E, Arrivillaga J, Hinojosa M, Liria J (2018) New kissing bug (Hemiptera: Reduviidae: Triatominae) records from Napo and Morona-Santiago provinces with distribution updates in Ecuador. Journal of Threatened Taxa 10(11): 12515–12522. https://doi.org/10.11609/jott.4345.10.11.12523-12530

Souza ES, Von Atzinger NCB, Furtado MB, Oliveira J, Nascimento JD, Vendramini DP, Gardim S, Rosa JA (2016) Description of *Rhodnius marabaensis* sp. n. (Hemiptera: Reduviidae: Triatominae) from Pará State, Brazil. ZooKeys 621: 45–62. https://doi.org/10.3897/zookeys.621.9662

Valente VC, Valente SAS, Carcavallo RU, Rocha, DS, Galvão C, Jurberg J (2001) Considerações sobreuma nova especies do genero *Rhodnius* Stål, do estado do Pará, Brasil (Hemiptera, Reduviidae, Triatominae). Entomología y Vectores 8: 65–80.

Weirauch C (2008) Cladistic analysis of Reduviidae (Heteroptera: Cimicomorpha) based on morphological characters. Systematic Entomology 2008 33(2): 229–74. https://doi.org/10.1111/j.1365-3113.2007.00417.x

WHO (2019) Chagas disease (American trypanosomiasis). https://www.who.int/chagas/disease/en/

Zhao P, Ren S, Wang B, Cai W (2015) *Cosmosycanus perelegans* (Hemiptera: Reduviidae: Harpactorinae), a new record from China, with report of its female genitalia. Zootaxa 3936(4): 567–574. https://doi.org/10.11646/zootaxa.3936.4.6

Supplementary material 1

TPS file of landmarks of *R. ecuadoriensis*

Authors: Yisheng Zhao, Cleber Galvão, Wanzhi Cai

Data type: measurement

Explanation note: This TPS file contains the landmark cordinates of *R.ecuadoriensis*.

Link: https://doi.org/10.3897/zookeys.1012.54779.suppl1

Supplementary material 2

TPS file of landmarks of *R. micki*

Authors: Yisheng Zhao, Cleber Galvão, Wanzhi Cai

Data type: measurement

Explanation note: This TPS file contains the landmark cordinates of *R. micki*.

Link: https://doi.org/10.3897/zookeys.1012.54779.suppl2

Supplementary material 3

TPS file of landmarks of *R. pallescens*

Authors: Yisheng Zhao, Cleber Galvão, Wanzhi Cai

Data type: measurement

Explanation note: This TPS file contains the landmark cordinates of *R. pallescens*.

Link: https://doi.org/10.3897/zookeys.1012.54779.suppl3

Supplementary material 4

TPS file of landmarks of *R. pictipes*

Authors: Yisheng Zhao, Cleber Galvão, Wanzhi Cai

Data type: measurement

Explanation note: This TPS file contains the landmark cordinates of *R. pictipes*.

Link: https://doi.org/10.3897/zookeys.1012.54779.suppl4

Supplementary material 5

TPS file of landmarks of *R. stali*

Authors: Yisheng Zhao, Cleber Galvão, Wanzhi Cai

Data type: measurement

Explanation note: This TPS file contains the landmark cordinates of *R. stali*.

Link: https://doi.org/10.3897/zookeys.1012.54779.suppl5

ZooKeys 1012: 95–134 (2021)
doi: 10.3897/zookeys.1012.57172
https://zookeys.pensoft.net

RESEARCH ARTICLE

A peer-reviewed open-access journal
ZooKeys
Launched to accelerate biodiversity research

Five new genera of the subfamily Cylapinae (Insecta, Heteroptera, Miridae) from Australia

Anna A. Namyatova[1,2,3], Gerasimos Cassis[4]

1 *St Petersburg State University, Faculty of Biology, Universitetskaya nab. 7/9, St. Petersburg, Russia* **2** *University of Tyumen, Volodarskogo ul. 6, Tyumen, Russia* **3** *Zoological Institute, Russian Academy of Sciences, Universitetskaya nab. 1, St Petersburg, Russia* **4** *University of New South Wales, Evolution and Ecology Research Centre, School of Biological, Earth and Environmental Sciences, Randwick, Sydney, Australia*

Corresponding author: Anna A. Namyatova (anna.namyatova@gmail.com)

Academic editor: L. Livermore | Received 2 August 2020 | Accepted 3 December 2020 | Published 26 January 2021

http://zoobank.org/C790EE76-C9F8-49DE-A47D-DDEBF88D5D22

Citation: Namyatova AA, Cassis G (2021) Five new genera of the subfamily Cylapinae (Insecta, Heteroptera, Miridae) from Australia. ZooKeys 1012: 95–134. https://doi.org/10.3897/zookeys.1012.57172

Abstract

Cylapinae is one of the poorly studied groups within the megadiverse family Miridae (Insecta: Heteroptera). In this paper, five monotypic genera from Australia are described as new to science. Two of those taxa, *Dariella rubrocuneata* **gen. nov.** and **sp. nov.**, and *Labriella fusca* **gen. nov.** and **sp. nov.** are assigned to the tribe Cylapini. Three taxa, *Callitropisca florentine* **gen. nov.** and **sp. nov.**, *Laetifulvius morganensis* **gen. nov.** and **sp. nov.** and *Micanitropis seisia* **gen. nov.** and **sp. nov.** are placed into the tribe Fulviini. Habitus images, SEMs of external characters, illustrations of male and female genitalia, and distribution maps are provided for each species where possible. The systematic position and possible relationships of the newly described taxa are discussed.

Keywords

Australian fauna, description, morphology, new species, plant bugs, taxonomy

Introduction

Miridae is one of the largest hemimetabolous insect families, currently comprising more than 11,000 species and with numerous taxa yet to be described. Cylapinae is among the smallest subfamilies within the Miridae with approximately 100 genera and 500 species.

Currently this subfamily includes the followings tribes: Bothriomirini, Fulviini, Cylapini, Rhinomirini, and Vanniini. Additionally, the subfamily Psallopinae is sometimes considered within Cylapinae as a tribe (Wolski and Henry 2015). These groups are very different morphologically and do not share any characters in common, which casts doubts on Cylapinae monophyly. The largest tribes, Fulviini and Cylapini, also seem to be groups of convenience and their generic composition will likely be revised in the future.

Most representatives of Cylapinae are distributed in tropical and subtropical regions. It is very likely the true diversity of this subfamily is still not comprehensive, as many of its representatives live in litter and under bark in tropical forests and cannot be collected using the most common mirid collection technique, plant sweeping and beating. During the last decade numerous Cylapinae taxa collected by hands, malaise traps, light traps, fogging, and bark spraying have been described from different regions (e.g., Carpintero and Cherot 2014; Wolski 2014, 2017; Wolski and Gorczyca 2014a; Wolski et al. 2016, 2017, 2018; Namyatova and Cassis 2019a; Tyts et al. 2020).

The Australian fauna of Cylapinae seems to be very little known, and currently it includes just 21 genera and 43 species from all tribes, except for Rhinomirini (Cassis and Gross 1995; Wolski and Gorczyca 2014b; Namyatova and Cassis 2016a, 2019a; Namyatova et al. 2019) and also four Psallopinae species (Namyatova and Cassis 2019b). It is estimated from museum collections, that Australian Cylapinae species diversity may reach at least 100 (Namyatova and Cassis 2016a). In this paper, we aim to further expand our knowledge on Australian cylapine fauna by describing five new monotypic Cylapinae genera within Cylapini and Fulviini and discussing their systematic position.

Materials and methods

Specimens

Eighty-two specimens were examined for this study. A unique specimen identifier (USI) was attached to each specimen, and collection event data were entered into the Arthropod Easy Capture Specimen Database (https://research.amnh.org/pbi/locality/index.php) and accessible through https://www.discoverlife.org/. The USI code starts with "UNSW_ENT" prefix for all the labels, except otherwise stated. The specimens are deposited in the following collections:

AM Australian Museum, Sydney, Australia;
AMNH American Museum of Natural History, New York, USA;
NTM Museum and Art Gallery of the Northern Territory, Darwin;
QM Queensland Museum, Brisbane, Australia;
TMAG Tasmanian Museums and Art Gallery, Hobart, Australia;
SAMA South Australian Museum, Adelaide, Australia;
WAM Western Australian Museum, Perth, Sydney.

Dissection and terminology

The specimen dissection methodology follows Kerzhner and Konstantinov (1999). Terminology of male genitalia follows Kerzhner and Konstantinov (1999) and Konstantinov (2003), the aedeagus is described in repose. Terminology of female genitalia follows Davis (1955).

Habitus and scanning electron micrograph images

The focus stacked habitus images were taken using Canon EOS 40D and Canon EOS 5D cameras, those stacks were concatenated using Helicon Focus ver. 6 software with standard setting. Scanning electron micrographs were made using a Hitachi TM-3000 tabletop electron microscope, the specimens were uncoated. The images were cropped and contrasted in Photoshop CS3 and CS5.1, the same software was used to create the figure plates.

Measurements

Measurements have been completed using a Leica graticule and × 10 eyepieces, through a Leica MZ16 stereomicroscope. Measurements are provided in Table 1 in millimetres. The scale bars are 1 mm for habitus images and 0.1 mm for genitalia.

Maps

The maps were completed using Simplemappr website (https://www.simplemappr.net/) (Shorthouse and Davis 2010) and processed with Photoshop CS5.1.

Results

Subfamily Cylapinae
Tribe Cylapini

***Dariella* gen. nov.**
http://zoobank.org/81EEFDFE-0ADE-4D5D-AC20-A4F3973EDCBB

Type species. *Dariella rubrocuneata* sp. nov. by original designation.

Diagnosis. *Dariella* differs from other Cylapinae in the following combination of characters: macropterous; vertical head with antennal fossa placed above mandibular plate (Fig. 3A); elongate body, covered with short adpressed simple setae; pronotum, corium, and clavus deeply punctate (Fig. 3B, M); eye not pedunculated; vertex carinate posteriorly (Fig. 3B); base of pronotum wider than head; total antennal length shorter than body; antennal segment II slightly incrassate towards apex; antennal segments III

Table 1. Measurements.

Species		Length					Width		
		Body	Cun-Clyp	Pronotum	AntSeg 1	AntSeg2	Head	Pronotum	InterOcDi
Dariella rubrocuneata									
♂ (N = 5)	M1	2.06	1.48	0.40	0.25	0.67	0.54	0.73	0.21
	M2	2.23	1.50	0.42	0.25	0.71	0.54	0.77	0.23
	M3	2.19	1.54	0.42	0.27	0.65	0.50	0.73	0.19
	M4	2.25	1.56	0.44	0.31	0.77	0.52	0.77	0.21
	M5	2.08	1.46	0.44	0.25	0.67	0.52	0.75	0.21
Labriella fusca									
♂ (N = 5)	M1	2.96	2.10	0.48	0.25	0.88	0.69	0.94	0.23
	M2	2.88	2.04	0.48	0.25	0.79	0.65	0.92	0.21
	M3	2.81	1.98	0.44	0.25	0.83	0.65	0.90	0.23
	M4	2.67	1.94	0.46	0.25	0.75	0.65	0.85	0.23
	M5	2.81	2.00	0.46	0.25	0.77	0.65	0.85	0.21
♀ (N = 5)	F1	2.85	2.10	0.50	0.27	0.65	0.67	0.88	0.23
	F2	2.69	2.00	0.48	0.25	0.58	0.63	0.88	0.23
	F3	2.65	2.02	0.44	0.25	0.63	0.65	0.81	0.23
	F4	2.75	2.08	0.44	0.23	0.63	0.65	0.83	0.23
	F5	2.92	2.10	0.46	0.25	0.58	0.63	0.90	0.25
Callitropisca florentine									
♂ (N = 1)	M1	3.13	2.13	0.44	0.29	0.92	0.54	1.02	0.25
♀ (N = 2)	F1	3.00	2.25	0.46	0.21	0.83	0.54	1.00	0.27
	F2	3.04	2.27	0.42	0.21	0.77	0.56	0.92	0.29
Laetifulvius morganensis									
♂ (N = 2)	M1	3.10	1.98	0.42	0.25	0.77	0.60	0.94	0.21
	M2	3.04	2.04	0.46	0.25	0.77	0.60	0.92	0.23
Micanitropis seisia									
♂ (N = 5)	M1	3.21	2.33	0.54	0.35	0.98	0.56	1.15	0.23
	M2	–	–	0.58	0.33	1.00	0.63	1.13	0.25
	M3	3.38	2.35	0.50	0.33	0.94	0.60	1.08	0.23
	M4	3.19	2.42	0.52	0.31	0.94	0.60	1.17	0.23
	M5	3.13	2.29	0.54	0.29	–	0.58	1.10	0.21
♀ (N = 5)	F1	3.35	2.46	0.56	0.33	1.02	0.54	1.23	0.23
	F2	–	2.19	0.52	0.33	1.02	0.50	1.10	0.21
	F3	3.06	2.33	0.52	0.29	0.94	0.56	1.13	0.25
	F4	3.48	2.48	0.54	0.29	0.92	0.63	1.17	0.25
	F5	3.73	2.71	0.56	0.29	0.90	0.63	1.15	0.25

and IV each shorter than segment II (Fig. 3E); buccula ring-like (Fig. 3A); apex of labium slightly surpassing posterior coxae; segments I and II not subdivided (Fig. 3D); collar delimited with deep groove (Fig. 3A, B); calli distinct with round shallow pit between them; scutellum flat (Fig. 3E, M); metathoracic scent gland evaporative area only slightly longer than wide with distinct vertical grove behind peritreme (Fig. 3F); outer margin of hemelytron slightly constricted anteriorly (Fig. 1); widest part of embolium subequal to 1/3 cuneus width at base; cuneus longer than wide at base (Fig. 3L); tarsal segment I shorter than segments II and III each (Fig. 3J); middle row of tiles on unguitractor reduced (Fig. 3K); parameres subequal in length and both with swelling in basal half directed outwards (Fig. 4D, F); phallotheca more extensively sclerotised apically, than basally; endosoma with single sclerotised area placed at right hand side (Fig. 4A, B).

Description. Male. Coloration (Fig. 1). Head, pronotum, mesoscutum, scutellum mostly brown to dark brown; hemelytron, labium and appendages mostly pale brown to yellow with reddish tinge. For details see species description. **Surface and vestiture.** Dorsum shiny, without net-like pattern of microsculpture; posterior part of pronotum, clavus and corium with deep punctures (Fig. 3B, M); scutellum mostly smooth, serrate laterally (Fig. 3M); head, calli, embolium, cuneus and pleura smooth (Fig. 3B, F, L); dorsum and legs clothed with adpressed short simple setae, those setae on head and pronotum sparse; head with long suberect seta near inner margin of each eyes in dorsal view (Fig. 3B, C); antennae clothed with suberect setae mostly as long as or longer than antennal segment II width (Fig. 3E); anterior part of mesopleuron with area of dense short adpressed setae; posterior part of mesopleuron and metapleuron with sparse semi-adpressed setae (Fig. 3F). **Structure**. ***Head.*** Vertical, in dorsal view wider than long; eye not covering anterior margin of pronotum, not protruding; vertex carinate posteriorly (Fig. 3B); in anterior view head wider than high; antennal fossa attached near ventral margin of eye; clypeus separated from frons with shallow depression, its base placed slightly below ventral margin of eye (Fig. 3C); in lateral view head twice as high as long; eye slightly upraised above vertex, covering lateral margins of pronotum; distance between eye and ventral margin of head subequal to half of eye height; antennal fossa adjacent to eye, placed slightly above mandibular plate; mandibular and maxillary plates separated from head by shallow depression posteriorly; labrum triangular, shorter than labial segment I (Fig. 3A); buccula twice as long as high, ring-like, almost reaching posterior margin of head (Fig. 3A). ***Antenna*** (Fig. 3E). Shorter than body, segment I shorter than head width; segment II longer than head width, slightly incrassate apically; segment III subequal to half of segment II; segment IV ca. 1.5 × as long as segment III; segments I and II subequal in width and wider than segments III and IV each. ***Labium*** (Fig. 3D). Apex slightly surpassing hind coxa, its segments not subdivided; labial segment I surpassing base of forecoxa; labial segments I–III subequal in length; segment IV slightly shorter than segment III. ***Thorax.*** Pronotum wider than long, lateral margins concave in dorsal view, not carinate (Fig. 3A, B); collar delimited with deep sulcus, as wide as antennal segment I; posterior margin rounded and convex; calli swollen, occupying less than half of pronotum, separated from each other by depression and round pit (Fig. 3B); scutellum flat; mesoscutum almost entirely covered with pronotum (Fig. 3E, M); propleural apodeme mostly straight, its apical part inclined anteriorly and merging with collar sulcus; mesopleural apodeme oval; mesothoracic spiracle slit-like, without microsculpture around it; metathoracic scent gland evaporative area large, lateral margin reaching base of hind coxae, triangular, with distinct vertical groove; peritreme only slightly upraised, elongate; metepimeron subequal to 1/4–1/3 of mesopleuron in width (Fig. 3F). ***Hemelytron.*** Outer margin of hemelytron slightly constricted anteriorly (Fig. 1); ridge on clavus shallow, almost indistinct; claval commissure slightly more than twice longer than scutellum; medial fracture distinct, surpassing middle of corium (Fig. 3M); ridge along medial fracture absent; embolium wide, its widest part subequal to 1/3 of cuneus width at base; R+M more distinct basally; cuneus delimited with small incision, longer than wide at base; membrane with single cell, distance from cell apex to membrane apex subequal to cell length (Fig. 3L). ***Legs.*** Forecoxa length shorter than pronotum;

coxae subequal in width and length; femora regular, not specifically widened; fore- and hind femora slightly wider than middle femur (Fig. 3G); segments II and III of hind tarsus subequal in length and each of them twice longer than segment I (Fig. 3J); claw with small subapical tooth; medial row of tiles on unguitractor reduced, having less tiles than lateral rows (Fig. 3K). ***Genitalia.*** See species description.

Female. Unknown.

Etymology. The genus is named after the sister of the first author (AN), Daria Namyatova. The gender is feminine.

Remarks. According to the present classification (Gorczyca 2000), *Dariella* does not belong to any Cylapinae tribe. It is similar to Cylapini and Bothriomirini in having punctate body (Fig. 3B, M), vertical head with antennal fossa placed above mandibular plate (Fig. 3A), and not subdivided labial segments I and II (Fig. 3D). See also Wolski (2017) and Namyatova et al. (2019) for detailed diagnoses of Cylapini and Bothriomirini respectively. However, most Cylapini species have antennae as long as or longer than body and antennal segments III and IV each longer than segment II (Wolski 2017), whereas in *Dariella* the antennae are shorter than body, and antennal segment III is shorter than segment II. In Bothriomirini, the body is more or less oval and stout, the collar is not delimited or weakly delimited, the scutellum is punctate, the tarsal segments are subequal in length (Namyatova et al. 2019), whereas in *Dariella* the body is elongate (Fig. 1), the collar is delimited with the deep sulcus (Fig. 3B), the scutellum is impunctate (Fig. 3M), and the tarsal segment I is shorter than each of segments II and III (Fig. 3J). Currently, we place *Dariella* in Cylapini, as it has affinities to some of its members, which also do not fully fit the diagnoses provided by Gorczyca (2000) and Wolski (2017).

Dariella is similar to the Neotropical genera *Corcovadocola* Carvalho, 1948 and *Cylapoides* Carvalho, 1952 as they also have short antennae (Carvalho 1948, 1952). Additionally, both those genera have a carinate vertex, apex of the labium reaches at least the hind coxa, and possess more or less developed calli. *Corcovadocola* and *Cylapoides* differ from *Dariella* in a convex scutellum and antennal segment III subequal in length to segment II. *Corcovadocola* additionally differs from *Dariella* in the lateral sides of pronotum being slightly carinate, and the narrower embolium. *Cylapoides* additionally differs in the eyes slightly pedunculate, the head width subequal to pronotum width and the cuneus as long as wide at the base (Carvalho 1952; Wolski 2017). *Dariella* is also similar to another Neotropical genus *Cylapinus*, as they both have a punctate body, wide embolium and pit between calli and very similar shape of parameres with the left and right parameres subequal in length and the basal half of both parameres with swelling directed outwards (Fig. 4B, F; Carvalho 1986: figs 12, 13). *Cylapinus* differs from the new genus in the body covered with erect setae and the cuneus being as long as wide (Carvalho 1986).

Dariella can be easily recognised externally from two Australian genera *Carvalhoma* Slater & Gross, 1977 and *Schizopteromiris*, currently placed in the Cylapini, as *Carvalhoma* has staphylinoid hemelytra and *Schizopteromiris* Schuh, 1986 has coleopteroid hemelytra in both sexes (Schuh 1986; Namyatova and Cassis 2016a). However, those two genera are similar to the new genus in having the antenna shorter than the body, a similar vertical head and punctate hemelytron. Additionally, *Carvalhoma* has a similar left paramere with the basal half having swelling directed outwards and the phallotheca sclerotised apically (Namyatova and Cassis 2016a), and most species of *Carvalhoma* also have the endosoma with the sclerite placed at right side, which is very similar to *Dariella* (cf. Fig. 4A, B; Namyatova and Cassis 2016a: figs 7A, B, 9A, B, 10A, B). Another character uniting *Carvalhoma*, *Schizopteromiris* and *Dariella* is the reduced middle row of tiles on the unguitractor (Fig. 3K; pers. obs. for *Schizopteromiris*; Namyatova and Cassis 2016a: fig. 2L). *Schizopteromiris* might be closely related to *Dariella*, as they both have paired setae near the inner margin of eye dorsally (Fig. 3B, C; pers. obs. for *Schizopteromiris*) and a very similar shape of the metathoracic scent gland evaporative area which is slightly longer than wide with distinct vertical grove behind peritreme (cf. Fig. 3F and Schuh 1986: fig 12).

Dariella rubrocuneata sp. nov.

http://zoobank.org/611929C3-2384-4614-A395-7D0CD9D4D369
Figs 1, 3, 4, 15A

Material examined. ***Holotype*: Australia: Qld:** Mt Boolbun Sth (summit), 15.95°S, 145.1333°E, 950 m, 05 Nov 1995–11 Jan 1996, Monteith, Cook, Roberts, 1♂ (00043357) (QM). ***Paratypes*: Australia: Qld:** Graham Ra, 17.28333°S, 145.95°E, 550 m, 08 Dec 1995–09 Dec 1995, Monteith, Cook, Thompson, 1♂ (00043361) (QM). Koombooloomba Dam, Upper Tully, 17.8353°S, 145.605°E, 08 Dec 1989, Monteith, Thompson and Janetzki, 1♂ (00043362) (QM). Millaa Millaa Falls,

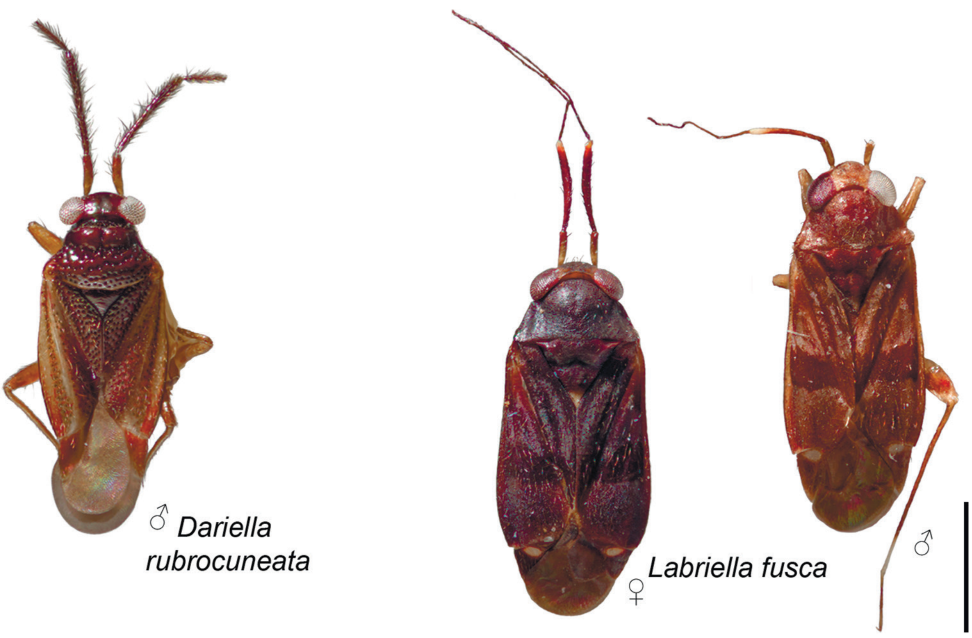

Figure 1. Habitus of *Dariella rubrocuneata* and *Labriella fusca*.

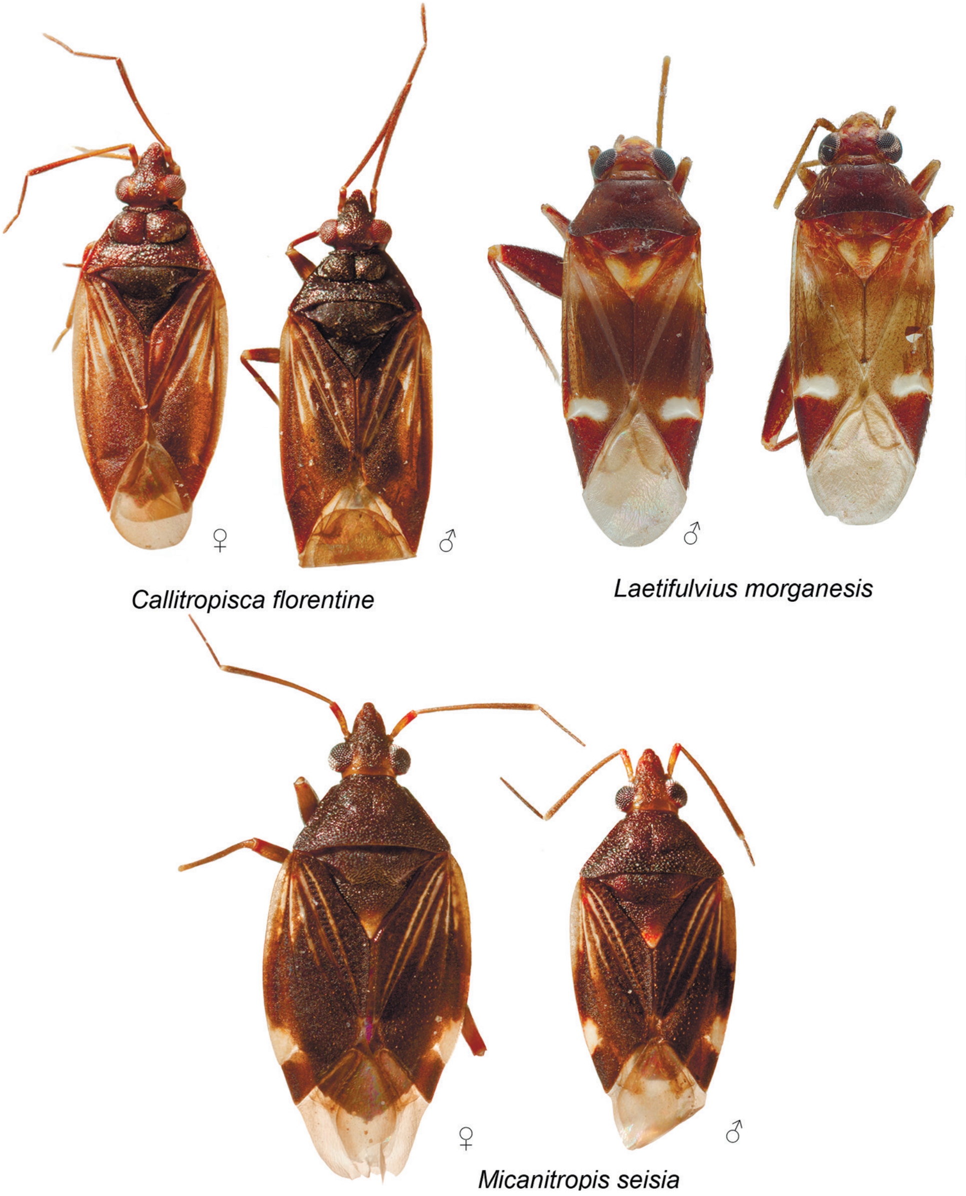

Figure 2. Habitus of *Callitropisca florentine*, *Laetifulvius morganensis*, and *Micanitropis seisia*.

17.46667°S, 145.6°E, 800 m, 17 May 1995, G. B. Monteith, 1♂ (00045284) (QM). Mt Boolbun Sth (summit), 15.95°S, 145.1333°E, 950 m, 05 Nov 1995–11 Jan 1996, Monteith, Cook, Roberts, 3♂ (00043358, 00043360, 00043359) (QM).

Diagnosis. Head, pronotum and pleura mostly brown to dark brown, corium and embolium yellow to pale brown with brown or reddish areas; antennal segment I yellow, reddish apically; segments II–IV mostly brown, segment IV whitish apically; labium yellow with reddish tinge; embolium reddish apically; cuneus red or pale brown

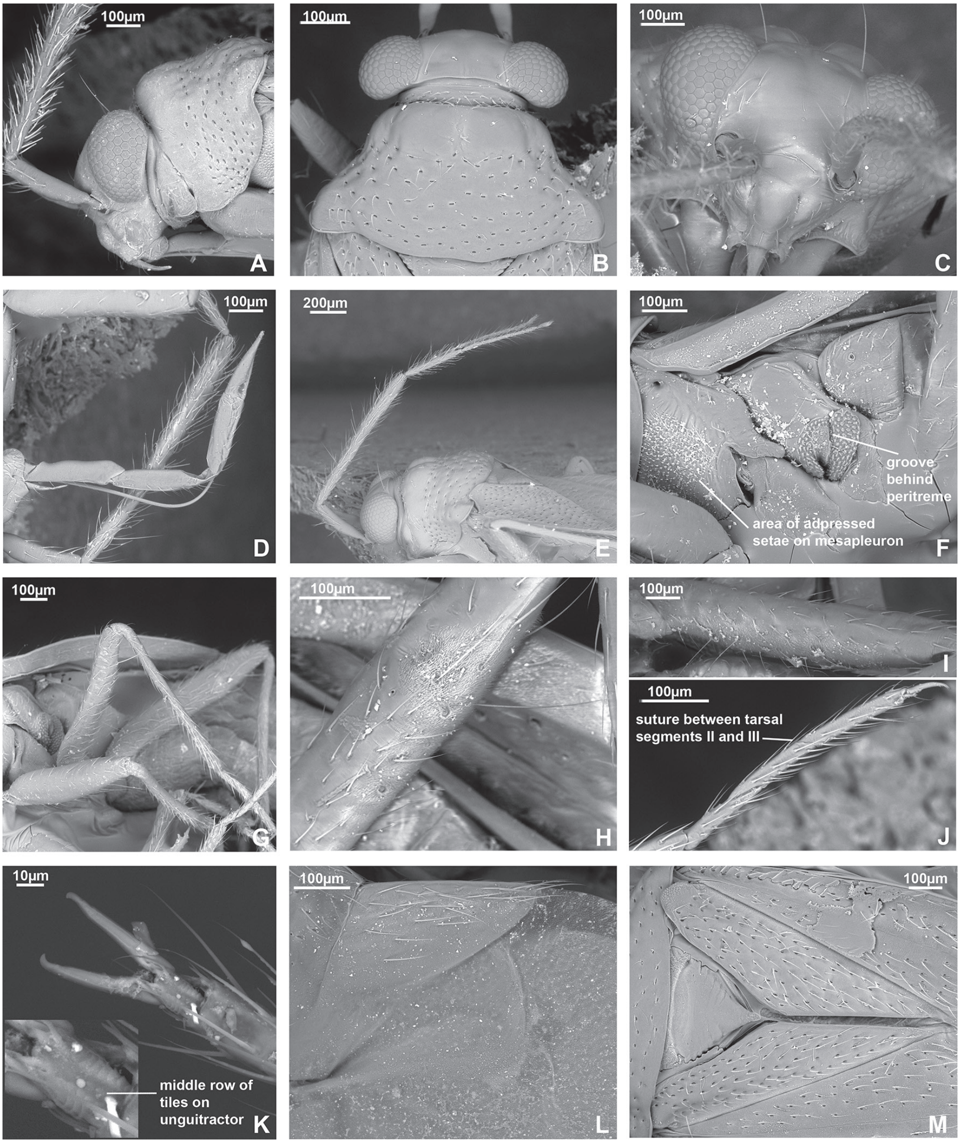

Figure 3. SEM images. *Dariella rubrocuneata* **A** head and pronotum, lateral view **B** head and pronotum, dorsal view **C** head, anterior view **D** labium **E** antenna **F** pleura **G** legs **H** trichobothria on hind femur **I** trichobothria on middle femur **J** hind tarsus **K** pretarsus, ventral view **L** cuneus and membrane cell **M** scutellum, clavus and corium.

with distinct reddish tinge (Fig. 1); endosoma with sclerotised area placed at right side and armed with small teeth (Fig. 4A, B).

Description. Male. Body length 2.1–2.3. **Coloration** (Fig. 1). Head mostly brown to dark brown, sometimes with reddish tinge; antennal segment I yellow, reddish apically; segments II and III brown; segment IV brown, whitish apically; labium yellow with reddish tinge; pronotum, mesoscutum and scutellum brown to dark brown, of-

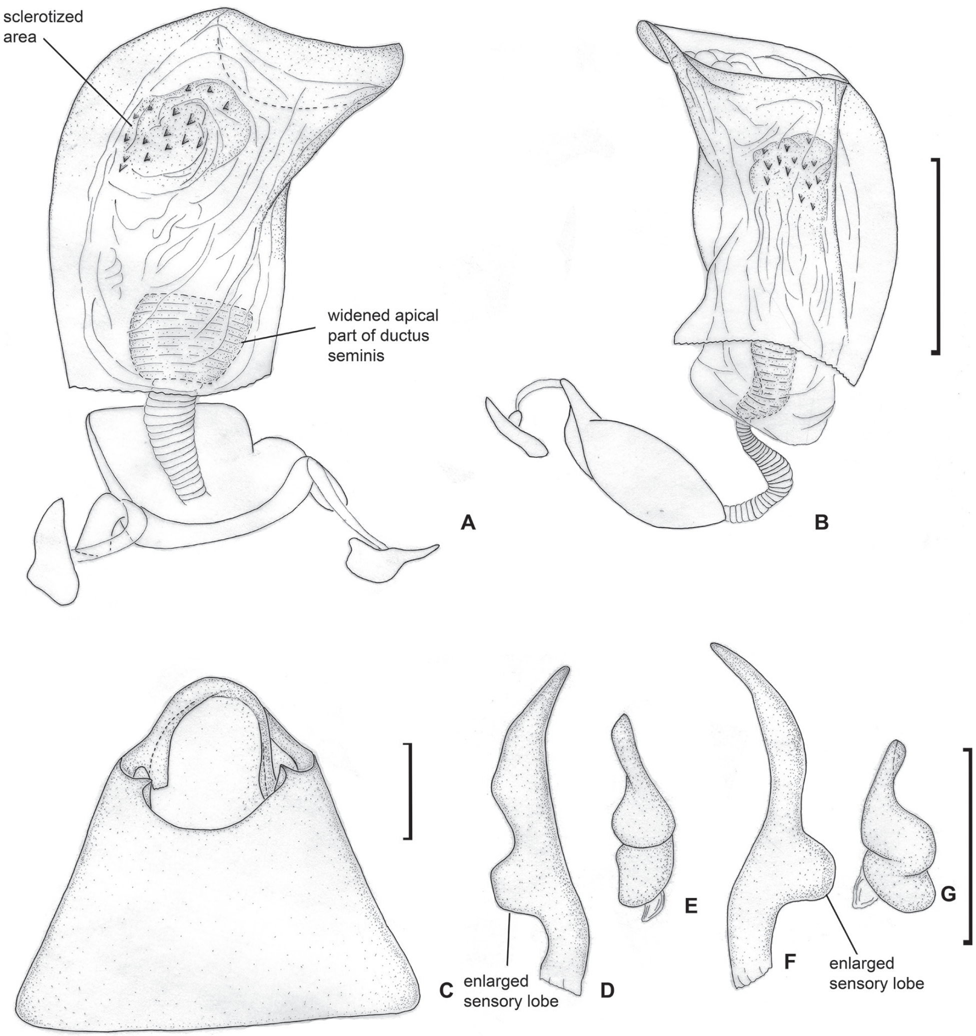

Figure 4. Male genitalia. *Dariella rubrocuneata* **A** aedeagus, dorsal view **B** aedeagus, left lateral view **C** genital capsule, dorsal view **D** left paramere, dorsal view **E** left paramere, posterior view **F** right paramere, dorsal view **G** right paramere, posterior view.

ten with reddish tinge; pleura mostly brown to dark brown; metathoracic scent gland evaporative area and metapleuron often reddish or with reddish tinge; clavus brown to reddish brown; corium and embolium yellow to pale brown with brown or reddish areas; embolium reddish apically; cuneus red or pale brown with distinct reddish tinge; membrane brown; legs mostly pale brown with red tinge; abdomen reddish brown. **Surface and vestiture.** See generic description. **Structure and measurements**. Body ca. 2.6–2.7 × as long as wide, ca. 2.8–3.0 × as long as pronotum width; head ca. 3.6–4.3 × as wide as long; vertex ca. 1.2–1.5 × as wide as eye; anterior view head ca. 1.3–1.4 × as wide as high; antennal segment I ca. 1.1–1.5 × as long as vertex, ca. 0.5–0.6 ×

as long as head width; segment II ca. 2.4–2.8 × as long as segment I, ca. 3.1–3.7 × as long as vertex, ca. 1.2–1.3 × as long as head width, ca. 0.9–1.0 × as long as pronotum width at base; segment III slightly shorter than segment I, and segment IV almost twice longer than segment III; pronotum ca. 1.7–1.9 × as wide as long, ca. 1.4–1.5 × as wide as head. ***Genitalia.*** Genital capsule triangular, without supragenital bridge (Fig. 4C); parameres subequal to each other in size and very similar in shape, slightly curved and with swelling in basal half directed outwards (Fig. 4D–G); phallotheca stronger sclerotised closer to apex than basally; ductus seminis short, its apical part widened and placed inside endosoma, somewhat sclerotised; endosoma not subdivided into vesica and conjunctiva, voluminous, with sclerotised area placed at right side and armed with small teeth (Fig. 4A, B).

Female. Unknown.

Distribution. Known only from Australian Wet Tropics (Fig. 15A).

Collection methods. The specimens were collected with flight intercept trap and pyrethrum knockdown.

Etymology. The species is named for its red cuneus, *ruber* from Latin, meaning red.

Labriella gen. nov.

http://zoobank.org/6C2CE837-63F7-46DD-A270-76413C12572D

Type species. *Labriella fusca* sp. nov. by original designation.

Diagnosis. *Labriella* is distinguished from other Cylapinae by the following combination of characters: labrum longer than labial segment I, oval, flattened at sides (Fig. 5D, E); head vertical with antennal fossa located above mandibular plate (Fig. 5A); eye not pedunculate; vertex carinate, concave (Fig. 5B, C); eye covering anterior angle of pronotum (Fig. 5A, B); buccula not ring shaped, declivous posteriorly (Fig. 5A); total antenna length shorter than body with antennal segment II as thick as segment I, segment IV longest (Fig. 5D); apex of labium reaching abdominal segments IV–V; labial segments I and II not subdivided (Fig. 5E); collar very narrow, delimited with deep depression (Fig. 5B); mesepimeral apodeme slit-like; mesothoracic spiracle with microsculpture along anterior margin dorsally (Fig, 5H); corium with ridge along medial fracture (Fig. 5I); impunctate brown body, covered with semi-adpressed setae; pronotum and hemelytron not constricted; hemelytron not modified or shortened (Figs 1, 5I); femora not significantly enlarged (Fig. 5K); parempodia setiform (Fig. 5F).

Description. Male. Coloration (Fig. 1). Mainly dark brown, for details see description of the species. **Surface and vestiture.** Dorsum and pleura glabrous, mostly matte, without punctation or rugosities (Fig. 5B, I, H); scutellum not serrate laterally (Fig, 5I); pleura with net-like pattern of microsculpture (Fig. 5H); body clothed with dark semi-adpressed setae, shorter than antennal segment II width, those setae shorter on appendages and almost absent on pleura (Fig. 5B, I, H). **Structure. *Head.*** In dorsal view head wider than long, vertical, vertex concave and carinate; eye covering anterior part of pronotum, not protruding (Fig. 5B); in anterior view head wider than high;

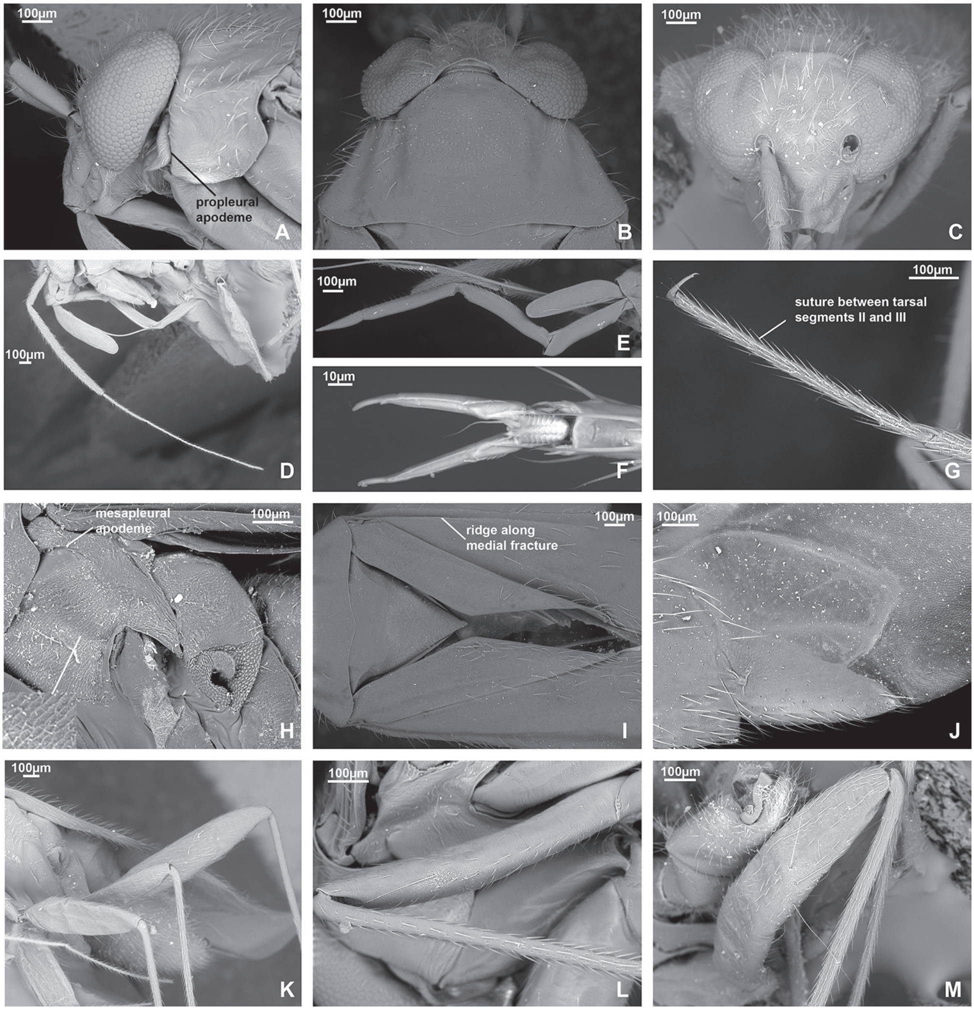

Figure 5. SEM images. *Labriella fusca* **A** head and pronotum, lateral view **B** head and pronotum, dorsal view **C** head, anterior view **D** antenna **E** labium **F** pretarsus, ventral view **G** hind tarsus **H** pleura **I** scutellum, clavus and corium **J** cuneus and membrane cell **K** legs **L** trichobothria on middle femur **M** trichobothria on hind femur.

antenna attached near ventral one third of eye, above ventral margins of eye; clypeus separated from frons by depression, its base placed slightly below antennal fossae, but above inferior margin of eye (Fig. 5C); in lateral view head ca. 1.5 × as high as long; eye slightly upraised above vertex, covering lateral margins of pronotum; distance from eye to ventral side of head subequal to third part of eye height laterally; eye covering anterior angles of pronotum; antennal fossa placed slightly above mandibular plate, adjacent to eye; mandibular and maxillary plate separated from head by distinct suture posteriorly; buccula twice as long as high, declivous posteriorly, not ring-like, almost reaching posterior margin of head (Fig. 5A); labrum as long as labial segment I, oval and flattened (Fig. 5D, E). ***Antenna*** (Fig. 5D). Total length shorter than body; segment I subequal to vertex width; segment II as wide as segment I, cylindrical and not incrassate apically; segment III and IV filiform, narrower than segments I and II; segment III subequal to half of segment II; segment IV ca. 2.5 × as long as segment III. ***Labium*** (Fig. 5D, E). Reaching abdominal segments IV–V, segments not subdivided; labial segment I slightly surpassing base of forecoxa; segments I, II and III subequal in length, segment IV subequal to half of segment III. ***Thorax.*** Pronotum wider than long; collar delimited, very narrow, narrower than antennal segment I (Fig. 5B); lateral margin of pronotum in dorsal view straight (Fig. 5B), in lateral view angulate, but not carinate (Fig. 5A); posterior margin of pronotum bisinuate (Fig. 5B); calli slightly upraised, occupying 2/3 of pronotum; calli separated with shallow depression between them; scutellum flat; mesoscutum exposed (Fig. 5I); propleural apodeme mostly straight, apical part inclined anteriorly (Fig. 5A), mesothoracic apodeme slit-like; mesothoracic spiracle open, slit-like, with small area of microsculpture along anterior margin dorsally; metathoracic gland evaporative area triangular, lateral margin reaching base of hind coxa; peritreme noticeably upraised, rounded, matte; metepimeron narrow (Fig. 5H). ***Hemelytron.*** Slightly narrowed anteriorly, and widened posteriorly; longitudinal ridge on clavus present, distinct; claval commissure almost twice longer than scutellum; medial fracture distinct, surpassing middle of corium; ridge along medial fracture present, surpassing middle of corium; embolium mostly narrow, apically widened, its width subequal to 1/6–1/7 of cuneus width at base (Fig. 1); R+M almost indistinct on posterior part of corium (Fig. 5I); cuneus delimited with pronounced incision, longer than wide; membrane with two cells (Fig. 5J). *Legs*. Forecoxa slightly longer than pronotum, slightly longer and as wide as middle and hind coxae; forefemur widened, approximately the same width as hind femur, each of them wider than middle femur (Fig. 5K); tarsus three-segmented, segment I and III subequal in length; segment II slightly longer than each of them; suture between segment II and III weak (Fig. 5G); claw with subapical tooth, middle row of tiles on unguitractor distinct, not reduced (Fig. 5F). ***Genitalia.*** See description for species.

Female. Similar to male, but antennal segment II wider and shorter. *Genitalia*. See species description.

Etymology. The genus is named for its enlarged labrum. The gender is feminine.

Remarks. *Labriella* cannot be confidently placed to any of the Cylapinae tribes based on the current classification and diagnoses (Gorczyca 2000). The combination of the vertical head, carinate vertex, antennae shorter than the body and the presence of the ridge along the medial fracture occurs in all representatives of Bothriomirini (Namyatova et al. 2019). However, bothriomirines are distinctly punctate, their labium not reaching the abdomen, they have a collar not delimited or shallowly delimited, the mesopleural apodeme round, and their mesothoracic spiracle without microsculpture. All those character states are absent in *Labriella* (see Diagnosis).

Labriella is similar to all Fulviini in that the total antennal length is shorter than the body, antennal segment II is as thick as segment I, and the labium is relatively long, the apex is reaching abdominal segments IV–V. However, *Labriella* differs from other Fulviini representatives in the possession of a vertical head (Fig. 5A), whereas in Fulviini it is mainly horizontal (Gorczyca 2000). Additionally, in all examined representatives of Fulviini the antennal fossa is located near the suture between the mandibular and maxillary plates (e.g., Figs 8F, 11C, 13I, see also Wolski 2010; Wolski et al. 2017, 2018; Namyatova and Cassis 2019a for more SEM images of Fulviini heads), whereas in *Labriella* it is located just above the mandibular plate (Fig. 5A).

Labriella fits many characters provided for the Cylapini diagnoses by Wolski (2017), e.g., the vertical head (Fig. 5B), labial segments I and II not subdivided (Fig. 5E), and the collar delimited with deep depression (Fig. 5B). However, some characters of *Labriella* do not fit the diagnoses. For example, in Cylapini, the anterior portion of the vertex is perpendicular to the rest of the vertex, the buccula is ring-like, the ventral margin of the eye barely reaches or does not reach the mandibular plate, and the antennae are thread-like. Whereas in *Labriella* the vertex is sloping more or less gradually, the eye reaches the maxillary plate, the buccula is not ring-like (Fig. 5A) and the antennae are not thread-like (Fig. 5D). We place *Labriella* into Cylapini based on the shared vertical head character. Based on the personal observations and the literature, all genera of Cylapini have this type of head, whereas the head is horizontal or sub-horizontal in all examined Fulviini and all other characters vary within both tribes.

Among species of Cylapini, *Corcovadocola* and *Cylapoides* Carvalho, 1952 are most similar to *Labriella* with the eyes being at least slightly covering the anterior angles of the pronotum and the antennal length being shorter than the body. *Cylapoides* differs from the new genus in the eyes being slightly pedunculate, the labium reaching the hind coxae and the body covered with erect setae (Carvalho 1952). *Corcovadocola* differs in having a brachypterous female, the vertex being only slightly concave and the lateral margins of pronotum being slightly emarginate (Carvalho 1948). The structure of the labrum was not included in the initial descriptions for all the above-mentioned genera (Poppius 1913; Carvalho 1948, 1952, 1986).

Labriella may be similar to the Neotropical genus *Tucuruisca* Carvalho, 1986 placed within the Fulviini and known only from the initial description. It also has a vertical head and the long labium, and its antennae are shorter than the body. According to the image, the eyes in *Tucuruisca* are also large, and are placed very close to or even slightly covering the anterior angles of the pronotum. *Tucuruisca* differs from *Labriella* in possessing a body covered with long erect hairs, the antennal segment IV being shorter than segment II and the thickened hind femora (Carvalho 1986).

***Labriella fusca* sp. nov.**

http://zoobank.org/A9574811-547D-4FEE-8878-92E250E6F481
Figs 1, 5, 6, 7, 15B

Material examined. ***Holotype*: Australia: Qld:** Mossman Bluff Track, 5–10 km W Mossman, site 6, 16.46667°S, 145.3667°E, 860 m, 16 Dec 1988–30 Dec 1988, Monteith, Thompson and ANZSES, 1♂ (UNSW_ENT 00043296) (QM).

Paratypes**:** **Australia: Qld:** 10 km SE El Arish, Laceys Creek nr Mission Beach, 17.86067°S, 146.08632°E, 40 m, 23 Jul 1982–05 Aug 1982, S. and J. Peck, 1♂ (00043320), 1 sex unknown (00043333) (AMNH). Bellenden Ker Range, 1 km S of Cable Tower 6, North Queensland, 17.23409°S, 145.86514°E, 500 m, 17 Oct 1981–05 Nov 1981, Earthwatch/QLD. Museum, 1♂ (00043312) (QM). Bellenden Ker Range, Cableway Base Stn, 17.271°S, 145.9°E, 100 m, 17 Oct 1981–09 Nov 1981, Earthwatch, 1 sex unknown (00043311) (QM). Cardwell Ra, Upper Broadwater Ck Valley, 18.3°S, 145.9333°E, 700 m, 17 Dec 1986–21 Dec 1986, Monteith, Thompson, Hamlet, 1♂ (00043317) (QM). Davies Ck Rd, 20 km SE Mareeba, 17.05°S, 145.6°E, 750 m, 04 Dec 1988–13 Dec 1988, Monteith and Thompson, 1♂ (00043319) (QM). Downey Ck, 25 km SE Millaa Millaa, 17.65°S, 145.7833°E, 400 m, 07 Dec 1988, G. Monteith and G. Thompson, 4♀ (00043291–00043294) (QM). Graham Ra, 17.28333°S, 145.9667°E, 550 m, 08 Dec 1995–09 Dec 1995, Monteith, Cook, Thompson, 3♀ (00043313, 00043314, 00043331) (QM). Hughes Rd, Topaz, 17.43333°S, 145.7°E, 650 m, 06 Dec 1993–25 Feb 1994, Monteith, Janetzki and Cook, 2♂ (00043309, 00043310) (QM). Lake Eacham, 17.28796°S, 145.62616°E, 750 m, 09 Dec 1989–14 Jan 1990, Monteith, Thompson and Janetzki, 1♂ (AMNH_PBI 00201880), 1 sex unknown (00043306) (QM). Mossman Bluff, 2 km ESE, 9 km W Mossman, 16.65°S, 145.5667°E, 1000 m, 17 Dec 1988–19 Dec 1988, Monteith and Thompson, 1♀ (AMNH_PBI 00404490) (QM). Mossman Bluff Track, 5–10 km W Mossman, N. Qld, Site 6, 16.46667°S, 145.3667°E, 860 m, 20 Dec 1989–15 Jan 1990, Monteith, Thompson and ANZSES, 1♂ (AMNH_PBI 00202018) (QM). Mossman Bluff Track,5–10 km W Mossman (Site1), 16.46667°S, 145.3667°E, 250 m, 20 Dec 1989–15 Jan 1990, Monteith, Thompson and ANZSES, 1♀ (AMNH_PBI 00404484), 1♂ (AMNH_PBI 00404486) (QM). Mossman Bluff Track, 5–10 km W Mossman (Site 5), 16.46667°S, 145.3667°E, 760 m, 16 Dec 1988–30 Dec 1988, Monteith, Thompson and ANZSES, 1♂ (00043297) (QM); 01 Jan 1989–16 Jan 1989, Monteith, Thompson and ANZSES, 1♂ (00043298) (QM); 20 Dec 1989–15 Jan 1990, Monteith, Thompson and ANZSES, 3♂ (00043117–00043119) (QM). Mossman Bluff Track, 5–10 km W Mossman, Site 7, 16.46667°S, 145.3667°E, 1000 m, 20 Dec 1989–15 Jan 1990, Monteith, Thompson and ANZSES, 3♂ (AMNH_PBI 00201868, AMNH_PBI 00201878, 00051481), 1♀ (AMNH_PBI 00404485) (QM). Mossman Bluff Track, 5–10 km W Mossman, site 6, 16.46667°S, 145.3667°E, 860 m, 16 Dec 1988–30 Dec 1988, Monteith, Thompson and ANZSES, 1♂ (00043295) (QM). Mossman Bluff Track, 9 km W Mossman, 16.44365°S, 145.29083°E, 1000 m, 17 Dec 1988, G. Monteith and G. Thompson, 1♂ (00043303) (QM). Mossman Bluff Track, 9 km W Mossman, Site 6, 16.44365°S, 145.29083°E, 860 m, 20 Dec 1989, Monteith and Thompson, 1♂ (00043302) (QM). Mossman Bluff Track, 10 km W Mossman, 16.45958°S, 145.27618°E, 1200 m, 17 Dec 1988, G. Monteith and G. Thompson, 1♂ (00043299), 2♀ (00043300, 00043301) (QM). Mt Finnigan summit, via Helenvale, 15.81667°S, 145.2833°E, 1100 m, 28 Nov 1985–30 Nov 1985, Monteith, Cook, Roberts, 1♂ (00043315) (QM). Mt Fisher, 7 km SW Millaa Millaa,Whiteing

Rd, 17.55°S, 145.5667°E, 1200 m, 05 May 1983, G. B. Monteith, D. K. Yeates, 1♀ (AMNH_PBI 00404493) (QM). Mt Lewis Rd, 11 km from H'way (Site 1), 16.05°S, 145.2667°E, 1000 m, 18 Dec 1889–13 Jan 1990, Monteith, Thompson and ANZSES, 1♂ (00043304) (QM). Mt Lewis Rd,16 km from H'way (Site 2), 16.56667°S, 145.2667°E, 950 m, 18 Dec 1989–13 Jan 1990, Monteith, Thompson and ANZSES, 1♂ (00043305) (QM). Mt Spurgeon; 2 km SE, via Mt Carbine, 16.45°S, 145.2°E, 1100 m, 20 Dec 1988, Monteith and Thompson, 3♂ (00043120, 00043307, 00043308), 4♀ (00043121, AMNH_PBI 00404487-AMNH_PBI 00404489) (QM). Mt Williams 0.5 km NW, 16.91667°S, 145.6667°E, 870 m, 28 Nov 1997, G. B. Monteith, 1♀ (AMNH_PBI 00404491) (QM). PEI road. Topaz, 17.4°S, 145.68333°E, 580 m, 06 Dec 1993–25 Feb 1994, Monteith, Janetzki and Cook, 1♂ (00043316) (QM). Paluma Dam Rd, Site 2, 19.23333°S, 146.2167°E, 720 m, 17 Nov 1990–08 Dec 1990, Monteith and Seymour, 1♂ (00043318) (QM). Polly Ck, (Hasenpusch property), 17.46667°S, 146.0167°E, 50 m, 25 Nov 1994–10 Jan 1995, Monteith and Hasenpusch, 1 sex unknown (00043332) (QM). Russell River at Bellenden Ker Landing, 17.25°S, 145.94°E, 5 m, 24 Oct 1981–09 Nov 1981, Earthwatch, 1♂ (AMNH_PBI 00404492) (QM). Tully R. Xing, 10 km S Koombooloomba Dam, 17.9318°S, 145.61902°E, 750 m, 08 Dec 1989, Monteith, Thompson and Janetzki, 1♀ (00043330) (QM).

Diagnosis. Body mostly brown to dark brown; clavus and corium with transversal stripe somewhat darker than rest of hemelytron (Fig. 1); labial segment III, scutellum apically, marking on cuneus at base, markings on abdomen, fore- and hind coxa at least basally, tibia apically, tarsi entirely or partly whitish yellow; endosoma with elongate sclerite, tapering apically; endosoma with sub-rectangular sclerite at base of elongate sclerite, and with sclerotised area on left side (Fig. 6A, B); dorsal labiate plate with semilunar sclerotised rings, those rings small, subequal to ca. 0.12–0.14 of dorsal labiate plate width (Fig. 7A).

Description. Male. Body length 2.7–3.0. **Coloration** (Fig. 1). Mainly brown to dark brown, sometimes with reddish tinge; antennal segment II apically, labial segment III, scutellum apically, base of cuneus, markings on abdomen, fore- and hind coxae at least basally, tibia apically, tarsi entirely or partly whitish yellow. Antennal segment I also sometimes pale brown to whitish yellow. **Surface and vestiture.** As in generic description. **Structure and measurements.** Body ca. 2.6–2.8 × as long as wide, ca. 3.1–3.3 × as long as pronotum width. Head ca. 2.2–2.5 × as wide as long; vertex ca. 1.0–1.1 × as wide as eye; in anterior view head ca. 1.2–1.3 × as wide as high; antennal segment I ca. 1.1–1.2 × as long as vertex; segment II ca. 3.0–3.5 × as long as segment I, ca. 3.3–3.8 × as long as vertex width, 1.2–1.3 × as long as head width, ca. 0.9 × as long as pronotum width; pronotum ca. 1.9–2.1 × as wide as long, ca. 1.3–1.4 × as wide as head. ***Genitalia.*** Genital capsule simple, without supragenital bridge; apical part of ventral wall curved dorsally (Fig. 6C). Right paramere short, with swelling on basal half directed outwards; right paramere also with widened apical half; apical process of right paramere narrow in dorsal view and flat in posterior view (Fig. 6D, E); left paramere L-shaped, slightly longer than right

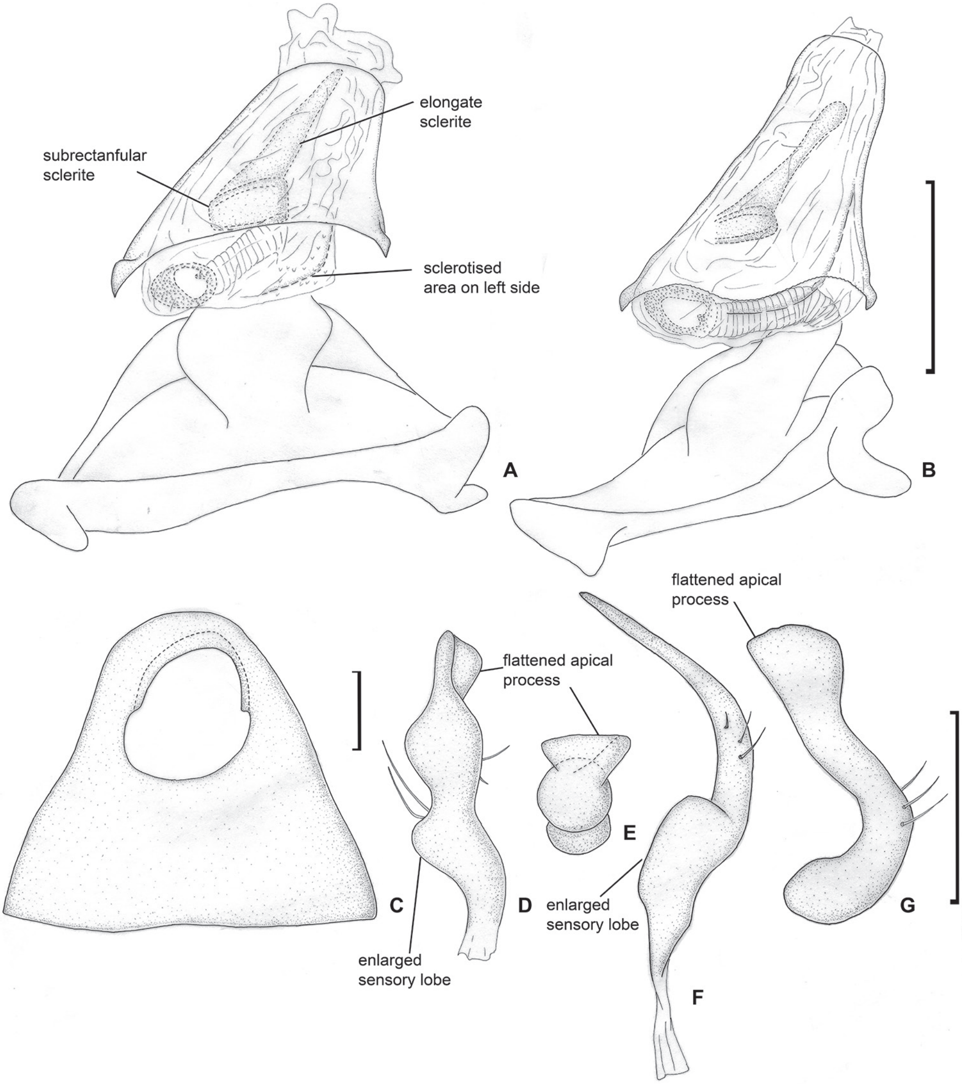

Figure 6. Male genitalia. *Labriella fusca* **A** aedeagus, dorsal view **B** aedeagus, left lateral view **C** genital capsule, dorsal view **D** left paramere, dorsal view **E** left paramere, posterior view **F** right paramere, dorsal view **G** right paramere, posterior view.

paramere, mostly narrow with swollen basal part, swelling directed upwards and inwards; apical process of left paramere flat in posterior view (Fig. 6F, G), aedeagus with phallobase wider than phallotheca; endosoma not subdivided into vesica and conjunctiva; endosoma voluminous with sclerotised area on the left, elongate spicule tapering apically, and subrectangular spicule at base of elongate spicula; ductus seminis mostly membranous with coils, it curved right side within endosoma with secondary gonopore placed near right basal angle of phallotheca; ductus seminis with

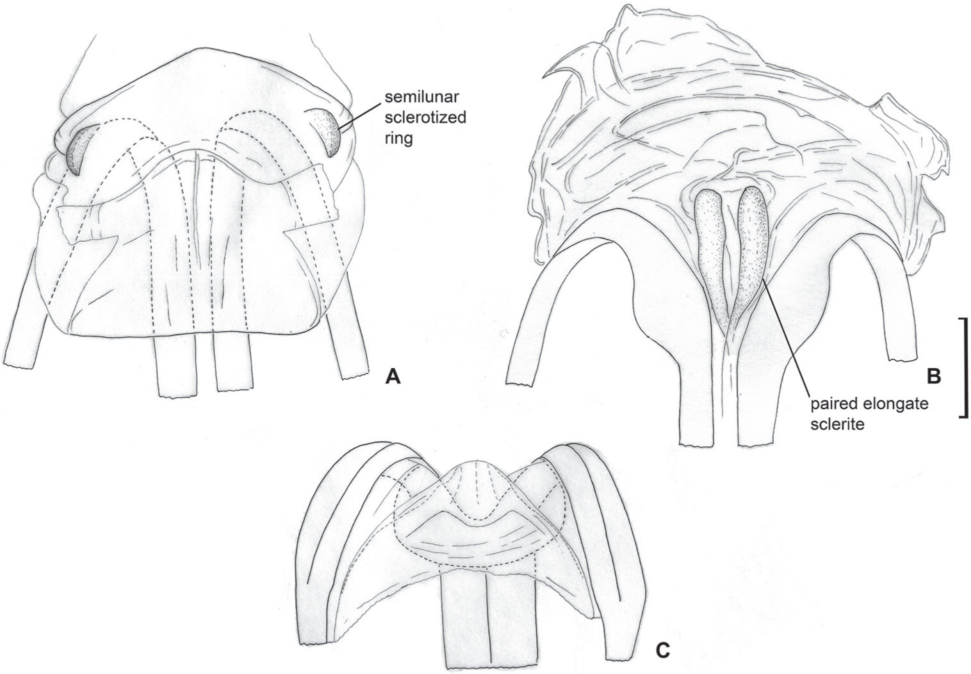

Figure 7. Female genitalia. *Labriella fusca* **A** dorsal wall **B** ventral wall of bursa copulatrix **C** posterior wall of bursa copulatrix.

basal part sclerotised; ductus seminis around secondary gonopore oval, sclerotised, armed with microsculpture (Fig. 6A, B).

Female. Body length 2.7–2.9. **Coloration** (Fig. 1). As in male. **Surface and vestiture.** As in generic description. **Structure and measurements.** Body ca. 2.6–2.7 × as long as wide, ca. 3.1–3.3 × as long as pronotum width. Head ca. 1.9–2.2 × as wide as long; vertex ca. 1.0–1.3 × as wide as eye; in anterior view head ca. 1.1–1.2 × as wide as high; antennal segment I ca. 1.1–1.2 × as long as vertex; segment II ca. 2.3–2.7 × as long as segment I, ca. 2.3–2.8 × as long as vertex width, ca. 0.9–1.0 × as long as head width, ca. 0.7–0.8 × as long as pronotum width; pronotum ca. 1.8–2.0 × as wide as long, ca. 1.3–1.4 × as wide as head. ***Genitalia.*** Dorsal labiate plate with semilunar sclerotised rings, those rings small, ca. 0.12–0.14 × as wide as dorsal labiate plate width, and placed near posterior margin of dorsal labiate plate; lateral oviducts attached in the middle of dorsal labiate plate (Fig. 7A); ventral wall with paired elongate sclerites near vulva (Fig. 7B); posterior wall membranous, without any sclerotisation (Fig. 7C).

Distribution. Known from numerous localities in the Australian Wet Tropics (Fig. 15B).

Collection methods. The specimens of *Labriella fusca* were collected using pitfall traps, intercept traps, pyrethrum spraying of trees and logs and baited window trap.

Etymology. Species is named so for its brown colour, *fuscus* from Latin meaning brown.

Tribe Fulviini

Callitropisca gen. nov.

http://zoobank.org/91DA3027-7449-4C4E-98FF-AEF2DA110A34

Type species. *Callitropisca florentine* sp. nov. by original designation.

Diagnosis. *Callitropisca* can be recognised using following combination of characters: swollen and rounded calli, separated from each other; collar and rest of pronotum with distinct depression (Fig. 8D); vertex upraised above eye in lateral view (Fig. 8G); in lateral view distance between eye and ventral margin of eye equal to 1/6 of eye height

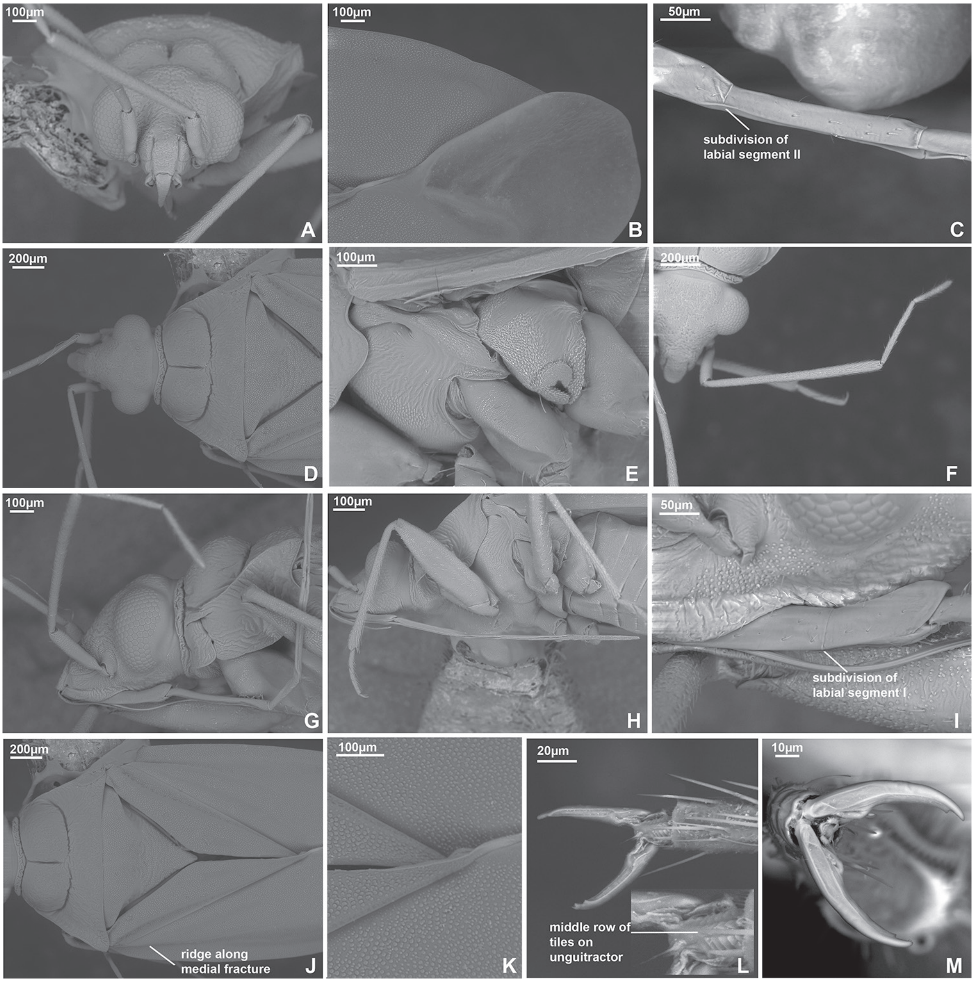

Figure 8. SEM images. *Callitropisca florentine* **A** head, anterior view **B** cuneus and membrane cell **C** apical part of labial segment II **D** head and pronotum, dorsal view **E** pleura **F** antenna **G** head and pronotum, lateral view **H** labium **I** labial segment I **J** scutellum, clavus and corium **K** tubercles on hemelytron **L** pretarsus, ventral view **M** pretarsus, dorsal view.

(Fig. 8G); vertex not carinate (Fig. 8D, G); lateral margins of pronotum strongly carinate (Fig. 8G); apex of labial segment I not reaching pronotum (Fig. 8G); antennal segment I subequal to vertex width; antennal segment II straight, cylindrical, not widened or swollen (Fig. 8G, F); body impunctate, head and pronotum rugose; pleura smooth, without distinct rugosities (Fig. 8D, E, I–K); body covered with very short and sparse simple setae and small tubercles (Fig. 8K); hemelytron full, not shortened or modified, with whitish stripes on clavus and corium (Fig. 2); claval commissure twice as long as scutellum (Fig. 8J); metathoracic evaporative area large and triangular (Fig. 8E); left paramere with large outgrowth on basal part directed outwards and upwards (Fig. 9G, H), apical part of ductus seminis widened, with two lobes having row of narrow outgrowths along outer margin (Fig. 9A–C); dorsal labiate plate without sclerotised rings (Fig. 10A).

Description. Male. Coloration (Fig. 2). Background colouration brown to dark brown, with yellow stripes on hemelytron. See species description for details. **Surface and vestiture.** Head and pronotum shiny, hemelytron matte (Fig. 2). Body impunctate; head and pronotum with distinct rugosities (Fig. 8D, G); pleura almost smooth, not visibly rugose (Fig. 8E); head laterally, scutellum and hemelytron clothed with small tubercles (Fig. 8G, J, K); net-like pattern of microsculpture present on mesopleuron ventrally (Fig. 8E); scutellum not serrate laterally (Fig. 8J). Body clothed with short adpressed setae, shorter than antennal segment II width; setae on dorsum very short and sparse (Fig. 8K); setae on antenna, pleura, legs and abdomen denser and longer; mesopleuron almost without setae; metapleuron with dense adpressed setae anteriorly (Fig. 8E); spines on tibiae short and pale; body impunctate (Fig. 8D, E, G, J, K). **Structure and measurements.** Body elongate. ***Head.*** Horizontal, dorsally as long as wide or slightly longer than wide, not carinate; eye not covering anterior margin of pronotum posteriorly, not protruding; vertex not carinate (Fig 8D); in anterior view head wider than high; base of clypeus not delimited with depression, located above ventral margin of eye and antennal fossa; antennal fossa located near ventral margin of eye (Fig. 8A); in lateral view head slightly longer than high; vertex upraised above eye; base of clypeus not delimited with depression; distance between eye and ventral margin of head subequal to 1/6 of eye height; eye placed close to lateral margin of pronotum, but not covering it; antennal fossa removed from eye at distance equal to antennal fossa width, and located close to suture between mandibular and maxillary plates; mandibular and maxillary plates not separated by suture or depression from head; labrum triangular, shorter than labial segment I length; buccula elongate, 5–6 × as long as wide; distance between buccula and pronotum as long as buccula length (Fig. 8G). ***Antenna.*** Total length shorter than body; antennal segment I not widened, shorter than head width; antennal segment II cylindrical, slightly thinner than segment I, longer than head width; segment III slightly thinner than segment II, cylindrical, slightly shorter than segment II; segment IV subequal to half of segment III, and as thick as segment III (Fig. 8G, F). ***Labium.*** Apex reaching abdominal segments IV–V (Fig. 8H); labial segment I not surpassing posterior margin of head, subdivided in apical half (Fig. 8G, I); segment II almost twice as long as segment I, subdivided subapically, its apical part 9–10 × as long as wide (Fig. 8C, G); segment III subequal to 2/3 of segment II, more than 10 × as long as wide; segment IV subequal to 2/3 of segment

III (Fig. 8H). ***Thorax.*** Pronotum wider than long; lateral margins straight in dorsal view, carinate; collar delimited dorsally and laterally (Fig. 8D, G); calli large, upraised, rounded, covering slightly more than half of pronotum, separated from each other and pronotum with distinct depression; posterior margin concave (Fig. 8D); scutellum flat, mesoscutum exposed, (Fig. 8J); propleural suture T-shaped (Fig. 8G); mesothoracic apodeme slit-like; mesothoracic spiracle oval, with one or two rows of microsculpture along anterior margin; metathoracic gland evaporative area large and triangular, lateral margin almost reaching base of hind coxa; peritreme upraised, rounded; metepimeron narrow (Fig. 8E). ***Hemelytron.*** Outer margin rounded (Fig. 2); ridge on clavus present, distinct; claval commissure twice longer than scutellum; medial fracture almost reaching middle of corium; ridge along medial fracture only basally visible; R+M basally visible and faint medially and apically (Fig. 8J); embolium wide, its widest part subequal to quarter of cuneus width at base (Fig. 2); cuneus delimited with faint suture, not incised; membrane with two cells; distance between cell and membrane longer than cell length (Fig. 8B). ***Legs.*** Forecoxa shorter than pronotum length, slightly wider and longer than middle and hind coxa; forefemur 4 × as long as wide, wider than and as long as middle femur (Fig. 8H); hind legs broken; claw with subapical tooth, unguitractor with medial row fully developed (Fig. 8L). ***Genitalia.*** See species description.

Etymology. The genus is so named because of its swollen calli. The gender is feminine.

Remarks. *Callitropisca* has all the diagnostic features for Fulviini, e.g., horizontal head, antenna shorter than body, forecoxae and forefemora enlarged, labium reaching middle of abdomen (Gorczyca 2000). It also has subdivided labial segments I and II, which is common for this group (Wolski and Henry 2015; Namyatova and Cassis 2019a). Therefore, we place *Callitropisca* into Fulviini. This genus differs from all other Fulviini representatives in the diagnostic characters, especially in possessing swollen and rounded calli, separated from each other, and the collar and rest of pronotum with a distinct depression (Fig. 8D).

Callitropisca is most similar, and, presumably, most closely related to *Micanitropis* and *Xenocylapidius*. *Callitropisca*, and *Micanitropis* have a similar colour pattern, with the body mainly brown to dark brown and whitish yellow longitudinal stripes on the clavus and corium (Fig. 2), the presence of rugosities on the head and pronotum (Figs 8A, D, G, J, 13A, E, I, M), the setae on the hemelytron sparse (Figs 8K, 13B), the presence of an outgrowth on the right side on posterior margin of genital capsule when viewed dorsally (Figs 9I, 14D), and the aedeagus with the ductus seminis having a row of narrow outgrowths along the apical margins (Figs 9A–C, 14A, B). The structure of the genital capsule for *Xenocylapidius* is unknown; however, it has a similar structure of the aedeagus (Wolski and Gorczyca 2014b). The authors named the structure "basal sac of endosoma". However, it has similar shape and position as the apical part of the ductus seminis in *Callitropisca* and *Micanitropis*. In all those species, the left paramere has a large outgrowth in the basal half (Figs 9G, H, 14G, H; Wolski and Gorczyca 2014b: figs 19, 24, 29, 35, 40). The hemelytron of *Callitropisca* and *Micanitropis* is covered with rounded small tubercles (Figs 8K, 13B), and similar microstructure, although more elongate in shape, was also observed in the examined species of *Xenocylapidius* by the first author. Both, *Xenocylapidius* and *Micanitropis* differ from *Callitropisca* in the calli being less developed, and not surrounded by a distinct depression (Fig. 13E; Wolski and Gorczyca 2014b: figs 1–8), the frons not raised above the eye in lateral view (Fig. 13I; Wolski and Gorczyca 2014b: figs 9–15), and the labial segment I reaching the pronotum (Fig. 13I, N; Wolski and Gorczyca 2014b: figs 9–15). *Micanitropis* additionally differs from *Callitropisca* in the pleura being noticeably rugose (Fig. 13J), the claval commissure being only slightly longer than clavus (Fig 13M) and the dorsal labiate plate possessing large sclerotised rings (Fig. 10B).

Callitropisca florentine **sp. nov.**

http://zoobank.org/F6544F7C-8B3F-4742-9075-ECCDC55352A6
Figs 2, 8, 9, 10A, C, E, 15A

Material examined. ***Holotype*****:** **Australia: Tas:** 29 km WNW Maydena on Eleven Rd, Florentine Valley, 42.76667°S, 146.4°E, 460 m, 01 Feb 1980–06 Feb 1980, A. F. Newton, M. K. Thayer, 1♂ (UNSW_ENT 00043066) (TMAG). ***Paratypes*****:** **Australia: Tas:** 29 km WNW Maydena on Eleven Rd, Florentine Valley, 42.76667°S, 146.4°E, 460 m, 01 Feb 1980–06 Feb 1980, A. F. Newton, M. K. Thayer, 1♀ (00043068) (AMNH). Strahan, 42.15°S, 145.3333°E, 52 m, Lea and Carter, 1♀ (00043067) (SAMA).

Diagnosis. Characterised by head, pronotum, scutellum and pleura dark brown, and hemelytron brown; antennal segments mostly pale brown to brown; labial segment I red; hemelytron with whitish yellow stripes on clavus, along claval suture and on corium, and embolium whitish basally; coxa mostly reddish brown or reddish, fore- and middle femora mostly brown; foretibia pale brown, middle tibia reddish basally and yellow apically (Fig. 2); vesica with three sclerites elongate and acute apically and two sclerotised areas, one of those areas convex and placed on the left, and another one bifurcate, placed at base of spicules (Fig. 9A–C).

Description. Male. Body length 3.1. **Coloration** (Fig. 2). ***Head.*** Dark brown with faint pale brown marking near inner margin of eye. Antennal segment I brown basally, yellow to pale brown medially and red apically; segments II–IV uniformly brown; labial segment I red, segments III and IV pale brown to brown. ***Thorax.*** Pronotum and scutellum dark brown to black; pleura dark brown. ***Hemelytron.*** Mostly brown with two whitish yellow stripes on clavus, whitish yellow stripe on claval suture and two stipes on corium; stripes not reaching or barely reaching middle of corium; embolium whitish yellow basally; membrane pale brown with brown cells. ***Legs.*** Coxae reddish brown, whitish yellow apically; fore- and middle femora brown with wide pale brown band in apical half and whitish yellow at extreme apex; foretibia pale brown; middle tibia reddish basally and yellow apically; tarsi pale brown. **Surface and vestiture.** See generic description. **Structure and measurements.** Body ca. 2.7 × as long as wide, ca. 3.1 × as long as pronotum width; head horizontal, as wide as long, in anterior view head ca. 1.4 × as long as high; antennal segment I ca. 1.2 × as long as vertex width, ca. 0.5 × as long as head width; antennal segment II ca. 3.1 × as long as segment I, ca. 3.7 × as long as vertex width, ca. 1.7 × as long as head width, ca. 0.9 × as long as pronotum width; pronotum ca. 1.9 × as wide as head, ca. 2.3 × as wide as long. ***Genitalia.*** Genital capsule as

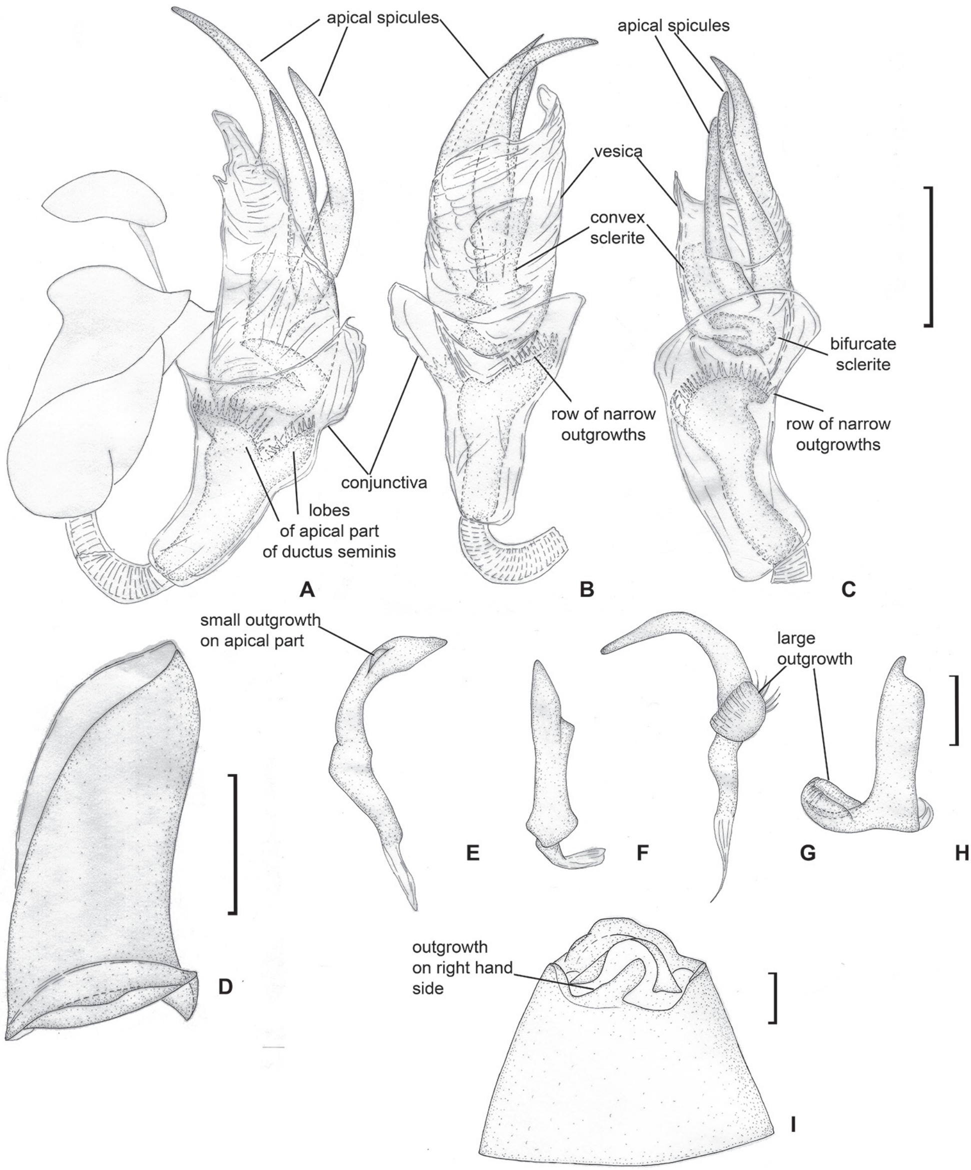

Figure 9. Male genitalia. *Callitropisca florentine* **A** aedeagus, left lateral view **B** aedeagus, dorsal view **C** aedeagus, ventral view **D** theca **E** left paramere, dorsal view **F** left paramere, posterior view **G** right paramere, dorsal view **H** right paramere, posterior view **I** genital capsule.

long as wide, with outgrowth on right hand side on posterior margin dorsally (Fig. 9I). Parameres r-shaped, subequal in length; basal part of right paramere with angulate swelling directed inwards and rounded outgrowth directed upwards; apical part of right paramere widened with small tubercle apically; left paramere with large outgrowth on basal part directed outwards and upwards, apical process narrow and elongate (Fig. 9E–H); theca without outgrowths (Fig. 9D); endosoma subdivided into vesica and conjunctiva;

vesica with three elongate spicules acute apically, and with two sclerites, one of them convex and placed on the left, and another one bifurcate, placed at base of spicules; apical part of ductus seminis strongly sclerotised, secondary gonopore surrounded by two wide lobes with row of narrow outgrowths along outer margin (Fig. 9A–C).

Female. Body length 3.0. **Coloration** (Fig. 2). Head dark brown with yellow marking near inner margin of eye, or reddish brown with dark brown area around antennal fossa, yellow marking near inner margin of eye and paired markings on vertex

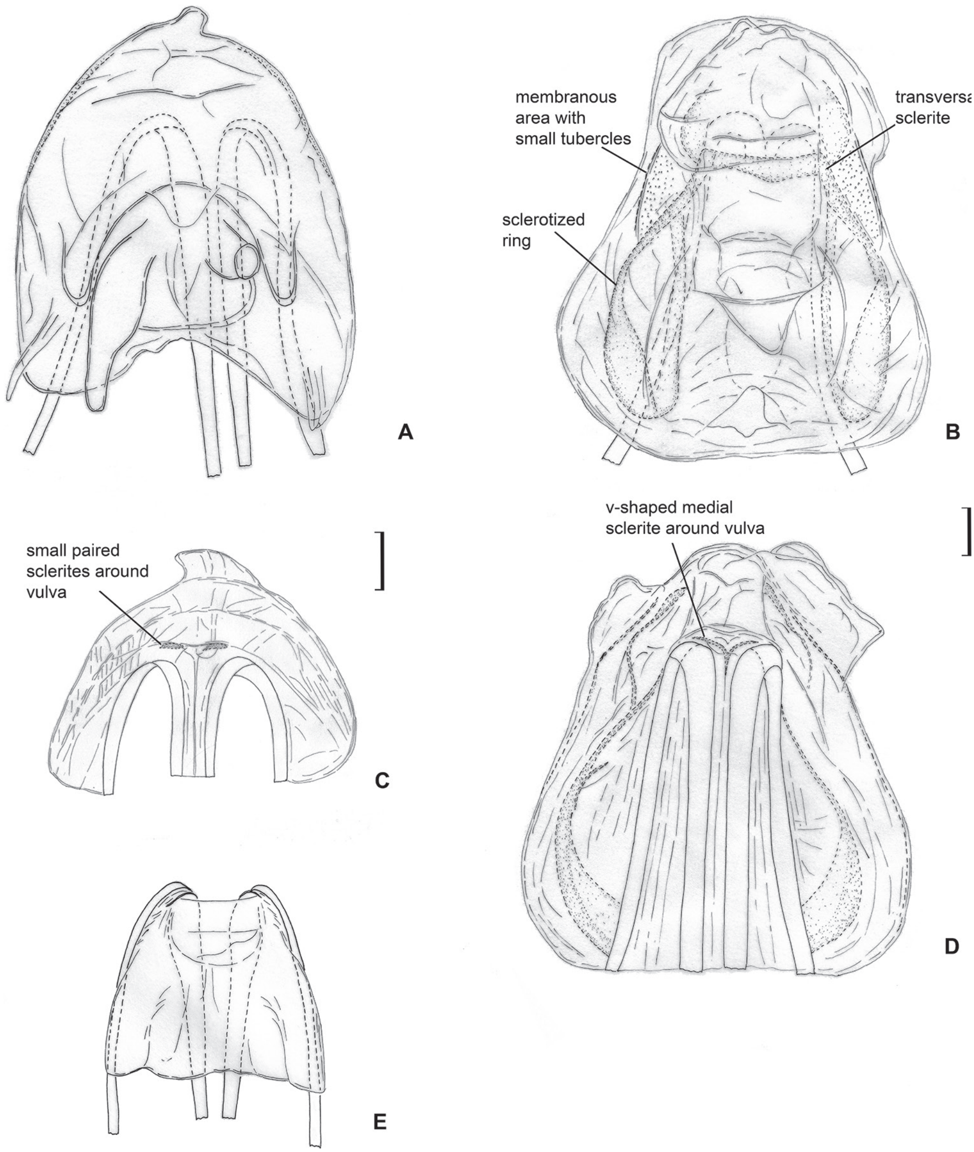

Figure 10. Female genitalia. *Callitropisca florentine* **A** dorsal wall **C** ventral wall of bursa copulatrix **E** posterior wall of bursa copulatrix. *Micanitropis seisia* **B** dorsal wall **D** ventral wall of bursa copulatrix.

medially closer to frons; antennal segment II changing colour gradually from pale brown to brown or from yellow to red; segment IV mostly brown, pale brown apically; pronotum brown to dark brown; pleura dark brown with reddish tinge or with red metapleuron including metathoracic scent gland evaporative area; coxae reddish brown or reddish, whitish yellow apically; legs as in male, but with more reddish tinge; abdomen reddish brown. **Surface and vestiture.** See generic description. **Structure and measurements.** Body ca. 2.5 × as long as wide, ca. 3.0–3.3 × as long as pronotum width; head horizontal, ca. 1.2 × as wide as long; in anterior view head ca. 1.4–1.5 × as long as high; antennal segment I ca. 0.7–0.8 × as long as vertex, ca. 0.3–0.4 × as long as head width; antennal segment II ca. 3.7–4.0 × as long as segment I, ca. 2.6–3.1 × as long as vertex, ca. 1.4–1.5 × as long as head width, ca. 0.8 × as long as pronotum width; pronotum ca. 1.6–1.9 × as wide as head, ca. 2.2 × as wide as long. ***Genitalia.*** Dorsal labiate plate without any sclerites; lateral oviducts placed in anterior half of dorsal labiate plate (Fig. 10A); ventral wall with small paired sclerites around vulva (Fig. 10C); posterior wall of bursa copulatrix without sclerites (Fig. 10E).

Distribution. Known only from western Tasmania (Fig. 15A).

Collection techniques. Unknown.

Etymology. The species is named after Florentine valley, where two specimens of this species were collected.

Laetifulvius gen. nov.

http://zoobank.org/0858F4B1-6362-4075-8AF9-31422D016EB1

Type species. *Laetifulvius morganensis* sp. nov. by original designation.

Diagnosis. Differs from other representatives of Cylapinae in the following combinations of characters: head semi-horizontal, antennal fossa attached near depression between mandibular and maxillary plates (Fig. 11C); antennal segment I length subequal to vertex width; eye located close to pronotum and slightly covering its anterior angle (Fig. 11B, C); vertex not carinate (Fig. 11B, C); labial segment I only slightly surpassing anterior margin of head, subdivided with suture (Fig. 11D, E), segment II subdivided with shallow suture apically (Fig. 11F); calli flat, indistinct (Fig. 6B); lateral margins of pronotum not carinate, rounded (Fig. 11C); collar delimited with shallow depression, relatively wide, wider than antennal segment I (Fig. 11B); evaporative area large and triangular (Fig. 11J); cuneus slightly longer than wide (Fig. 11I); forefemora not enlarged; hind femur twice wider than forefemur; tarsal segments subequal in length (Fig. 11L); body impunctate, clothed with simple semi-adpressed setae (Figs 2, 11B, H–J); endosoma not subdivided into vesica and conjunctiva (Fig. 12A, B).

Description. Male. Coloration (Fig. 2). Mainly reddish brown with whitish yellow, yellow and pale brown markings. **Surface and vestiture** (Fig. 11B, C, H–J). Dorsum glabrous, shiny, impunctate and not rugose, without distinct tubercles or net-like pattern of microsculpture on dorsum and pleura; scutellum not serrated laterally; body clothed with pale sparse simple semi-adpressed setae, shorter than antennal segment II

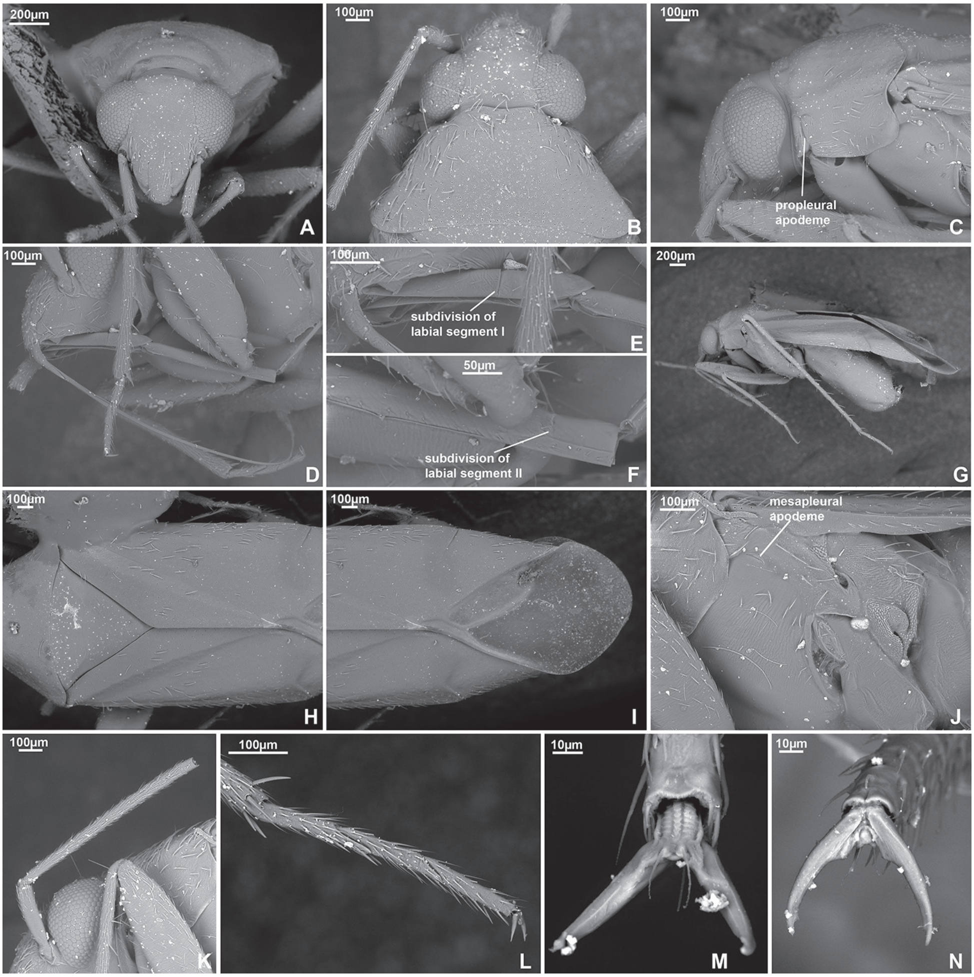

Figure 11. SEM images. *Laetifulvius morganensis* **A** head, anterior view **B** head and pronotum, dorsal view **C** head, lateral view **D** labial segments I and II **E** labial segment I **F** apical part of labial segment II **G** legs **H** scutellum, clavus and corium **I** cuneus and membrane cell **J** pleura **K** antennal segments I and II **L** hind tarsus **M** pretarsus, ventral view **N** pretarsus, dorsal view.

width, those setae denser on antennae and tibiae and very rare on pleura. **Structure.** ***Head.*** Semi-horizontal, in dorsal view head wider than long; vertex not carinate posteriorly; eye not protruding, covering anterior part of pronotum (Fig. 11B); in anterior view head slightly wider than high; antenna attached near ventral margin of eye; clypeus not separated from frons by depression, its base placed slightly above ventral margin of antennal fossae (Fig. 11A); in lateral view head as high as long; vertex not upraised above eye; eye removed from ventral side of head at distance subequal to fifth part of eye height, not covering anterior angles of pronotum; antennal fossa adjacent to eye, placed near suture between mandibular and maxillary plates, mandibular and maxillary plates not separated from head by suture posteriorly; labrum triangular, shorter than labial segment I; buccula elongate, ca. 5–6 × as long as high; distance between buccula and pronotum subequal to buccula length (Fig. 11C, D). ***Antenna.*** Segment I subequal to vertex width; segment II as wide as segment I, cylindrical, not incrassate apically (Fig. 11K). ***Labium.*** Labial segment I subdivided in apical half (Fig. 11E), apex reaching base of forecoxa (Fig. 11D); segment II slightly longer than segment I, subdivided apically with shallow suture (Fig. 11F). ***Thorax.*** Pronotum wider than long, lateral margins straight in dorsal view (Fig. 11B), in lateral view not carinate, rounded (Fig. 11C); collar delimited with shallow suture, relatively wide, wider than antennal segment I (Fig.11B); posterior margin of pronotum concave (Fig. 11B, H); calli flat, almost indistinct, occupying less than half of pronotum (Fig. 11B); scutellum flat; mesoscutum exposed (Fig. 11H); propleural apodeme T-shaped (Fig. 11C); mesepimeral apodeme slit-like; mesepimeral spiracle oval, with wide area of microsculpture along anterior margin dorsally; metathoracic gland evaporative area triangular, lateral margin almost reaching base of hind coxa; peritreme upraised, rounded; metepimeron narrow (Fig. 11J). ***Hemelytron*** (Fig. 11H, I). Outer margin almost straight; clavus with longitudinal ridge; claval commissure longer than scutellum; medial fracture reaching middle of corium, but not surpassing it; ridge along medial fracture shallow, present basally and medially; white marking on corium posteriorly slightly upraised; R+M visible over entire length; embolium narrow, its widest part subequal to 1/5–1/6 of cuneus width; cuneus delimited, slightly longer than wide, its base not incised; membrane with singe cell, distance between cell and apex of membrane longer than cell length. ***Legs.*** Forecoxa as long as pronotum; fore- and hind coxae subequal in size, middle coxa slightly smaller than forecoxa; forefemur slightly longer than pronotum, ca. 4 × as long as wide, as long as and slightly wider than middle femur; hind femur twice as wide and ca. 1.5 × as long as forefemur (Fig. 11G); hind tarsus three-segmented, segments subequal in length (Fig. 11L); claw with subapical tooth, middle row of tiles on unguitractor full (Fig. 11M). ***Genitalia.*** See species description.

Female. Unknown.

Etymology. The species is named for its colourful appearance, *laetus* from the Latin meaning colourful. The gender is masculine.

Remarks. In Cylapinae tribe diagnoses, the length of the antennae and labium are among the most important characters (Gorczyca 2000; Cassis et al. 2003; Wolski 2017; Namyatova et al. 2019; Namyatova and Cassis 2019a), and *Laetifulvius* representatives do not match the diagnoses for these traits. However, they do have antennal segments I and II subequal in width, an impunctate body, labial segments I and II subdivided, antennal fossa placed near suture between mandibular and maxillary plates, and this combination of characters is typical for Fulviini. Therefore, we place *Laetifulvius* in this tribe. Although most Fulviini have a horizontal head, in some its genera it is also subhorizontal, e.g., *Mycetocylapus* Poppius, 1914 (Namyatova and Cassis 2019a), *Trynocoris* Herring, 1976 (Herring 1976), *Fulviella* Carvalho, 1991 (Carvalho 1991).

Laetifulvius may be related to *Phylocylapus* Poppius, 1913, as according to the initial description, the latter has a vertical head, wide collar, flat calli and a large evaporative area. *Phylocylapus* differs from *Laetifulvius* in the leaf-like forefemora, the labial segment I reaching the middle of the forecoxa, and tarsal segment I being longer than segments II and III (Poppius 1913). Many characters in the description of the Neotropical genus *Tucuruisca* also fit those of *Laetifulvius*. Both of these genera have an inclined head, wide collar, large hind femur, and tarsal segments subequal in length (Carvalho 1986). *Tucuruisca* differs in the long setae covering the body, the antennal segment I being shorter than the clypeus length and the wide embolium.

Laetifulvius is not very similar to any other Australian genus, although it may be related to *Fulviella* and *Phyllofulvius* Carvalho, 1991 as they have a similar structure of the aedeagus with a voluminous endosoma not subdivided into conjunctiva and vesica and bearing

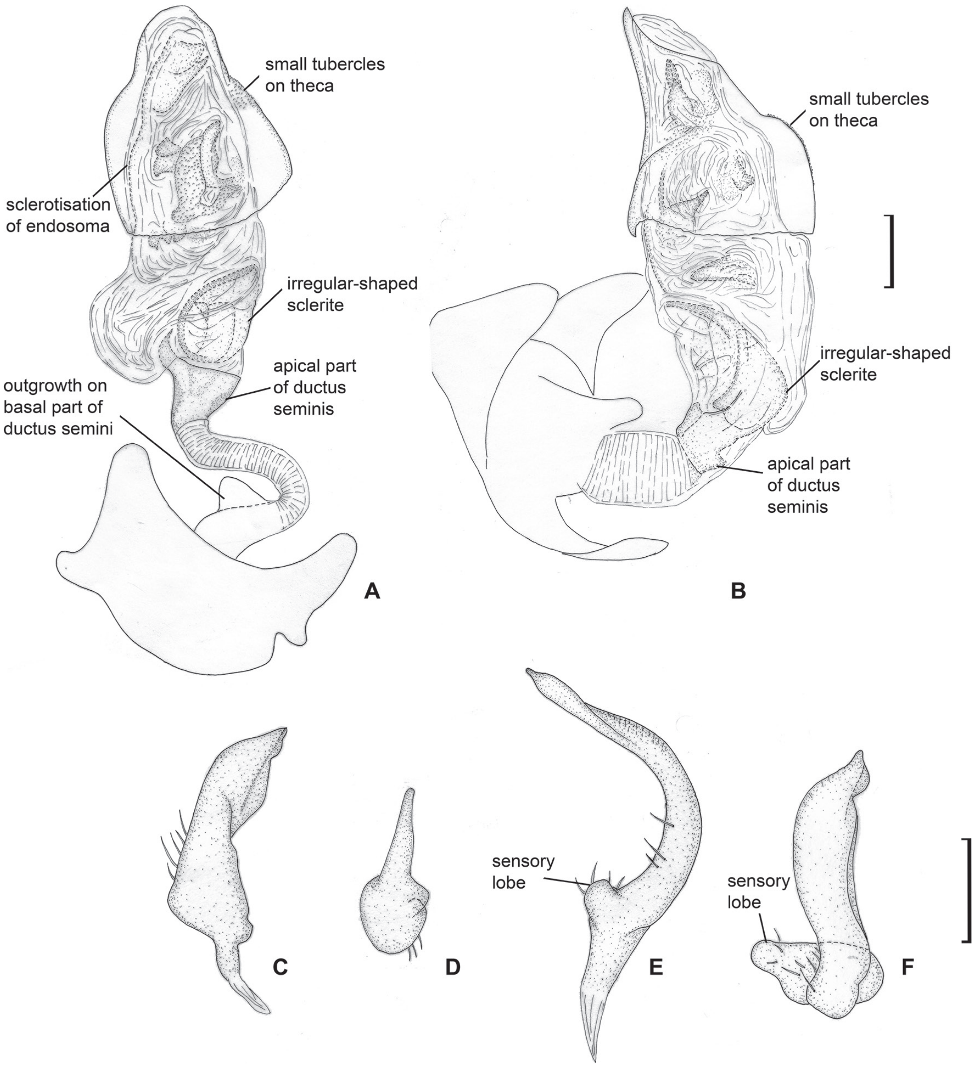

Figure 12. Male genitalia. *Laetifulvius morganensis* **A** aedeagus, dorsal view **B** aedeagus, left lateral view **C** left paramere, dorsal view **D** left paramere, posterior view **E** right paramere, dorsal view **F** right paramere, posterior view.

numerous sclerites (Fig. 12A, B; Carvalho 1991: figs 4, 11). Both genera differ from *Laetifulvius* in the forefemora being widened. *Fulviella* also differs from *Laetifulvius* in the vertex and the lateral margins of pronotum being carinate, the antennal segment I shorter than the vertex and the tarsal segment I longer than segments II and III each. *Phyllofulvius* differs from *Laetifulvius* in the leaf-shaped antennal segment II (Carvalho 1991).

Laetifulvius morganensis **sp. nov.**
http://zoobank.org/88354C89-E808-4409-A64F-4CD0E4B6593F
Figs 2, 11, 12, 15B

Material examined. ***Holotype*:** Australia: South Australia: 51 km NW of Morgan, 33.58333°S, 140°E, 150 m, 01 Nov 1995, Schuh, Cassis, and Gross, 1♂ (UNSW_ENT 00042973) (SAMA). Paratype. AUSTRALIA: South Australia: 51 km NW of Morgan, 33.58333°S, 140°E, 150 m, 01 Nov 1995, Schuh, Cassis, and Gross, 1 sex unknown (00042974) (AM).

Diagnosis. Head reddish brown, antennal segments I and II pale brown; segment II whitish yellow apically; labial segment I reddish brown, segments II and III pale brown to brown; pronotum uniformly brown; scutellum mostly yellow with reddish brown base; pro- and mesopleuron brown; metapleuron whitish yellow with reddish marking dorsally; metathoracic scent gland evaporative area whitish yellow; hemelytron mostly brown, corium with white oval marking posteriorly adjacent to cuneus; cuneus reddish brown; coxae mostly whitish yellow; femora reddish brown with whitish yellow apices; fore- and middle tibiae mostly pale brown; basal part of hind tibia reddish brown, its apical third or half whitish yellow (Fig. 2); endosoma sclerotised at right side, with large irregularly shaped sclerite near apical part of ductus seminis and numerous small sclerites and sclerotised areas (Fig. 12A, B).

Description. Male. Body length 3.0–3.1. **Coloration** (Fig. 2). Head reddish brown, with yellow and whitish yellow markings anteriorly; antennal segments I and II pale brown, segment II whitish yellow apically; labial segment I reddish brown, segments II and III pale brown to brown; pronotum uniformly brown; mesoscutum brown with reddish tinge laterally; scutellum mostly yellow, with base and longitudinal stripe reddish brown; pro- and mesopleuron brown; metapleuron whitish yellow with reddish marking dorsally; metathoracic scent gland evaporative area whitish yellow; hemelytron mostly brown, with reddish tinge anteriorly; embolium with reddish tinge posteriorly; corium with white oval marking posteriorly adjacent to cuneus; cuneus reddish brown; membrane pale brown; coxae uniformly whitish yellow or with brown bases; femora reddish brown with whitish yellow apices; fore- and middle tibiae mostly pale brown, reddish brown basally, foretibia sometimes red apically; basal part of hind tibia reddish brown, its apical third or half whitish yellow; tarsi whitish yellow to pale brown. **Surface and vestiture.** As in generic description. **Structure and measurements.** Body ca. 3.0–3.2 × as long as wide, ca. 3.3 × as long as pronotum width; head ca. 2.1–2.2 × as wide as long; vertex ca. 1.1–1.2 × as wide as eye; in anterior view head ca. 1.2–1.3 × as wide as high; antennal segment I ca. 1.1–1.2 × as long as vertex width, ca. 0.4 × as wide as head width; segment II ca. 3.1 × as long as segment I, ca. 3.4–3.7 × as long as vertex width, ca. 1.3 × as long as head width, ca. 0.8 × as long as pronotum width; pronotum ca. 2.0–2.3 × as wide as long, ca. 1.5–1.6 × as wide as head. ***Genitalia.*** Right paramere short, broad, r-shaped, its apical part broad in dorsal view and narrow in posterior view; left paramere ca. 1.5 × as long as right paramere, r-shaped, its apical part twisted in dorsal view and widened in posterior view; basal half of left paramere with wide outgrowth directed inwards (Fig. 12C–F); theca triangular with small tubercles on left hand side (Fig. 12A, B); endosoma not subdivided into vesica and conjunctiva, most part of ductus seminis membranous and coiled, basal part sclerotised with outgrowth directed upwards, apical part sclerotised and widened, subtriangular in dorsal view, with right side elongate; endosoma sclerotised at right side, with large irregularly shaped sclerite near apical part of ductus seminis and numerous small sclerites and sclerotised areas (Fig. 12A, B).

Distribution. Known only from type locality in South Australia (Fig. 15B).

Collection techniques. Both specimens were collected at light.

Etymology. The species is named after town Morgan, as it was collected nearby.

Micanitropis **gen. nov.**

http://zoobank.org/D54217ED-80D8-49C8-8BC1-4B7D7B9C911B

Type species. *Micanitropis seisia* sp. nov. by original designation.

Diagnosis. *Micanitropis* can be separated from other representatives of Cylapinae using the following combination of characters: body impunctate; dorsum without net-like pattern of microsculpture on head, pronotum and pleura; dorsum clothed with rare short adpressed setae; hemelytron covered with small tubercles and sparse setae; head, pronotum and pleura with distinct rugosities (Fig. 13A, B, E, F, I, J, M); head horizontal, in lateral view longer than high (Fig. 13I); vertex not carinate (Fig. 13E), not raised above eyes (Fig. 13I); length of antennal segment I subequal to vertex width; antennal segment II not modified (Fig. 13K); labium reaching or almost reaching genital segment (Fig. 13N); calli moderately raised, not delimited with depression laterally and posteriorly, delimited from each other with shallow depression; collar narrow, delimited with shallow depression (Fig. 13E); lateral margin of pronotum strongly carinate (Fig. 13I); corium and hind femora without translucent patches; cuneus as long as wide at base (Fig. 13F); hemelytron full, lateral margins rounded, not concave or constricted anteriorly (Fig. 2); metathoracic scent gland evaporative area triangular and large, reaching base of hind coxa (Fig. 13J); forefemur wider than middle and hind femora; tarsal segment I longer than segments II and III each (Fig. 13O); apical part of ductus seminis widened, with two lobes around secondary gonopore both having row of narrow outgrowths along outer margin (Fig. 14A, B).

Description. Male. Coloration (Fig. 2). Background colouration brown to dark brown with whitish yellow to pale brown markings and stripes, sometimes with reddish tinge. **Surface and vestiture** (Fig. 13B, E, I, J, M). Body impunctate; scutellum not serrate laterally (Fig. 13M); head, pronotum, scutellum and pleura with distinct

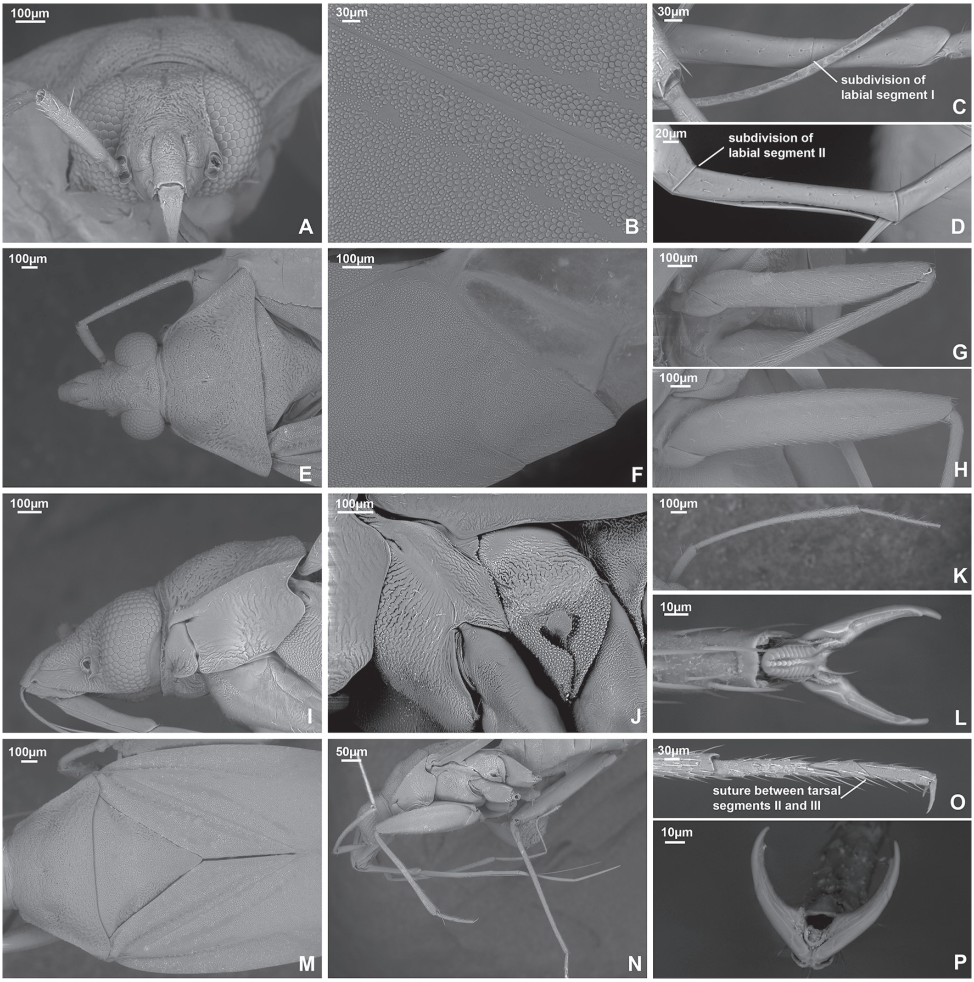

Figure 13. SEM images. *Micanitropis seisia* **A** head, anterior view **B** tubercles on hemelytron **C** labial segment I **D** apical part of labial segment II **E** head and pronotum, dorsal view **F** cuneus and membrane cell **G** trichobothria on middle femur **H** trichobothria on hind femur **I** head and pronotum, lateral view **J** pleura **K** antennal segments I, II **L** pretarsus, ventral view **M** scutellum, clavus and corium **N** legs **O** hind tarsus **P** pretarsus, dorsal view.

rugosities (Fig. 3A, E, I, J, M); hemelytron clothed with small tubercles (Fig. 13B); dorsum and pleura without net-like pattern of microsculpture (Fig. 3A, E, I, J, M). Body clothed with short sparse adpressed setae (Fig. 13B, J); setae on dorsum very short, setae on antenna, pleura, legs and abdomen longer; spines on tibiae short and pale. **Structure.** Body elongate oval. ***Head.*** Horizontal, dorsally as long as or slightly longer than wide (Fig. 13E), vertex not carinate, eye not protruding, not covering anterior margin of pronotum posteriorly (Fig. 13E); in anterior view head wider than high, antennal fossa placed near ventral 1/3 of eye, above ventral margin of eye; base of clypeus not delimited with depression, placed near median of eye (Fig. 13A); in lateral view head longer than high; vertex not raised above eyes; eye large, producing to ventral margin of head; eye located close to lateral margin of pronotum or slightly covering it; antennal fossa slightly removed from eye and placed close to suture between mandibular and maxillary plates; mandibular and maxillary plates not separated from head with suture or depression; labrum triangular, not modified, shorter than labial segment I; buccula elongate, ca. 5–6 × as long as high; distance between buccula and pronotum longer than buccula length (Fig. 13I). ***Antenna.*** Shorter than body, antennal segment I not widened, shorter than head width; antennal segment II slightly widened towards apex, slightly thinner than segment I, longer than head width; segment III slightly shorter than half of segment II; segment IV ca. 1.5 × as long as segment III; segment III as thick as segment IV, and both thinner than segment II (Fig. 13K, N). ***Labium.*** Apex almost reaching or reaching genital segment; labial segment I almost reaching posterior margin of head, subdivided in apical half (Fig. 13C, I, N); segment II almost twice as long as segment I, subdivided subapically, its apical part 9–10 × as long as wide (Fig, 13D, N); segment III subequal to half of segment II, more than 10 × as long as wide; segment IV slightly shorter or same length as segment III (Fig. 13N). ***Thorax.*** Pronotum wider than long (Fig. 13E), lateral margins straight in dorsal view, strongly carinate in lateral view (Fig. 13E, I); collar relatively narrow, narrower than antennal segment I, separated with weak depression; calli large and moderately upraised, covering 2/3 of pronotum surface, separated from each other with weak depression; posterior margin of pronotum slightly concave (Fig. 13E, M); mesoscutum exposed; scutellum flat (Fig. 13M); propleural apodeme T-shaped (Fig. 13I); mesopleural apodeme slit-like; mesothoracic spiracle slit-like, with row of microsculpture along anterior margin; metathoracic gland evaporative area triangular, lateral margin reaching base of hind coxa; peritreme upraised, rounded; metepimeron narrow (Fig. 13J). ***Hemelytron*** (Fig. 13F, M). Outer margins rounded, not concave or constricted anteriorly; clavus with longitudinal ridge; claval commissure slightly longer than scutellum; medial fracture almost reaching middle of corium; ridge along medial fracture distinct basally; embolium relatively wide, its widest part subequal to 1/3 of cuneus width; R+M distinct only basally; cuneus visibly delimited, as wide as long, not incised at base; membrane with two cells, distance between cell and membrane apex slightly longer than cell length. ***Legs.*** Forecoxa slightly shorter than pronotum length, longer and wider than middle and hind coxae; forefemur widened, 3–4 × as long as wide, wider and slightly longer than middle femur, slightly wider and shorter than hind femur (Fig. 13G, H, N), segment I of hind tarsus twice longer than segment II; segment III slightly longer than segment II (Fig. 13O); claw with subapical tooth; middle row of tiles on unguitractor full (Fig. 13L). ***Genitalia.*** See species description.

Female. Similar to male. ***Genitalia.*** See species description.

Etymology. The genus is named for its sparkling appearance, *micans* from Latin meaning sparkling, glittering. The genus is masculine.

Remarks. *Micanitropis* belongs to Fulviini as its structure fits the diagnosis for this tribe, in particular, it has the prognathous head, the antenna shorter than the body, the body impunctate, and its labium is long, reaching or almost reaching the genitalia segment (Gorczyca 2000).

Micanitropis is similar to *Peritropis* Uhler, 1891, as they both have the moderately elevated calli, the carinate lateral margins of pronotum, the eyes elongate in lateral view and reaching gula, and the hemelytron, at least in some species, including type species *P. saldaeformis* Uhler, 1891, is covered with small tubercles (Moulds and Cassis 2006; Wolski and Henry 2012). Currently *Peritropis* includes ca. 90 species worldwide, with only the Australian and American fauna having been revised (Moulds and Cassis 2006; Wolski and Henry 2012). According to the previous works and personal observations, *Peritropis* differs from *Micanitropis* in the collar being indistinct, the vertex usually more or less carinate, the metathoracic scent gland evaporative area usually being reduced or at least its anterior angle being rounded, and the head, pronotum and pleura not being covered with rugosities, but instead with a net-like pattern of microsculpture. The anterior margin of pronotum of *Peritropis* is also often concave and angulate at sides, and the apical part of ductus seminis does not have the row of outgrowths along margin (Moulds and Cassis 2006; Wolski and Henry 2012).

As mentioned in the remarks for *Callitropisca*, this genus, *Micanitropis*, and *Xenocylapidius* share similar genitalic structures, with the apical part of the ductus seminis having two lobes, bearing a row of long outgrowths along outer margin. See comparison of *Callitropisca* and *Micanitropis* in the Remarks section for *Callitropisca*. *Xenocylapidius* and *Micanitropis* are similar in the head being longer than high in lateral view, the vertex flat (Fig. 13I; Wolski and Gorczyca 2014b: figs 9–15), and the tarsal segment I being longer than tarsal segments II and III each (Fig. 13O). However, *Xenocylapidius* differs from *Micanitropis* in the antennal segment I being longer than the vertex, the setae covering the dorsum are either dense and short or long and sparse, and the head, pronotum, and scutellum are not rugose or only slightly rugose (pers. obs.; Wolski and Gorczyca 2014b).

Micanitropis seisia sp. nov.

http://zoobank.org/B2AE0B02-5998-4EA5-9237-2540B9C2747E
Figs 2, 13, 14, 15B

Material examined. ***Holotype*:** Australia: Queensland: Seisia via Bamaga, 10.85283°S, 142.37132°E, 10 Jan 2011, J. Sailor, 1♂ (UNSW_ENT 00027641) (QM). ***Paratypes*:** Australia: Northern Territory: Crocodile Ck nr Dorisvale M.T., 14.29°S, 131.22°E, 17 Nov 1984, M. B. Malipatil, 1♂ (00043059) (NTM). Kakadu National Park, Nourlangie Camp, 12.759°S, 132.659°E, 17 Nov 1979–18 Nov 1979, M. B. Malipatil, 1♀ (00043063) (NTM). Lake Bennett, 19 km SE off Stuart Hwy nr Manton Dam, 12.86449°S, 131.11889°E, 30 Mar 1979, M. B. Malipatil, 3♂ (00043052–00043054), 1♀ (00043055) (NTM), 1 sex unknown (00043056) (NTM). Tindal, 14.516°S, 132.383°E, 01 Dec 1967–20 Dec 1967, W. Vestjens, 1♂ (00043060) (NTM). Queensland: Clermont, 22.823°S, 147.638°E, Nov 1929, K. K. Spence, 1♂ (00043061) (AM). Proserpine, Thompson Creek, (site XY15), 20.51888°S, 148.55694°E, 21 m, 11 Nov 2007, C. J. Burwell, 1♂ (00043046) (QM). Proserpine, Thompson Creek, site XY15, 20.519°S, 148.557°E, 30 m, 11 Nov 2007, C. J. Burwell, 2♀ (00043048, 00043049) (QM). Western Australia: Kimberley Research Station, via Kununura, 15.70777°S, 128.69947°E, 25 Nov–26 Nov 1997, A. Postle and C. Brockway, 1♀ (00043062) (WAM). Roebuck Plains, via Broome, 17.96°S, 122.435°E, 30 Dec 1997–02 Jan 1998, C. Johnstone, 1♂ (00043057) (WAM).

Diagnosis. Head mostly brown to dark brown dorsally; antennal segment I yellow basally and reddish apically; segment II pale brown to brown, whitish yellow apically; segments III and IV pale brown to brown; pronotum, mesoscutum and scutellum brown to dark brown; scutellum whitish yellow to yellow apically; pleura mostly brown to dark brown or reddish brown; hemelytron mostly brown; clavus with three longitudinal whitish yellow stripes, inner stripe sometimes faint or indistinct; corium with two longitudinal whitish yellow stripes reaching or almost reaching middle of corium (Fig. 2); vesica with two elongate sclerites, one of them straight and placed dorsally, second one curved and widened basally, vesica also with triangular semi-sclerotised area apically (Fig. 14A, B).

Description. Male. Body length 3.1–3.4. **Coloration** (Fig. 2). Background colouration brown to dark brown. ***Head.*** Brown to dark brown dorsally with yellow marking near inner margin of eye; mandibular and maxillary plates and ventral side of head pale brown often with reddish tinge; antennal segment I yellow basally and reddish apically; segment II pale brown to brown, whitish yellow apically; segments III–IV pale brown to brown; labium yellow to brown, labial segment I sometimes with reddish tinge. ***Thorax.*** Pronotum uniformly brown to dark brown. Mesoscutum and scutellum brown to dark brown; mesoscutum often with pale brown or reddish marking laterally; scutellum whitish yellow to yellow apically; pleura brown to dark brown, sometimes reddish brown; evaporative area often slightly paler than metapleuron. ***Hemelytron.*** Mostly brown; clavus with three longitudinal whitish yellow stripes, inner stripe sometimes faint or indistinct; corium with two longitudinal whitish yellow stripes reaching or almost reaching middle of corium; embolium whitish yellow anteriorly; corium and embolium with yellow marking adjacent to cuneus, sometimes with reddish tinge; membrane pale brown with brown cells. ***Legs.*** Forecoxa brown to dark brown, often with whitish apex; middle and hind coxae whitish yellow to pale brown; femora brown, yellow or reddish yellow apically; forefemur often darker than middle and hind femora; tibiae pale brown to dark brown, often yellow apically; tarsi whitish yellow to pale brown. ***Abdomen.*** Brown to dark brown, sometimes with reddish tinge. **Surface and vestiture.** See generic description. **Structure and measurements.** Body ca. 2.5–2.8 × as long as wide, ca. 2.7–3.1 × as long as pronotum width; head ca. 1.0–1.3 × as wide as long, in lateral view head ca. 1.4–1.5 × as long as high; antennal segment I ca. 1.3–1.6 × as long as vertex, ca. 0.5–0.6 × as long as head width; antennal segment II ca. 2.8–3.0 × as long as segment I, ca. 4.0–4.3 × as long as vertex width, ca. 1.6–1.7 × as long as head width, ca. 0.8–0.9 × as long as pronotum width; pronotum ca. 1.8–2.0 × as wide as head, ca. 1.9–2.2 × as wide as long. ***Genitalia.*** Genital capsule as long as wide, with outgrowth on right hand side on posterior margin dorsally (Fig. 14D). Parameres r-shaped, subequal in length; basal part of right paramere with angulate swelling directed inwards and rounded outgrowth directed upwards, apical part of right paramere widened with small tubercle apically; left paramere with large

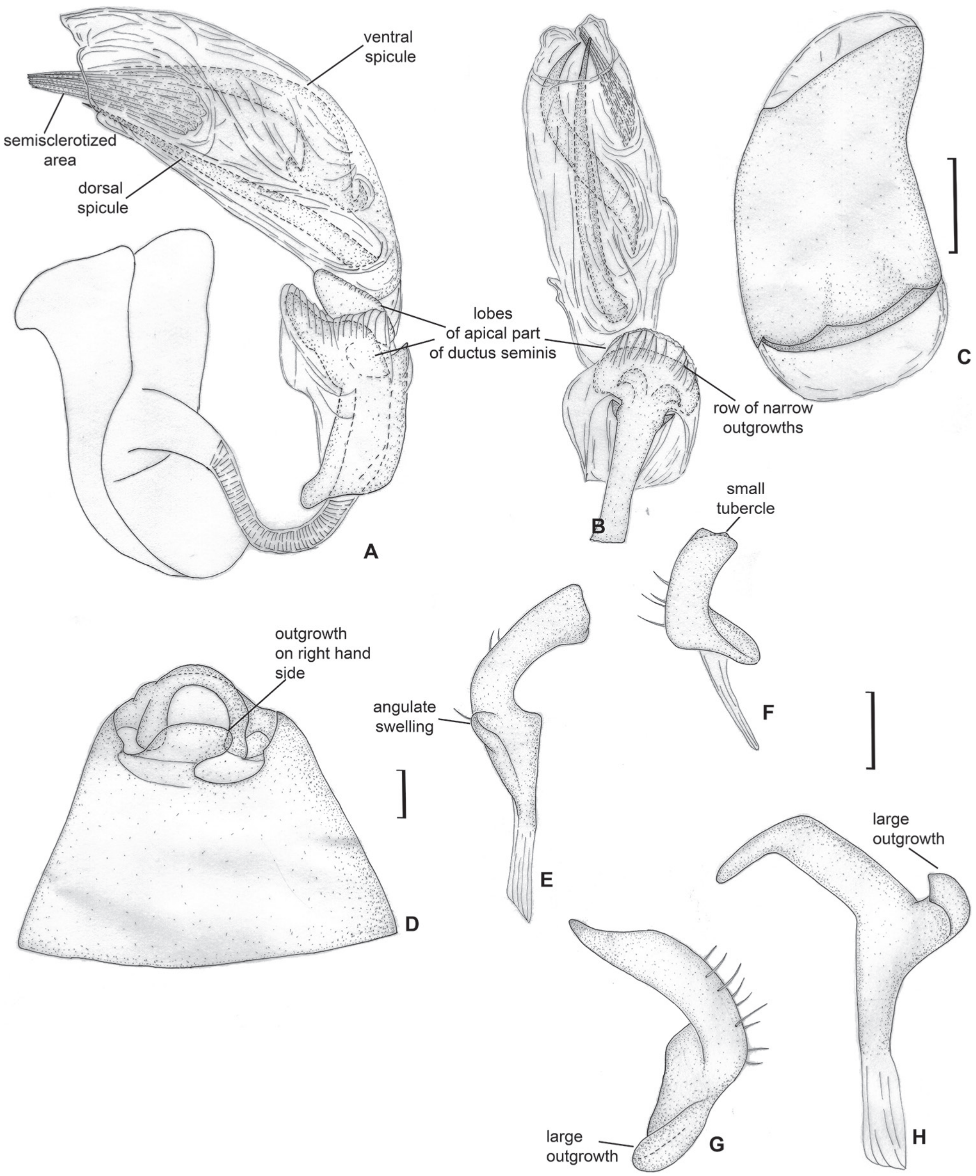

Figure 14. Male genitalia. *Micanitropis seisia* **A** aedeagus, left lateral view **B** aedeagus, dorsal view **C** theca **D** genital capsule **E** left paramere, dorsal view **F** left paramere, posterior view **G** right paramere, posterior view **H** right paramere, dorsal view.

outgrowth on basal part directed outwards and upwards, apical process narrow and elongate (Fig. 14E–H); theca without outgrowths (Fig. 4C); endosoma subdivided into vesica and conjunctiva; vesica with two elongate spicules, tapering apically, dorsal spicule straight, not particularly widened basally; ventral spicule curved, and widened basally in lateral view; vesica also with triangular semi-sclerotised area apically; ductus seminis widened and sclerotised apically; secondary gonopore surrounded with two

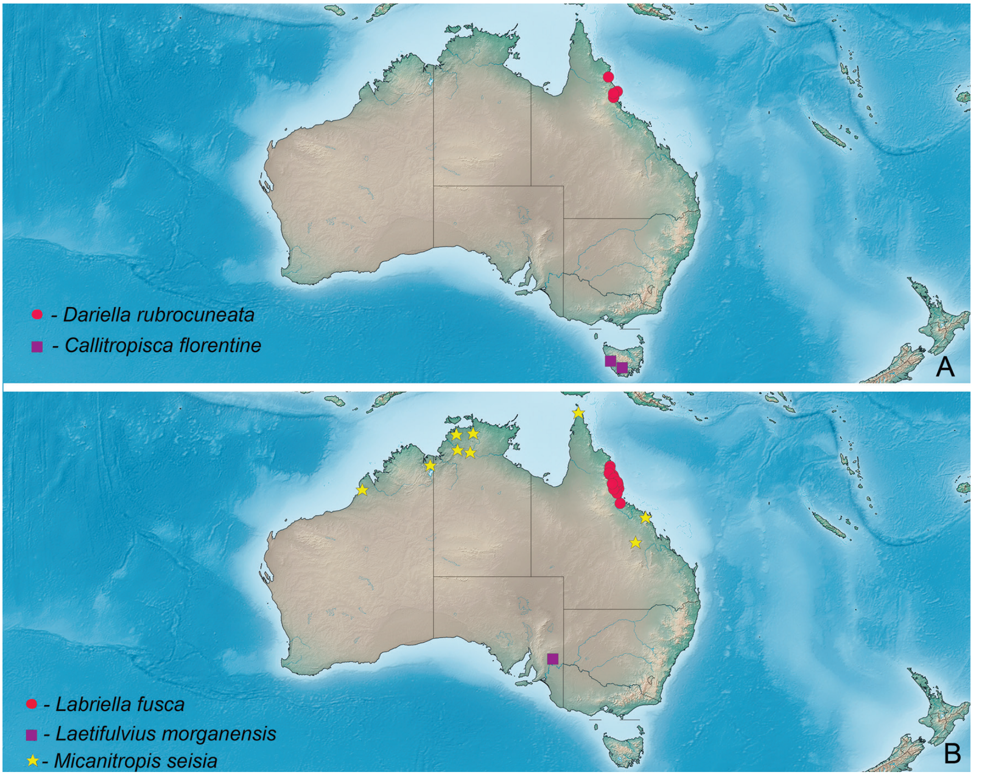

Figure 15. Distribution maps **A** *Dariella rubrocuneata*, *Callitropisca florentine* **B** *Labriella fusca*, *Laetifulvius morganensis*, *Micanitropis seisia*.

wide lobes, with row of narrow outgrowths along outer margin, one of those lobes placed dorsally and another one ventrally (Fig. 14A, B).

Female. Body length 3.1–3.7. **Coloration** (Fig. 2). As in male, marking near eye sometimes absent, cuneus sometimes almost entirely whitish yellow. **Structure and measurements.** Body ca. 2.2–2.7 × as long as wide, ca. 2.7–3.3 as long as pronotum width; head ca. 0.9–1.0 × as wide as long, in lateral view head ca. 1.5 × as long as high; antennal segment I ca. 1.2–1.6 × as long as vertex, ca. 0.5–0.7 × as long as head width; antennal segment II ca. 3.1–3.2 × as long as segment I, ca. 3.6–4.9 × as long as vertex width; ca. 1.4–2.0 × as long as head width, ca. 0.8–0.9 × as long as pronotum width; pronotum ca. 1.8–2.3 × as wide as head, ca. 2.0–2.2 × as wide as long. ***Genitalia.*** Dorsal labiate plate as long as wide, with large elongate sclerotised rings, each of them ca. 0.2 × as wide as dorsal labiate plate, and only slightly shorter than dorsal labiate plate; sclerotised rings connected with each other with transversal sclerite anteriorly; posterior part of dorsal labiate plate with paired sclerotised areas and paired membranous areas with small tubercles (Fig. 10B); ventral wall with v-shaped medial sclerite surrounding vulva (Fig. 10D).

Distribution. Known from different locations in the dry areas in the northern parts of Western Australia, Northern Territory and Queensland (Australia) (Fig. 15B).

Collection techniques. The specimens were collected with hands at night, at light, at MV light, and using pyrethrum knockdown of mango trees.

Etymology. Named after the town Seisia in the Cape York (Queensland, Australia), where the holotype was collected (Fig. 15B).

Discussion

The subfamily Cylapinae is characterised by long and narrow tarsi, as well as the combination of characters in the pretarsus, specifically the setiform and often asymmetrical parempodia, the lack of pulvilli, the slender claws usually toothed apically, and the three rows of tiles on the unguitractor with the tiles of the medial row acute (Schuh 1976; Gorczyca 2000; Namyatova et al. 2016). The listed characters occur in Bothriomirini, Cylapini, Fulviini and Rhinomirini (Wolski et al. 2016; Namyatova and Cassis 2016a; Wolski 2017; Namyatova et al. 2016, 2019). However, Vanniini has a different structure of the pretarsus with flattened spatulate parempodia and without a middle row of tiles on the unguitractor plate (Namyatova et al. 2016). A combination of characters similar to that possessed by the most cylapines was found in Isometopinae and Psallopinae. Isometopinae are different from Cylapinae in the presence of ocelli (Namyatova and Cassis 2016b), and Psallopinae are often very small (1–2 mm), fragile and have the vertex width shorter than eye diameter (Namyatova and Cassis 2019b). All genera described in this paper have the abovementioned structures of the pretarsus and do not fit the diagnoses of Isometopinae and Psallopinae, and, therefore, we place them into Cylapinae.

The current diagnoses for Cylapini and Fulviini cannot be applied to all representatives of those tribes, and this complicates the tribal assignment of the new genera. *Callitropisca* and *Micanitropis* possess all the features typical for Fulviini. Although *Laetifulvius* has the head strongly inclined, its morphological features also fit the current understanding of Fulviini in all other respects.

Labriella and *Dariella* do not fit the diagnoses for any of the Cylapinae tribes. They have a vertical head, which is true for Cylapini, Bothriomirini and Vanniini. However, according to the diagnoses, the Cylapini and Vanniini typically have antennae longer than the body, whereas they are shorter than the body in *Labriella* and *Dariella*. The combination of the vertical head and short antennae is characteristic for Bothriomirini. All representatives of Bothriomirini form a well-defined group with some important characters not occurring in *Dariella* and *Labriella* (see Remarks section for those genera). However, Cylapini have other genera which also have short antennae, and those taxa are similar to *Dariella* and *Labriella*. In particular, *Dariella* has the male genitalia and pretarsus structure very similar to another Australian genus *Carvalhoma*, and the metathoracic scent gland evaporative area similar to *Schizopteromiris*, which is also known from Australia. Therefore, we place *Dariella* and *Labriella* in Cylapini based on their affinities to other genera assigned to this tribe, although not its typical representatives. We are awaiting the phylogenetic study of Cylapinae to clarify the position of those two new genera.

With five new monotypic genera, Australian Cylapinae fauna now includes 26 genera and 48 species currently assigned to four tribes, Bothriomirini, Cylapini, Fulviini and Vanniini. The Cylapini fauna is composed of the genera *Carvalhoma*, *Dariella*, *Labriella* and *Schizopteromiris*. None of these genera fully fit the diagnosis of this tribe, and the position of those genera can be reassessed in the future.

Acknowledgements

This work was supported by the Australian Biological Resources Study postdoctoral fellowship to AAN, and its final stages were supported by the Russian Foundation for Basic Research (RFBR) (grant number 20–04–01040 A). The majority of the work was performed in the facilities in the G. Cassis' lab, University of New South Wales (Australia). Facilities were also provided by the Zoological Institute of the Russian Academy of Sciences, sponsored by the state research project AAAA–A19–119020690101–6 and the St Petersburg State University. We are grateful to the following curators for lending us the material: Dave Britton (AM), Randall T. Schuh (AMNH), Michael Braby (NTM), Christine Lambkin (QM), Peter Hudson (SAMA), and Terry Houston (WAMP). We also thank Cynthia Chan and Yeewei Chin (UNSW) for assisting with taking the SEM images and processing them. We also thank Eric Gordon (University of Connecticut, USA) for helping to revise the manuscript.

References

Carpintero DL, Chérot F (2014) Liste commentée des Cylapinae d'Argentine et du Chili avec la description d'un nouveau genre et d'une nouvelle espèce (Hemiptera, Heteroptera, Miridae). Bulletin de la Societe entomologique de France 119(1): 59–66. https://www.persee.fr/doc/bsef_0037-928x_2014_num_119_1_2563

Carvalho JCM (1948) Mirideos neotropicais, 35: Generos *Corcovadocola* n. g., *Guanabarea* n. g. e *Caulotops* Bergroth (Hemiptera). Revista Brasileira de Biologia 8: 525–533.

Carvalho JCM (1952) Neotropical Miridae, 56: Description of three new genera and five new species from Brazil and British Honduras (Hemiptera). Revista Brasileira de Biologia 12: 265–273.

Carvalho JCM (1986) Mirideos neotropicais, CCLVI: Dois generos e seis espécies novos da tribo Cylapini (Hemiptera). Acta Amazonica 16/17: 589–598. https://doi.org/10.1590/1809-43921987171598

Carvalho JCM (1991) Tres generos e espécies novos de cilapineos da Australia (Hemiptera, Miridae). Anais da Academia Brasileira de Ciencias 63: 403–408.

Cassis G, Gross GF (1995) Zoological Catalogue of Australia. Heteroptera. Volume 27.3 A. CSIRO, Canberra, 506 pp.

Cassis G, Schwartz MD, Moulds T (2003) Systematics and new taxa of the *Vannius* complex (Hemiptera: Miridae: Cylapinae) from the Australian Region. Memoirs of the Queensland Museum 49: 123–151.

Davis NT (1955) Morphology of the female organs of reproduction in the Miridae (Hemiptera). Annals of the Entomological Society of America 48: 132–150. https://doi.org/10.1093/aesa/48.3.132

Gorczyca J (2000) A systematic study on Cylapinae with a revision of the Afrotropical Region (Heteroptera, Miridae). Wydawnictwo Uniwersytetu Śląskiego, Katowice, 174 pp. https://core.ac.uk/display/225721895

Herring JL (1976) A new genus and species of Cylapinae from Panama (Hemiptera: Miridae). Proceedings of the Entomological Society of Washington 78: 91–94. https://www.biodiversitylibrary.org/page/16252566

Kerzhner IM, Konstantinov FV (1999) Structure of the aedeagus in Miridae (Heteroptera) and its bearing to suprageneric classification. Acta Societatis Zoologicae Bohemicae 63: 117–137.

Konstantinov FV (2003) Male genitalia in Miridae (Heteroptera) and their significance for suprageneric classification of the family. Part I: general review, Isometopinae and Psallopinae. Belgian Journal of Entomology 5: 3–36. http://www.srbe-kbve.be/cm/sites/default/files/publications/BJE/BJE%202003/BJE%202003%20vol%205%20%281-2%29%20Konstantinov.pdf

Moulds T, Cassis G (2006) A review of Australian species of *Peritropis* (Insecta: Heteroptera: Miridae: Cylapinae). Memoirs of the Queensland Museum 52: 171–190.

Namyatova AA, Cassis G (2016a) Revision of the staphylinoid and ground-dwelling genus *Carvalhoma* Slater and Gross (Insecta: Heteroptera: Miridae: Cylapinae) of Australia. European Journal of Taxonomy 253: 1–27. https://doi.org/10.5852/ejt.2016.253

Namyatova AA, Cassis G (2016b) Review of the seven new species of Isometopinae (Heteroptera: Miridae) in Australia and discussion of distribution and host plant associations of the subfamily on a worldwide basis. Austral Entomology 55(4): 392–422. https://doi.org/10.1111/aen.12202

Namyatova AA, Cassis G (2019a) Total-evidence phylogeny of the Rhinomirini, taxonomic review of its subgroupings (Insecta: Heteroptera: Miridae: Cylapinae) and description of new Australian taxa. Zoological Journal of the Linnean Society 187(4): 1196–1252. https://doi.org/10.1093/zoolinnean/zlz058

Namyatova AA, Cassis G (2019b) First record of the subfamily Psallopinae (Heteroptera: Miridae) from Australia and discussion of its systematic position and diagnostic characters. Austral Entomology 58(1): 156–170. https://doi.org/10.1111/aen.12350

Namyatova AA, Contos P, Cassis G (2019) New species, taxonomy, phylogeny, and distribution of the tropical tribe Bothriomirini (Insecta: Heteroptera: Miridae: Cylapinae). Insect Systematics and Evolution 50(1): 83–146. https://doi.org/10.1163/1876312X-00002179

Namyatova AA, Konstantinov FV, Cassis G (2016) Phylogeny and systematics of the subfamily Bryocorinae based on morphology with emphasis on the tribe Dicyphini sensu Schuh. Systematic Entomology 41(1): 3–40. https://doi.org/10.1111/syen.12140

Poppius B (1913) Zur Kenntnis der Miriden, Isometopiden, Anthocoriden, Nabiden und Schizopteriden Ceylon's. Entomologisk Tidskrift 34: 239–260. https://doi.org/10.5962/bhl.part.1634

Shorthouse DP (2010) SimpleMappr, an online tool to produce publication-quality point maps. https://www.simplemappr.net [Accessed 03 December 2020]

Schuh RT (1976) Pretarsal structure in the Miridae (Hemiptera), with a cladistic analysis of relationships within the family. American Museum Novitates 2601: 1–39. http://hdl.handle.net/2246/2919

Schuh RT (1986) *Schizopteromiris*, a new genus and four new species of coleopteroid cylapine Miridae from the Australian Region (Heteroptera). Annales de la Société Entomologique de France 22: 241–246.

Tyts VD, Namyatova AA, Damken C, Wahab RA, Konstantinov FV (2020) *Tatupa grafei*, a new genus and species of Cylapinae (Heteroptera, Miridae) from Brunei Darussalam. ZooKeys 946: 37–52. https://doi.org/10.3897/zookeys.946.51780

Wolski A (2010) Revision of the *Rhinocylapus*-group (Hemiptera: Heteroptera: Miridae: Cylapinae). Zootaxa 2653(1): 1–36. https://doi.org/10.11646/zootaxa.2653.1.1

Wolski A (2014) Revision of the plant bug genus *Xenocylapus* Bergroth (Hemiptera: Heteroptera: Miridae: Cylapinae), with a description of *Henryfulvius gracilis* – a new cylapine genus and species from Ecuador. Annales de la Société entomologique de France (NS) 50(3–4): 311–335. https://doi.org/10.1080/00379271.2014.990251

Wolski A (2017) Taxonomic review of the plant bug genera *Amapacylapus* and *Cylapus* with descriptions of two new species and a key to the genera of Cylapini (Hemiptera: Heteroptera: Miridae). Acta Entomologica Musei Nationalis Pragae 57(2): 399–455. https://doi.org/10.1515/aemnp-2017-0084

Wolski A, Gorczyca J (2014a) Notes on the genera *Peritropisca* Carvalho and Lorenzato and *Rewafulvius* Carvalho (Hemiptera: Heteroptera: Miridae: Cylapinae), with the description of a new species of Peritropisca from Indonesia. Zootaxa 3753(2): 155–166. https://doi.org/10.11646/zootaxa.3753.2.5

Wolski A, Gorczyca J (2014b) Revision of the plant bug genus *Xenocylapidius* (Hemiptera, Heteroptera, Miridae, Cylapinae), with descriptions of five new species from Australia and New Caledonia. ZooKeys 459: 73–94. https://doi.org/10.3897/zookeys.459.8015

Wolski A, Gorczyca J, Herczek A (2016) A new species of the genus *Hemiophthalmocoris* from the Oriental Region (Hemiptera: Heteroptera: Miridae: Cylapinae). Entomologica Americana 122(1): 97–103. https://doi.org/10.1664/15-RA-042

Wolski A, Gorczyca J, Yasunaga T (2018) Taxonomic review of the bifenestratus species group of the genus *Fulvius* Stål with descriptions of two new species (Hemiptera, Heteroptera, Miridae, Cylapinae). ZooKeys 796: 107–129. https://doi.org/10.3897/zookeys.796.21293

Wolski A, Henry TJ (2012) Revision of the new world species of *Peritropis* Uhler (Heteroptera: Miridae: Cylapinae). Insect Systematics and Evolution 43(3–4): 213–270. https://doi.org/10.1163/1876312X-04303002

Wolski A, Henry TJ (2015) Review and a new subfamily placement of the plant bug genus *Isometocoris* Carvalho & Sailer, 1954 (Hemiptera: Heteroptera: Miridae), with the description of a new species from Brazil. Proceedings of the Entomological Society of Washington 117(3): 407–418. https://doi.org/10.4289/0013-8797.117.3.407

Wolski A, Yasunaga T, Gorczyca J, Herczek A (2017) *Sulawesifulvius thailandicus* – a new species of the genus *Sulawesifulvius* Gorczyca, Chérot and Štys from Thailand (Hemiptera, Heteroptera, Miridae, Cylapinae). ZooKeys 647: 109–119. https://doi.org/10.3897/zookeys.647.10960

ZooKeys 1012: 135–150 (2021)
doi: 10.3897/zookeys.1012.59035
https://zookeys.pensoft.net

RESEARCH ARTICLE

A peer-reviewed open-access journal
ZooKeys
Launched to accelerate biodiversity research

Complete mitochondrial genome sequence of *Lepus yarkandensis* Günther, 1875 (Lagomorpha, Leporidae): characterization and phylogenetic analysis

Wenjuan Shan[1], Mayinur Tursun[1], Shiyu Zhou[1], Yucong Zhang[1], Huiying Dai[1]

1 *Xinjiang Key Laboratory of Biological Resources and Genetic Engineering, College of Life Science and Technology, Xinjiang University, Urumqi, China, 830046*

Corresponding author: Wenjuan Shan (swj@xju.edu.cn)

Academic editor: P. Stoev | Received 29 September 2020 | Accepted 28 December 2020 | Published 26 January 2021

http://zoobank.org/8A07FC9B-3091-40E3-986E-71D9E2CE326A

Citation: Shan W, Tursun M, Zhou S, Zhang Y, Dai H (2021) Complete mitochondrial genome sequence of *Lepus yarkandensis* Günther, 1875 (Lagomorpha, Leporidae): characterization and phylogenetic analysis. ZooKeys 1012: 135–150. https://doi.org/10.3897/zookeys.1012.59035

Abstract

Lepus yarkandensis is a national second-class protected animal endemic to China and distributed only in the hot and arid Tarim Basin in Xinjiang. We sequenced and described the complete mitogenome of *L. yarkandensis* to analyze its characteristics and phylogeny. The species' DNA is a 17,047 bp circular molecule that includes 13 protein-coding genes (PCGs), two rRNA genes, 22 tRNA genes, and one control region. The overall base composition was as follows: A, 31.50%; T, 29.40%; G, 13.30% and C, 25.80%, with a high A+T bias of 60.9%. In the PCGs, ND6 had deviation ranges for AT skew (–0.303) and GC skew (0.636). The Ka/Ks values of ND1 (1.067) and ND6 (1.352) genes were >1, indicating positive selection, which might play an important role in the adaptation of *L. yarkandensis* to arid and hot environments. The conserved sequence block, the central conserved domain, and the extended termination-associated sequences of the control region and their features were identified and described. The phylogenetic tree based on the complete mitogenome showed that *L. yarkandensis* was closely related to the sympatric *Lepus tibetanus pamirensis*. These novel datasets of *L. yarkandensis* can supply basic data for phylogenetic studies of *Lepus* spp., apart from providing essential and important resource for further genetic research and the protection of this species.

Keywords

mitogenome, molecular phylogeny, synonymous/non-synonymous substitution, Yarkand hare

Introduction

The Yarkand hare (*Lepus yarkandensis*) is endemic to China and is restricted to scattered oases around the Taklamakan Desert in the Tarim Basin of Xinjiang (Luo 1988; Smith et al. 2008, 2018). These hares live in hot, arid environments with scarce food and open terrain. Thus, this species is highly morphologically specialized, with smaller bodies, longer ears, and larger tympanic bullae than other *Lepus* species in China (Shan et al. 2011; Wu et al. 2011). This species is also listed as a second-class protected animal (Wang 1998). Several studies have been published on *L. yarkandensis*, including its morphology, skull morphometrics, genetic diversity, and genetic structures based on partial mitochondrial DNA (mtDNA) markers, microsatellites, and several nuclear genes (Li et al. 2005; Li et al. 2006; Aerziguli et al. 2010; Shan et al. 2011). The complete mtDNA sequence of *L. yarkandensis* has been reported (Huang et al. 2019), but without the details given of its characteristics, particularly those adapting to such extremely arid environments.

Characterized by small size, stable gene content, high evolutionary rate, relatively conserved gene arrangement, high information content, and maternal inheritance, animal mitogenomes are powerful tools used to investigate molecular evolution, phylogenetic relationships, and protective biology for many animals (Yu et al. 2017; Zhang et al. 2018; Song et al. 2019; Hu et al. 2020; Wu et al. 2020).

In the present study, we successfully sequenced and characterized the complete mtDNA of *L. yarkandensis*, including its base composition, gene structure, and arrangement of protein-coding genes (PCGs) and a control region. We also constructed a phylogenetic tree based on complete mitogenome sequences to elucidate the relationship of *L. yarkandensis* with other *Lepus* spp. Therefore, this study provides essential scientific data and contributes to population genetics, adaptation, and phylogenetic studies of *L. yarkandensis*.

Materials and methods

A male adult *L. yarkandensis* was collected from Alar, Xinjiang, China (40°34'00"N, 81°19'33"E) on 24 December 2016. Complete mtDNA was extracted from muscle tissue using standard phenol-chloroform (Psifidi et al. 2010). The complete mitogenome of the species was sequenced by next-generation sequencing using an Illumina HiSeq platform by Hengchuang Gene Technology Co., Ltd (Shenzhen, China) and assembled using SOAPdenovo 12.04 (Luo et al. 2012). The genome structure was mapped using the CGView software (Stothard et al. 2005). The complete mitogenome sequences of 25 other lagomorph species were downloaded from GeneBank (Table 1). The base composition, Ka and Ks (Ka, Ks, Ka/Ks) values, and composition skew were analyzed using MEGA7, together with the following formulas: AT skew = [A – T]/[A + T] and GC skew = [G – C] / [G + C] (Perna et al. 1995). A conserved sequence block (CSB) in the control region was identified based on previously published se-

Table 1. Lagomorph mitogenomes used in the phylogenetic analysis of the present study.

Name	Accession number	Collection places	Size
Lepus americanus1	NC024043	Montana, USA	17042
Lepus americanus2	KJ397613	Montana, USA	17042
Lepus capensis	GU937113	Yancheng, Jiangsu	17722
Lepus coreanus	KF040450	Incheon, Korea	17472
Lepus europaeus1	AJ421471	Skane, Sweden	17734
Lepus europaeus2	KY211025	North-east Greece	16680
Lepus granatensis1	NC024042	León, Spain	16916
Lepus granatensis2	KJ397610	León, Spain	16916
Lepus hainanus	JQ219662	Hainan, China	16646
Lepus sinensis	KM362831	Hefei Anhui	17438
Lepus tibetanus pamirensis	LC073697	Aketao, Xinjiang,	17597
Lepus timidus1	KR019013	Haerbin, Heilongjiang	17762
Lepus timidus2	KJ397605	Finland	17755
Lepus timidus3	KR030070	Harbin, Heilongjiang	17748
Lepus timidus4	KR030072	Harbin, Heilongjiang	17749
Lepus timidus5	KR030069	Harbin, Heilongjiang	17744
Lepus timidus6	KR013248	Harbin, Heilongjiang	17759
Lepus tolai	KM609214	Hefei Anhui	17472
Lepus townsendii1	NC024041	Wyoming, USA	17732
Lepus townsendii2	KJ397609	Wyoming, USA	17732
Lepus yarkandensis1	MG279351	Alaer, Xinjiang	17047
Ochotona curzoniae	EF535828	Qinghai, China	17313
Ochotona collaris	AF348080	Not mentioned	16968
Ochotona princeps	AJ537415	Not mentioned	16481
Lepus yarkandensis2	MN450151	Kuqa, Xinjiang	17011
Oryctolagus cuniculus	AJ001588	Not mentioned	17245

quence data from several mammals (Sbisà et al. 1997). All tRNA secondary structures, except for tRNA-Ser (AGN), were verified using the tRNAscan-SE Webserver (Lowe and Eddy 1997). A phylogenetic tree was constructed by neighbor-joining (NJ) using MEGA7 and Bayesian analysis using MrBayes (Ronquist et al. 2012; Kumar et al. 2016). An NJ tree was constructed with default settings. Bayesian analyses were performed using MrBayes v. 3.2.6 ×64 for the best-fit model, GTR+I+F+G4, as determined by IQ-TREE (Nguyen et al. 2015). With the final model, analyses were run for 5,000,000 generations.

Results and discussion

Mitochondrial genome organization

The mitogenome of *L. yarkandensis* was a circular, double-stranded DNA molecule 17047 bp in size (GenBank accession number: MG279351) which is slightly longer than reported *L. yarkandensis* (MN450151) with 17011 bp (Huang et al. 2019). It contained all 37 typical vertebrate mitogenomes–13 PCGs, two rRNA genes, 22 tRNA genes, and one control region-among which 28 genes were encoded on the heavy strand (H strand), except for eight tRNA genes and the ND6 gene (Fig. 1; Table 2). Eleven

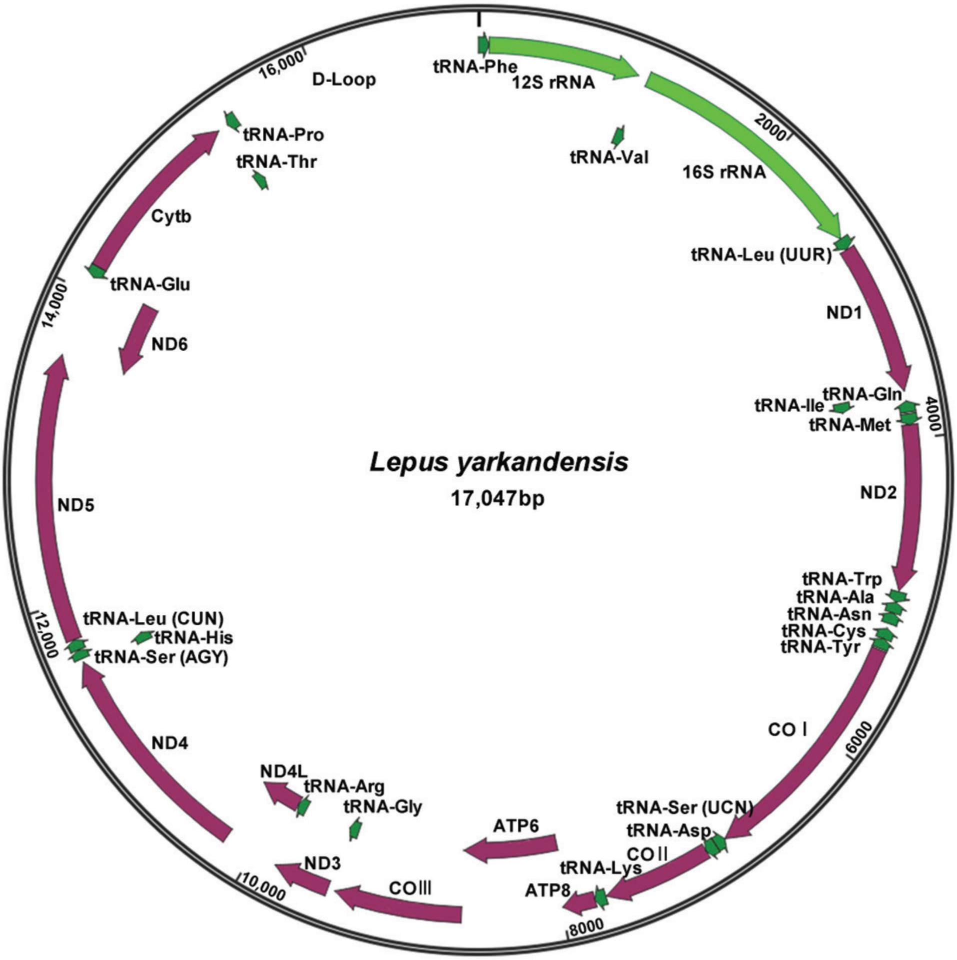

Figure 1. Complete mitochondrial genome map of *Lepus yarkandensis*. Genes encoded on the heavy and light strands are shown outside and inside the circle, respectively.

overlapping nucleotides with lengths ranging from 1 bp to 47 bp were present in the *L. yarkandensis* mitogenome, comprising a total length of 140 bp, with the longest nucleotide located between ND4 and tRNA-His. Moreover, 70 bp of intergenic spacer sequences spread over 12 regions in the hare mitogenome, ranging from 1 bp to 32 bp in size, with the longest was located between tRNA-Asn and tRNA-Cys (Table 2).

Genome composition and skewness

AT skew, GC skew, and A + T content were selected as parameters for investigating the pattern of the mitogenome nucleotide composition (Wei et al. 2010; Hassanim et al. 2005). The *L. yarkandensis* mitogenome had a base nucleotide composition of 31.50% for A,

Table 2. Mitochondrial genome organization of *Lepus yarkandensis*.

Gene name	Position		Size	Location	Codon		Intergenic nucleotide bp
	From	To	(bp)	H/L strand	Start	Stop	
tRNA-Phe	1	67	67	H			0
12S rRNA	68	1022	955	H			0
tRNA-Val	1023	1088	66	H			0
16S rRNA	1087	2668	1582	H			–2
tRNA-Leu (UUR)	2669	2743	75	H			0
ND1	2746	3702	957	H	ATG	T	+2
tRNA-Ile	3701	3769	69	H			–2
tRNA-Gln	3767	3838	72	L			–3
tRNA-Met	3848	3916	69	H			+9
ND2	3917	4960	1044	H	ATT	TAA	0
tRNA-Trp	4966	5032	67	H			+5
tRNA-Ala	5035	5101	67	L			+2
tRNA-Asn	5102	5174	73	L			0
tRNA-Cys	5207	5273	67	L			+32
tRNA-Tyr	5274	5339	66	L			0
COI	5347	6888	1542	H	ATG	TAA	+7
tRNA-Ser (UCN)	6891	6959	69	L			+2
tRNA-Asp	6963	7031	69	H			+3
COII	7032	7715	684	H	ATG	TAG	0
RNA-Lys	7719	7789	71	H			+3
ATP8	7791	7994	204	H	ATG	TAA	+1
ATP6	7952	8632	681	H	ATG	TAA	–43
COIII	8632	9435	804	H	ATG	T	–1
tRNA-Gly	9416	9485	70	H			–20
ND3	9486	9842	357	H	ATT	TA	0
tRNA-Arg	9833	9899	67	H			–10
ND4L	9901	10197	297	H	ATG	TAA	+1
ND4	10191	11615	1425	H	ATG	T	–7
tRNA-His	11569	11637	69	H			–47
tRNA-Ser (AGY)	11638	11696	59	H			0
tRNA-Leu (CUN)	11697	11766	70	H			0
ND5	11767	13578	1812	H	ATT	TAA	0
ND6	13575	14099	525	L	ATG	TAG	–4
tRNA-Glu	14100	14167	68	L			0
Cytb	14171	15310	1140	H	ATG	AGG	+3
tRNA-Thr	15310	15377	68	H			–1
tRNA-Pro	15378	15443	66	L			0
D-Loop	15444	17047	1604	H			0

(Overlap is denoted as "–". Spacer regions are denoted as "+". No overlap or interval is denoted as "0".)

29.40% for T, 13.30% for G, and 25.80% for C, with an A+T bias of 60.90%. Moreover, A and C were more popular than T and G with overall AT skew = 0.034 and GC skew = –0.320 in the entire *L. yarkandensis* mitogenome (Table 3). These overall genome composition and skewness are highly similar to those of other *Lepus* spp., such as *L. yarkandensis* (MN450151), *Lepus coreanus* and *Lepus tolai* (Yu et al. 2015; Huang et al. 2019; Shan et al. 2020). However, in species such as *Caenorhabditis elegans*, *Ascaris suum*, and *Mytilus edulis*, different AT and GC skew values were determined-negative AT skew and positive GC skew (Perna et al. 1995). In *Arbacia lixula* and *Anopheles cracens*, both AT and GC skews were negative (Perna et al. 1995; Mao et al. 2019). Moreover, an AT-rich region

Table 3. Nucleotide composition and skewness of the *Lepus yarkandensis* mitogenome.

	A%	T%	G%	C%	Size	A+T%	ATskew	GCskew
Total PCGs	30.50	30.90	12.00	26.50	11417	61.40	–0.007	–0.377
Overall	31.50	29.40	13.30	25.80	17047	60.90	0.034	–0.320
rRNAs	36.10	24.70	17.80	21.40	2535	60.80	0.188	–0.092
tRNAs	31.20	29.90	12.30	26.70	8295	61.10	0.021	–0.369
D-Loop	28.70	27.40	13.00	30.90	1604	56.10	0.023	–0.408
CDs	21.80	27.10	21.10	30.0	317	48.90	-0.108	–0.174
CSB	30.00	26.2	11.4	32.4	920	56.2	0.068	–0.480
ETAS	31.60	30.80	9.80	27.80	367	62.40	0.013	–0.479

is typically observed in vertebrates (Quinn et al. 1993; Zhao et al. 2016; Sarvani et al. 2018). Thus, this variation in AT and GC skews shows a degree of similarity within the same genus but not in different classes, which can also be used as an auxiliary reference for evaluating phylogenetic relationships.

Protein-coding genes

The total length of PCGs in the *L. yarkandensis* mitogenome was 11,417 bp, and its base composition was 30.50% for A, 30.90% for T, 12.00% for G, and 26.50% for C with an A+T bias of 61.40%. Among the 13 PCGs, 12 were located on the heavy strand (H strand), whereas ND6 was located on the light strand (Tables 2, 3), as observed in other *Lepus* species (Ding et al. 2014; Shan et al. 2020).

The skewness of the entire PCGs in *L. yarkandensis* (Table 3) indicated a higher occurrence of T than A, with a negative AT skew (–0.007), and C than G with a negative GC skew (–0.337) (Table 3). The negative AT skew value was inconsistent with that for most mammalians, which had positive AT skew values (Sarvani et al. 2018; Priyono et al. 2020). However, the result of the current study is highly similar to the result obtained for *Camelus dromedarius* (both AT and GC skews were negative), a heat-tolerant mammal (Sarvani et al. 2018; Manee et al. 2019).

To further estimate and understand the level of base bias between all PCGs, we calculated the AT and GC skew ratios for each PCG in the mtDNA genome of *L. yarkandensis* (Fig. 2). All values for the skewness of GC (except for ND6) in PCGs were negative, with C being more prevalent that G in the nucleotide composition. The ATP6, ATP8, ND2, and ND3 genes had positive AT skews, whereas the remaining genes (9 of 13) had negative values. Notably, ND6 had deviation ranges for AT skew (–0.303) and GC skew (0.636) when compared with the other 12 PCGs in the *L. yarkandensis* mtDNA sequence, and the deviation range is highly similar to some mammalians, such as *Moschiola indica*, *Camelus dromedarius*, and *Bubalus quarlesi* (Sarvani et al. 2018; Manee et al. 2019; Priyono et al. 2020).

As with the vertebrate mtDNA genome, the majority of PCGs in the *L. yarkandensis* mitogenome used ATG as the start codon, although ND2, ND3, and ND5 used ATT as the start codon. Most PCGs used typical stop codons (TAA for ND2, COI, COII, ATP8, ATP6, ND4L, and ND5; TAG for ND6 and COII), whereas a small

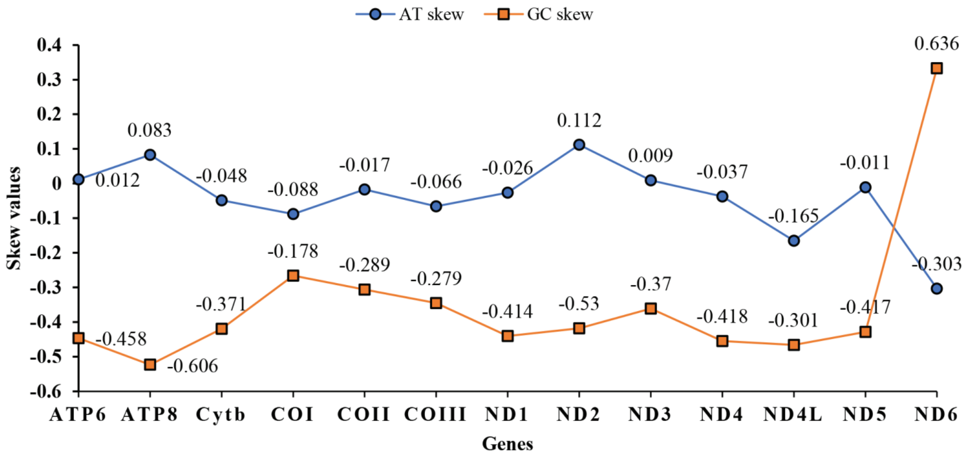

Figure 2. GC and AT skews for mitochondrial PCGs in *Lepus yarkandensis.*

number of abnormal stop codons were observed, including AGG (Cytb), T (ND1, COIII, ND4), and TA (ND3). Moreover, nine of 13 PCGs had complete stop codons, and four genes had incomplete stop codons (Table 2), which could be completed via posttranscriptional polyadenylation (Anderson et al. 1981; Ojala et al. 1981). Both PCGs of our *L. yarkandensis* (MG279351) and reported Yarkand hare (MN450151) have identical start and end codons, but different skewness.

The Ka, Ks, and Ka/Ks values of PCGs were estimated using substitution rates (Fig. 3). If Ka/Ks > 1, a positive selection effect was considered; if Ka/Ks = 1, a neutral effect was assumed; and if Ka/Ks < 1, purification selection was considered (Hurst et al. 2002). Except for ND1 and ND6, all PCGs in *L. yarkandensis* had average Ka/Ks values < 1, indicating purification selection. Meanwhile, for ND1 and ND6, Ka/Ks > 1 indicated positive selection. The function of the mitochondrial genome is crucial because it mainly undergoes evolutionary neutral or purifying selection. Other studies have reported that mitochondrial genes are also influenced by positive selection, particularly in animals adapting to harsh environments (Luo et al. 2008; Hichem et al. 2017; Jin et al. 2018). In the present study, positive selection in ND1 and ND6 might be beneficial to organisms and may confer to *L. yarkandensis* the ability to adapt to harsh and arid environments.

Control region

The control region 1604 bp in length was organized between *trnP* and *trnF* genes in the *L. yarkandensis* mitogenome (Table 2; Fig. 4). In vertebrate mitogenomes, the control region is a noncoding segment and consists of several control elements. These elements regulate genome replication and transcription (Boore 1999). In the current study, we successfully identified several highly conserved domains within the control region of the *L. yarkandensis* mitogenome-conserved sequence blocks (CSB) I–III, con-

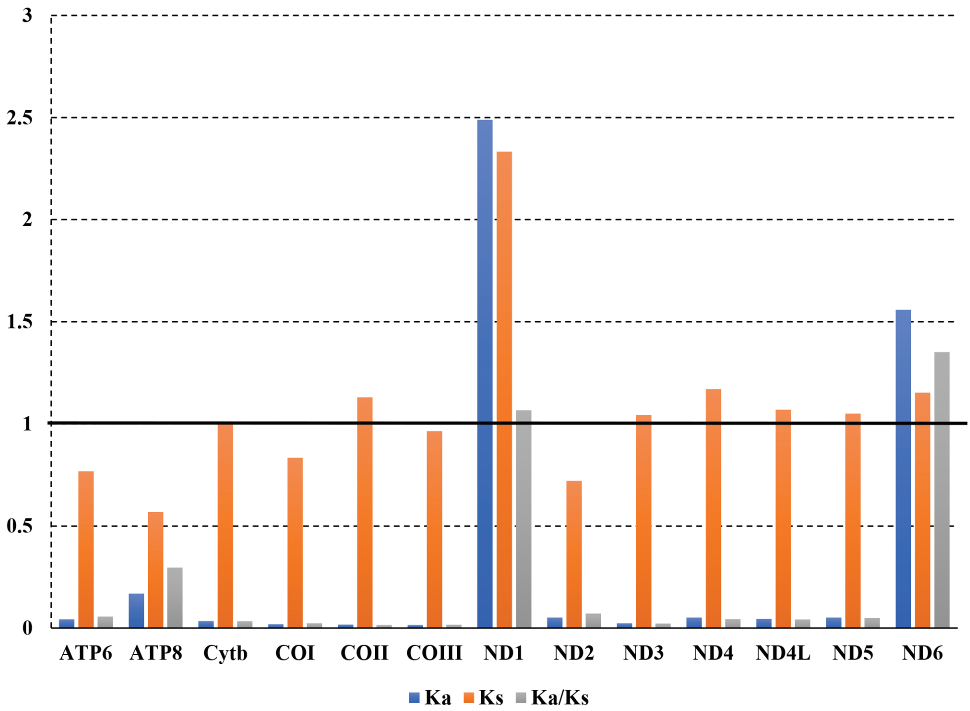

Figure 3. Evolutionary rates of the *Lepus yarkandensis* mitogenome by Ka/Ks.

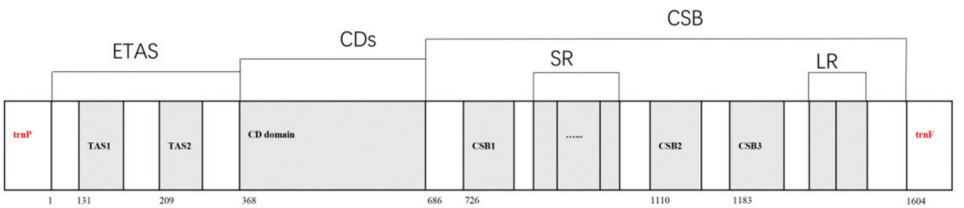

Figure 4. A schematic of the structural organization of the mitochondrial control region in *Lepus yarkandensis.* Control region flanking genes tRNA-Phe and tRNA-Pro presented in red. Conserved elements in the control region denoted by gray boxes: TAS, termination associated sequence; CD, central conserved domain; CSB, conserved sequence block. SR, short repeat; LR, long repeat.

served domain (CD), and extended termination associated sequence (ETAS) I–II–on the basis of their homology with other members of Lagomorpha and mammals (Elisabetta et al. 1997) (Table 4; Fig. 4). Characteristic motifs were used to detect the CSB domains: CSBI (GACATA), CSBII (CAAACCCCCC), and CSBIII (TGCCAAACCCCAAAAAC) (Gemmell et al. 1996; Elisabetta et al. 1997). We found from the sequence alignment results among hares and other mammals (Elisabetta et al. 1997) that more variations existed in Yarkand hare, including base insertions and deletions in the whole control region. CD was conservative with a narrow length range. The ETAS and

Table 4. Sequences of the conserved regions in the control region of *Lepus yarkandensis*.

Functional domains	Nucleotide sequences
TAS	
ETAS1	ACCATTATATGTTTAATCGTACATTAAAGCTTTACCCCATGCATATAAGCTAGTACATTC
ETAS2	CACATACACCTACTCAACTCCACAAAACCTTATCATCAACACGGATATCCAAACCCATTACCCA
CSB	
CSB1	TATCTTTTCATGCTTGACGGACATA
CSB2	AAACCCCCCCTACCCCC
CSB3	TGCCAAACCCCAAAAAC

CSB regions widely varied in the length of the control region, which is also the main reason for variations in mitogenome size in different species (Xu et al. 2012).

In CSB regions, CSB1 and CSB3 were relatively conservative, and CSB2 widely varied in *L. yarkandensis*. This finding contradicted the results for *Felis catus* and Mustelidae species (Elisabetta et al. 1997l; Zhang et al. 2009). In the present study, an ACCCC motif in the ETAS I sequence of *L. yarkandensis* was found, similar to that of the horseshoe bat (Sun et al. 2009). In some taxa such as species of Mustelidae, cattle, and Cervidae, the sequences were GCCCC (Zhang et al. 2009; Douzary et al. 1997). Between CSB I and CSB II, a number of short tandem repeat motifs, which commonly characterize mitogenomes, were observed in the *L. yarkandensis* mitogenome (Ren et al. 2009). The short repeat CGTCTACGCGCACGTACACCCA was 22 bp with 14 repetitions (Table 4), whereas the long repeat ACAATACTGACATAGCACTCAGCCTTTTATTTTTCCTCCAACAGGCATAACCCTAATTAAATTTTTCCAAAAAAAA occurred twice. Similarly, the short repeats CSB3 CGTCTACGCGCACGTACACCCA in *L. yarkandensis* (Fig. 4) occurred twice, which was also found in other *Lepus* species in this study. Notably, tandem repeats have been described in the control region of metazoans (Lunt et al. 1998; Rand et al. 1993; Yokobori et al. 2004) and the family Veneridae.

Transfer RNAs and ribosomal RNAs

Except for tRNA-ser (AGY), which lacked a D stem, the other 21 tRNAs formed complete secondary structures (Suppl. material 1). Aberrant loops have been found in some tRNA genes. These mismatches could be rectified by the post-transcriptional RNA-editing mechanism to maintain tRNA functions (Tomita et al. 2002).

Phylogenetic analysis

We constructed NJ and Bayesian trees based on the complete mtDNA genome of *L. yarkandensis* in this study and 25 other lagomorphs published on NCBI (Fig. 5). The topological structures of both trees were consistent and supported by high bootstrap values. The phylogenetic tree confirmed the existence of three distinct lineages-hares, rabbits, and pikas-which is consistent with Smith et al. (2018). In the present study, *L. yarkandensis* was not closely related to neither *Lepus europaeus* nor *Lepus americanus*

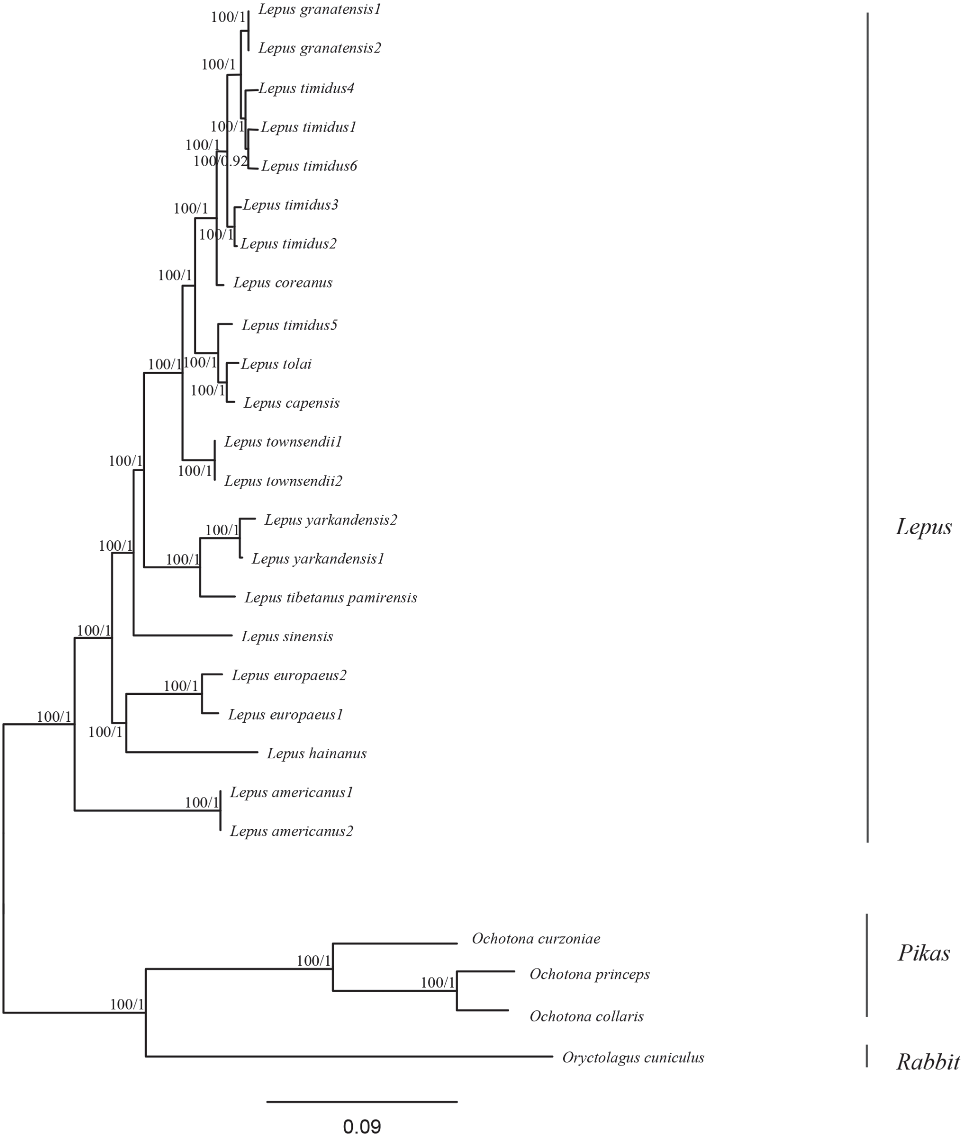

Figure 5. Neighbor-joining and Bayes trees based on the complete mtDNA sequences of 25 lagomorphs. Values separated by slash (/) represent bootstrap support values for the NJ and Bayes trees.

but was closely related to *Lepus tibetanus* in Xinjiang, China. The latter was misnamed as *Lepus capensis pamirs* in our previous study (Shan et al. 2015) and was renamed by Smith et al. (2018). Our *L. yarkandensis and L. yarkandensis* (MN450151) were clustered on the same branch. One reason for this close relationship could be the relatively close habitat. *Lepus t. pamirensis* are mainly distributed in the Pamir plateau of southeastern Kashgar, Xinjiang, China, bordering the Tarim Basin. The *L. yarkandensis* sample used in the current study was from Alar City in western Tarim Basin, which is near the *L. t. pamirensis* distribution. Another reason could be similarly extreme environments. Both habitats are dry with scarce rainfall and a lack of food (Shan et al. 2011). However, the phylogenetic relationship between *L. yarkandensis* and *L. t. pamirensis* remains uncertain, as hybridization has occurred between them (Wu et al. 2011). Further analysis with more samples and more extensive markers is required.

Acknowledgements

We are grateful for the financial support received from the National Natural Science Foundation of China (grant numbers 31860599, 31301006) and Xinjiang Natural Science Foundation (grant number 2018D01C060).

References

Aerziguli S, Mairepati P, Dilixiati A, Mahemut H (2010) Comparison of skull morphological characters of Yarkand Hare (*Lepus yarkandensis*) of different geographical populations. Xinjiang Agricultural Sciences 47: 1627–1631.

Anderson S, Bankier AT, Barell BG, De-Bruijn MH, Coulson AR, Drouin J (1981) Sequence and organization of the human mitochondrial genome. Nature 290: 457–465. https://doi.org/10.1038/290457a0

Boore JL (1999) Animal mitochondrial genomes. Nucleic Acids Research 27: 1767–1780. https://doi.org/10.1093/nar/27.8.1767

Ding L, Chen CM, Wang H, Zhang BW (2014) Complete mitochondrial DNA sequence of *Lepus tolai* (Leporidae: *Lepus*). Mitochondrial DNA 27: 1711–1712. https://doi.org/10.3109/19401736.2014.982568

Douzery E, Randi E (1997) The mitochondrial control region of Cervidae: evolutionary patterns and phylogenetic content. Molecular Biology and Evolution 14: 1154–1166. https://doi.org/10.1093/oxfordjournals.molbev.a025725

Elisabetta S, Tanzariello F, Reyes A, Pesole G, Saccone C (1997) Mammalian mitochondrial d-loop region structural analysis: identification of new conserved sequences and their functional and evolutionary implications. Gene 205: 125–140. https://doi.org/10.1016/S0378-1119(97)00404-6

Gemmell NJ, Western PS, Watson JM (1996) Evolution of the mammalian mitochondrial control region-comparisons of control region sequences between monotreme and therian mammals. Molecular Biology and Evolution 13: 798–808. https://doi.org/10.1093/oxfordjournals.molbev.a025640

Hassanin, A, Léger N, Deutsch J (2005) Evidence for multiple reversals of asymmetric mutational constraints during the evolution of the mitochondrial genome of Metazoa, and consequences for phylogenetic inferences. Systematic Biology 54: 277–298. https://doi.org/10.1080/10635150590947843

Hichem BS, Helmut S, Felix K, Franz S (2017) Selection on the mitochondrial ATP synthase6 and the *NADH dehydrogenase 2* genes in hares (*Lepus capensis* L., 1758) from a steep ecological gradient in North Africa. BMC Evolutionary Biology 17: e46. https://doi.org/10.1186/s12862-017-0896-0

Hu CY, Wang SB, Huang BS, Liu HG, Xu L, Hu ZG, Liu YF (2020) The complete mitochondrial genome sequence of *Scolopendra mutilans* L. Koch, 1878 (Scolopendromorpha, Scolopendridae), with a comparative analysis of other centipede genomes. ZooKeys 925: 73–88. https://doi.org/10.3897/zookeys.925.47820

Huang YL, Chen YX, Guo HT, Xu YH, Liu HY, Liu DW (2019) The complete mitochondrial genome sequence of Yarkand hare (*Lepus yarkandensis*). Mitochondrial DNA Part B 4: 3727–3728. https://doi.org/10.1080/23802359.2019.1681321

Hurst LD (2002) The Ka/Ks ratio: Diagnosing the form of sequence evolution. Trends in Genetics 18: 486–487. https://doi.org/10.1016/S0168-9525(02)02722-1

Jin YT, Wo YB, Tong HJ, Song S, Zhang LX, Brown RP (2018) Evolutionary analysis of mitochondrially encoded proteins of toad-headed lizards, *Phrynocephalus*, along an altitudinal gradient. BMC Genomics 19: e185. https://doi.org/10.1186/s12864-018-4569-1

Kumar S, Stecher G, Tamura K (2016) MEGA7: molecular evolutionary genetics analysis version 7.0 for bigger datasets. Molecular Biology and Evolution 33: 1870–1874. https://doi.org/10.1093/molbev/msw054

Li Z, Xia L, Li Y, Yang Q, Liang M (2006) Mitochondrial DNA variation and population structure of the yarkand hare *Lepus yarkandensis*. Acta Theriologica 51: 243–253. https://doi.org/10.1007/BF03192676

Li ZC, Xia L, Yang QS, Liang MY (2005) Population genetic structure of the Yarkand hare (*lepus yarkandensis*). Acta Theriologica Sinica 25: 224–228.

Lowe TM, Eddy SR (1997) tRNAscan-SE: a program for improved detection of transfer RNA genes in genomic sequence. Nucleic acids research 25: 955–964. https://doi.org/10.1093/nar/25.5.955

Lunt DH, Whipple LE, Hyman BC (1998) Mitochondrial DNA variable number tandem repeats (VNTRs): utility and problems in molecular ecology. Molecular Ecology 7: 1441–1455. https://doi.org/10.1046/j.1365-294x.1998.00495.x

Luo R, Liu B, Xie Y, Li Z, Huang W, Yuan J, He GZ, Chen YX, Pan Q, Liu YJ, Tang JB, Wu GX, Zhang H, Shi YJ, Liu Y, Yu C, Wang B, Lu Y, Han CL, Cheung DW, Yiu SM, Peng SL, Zhu XQ, Liu GM, Liao XK, Li YR, Yang HM, Wang J, Lam TW, Wang J (2012) Soapdenovo2: an empirically improved memory-efficient short-read *de novo* assembler. Giga Science 1: 1–18. https://doi.org/10.1186/2047-217X-1-18

Luo YJ, Gao WX, Gao YQ, Tang S, Huang QY, Tan XL, Chen J, Huang TS (2008) Mitochondrial genome analysis of *Ochotona curzoniae* and implication of cytochrome c oxidase in hypoxic adaptation. Mitochondrion 8: 352–357. https://doi.org/10.1016/j.mito.2008.07.005

Luo ZX (1988) The Chinese Hare. China Forestry Publishing House, Beijing.

Manee MM, Alshehri MA, Binghadir SA, Aldhafer SH, Alswailem RM, Algarni AT, Al-Shomrani BM, Al-Fageeh MB (2019) Comparative analysis of camelid mitochondrial genomes. Journal of Genetics 98: e88. https://doi.org/10.1007/s12041-019-1134-x

Mao QM, Li TJ, Fu WB, Yan ZT, Chen B (2019) Sequencing of the complete mitochondrial genome of *Anopheles lindesayi* and a phylogenetic analysis of the genus *Anopheles* (Diptera: Culicidae) based on mitochondrial genomes. ACTA Entomologica Sinica 62: 101–116.

Nguyen LT, Schmidt HA, von Haeseler A, Minh BQ (2015) IQ-TREE: a fast and effective stochastic algorithm for estimating max imum-likelihood phylogenies. Molecular Biology and Evolution 32: 268–274. https://doi.org/10.1093/molbev/msu300

Ojala D, Montoya J, Attardi G (1981) tRNA punctuation model of RNA processing in human mitochondria. Nature 290: 470–474. https://doi.org/10.1038/290470a0

Perna NT, Kocher TD (1995) Patterns of nucleotide composition at fourfold degenerate sites of animal mitochondrial genomes. Journal of Molecular Evolution 41: 353–358. https://doi.org/10.1007/BF01215182

Priyono DS, Solihin DD, Farajallah A, Purwantara B (2020) The first complete mitochondrial genome sequence of the endangered mountain anoa (*Bubalus quarlesi*) (Artiodactyla: Bovidae) and phylogenetic analysis. Journal of Asia-Pacific Biodiversity 13: 123–133. https://doi.org/10.1016/j.japb.2020.01.006

Psifidi A, Dovas CI, Banos G (2010) A comparison of six methods for genomic DNA extraction suitable for PCR-based genotyping applications using ovine milk samples. Mol Cell Probes 24: 93–98. https://doi.org/10.1016/j.mcp.2009.11.001

Quinn TW, Wilson AC (1993) Sequence evolution in and around the mitochondrial control region in birds. Journal of Molecular Evolution 37: 417–425. https://doi.org/10.1007/BF00178871

Rand DM (1993) Endotherms, ectotherms, and mitochondrial genome-size variation. Journal of Molecular Evolution 37: 281–295. https://doi.org/10.1007/BF00175505

Ren J, Shen X, Sun M, Jiang F, Yu Y, Chi Z (2009) The complete mitochondrial genome of the clam *Meretrix petechialis* (Mollusca: Bivalvia: Veneridae). Mitochondrial DNA 20: 78–87. https://doi.org/10.1080/19401730902964425

Ronquist F, Teslenko M, van der Mark P, Ayres DL, Darling A, Höhna S, Larget B, Liu L, Suchard MA, Huelsenbeck JP (2012) MrBayes 3.2: efficient Bayesian phylogenetic inference and model choice across a large model space. Systematic Biology 61: 539–542. https://doi.org/10.1093/sysbio/sys029

Song R, Zhang D, Gao JW, Cheng XF, Xie M, Li H, Wu YA (2019) Characterization of the complete mitochondrial genome of *Brentisentis yangtzensis* Yu & Wu, 1989 (Acanthocephala, Illiosentidae). ZooKeys 861: 1–14. https://doi.org/10.3897/zookeys.861.34809

Sun KP, Feng J, Jin LR, Liu Y, Shi LM, Jiang TL (2009) Structure, DNA sequence variation and phylogenetic implications of the mitochondrial control region in horseshoe bats. Mammlian Biology 74: 130–144. https://doi.org/10.1016/j.mambio.2008.09.002

Sarvani R K, Parmar D R, Tabasum W, Thota N, Sreenivas A, Gaur A (2018) Characterization of the complete mitogenome of Indian Mouse Deer, *Moschiola indica* (Artiodactyla: Tragulidae) and its evolutionary significance. Scientific reports 8: e2697. https://doi.org/10.1038/s41598-018-20946-5

Sbisà E, Tanzariello F, Reyes A, Pesole G, Saccone C (1997) Mammalian mitochondrial D-loop region structural analysis: identification of new conserved sequences and their functional and evolutionary implications. Gene 205: 125–140. https://doi.org/10.1016/S0378-1119(97)00404-6

Shan WJ, Liu J, Yu L, Robert WM, Mahmut H, Zhang YP (2011) Genetic consequences of postglacial colonization by the endemic Yarkand hare (*Lepus yarkandensis*) of the arid Tarim Basin. Chinese Science Bulletin 56: 1370–1382. https://doi.org/10.1007/s11434-011-4460-9

Shan WJ, Liu YG (2015) The complete mitochondrial DNA sequence of the cape hare *Lepus capensis pamirensis*. Mitochondrial DNA 27: 4572–4573. https://doi.org/10.3109/19401736.2015.1101569

Shan WJ, Tursun M, Zhou SY, Zhang YC, Dai HY (2020) The complete mitochondrial genome sequence of *Lepus tolai* in Xinjiang. Mitochondrial DNA Part B 5: 1336–1337. https://doi.org/10.1080/23802359.2020.1735267

Smith AT, Johnston CH, Alves PC, Hacklander K (2018) Lagomorphs: Pikas, Rabbits, and Hares of the World. Johns Hopkins University Press, Baltimore.

Smith AT, Xie Y (2008) Mammal of China. Princeton university press, Princeton, New Jersey

Stothard P, Wishart DS (2005) Circular genome visualization and exploration using CGView. Bioinformatics 21: 537–539. https://doi.org/10.1093/bioinformatics/bti054

Tomita K, Yokobori S, Oshima T, Ueda T, Watanabe K (2002) The cephalopod *Loligo bleekeri* mitochondrial genome: multiplied noncoding regions and transposition of tRNA Genes. Journal of Molecular Evolution 54: 486–500. https://doi.org/10.1007/s00239-001-0039-4

Wang S (1998) China Red Data Book of Endangered Animals. Science Press, Beijing, 247 pp.

Wei SJ, Shi M, Chen XX, Sharkey MJ, van Achterberg C, Ye GY, He JH (2010) New Views on Strand Asymmetry in Insect Mitochondrial Genomes. PloS ONE 5: e12708. https://doi.org/10.1371/journal.pone.0012708

Wu Y, Xia L, Zhang Q, Yang Q, Meng X (2011) Bidirectional introgressive hybridization between *Lepus capensis* and *Lepus yarkandensis*. Molecular Phylogenetics & Evolution 59: 545–555. https://doi.org/10.1016/j.ympev.2011.03.027

Wu YA, Gao JW, Cheng XF, Xie M, Yuan XP, Liu D, Song R (2020) Characterization and comparative analysis of the complete mitochondrial genome of *Azygia hwangtsiyui* Tsin, 1933 (Digenea), the first for a member of the family Azygiidae. ZooKeys 945: 1–16. https://doi.org/10.3897/zookeys.945.49681

Xu XD, Wu XY, Yu ZN (2012) Comparative studies of the complete mitochondrial genomes of four *Paphia clams* and reconsideration of subgenus *Neotapes* (Bivalvia: Veneridae). Gene 494: 17–23. https://doi.org/10.1016/j.gene.2011.12.002

Yokobori S, Fukuda N, Nakamura M, Aoyama T, Oshima T (2004) Long-Term Conservation of Six Duplicated Structural Genes in Cephalopod Mitochondrial Genomes. Molecular Biology and Evolution 21: 2034–2046. https://doi.org/10.1093/molbev/msh227

Yu J, Nam B, Yoon J, Kim E B, Park J Y, Kim H, Yon SH (2017) Tracing the spatio-temporal dynamics of endangered fin whales (*Balaenoptera physalus*) within baleen whale (Mysticeti) lineages: a mitogenomic perspective. Genetica 145: 603–612. https://doi.org/10.1007/s10709-017-9988-4

Yu JN, Chung CU, Kwak M (2015) The complete mitochondrial genome sequence of the Korean hare (*Lepus coreanus*). Mitochondrial DNA 26: 129–130. https://doi.org/10.3109/19401736.2013.815170

Zhao C, Zhang HH, Liu GS, Yang XF, Zhang J (2016) The complete mitochondrial genome of the *tibetan fox* (vulpes ferrilata) and implications for the phylogeny of Canidae. Comptes Rendus Biologies 339: 68–77. https://doi.org/10.1016/j.crvi.2015.11.005

Zhang H, Xu C, Ma J (2009) Structure of the mtDNA control region and phylogeny of the Mustelidae species. Journal of Ecology 29: 3585–3592.

Zhang QH, Huang P, Chen B, Li TJ (2018) The complete mitochondrial genome of *Orancistrocerus aterrimus aterrimus* and comparative analysis in the family Vespidae (Hymenoptera, Vespidae, Eumeninae). ZooKeys 790: 127–144. https://doi.org/10.3897/zookeys.790.25356

Supplementary material 1

Figure S1a, S1b

Authors: Wenjuan Shan, Mayinur Tursun, Shiyu Zhou, Yucong Zhang, Huiying Dai

Data type: multimedia

Link: https://doi.org/10.3897/zookeys.1012.59035.suppl1